From Proteome Center Rostock
Director: Prof. Dr. Michael O. Glocker

Molecular recognition studies by nanoESI mass spectrometry

Dissertation
For the acquirement of the academic degree
Doctor rerum humanarum: "Dr. rer. hum."

Faculty of Medicine, University of Rostock

Submitted by
Bright Djan Danquah, 04.05.1987
From Ghana

Rostock, 17.06.2019

https://doi.org/10.18453/rosdok_id00002661

Printed with the support of the German Academic Exchange Service

Reviewers:

Prof. Dr. Michael O. Glocker, Universität Rostock, Proteom Zentrum Rostock

Prof. Dr. Christopher Gerner, Universität Wien, Institut für Analytische Chemie

Prof. Dr. Georg Füllen, Universität Rostock, Institut für Biostatistik und Informatik in Medizin und Alternsforschung

Month/Year of submission: June, 2019

Month/Year of examination: December, 2019

Personal declaration

I hereby declare that the submitted dissertation is the result of my original work, and that it has not been previously accepted for any degree. To the best of my knowledge, it is also not being concurrently submitted for any degree or examination in any other university/institution. All sources of information utilized have been duly acknowledged and references provided in the dissertation.

Bright Djan Danquah

I dedicate this work to my parents, Mr. Daniel A. Danquah and Ms. Margaret Gyekye.

Acknowledgements

I would like to express my deepest appreciation and gratitude to my PhD supervisor, Prof. Dr. Michael O. Glocker, for the opportunity he offered me to perform my PhD work in the Proteome Center Rostock. His excellent scientific advice and suggestions have helped me to tremendously appreciate and understand key topics in the subject area. I am also thankful for his encouragements and for always challenging me as a student to utilize my intellect to solve problems that will benefit humanity. I am not leaving this challenge behind at the Proteome Center Rostock.

The support I received from my second supervisor, Prof. Dr. Michael Przybylski, also enormously helped me to progress with my PhD work. He always provided great scientific discussions and was very supportive throughout my studies. I am therefore grateful unto him as well.

I would also extend my sincere thanks to Dr. Cornelia Koy, Dr. Stefan Mikkat, Ms. Manuela Ruß and Dr. Claudia Röwer, who were very helpful in guiding my first steps in the laboratory and introducing me to the various instruments available at the Proteome Center Rostock.

I would like to use this opportunity to also thank Dr. Samuel Asare-Nkansah and Dr. Kwabena Frimpong Manso Opuni for continually providing words of encouragement throughout my PhD studies. I am particularly grateful for the information and advice they both offered me which led me to become a PhD student at the Proteome Center Rostock.

I thank Prof. Dr. Hans-Jürgen Thiesen for his fruitful discussions on my research work during our weekly departmental seminars. I must admit his constructive criticisms helped improve the quality of my work and I am therefore appreciative. I am also thankful to Mr. Michael Kreutzer for always sharing his valuable expertise in bioinformatics.

I also want to thank all my former and current colleagues at the Proteome Center Rostock and Institute of Immunology; Dr. Jingzhi Yang, Dr. Yelena Yefremova, Ms. Teresa Melder, Mr. Duc Nguyen, Mr. Niklas Menz, Mr. Charles Ayensu Okai, Mr. Hassan Albony and Mr. Mohanned Al-Chiblak for creating all the time, a nice and friendly working environment.

I am extremely thankful to my wife, Edith Danquah and my daughter, Naana Adjepongmaa Danquah for their patience, love and support. I also thank all my siblings especially my brother Samuel Adjepong Danquah for encouraging me to always aspire higher and for his support throughout my studies.

I would also like to thank my good friend I found in Rostock, Dr. Andres Velasco for his friendship, help and kindness.

Lastly, but not the least, what shall I say unto the Lord? All I have to say is thank you Lord for your divine grace and protection throughout this challenging phase in my life.

Table of Contents

1 Summary

1.1 Introduction

Biological systems are continuously exchanging messages with their environment, both chemical and electrical in nature [1]. The biological effects that result from interactions between biomacromolecules and small molecules, hormones, co-factors and ligands are based on physical contacts between the interactors and specific interaction between two or more molecules which requests molecular recognition [2]. Molecular recognition, thus, plays pivotal roles in all biological systems as it is involved in essential elements of life affecting metabolism, cellular signaling, immune responses, etc. For example, enzymes which catalyze chemical reactions in biological systems do so by bringing their substrates in close proximity within the active site so that reactions can be accelerated by lowering the activation energy [3-5].

The genome of unicellular *S. cerevisiae* has currently been estimated to consist of 5,858 genes and it was concluded that in an average yeast cell the number of proteins, i.e. the gene products, would amount to approximately 42 million [6]. It is legitimate to reason that in all organisms, and the more so in more complex multicellular organism like humans, the wide range of molecules present in eukaryotic cells must possess unique features that permit recognition which, consequently, leads to specific interactions. In other words, in order to achieve sanity in a living system consisting of some millions of molecules, there must be certain features or defined properties of these molecules that cause them to differentiate and recognize their interacting partners and then bind to them, once a matching recognition pattern is revealed.

All of the different classes of biomacromolecules express recognition patterns, including protein – carbohydrate ligand systems [7] and DNA / RNA − protein assemblies (e.g. DNA and the zinc-finger protein assembly) [8,9], to name only a few. All these molecular interactions are innately encoded in the molecule´s structure which by itself is encoded in the genome, and recognition motifs are thereby reliably provided to the organism by simply expressing and/or producing the respective biomolecules.

1.1.1 Molecular recognition in biomacromolecules

Whereas “recognition” has been proposed to apply to both, inter- and intramolecular phenomena, alternative terminologies such as “host-guest chemistry”, “supramolecular chemistry”, and “self-assembly” are limited to intermolecular processes; the first two by definition and the third by convention [2].

The Three-Dimensional Force Code

The interaction between macromolecules like proteins in general, and between antibodies and antigens in particular, can be described at various structural levels (Table 1). The specific binding of proteins to other proteins does not generally rely on all the amino acids located at the contact interface (paratope – epitope in case of antibody recognition), but on a limited set of atoms of some of the key amino acid residues of the epitope or the paratope. In order for molecular recognition of their cognate partners, specific atoms on binding interfaces must become part of a “three-dimensional force code” (not to be confused with the “three dimensional N-body code” [10]). The three-dimensional force code to which is referred to in this thesis is situated or stored as hotspot(s) on the surface of the interacting biomacromolecules, such as proteins. The atoms which constitute the three-dimensional force code are therefore to be elucidated in order to understand their altruistic nature and ultimately to obtain detailed knowledge on molecular recognition.

The three-dimensional force code is what determines which molecule or set of molecules is being recognized and bound to e.g. by a given protein. Moreover, the three dimensional force code not only defines specificity but also determines how strong interactions between binding partners shall be. General forces that keep molecules in physical contact upon molecular recognition occur mainly through hydrogen bonds, ionic forces, Van der Waals forces as well as by hydrophobic effects between the respective surface atoms. In other words, the three dimensional force code serves as the “eye” with which a molecule “sees” and simultaneously as the “hand” with which it holds on or clings to its binders.

Table 1: Structural levels and functional elements of a “Three-Dimensional Force Code”

structural level [a)]	functional elements	
	donor	acceptor
domain [b)]	antibody´s V_L and V_H (Ab)	antigen (Ag)
sub-domain	paratope (para)	epitope (epi)
peptide	complementarity determining regions (CDR)	complex determining peptides (CDP)
residue	specificity determining residues (SDR)	specificity determining positions (SDP)
atom	force donors and/or receptors (FDR)	force depending patches (FDP)

a) exemplified on antibody – antigen pairs

b) equals the molecular level in single domain proteins

In case of antibody - antigen interaction the three dimensional force code which is located within the antibody´s paratope defines both, the antibody´s specificity and its affinity. The paratope on the antibody molecule, i.e. the region that recognizes and permits antigen binding to occur is also called antigen binding site [11]. Within an antibody molecule, the six hypervariable loops, termed the complementarity determining regions (CDRs), are widely accepted as being the most responsible for antigen recognition. They together form the paratope. Even though the term specificity determining residues (SDRs) has been previously used in some cases to refer to key amino acid residues that determine the specificity of an antibody[12-14], specificity determining residues (SDRs) [15,16] as well as specificity determining positions (SDPs) [17,18] have been used interchangeably to refer to the amino acid residues that are very important for molecular binding specificity of a protein [15-19]. For improving clarity, the two terms are differentiated in this thesis, such that when speaking of specificity determining residues (SDRs) amino acid residues which are located on the antibody surface are addressed, whereas the term specificity determining positions (SDPs) shall be reserved to describe regions of the antigen´s epitope. To zoom in further, the set of atoms of the specificity determining residues (SDRs) on the antibody molecule which make intimate contacts with the antigen surface and, in addition, supply binding forces are described as those atoms that function as force donors and/or force receptors (FDRs).

The antigens which are recognized and bound by antibodies vary widely in both their chemical and physical properties, such as in size, hydrophilicity / hydrophobicity, sugar or

amino acid composition, etc. [20]. Typical antigens encountered by antibodies can be proteins, such as receptors which are expressed on cell surfaces, carbohydrates on bacterial and viral cell surfaces, hormones, chemical compounds, or nucleic acid structures [21-24]. The area / region on an antigen molecule that interacts or binds with an antibody is known as the “antigenic determinant” or the epitope [25]. In analogy to CDRs on antibodies, the respective peptides that are included in the antigen´s epitope are named complex determining peptides (CDPs). The different arrangements of complex determining peptides (CDPs) on the antigen surface that one can distinguish, allows to subdivide epitopes into different classes (Fig. 1). As previously summarized [25], epitopes may be classified as (i) consecutive, (ii) hybrid, or (iii) assembled.

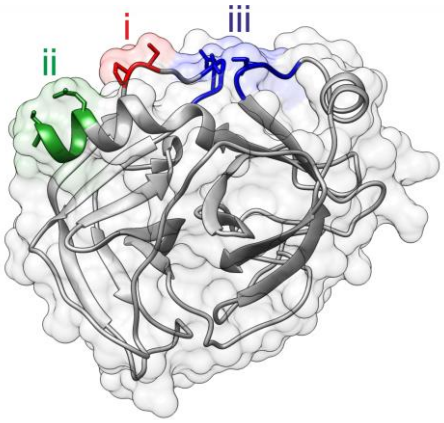

Fig. 1 The three dimensional epitope structures on a protein antigen molecule surface. A primary structure motif defines a “consecutive” epitope (i, red), a secondary structure motif determines a “hybrid” epitope (ii, green), and a tertiary structure motif is needed to form an “assembled” epitope (iii, blue). Adapted from *Opuni et al, 2018*

However, defining epitope subclasses, i.e the complex determining peptides (CDPs) along a proteins´s higher order structural elements [26], may perhaps be preferable. It is suggested to consider a “consecutive epitope” as an epitope which consists of one CDP that solely comprises primary structure elements (i). In analogy, a “hybrid” epitope also consists of one CDP which, however, is kept in position by secondary structure motifs like alpha helices (ii). At last, an “assembled” epitope consists of more than one CDP and is constructed by the tertiary structure of the antigen (iii).

Finally, the set of atoms within the antigens complex determining peptides (CDPs) are then termed, again in analogy to the respective atoms on the antibody´s CDRs “force depending patches (FDPs)”. Their positioning in space is predetermined by the protein surface which itself is defined by the protein fold that results as predetermined higher order structure which is formed by the amino acid sequence which finally is encoded in the respective genome. FDPs are typically identified by X-ray crystallography or by NMR as being in contact with atoms of the antibody in such distances which are consistent with those from known bond structures, e.g. hydrogen bonds have a typical length of ca. 3 - 4 Å in proteins [27,28]. FDPs have in some cases been termed “structural epitopes” [11].

1.1.2 The humoral immune system

The humoral immune system involves macromolecules which are found in extracellular spaces of the body, and is largely mediated by secreted immunoglobulins (antibodies) of the B cells and/or the plasma cells [29]. Complement proteins and certain antimicrobial peptides like α and β defensins, RegIIIα etc. are involved in humoral immunity [30]. The

aspect of humoral immunity that involves antibodies is often referred to as antibody - mediated immune response. Antibodies (also named immunoglobulins) are glycoproteins naturally amplified in response to invading foreign particles such as bacteria, viruses, and other microorganisms [31,32]. As many of the bacteria that cause infections multiply in the extracellular space, and most intracellular pathogens spread by moving from cell to cell through extracellular fluids, the extracellular spaces are protected by the humoral immune response during a microbial attack [29].

One must remember that even before an individual´s immune system comes into contact with a foreign particle (antigen), the B cells of the immune system is capable of producing enormous repertoires of antibodies [29,33]. The antibodies, which are part of the humoral immune system, are generated to potentially recognize a plethora of antigens beforehand. One must keep in mind though, that just like any other cellular protein, antibodies are encoded by genes. The final genes responsible for encoding antibodies are assembled on the DNA-level from separate gene segments during B cell development [33]. This irreversible process ensures that an individual can generate a sufficiently diverse repertoire of antibodies to react with the numerous toxic and pathogenic organisms present in the environment. The joining of antibody gene segments before they are transcribed, as well as the assembly of heavy and light chains during antibody formation has been described in several papers and textbooks in detail [33-36].

During B cell development in the bone marrow, the antibody molecules are at first embedded into the B cell membrane as receptors and then in a slightly different form are later produced as secreted molecules [37]. Depending on the strength and duration of the B cell antigen receptor (BCR) signaling, upon antigen binding, the BCRs may or may not require co-stimulatory signals for B cell activation to proliferate and differentiate into either memory cells or antibody-secreting effector cells [37]. By this, only those B cells that encounter an antigen to which their receptor binds will be activated to proliferate and differentiate into effector cells. In sum, quite to the contrary of other protein – protein interactions, antibody − antigen recognition [38] is based on a learning system. The immunity developed as a result of this learning system, known as the clonal selection theory, is a central principle in adaptive immunity [39].

1.1.3 Structure – function correlation of binding sites on immunoglobulin G

Antibodies play a critical role in the immune system's defense against infection and disease [21,32]. There are five classes of antibodies known to occur in mammals (IgG, IgA, IgM, IgE and IgD) [40,41]. Subclasses of IgG and IgA are also known to exist [40,42]. In human serum, the abundances as well as biological effects of the various classes and subclasses of antibodies vary widely [40,41] but they ultimately mediate specific biologic functions that are essential for responding to pathogens. In practice they are distinguished by immunoanalytical assays in which specific antibodies are applied. Once B lymphocytes have matured into plasma cells, each cell clone produces antibody molecules with a unique antigen binding site [43].

IgG is the most abundant class of antibody in serum as it constitutes about 75% of the antibody in serum [29,39]. The four subclasses of IgG known to exist in humans are IgG1, IgG2, IgG3, and IgG4, with relative amounts of ca. 60%, 25%, 10%, and 5% respectively in normal serum [42]. The molecular mass of an IgG molecule is approx. 150 kDa, and it is composed of a pair of two different kinds of polypeptide chains. One, of ca. 50 kDa in mass, is termed the heavy chain or H chain, and the other, of ca: 25 kDa in mass, is termed the light chain or L chain. Each IgG molecule consists of two heavy chains and two light chains (Fig. 2). The two heavy chains are linked to each other by disulfide bridges and each heavy chain is linked to a light chain by a disulfide bridge as well as by non-

covalent interactions to form the arms of a Y-shaped antibody molecule. In any given immunoglobulin G molecule, the two heavy chains and the two light chains are identical, giving an antibody molecule two identical antigen-binding sites. This implies that an IgG molecule has the ability to bind simultaneously to two antigens.

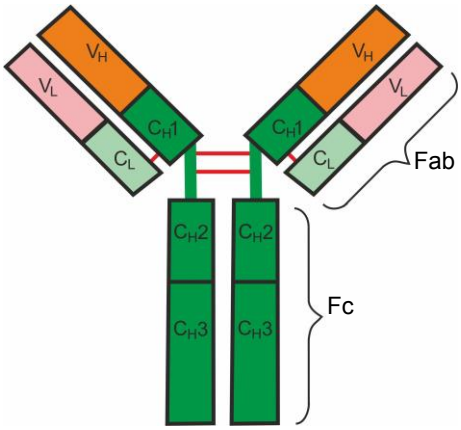

Fig.2 Schematic representation of an IgG molecule. Domains are shown as boxes (orange and pink: variable domains; green: constant domains) which are connected by disulfide bonds (red lines) and linker regions (green lines). Each light chain is composed of two domains (V_L and C_L), whereas each heavy chain contains four (V_H, C_H1, C_H2 and C_H3)

The amino acid composition of IgG heavy and light chains show that each chain consists of a series of similar, although not identical, sequences, each ca. 110 amino acids long and each of these repeats corresponds to a discrete, compactly folded region of protein structure known as a protein domain [29,42]. An important feature revealed by comparing the amino acid sequences is that the amino-terminal sequences of both the heavy and light chains vary widely between different antibodies. Thus, the variability in amino acid sequence is limited to the residues located in the variable domains (V_L and V_H). The remaining domains are constant between IgG chains of the same subclass.

The variable domains of the heavy and light chains (V_H and V_L, respectively) together make up the variable region (V of Fv domains) of the antibody and confer on an IgG the ability to bind a specific antigen, whereas the constant domains (C domains) of the heavy chain (C_H1, C_H2 and C_H3) and light chain (C_L) make up the C regions. The Fab is composed of two variable domains (V_H in the heavy chain and V_L in the light chain) and two constant domains (C_H1 and C_L). Two additional domains, C_H2 and C_H3 of both of the heavy chains compose the Fc region which is responsible for mediating the biological activity of the IgG molecule [29].

The most widely studied immunoglobulin class, the IgG class, has found a broad variety of applications including treatment of numerous autoimmune diseases and cancer [44-46]. Consequent to the clinical and biotechnological applications of IgGs, a variety of strategies are currently available for improving the manufacturability of IgG on a large scale either by recombinant DNA technology or hybridoma techniques [47]. Moreover, as reagents, antibodies have varying applications in disease diagnostics and biotechnological assays due to their striking specificities in recognizing their cognate antigens [48-50]. The principle underlying the different kinds of molecular recognition patterns is utilized also in a variety of other biotechnological applications, such as the purification [51-53] and immobilization of biomolecules [54,55], labeling of proteins [56,57], targeting approaches in therapeutics [58-60], and design of molecular probes for disease diagnosis [61,62]. Although various bio-recognition elements such as lectins [63], aptamers [64], enzymes [65,66] exist as well, antibodies, have

particularly and widely been used as molecular recognition elements in a variety of biotechnology platforms due to their exquisite specificities for their cognate antigens [67].

Paratope - Epitope interactions

The V_H and V_L domains of an IgG combine in a non-covalent manner to form the Fv, also known as the variable domain which harbors the paratope [68] (Fig. 3). The variable loops of β-strands, three on each of the V_L and V_H domains, referred to as the complementarity determining regions (CDRs), are responsible for binding to the antigen [69]. In essence, each of the two arms of the Y shaped antibody monomer is tipped with a paratope, which consists of residues originating from most or all the complementarity determining regions [11]. The partial surface of the antigen to which the paratope binds is called an epitope or antigenic determinant [11,25,68]. The ability of antigen structures to be recognized and bound by antibodies forms the molecular basis of antigenicity [70].

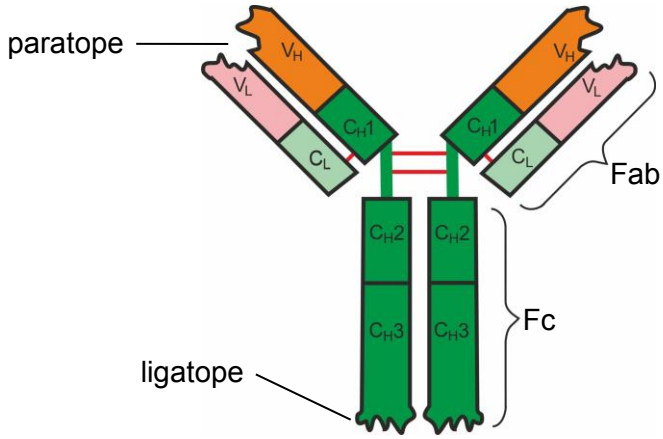

Fig.3 Schematic representation of an antibody molecule showing its antigen binding site (paratope) and its receptor binding site (ligatope).

IgGs are not only responsible for binding to diverse antigens via paratope - epitope interaction but also bind to the various effector molecules to which their constant regions (Fc domains) engage [71], thereby mediating diverse effector activities through the various classes of Fc receptors (FcRs) [72].

Ligatope – Efcetope interactions

Fc receptors (FcRs) are protein molecules found on a variety of immune cells including macrophages, neutrophils, monocytes, eosinophils, and lymphocytes of the innate immune system (natural killer cells) or adaptive immune system (e.g., B cells) [73-76]. Several classes of FcRs exist. They are classified based on the type of antibody that they recognize and bind [77]. For instance, FcRs that bind the most predominant class of antibody, IgG, are called Fc-gamma receptors (FcγR), those that bind IgA are called Fc-alpha receptors (FcαR) and those that bind IgE are called Fc-epsilon receptors (FcεR). The recently identified FcR found to bind to IgM was also named FcμR [78]. Subtypes of receptors are also denoted by capital Roman numerals, such as: FcγRI, II and III (numerals are in the order of affinity for IgG) [77]. Although the FcRs can consist of up to several hundreds of amino acids, only a set of few amino acid residues are in contact with the antibody Fc at the binding interface [79,80]; another example for realization of the three-dimensional force code.

Interaction between Fc receptors on phagocytic cells and antibodies play a critical role in both innate and adaptive immune responses [73,81]. Various immune responses are mediated through FcR-antibody recognition [73]. The most common is the activation of phagocytes such as macrophages to ingest and kill IgG-decorated pathogens by a process known as phagocytosis [82]. Another common process involving Fc receptors is the so-called antibody-dependent cell-mediated cytotoxicity (ADCC), where FcγRIII receptors on the surface of natural killer (NK) cells stimulate the NK cells to release cytotoxic molecules from their granules to kill antibody-covered target cells [76,83].

FcRs recognize and bind to antibodies that are attached to the surfaces of microbes or microbe infected cells and activate these cells to eliminate microbial pathogens. Since the antibody functions as a ligand in the antibody-FcR recognition, the term “ligatope” may be used to appropriately describe the specific area on the antibody that recognizes and binds to the FcR (Fig. 3). The restricted area on the FcR that makes contact with the ligatope of the antibody could therefore be named an efcetope (efce; Fc and topos; place). The capacity of antigenic determinants or structures to induce cellular and humoral immune responses is termed immunogenicity [70].

In recent years, much has been learned about the structural details of the interaction between various kinds of FcRs and IgG Fc parts using predominantly X-ray crystallography [79,84,85]. From crystallographic studies, the FcγRIII has been shown to bind between the two C_H2 regions of Fc part of IgG1 and make contact with residues in the hinge region [79,86]. The total buried surface area on both C_H2 domains upon FcγRIII-IgG-Fc complex formation was estimated to be 895 $Å^2$ suggesting that only a few residues are involved in the binding interface [79]. Additionally, some low affinity FcRs have been shown to bind to C_H3 domains of IgG [87].

In light of the modern advancements in mass spectrometry, attempts have been made to understand and characterize ligatope - effcetope interactions by using mass spectrometry [88-90]. Studies on the interaction between a full length IgG1 and a human neonatal Fc receptor (FcRn) by hydrogen/deuterium exchange mass spectrometry (HDX-MS) showed that regions in the antibody Fc and the FcRn were protected from exchange upon complex formation- a result that was in good agreement with previous crystallographic studies of FcRn in complex with Fc fragment of IgG[89]. There is therefore no doubt that mass spectrometry can be used as an analytical tool to probe ligatope - efcetope interactions.

Classotope, Idiotope, Allotope – Paratope interactions

IgGs themselves can be antigenic [91-93]. Thus, they can trigger the production of antibodies (anti-antibodies) in the appropriate recipient. For instance, injecting a patient with purified mouse derived IgG can cause very undesirable immune reactions [94] because the patient’s immune system recognizes the purified mouse IgG as foreign. It is also worth noting that the use of even humanized and fully human IgG as therapeutics may still carry some immunological risk [92]. There is therefore untold need to elucidate structures on IgGs that make them immunogenic.

Antibodies which are produced to recognize human antibodies enables their classification into isotypes, allotypes, and idiotypes [91,95] (Fig. 4) which is used to categorize antibodies into the five antibody classes (isotypes) - IgG, IgA, IgM, IgE and IgD and into subclasses, such as IgG1 through IgG4 [40,95]. The different heavy and light chain classes account for the isotypic variation in antibodies [40]. Since the isotypic variation allows antibodies to be grouped broadly into their classes and sub-classes [96], regions on the antibody molecule that contain the isotypic markers may be referred to as “classotopes” (Fig. 4).

Allotypic variations are mostly known to occur in the constant region of H and L chains, but some have been found to appear in the framework residues of V regions [97-99]. The region on an antibody molecule that defines the allotypic determinants of the antibody can therefore be termed as the allotope. Allotypic determinants (allotopes) are encoded by one allele (variation) of a given antibody gene and are present on the antibodies of some members of a species.

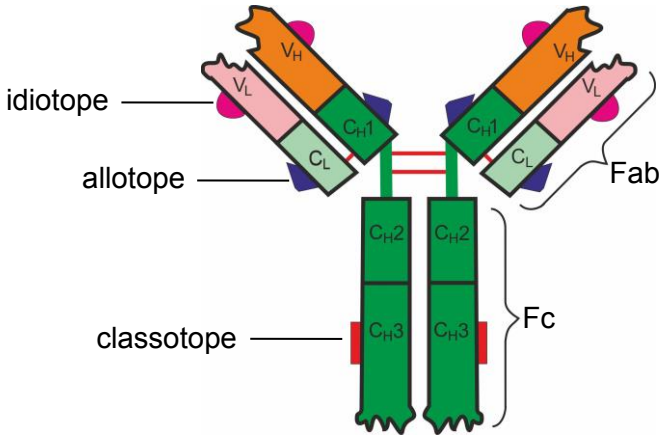

Fig.4 Schematic representation of an antibody molecule showing its classotope, allotope and idiotope locations.

Although antibodies have been humanized to diminish the adverse effects of immunogenicity, the differences in allotope sequences still creates a potential for immune response from the patient to the antibody if the allotype of patient and antibody do not match [93]. Consequently, the choice of allotype to select for a therapeutic antibody is difficult since allotypic distribution in humans is known to vary within and across ethnic groups [93,100]. It therefore makes it imperative to develop novel methods that can be used to map the allotopes of antibodies to better understand immunogenicity arising from allotypic variations.

Idiotypy has previously been coined to define the phenomenon where an antigenic determinant is found to be unique to particular antibody molecules of a given individual [91]. Idiotopes (idiotypic determinants) are found in the V region near the antigen-binding site of the antibody molecule[91] (Fig. 4). These determinants are common to antibodies exhibiting specificity for the same antigenic determinant and are therefore used to define the monoclonality of an antibody [96]. Idiotopes are known to be individual-specific and each individual has as many different idiotypes as it has different antibodies. Of note, idiotopes of therapeutic antibodies may be responsible for triggering immune reactions in patients.

Constatope – Cementotope interactions

Apart from the fragment antigen binding (Fab) domains where cognate antigens bind to antibodies with high selectivity and specificity, the Fc regions of human immunoglobulins are also the primary recognition site for other proteins, such as the bacterial proteins, protein A (from Staphylococcus origin) and protein G (from Streptococcal origin).

Protein G binds to the interface between the second and third heavy chain constant domains (C_H2 and C_H3) of Fc which is roughly the same binding site for protein A [101]. Since the amino acid residues of the fragment crystallizable (Fc) regions that serve as their primary recognition site are almost identical (constant regions), we name the area on the Fc where the proteins bind a constatope (Fig. 5). Due to the extremely high affinity with which protein G binds to the constatope on the Fc of the antibody, we call the area on the

protein G that makes contact with the constatope a cementotope. From X-ray crystallographic data and an NMR study, the interface between the Fc binding region (cementotope) of the protein G and that of the of the antibody (constatope) comprises of about 8-11 amino acid residues from the constatope in contact with about the same number of residues of the cementotope [101,102].

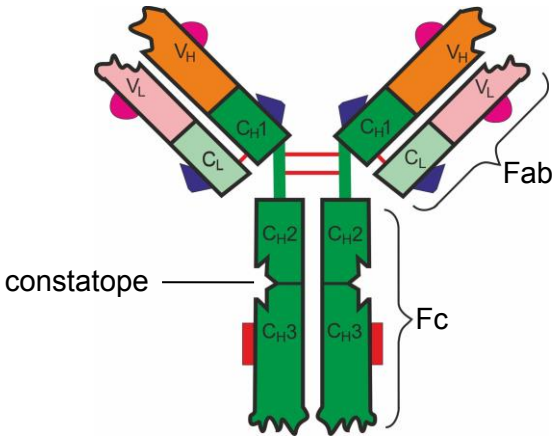

Fig.5 Schematic representation of an antibody molecule showing its constatope location.

Although the binding of these bacterial proteins to the Fc part of IgGs have been widely applied for purification [103-105], immobilization [106] and affinity capturing [107] of antibodies in biotechnological assays, a major drawback of using the full length of these bacterial IgG binders is that their recognition profile may not be suitable for specific usages. When used as a ligand for affinity capturing of antibodies in immunoassays, the additional binding of the ligand to Fab regions of the antibodies can limit its application [108]. In addition, the binding affinities of both protein A and protein G vary with different IgG subclasses [109-112].

In spite of the aforementioned limitations, the tremendous importance of IgG Fc-binding proteins continues to stimulate research directed to improve their use as high affinity ligands [113]. A prerequisite to designing ligands with enhanced specificities and affinities is a good understanding of their recognition motifs. Current understanding of their recognition sites through structural and functional studies has led to for example the design of artificial ligands that have high affinity for immunoglobulins, yet improved specificities [114,115].

Recently, we reported the development of an electrospray ionization mass spectrometry-based method by which thermodynamic properties of protein G-antibody interactions can be determined in the gas phase [116].

At last, when constructing a “cementotope” as a part of an antibody´s heavy chain and simultaneously creating a “constatope” on a second heavy chain, the so tailored molecular recognition pattern and resulting specific interaction leads to novel designer antibodies, which then become bispecific antibodies. The engineering process has been coined “knob-in-hole” [117,118], which involves creating a “knob” in the C_H3 domain of an antibody and a “hole” in the C_H3 domain of another antibody with a different specificity, thereby resulting in heterodimerization of the heavy chains of the two IgGs. Bispecific antibodies are IgG molecules which contain two different antigen binding sites. The design of such antibodies has largely been successful because of the sufficient understanding of the molecular recognition of IgG molecules. The emergence of bispecific antibodies [119-121] in the past years has developed into a promising field of research and for novel antibody based biotherapies.

Carvotope – Meditope interactions

A unique binding site for a small peptide in the center of the Fab cavity of cetuximab, a chimeric, anti-epidermal growth factor receptor monoclonal antibody was identified via diffraction studies and because of the position of the binding interface (Fig. 6), the peptide was named "meditope" (*medius*, middle; *topos*, place) [122]. Structural analysis using X-ray crystallography showed that the meditope-binding site or "carvotope" on the Fab is not only distinct from the antibody's antigen binding site (paratope) but also very distinct from the binding sites of other well established Fab binding proteins such as protein A, G, or L. The meditope-Fab recognition was found to involve all four domains of the Fab of cetuximab [122,123]. The binding of the meditope to the carvotope of the antibody occurs via a noncovalent interaction that does not significantly disrupt the antibody's ability to bind to its target antigen [59,122]. A meditope can therefore be defined as any small peptide that specifically binds to a unique site located in the center of a cavity formed by the light and heavy chains of an antibody and does not interfere with antigen binding affinity, specificity and stability.

In order to better understand the specificity of the meditope-Fab recognition and also to test whether this recognition could be expanded to other monoclonal antibodies, the meditope binding site of cetuximab has been grafted onto other monoclonal antibodies by the so called "SnAP" technology (Site specific novel Antibody Platform) [59]. The core technique in this strategy is the generation of meditope-enabled antibodies by site-specific carving which is made possible because the cetuximab carvotope-meditope recognition has been studied in details. This novel strategy has enabled antibody-drug conjugates (ADCs) to be customized for variety of applications in diagnostics, therapeutic delivery and imaging [58,122,124].

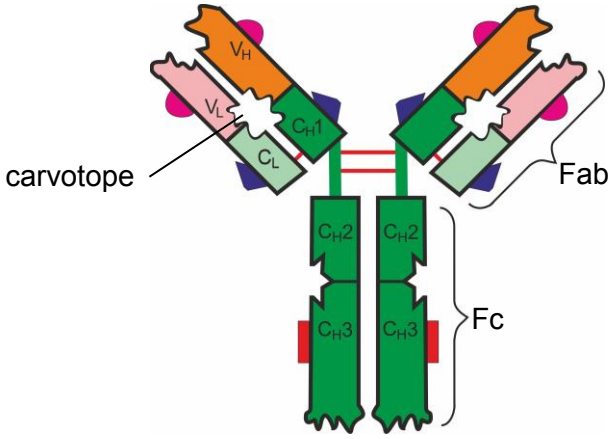

Fig.6. Schematic representation of an antibody molecule showing its carvotope location.

In general, the "Lego®-like" cave sites are created on Fab regions of a monoclonal antibody (mAb) by replacing a few amino acid residues using antibody engineering. These cave sites, termed as "meditope-binding site" or "carvotopes" of the antibody is then able to recognize and bind specifically to its cognate meditope without the need for a covalent chemical conjugation. Thus, by adjusting and optimizing engineered meditope-enabled antibodies, a stable non-covalent, yet site-specific conjugation can be accomplished. Considering the tremendous potential ADCs promise in the treatment of cancer [125-127], efforts have been made to design site-specific ADCs with high homogeneity [128,129] with the aim of identifying which conjugate species produce the most desirable pharmacological properties and also to aid accurate characterization of ADCs throughout all phases of discovery [130]. Whereas creating ADCs by chemical conjugation of a cytotoxin to a mAb

(typically involving lysines, reduced cysteines, or sugars on the mAb) has generally been reported to yield heterogeneous mixtures which can adversely affect the specificity and stability of the mAb and alter its bio-distribution [131-133], the use of meditope-enabled antibodies has been shown to be advantageous as it results in homogeneous ADC products with a predictable drug-to-antibody ratio (DAR).

An in-depth understanding of the molecular recognition of meditope-carvotope interactions has led to efforts to improve binding affinity by altering the cyclization and side chains of the meditope [123,134]. For example, to increase the affinity of the interaction between a cyclic 12-residue meditope which binds to a carvotope on the cetuximab Fab, extension of the side chain of Arg8 in the meditope by carboxyethylarginine substituition increased the half-life of the complex by three folds compared to the unmodified meditope [135].

The concept of Darthotopes and Jeditopes

As the lack of appropriate definitions and precise nomenclature has led to somewhat ambiguous terminologies in the past, the systematic and practical nomenclature that is suggested here (Table 2) intends to help reduce confusion in the field of molecular recognition investigations. For example, although an epitope is widely accepted as the region on an antigen molecule that makes contact with the paratope of an antibody, this definition had been abandoned when the region on an Fc receptor that binds to the Fc part of an antibody had been termed an epitope as well [80].

Unambiguous verbalization of the components of a bipolar concept of inverse complementarity, which clearly characterizes the most prominent characteristics of molecular recognition based on a three dimensional force code is required. Motivated by the instantly recognized and easy to capture analogy of a “yin and yang” concept that every student knows from the famous Star Wars movies, the recognition motifs on the antibody shall be termed the darthotopes (“darth” and topos: place) and the oppositely corresponding set of amino acids, peptides or surface regions on the antigen which bind to the antibody shall be defined as the jeditopes (“jedi” and topos: place). Thus, a darthotope is the set of amino acids or the restricted area on the IgG that forms its three dimensional force code responsible for recognition. By this definition, the amino acid residues in an IgG’s darthotope are considered to be required for bringing balance to the force code situated on the antigen surface.

Table 2. List of darthotope - jeditope pairs in antibody - antigen recognition.

darthotopes	jeditopes
paratope	epitope [a)]
ligatope	efcetope
constatope	cementotope
carvotope	meditope

a) classotopes, allotopes, and idiotopes are epitopes.

From an IgG molecule’s perspective, it recognizes a certain force code regardless of which molecule this force resides on. This implies that if atoms of amino acids of different and

unrelated protein antigens share a similar force code that can be recognized by an IgG molecule, chances are that the IgG will to some degree bind to these “unrelated” antigens [136]. Deciphering and learning into details about these recognition motifs and their force codes will thus arguably help to answer the problem of cross reactivities observed with antibody interactions as well as will help to broaden their applicability in life sciences.

1.2 Objectives

With the advent of therapeutic antibodies for treatment of patients, there is a huge demand for antibody characterization, both structurally and functionally. As the most specific property of an antibody is arguably its ability to bind its antigen through paratope - epitope recognition, the two prime objectives of this thesis were to develop simple but accurate mass spectrometric methods that can be used (i) to identify epitopes of antigens as well as (ii) to estimate the strength of antibody – antigen binding.

First, a mass spectrometric approach was developed that enabled rapid and accurate determination of epitope peptides: the “Intact Transition Epitope Mapping (ITEM)” method. This method is now renamed to “Intact Transition Epitope Mapping – One-step Non-covalent force Exploitation (ITEM-ONE)” since it has been surpassed by our most recently developed method which is entitled “Intact Transition Epitope Mapping – Targeted High-Energy Rupture of Extracted Epitopes (ITEM - THREE)”. Both methods make use of ion mobility mass spectrometry for rapid and accurate determination of antigen-derived peptides, the epitopes, that undergo specific in-solution interactions with an antibody of interest.

Second, within this thesis was developed a mass spectrometry-based method by which protein complex stabilities in the gas phase can be estimated. Once an immune complex had been isolated and translated into the gas phase, its stability was readily checked in one step by applying special experimental conditions through which one directly determined “apparent energies of dissociation activation ($E_A^{\#}{}_{m0g}$)” of charged antibody-protein complexes by application of the Rice Ramsperger Kassel Marcus - Quasi Equilibrium Theory (RRKM-QET). The example of choice in this thesis was the already established Immunoglobulin G Fc - protein G pair which according to our nomenclature resembles a “constatope - cementotope” recognition motif.

All three methods, although developed with antibody – antigen pairs, can principally be used to study apparent gas phase dissociation energies and identify substructures of protein - protein interactions of all kinds of biomacromolecular complexes. Because mass spectrometry offers the advantages of speed and low sample consumptions the here developed methods can be applied for many bio-medical purposes, such as to investigate stabilities of any disease-related interaction of biomacromolecules, hence opening avenues to functional testing of targeted personalized medicine concepts.

1.3 Methods

1.3.1 Protein epitope mapping in the gas phase

The most specific property of an antibody is arguably its ability to bind its cognate antigen in a unique fashion via precise paratope- epitope recognition. The experimental determination of antigenic determinants (epitopes), i.e. the region on the antigen that binds to the antibody, is of tremendous importance for antibody characterization. The relatively low amount of sample required for mass spectrometric epitope mapping makes it a method of choice. However, a major drawback to all the currently available experimental epitope mapping methods including mass spectrometric work-ups lies in the rather

sophisticated, but up to now unavoidable lengthy in-solution procedures. There is therefore an unmet need for rapid and accurate epitope mapping procedures. As a result, a method that facilitates in-solution handling is expected to generate a real breakthrough in routine epitope mapping.

In this thesis the “Intact Transition Epitope Mapping” method (ITEM) has been developed and applied as an epitope mapping procedure that identifies the epitope peptide of an antibody of interest in a fast and easy fashion. In-solution handling is reduced to mixing of peptide and antibody solutions using native mass spectrometry compatible volatile solvents whose pH allow antibodies to maintain their property to bind their cognate antigens. The entire antibody - peptide mixtures are electro-sprayed directly into the mass spectrometer, the unbound peptides (UBPs) are separated from the immune-complexes in the gas phase in an ion mobility separation chamber. Next, the immune-complexes are dissociated via collision induced dissociation (CID) and the masses of the complex-released peptides (CoRPs) are subsequently determined leading to unequivocal identification of epitopes in an easy to interpret “arrival time over *m/z*, atomz” plots.

Using both epitope extraction and excision work-ups, we applied the ITEM method to rapidly and accurately identify the epitope of the anti-RA33 antibody from a crude digest of rhRA-33 and the His-tag epitope from recombinantly expressed protein G´e.

For more information on protein epitope mapping in the gas phase see Chapter 1.4.1.

1.3.2 Identification of epitope peptides from unknown antigens

Information provided by results of epitope mapping experiments is extremely valuable in the process of antibody humanization, as well as in vaccine design. Mass spectrometric epitope mapping methods that identify epitopes at amino acid resolution are not only useful for identifying the regions on the antigens antibodies bind to but also are essential for identifying potential post-translational modifications on these regions and their effects on antibody recognition. Equally important is an epitope mapping method that allows scientist in life sciences to identify unknown antigens by first identifying the amino acid sequence of epitopes and with the aid of a protein database, identifying the antigen that contains the identified epitope.

In this thesis, we thus present the development and application of “Intact Transition Epitope Mapping - Targeted High-energy Rupture of Extracted Epitopes” method (ITEM-THREE) which allow identification of epitopes at amino acid resolution and subsequently identification of unknown antigens via a protein database search.

To perform ITEM-THREE experiments, three electrospray-compatible solutions with neutral pH, in which the antibodies maintain their in-solution activities, are prepared. Solution 1 is either a mixture of epitope peptides in 200 mM ammonium acetate (we mixed seven synthetic peptides) or a proteolytic digest of an antigen. Solution 2 contains one antibody in 200 mM ammonium acetate (in our case antiRA33, antiTRIM21, antiHis-tag or antiTNFalpha antibody). Solution 3 is a mixture of solutions 1 and 2, in which the specific immune complexes form (molar ratios: 2.2 : 1).

Without any purification steps solution 3 is then electrosprayed and the quadrupole analyzer is first used as a mass filter by setting it to block transmission of lower molecular weight ions (unbound peptides). The traversing antibody-peptide complexes are then dissociated in a first collision cell (TRAP) by increasing the collision cell voltage difference. The dissociated complexes then transit into the ion mobility separation chamber where they are separated according to their *m/z*, sizes and shapes. Finally, the collision cell

voltage difference in a second collision cell (TRANSFER) is also increased to cause fragmentation of the complex released peptides (CoRPs).

The collision voltages in the two collision cells (TRAP AND TRANSFER) are raised in a stepwise manner (5-20V/step) and optimized for each experiment to ensure adequate dissociation of the antibody - peptide complex and subsequent fragmentation of the complex released peptides. Appropriate control experiments using rituximab as a non-specific antibody were also carried out. Also, we performed control experiments by individually electrospraying the antibody solutions and the peptide mixtures (digests) alone and following the procedure described above. The resulting spectra were processed with Masslynx software version 4.1. The processed data was submitted to a Mascot search against a protein sequence database search to obtain partial amino acid sequence of the extracted epitope peptide which then allows one to identify the amino acid sequence of the full length antigen through a database search. ITEM-THREE thus provides a means of direct identification of antigens from which the epitope peptide has been extracted.

For more information on identification of epitopes from unknown antigens see Chapter 1.4.2.

1.3.3 Gas phase thermodynamic analysis of protein-protein complex dissociation

Protein-protein complexes are characterized in solution by determining thermodynamic properties like dissociation constants (K_D) and Gibbs free binding energies (ΔG^0_s) at equilibrium. Whereas methods to determine kinetic and/or thermodynamic properties of proteins and protein complexes in solution are well-established and broadly applied, approaches for studying such interactions in the gas phase are lacking. Electrospray mass spectrometry enables transfer of intact protein - protein complexes into the gas phase.

Since in vacuo measurement of analyte molecules are free of intermolecular interactions with surrounding solvent spheres, it allows the energy of intramolecular and intermolecular forces to be studied independently from interference of the solvent environment. The dissociation of complexes in the gas phase is unidirectional and irreversible, hence not reaching equilibrium conditions but we applied the so-called Rice-Ramsperger-Kassel-Marcus quasi-equilibrium theory which is based on a statistic model.

We estimated apparent activation energies in the gas phase using three closely related protein-protein complexes consisting of Fc parts of immunoglobulins (IgG) and protein G´e (IgG-Fc*****G´e; IgG-Fc*****G´f , and IgG-Fc*****G´g). Proteins G´e, G´f, and G´g as well as IgG-Fc were subjected to buffer exchange using 200 mM NH_4OAc. Immune complexes were formed by individually mixing of IgG-Fc with slight molar excesses of proteins G´s (1.3 : 1 molar ratios). Protein complexes (ca. 3 µl solution, each) were introduced into a Synapt G2S mass spectrometer via nanoelectrospray ionization. Non-complexed starting materials were separated from immune complexes by ion mobility separation. Upon ion mobility drift separation of the ionized intact complexes from excess of non-complexed constituent ions, dissociation of the complexes was induced by raising the transfer collision energy (TCE) in a stepwise manner to induce dissociation of the complexes via collision induced dissociation (CID).

The ion intensities of the surviving complexes and dissociated complex constituents were recorded in a mass spectrum and were used to calculate apparent activation energies of dissociation in the gas phase ($E_A^{\#}{}_{m0g}$) and apparent gas phase dissociation constants ($K_D^{\#}{}_{m0g}$). Comparing the calculated $K_D^{\#}{}_{m0g}$ values in the gas phase with those obtained from in-solution investigations, we were able to establish that the amino acid sequence of the IgG-binding domains of protein G´ plays a crucial role in high affinity binding between

protein G´ isoforms and IgG while neither the N-terminal nor the C-terminal flanking sequences were significantly influencing binding to IgG.

For more information on determination of gas phase thermodynamic parameters of protein complexes see Chapter 1.4.3.

1.4 Results

The sections within this chapter are a compilation of the abstracts of the published work from this thesis.

1.4.1 Intact Transition Epitope Mapping (ITEM)

"Intact Transition Epitope Mapping" enables rapid and accurate determination of protein antigen-derived epitopes by either epitope extraction or epitope excision. Upon formation of the immune-complex in solution, the entire mixture is electro-sprayed to translate all constituents as protonated ions into the gas phase. There, ions from antibody-peptide complexes are separated from unbound peptide ions according to their masses, charges, and shapes either by ion mobility drift or by quadrupole ion filtering. Subsequently, immune-complexes are dissociated by collision induced fragmentation and the ion signals of the “complex-released peptides”, which in effect are the epitope peptides, are recorded in the time-of-flight analyzer of the mass spectrometer. Mixing of an antibody solution with a solution in which antigens or antigen-derived peptides are dissolved is, together with antigen proteolysis, the only required in-solution handling step. Simplicity of sample handling and speed of analysis together with very low sample consumption makes "Intact Transition Epitope Mapping" faster and easier to perform than any other experimental epitope mapping methods.

For detailed information on epitope mapping using the ITEM method see Chapter 2.1.

1.4.2 Intact Transition Epitope Mapping - Targeted High-Energy Rupture of Extracted Epitopes (ITEM-THREE)

Epitope mapping, which is the identification of antigenic determinants, is essential for the design of novel antibody-based therapeutics and diagnostic tools. ITEM-THREE is a mass spectrometry-based epitope mapping method which is capable to identify epitopes on antigens upon generating an immune complex in electrospray-compatible solutions by adding an antibody of interest to a mixture of peptides from which at least one holds the antibody´s epitope. This mixture is nano-electrosprayed without purification. Identification of the epitope peptide is performed within a mass spectrometer which provides an ion mobility cell sandwiched in-between two collision cells and where this ion manipulation setup is flanked by a quadrupole mass analyzer on one side and a time-of-flight mass analyzer on the other side. In a step-wise fashion, immune-complex ions are separated from unbound peptide ions and dissociated to release epitope peptide ions. Immune complex-released peptide ions are separated from antibody ions and fragmented by collision induced dissociation. Epitope-containing peptide fragment ions are recorded and mass lists are submitted to unsupervised data base search thereby retrieving both, the amino acid sequence of the epitope peptide and the originating antigen. ITEM-THREE was developed with antiTRIM21 and antiRA33 antibodies for which the epitopes were known, subjecting them to mixtures of synthetic peptides of which one contained the respective epitope. ITEM-THREE was then successfully tested with an enzymatic digest of His-tagged recombinant human β-actin and an antiHis-tag antibody, as well as with an

enzymatic digest of recombinant human TNFα and an antiTNFα antibody whose epitope was previously unknown.

For detailed information on epitope mapping using the ITEM-THREE method see Chapter 2.2.

1.4.3 Determining Apparent Activation Energies of Protein Complex Dissociations in the Gas Phase by Electrospray Mass Spectrometry

We have developed a method to determine apparent activation energies of dissociation for ionized protein-protein complexes in the gas phase using electrospray ionization mass spectrometry following the Rice-Ramsperger-Kassel-Marcus quasi-equilibrium theory. Protein-protein complexes were formed in solution, transferred into the gas phase and separated from excess free protein by ion mobility filtering. Afterwards, complex disassembly was initiated by collision induced dissociation with step-wise increasing energies. Relative intensities of ion signals were used to calculate apparent activation energies of dissociation in the gas phase by applying linear free energy relations. The method was developed using streptavidin tetramers. Experimentally determined apparent gas phase activation energies for dissociation ($E_{A\,m0g}^{\#}$) of complexes consisting of Fc parts from immunoglobulins (IgG-Fc) and three closely related protein G´ variants (IgG-Fc•protein G´e, IgG-Fc•protein G´f, and IgGFc•protein G´g) show the same order of stabilities as can be inferred from their in-solution binding constants. Differences in stabilities between the protein-protein complexes correspond to single amino acid residue exchanges in the IgG-binding regions of the protein G´ variants.

For detailed information on determination of gas phase apparent activation energies of protein complexes see Chapter 2.3.

1.5 Discussion

Mass spectrometry has been used more and more as an analytical tool to study molecular recognition of biomolecules and has been shown to have real advantages such as low sample consumption and speed over other available methods [25,137]. Mass spectrometry-based techniques have also been successfully used to identify epitopes of protein antigens [25,137,138]. Although typical lengths of investigated antigens using mass spectrometric methods (epitope excision and epitope extraction) have increased up to several 100 amino acids, experimentally determined epitope peptides have been shown to comprise of 10-15 amino acid residues on average [25]. Also, X-ray crystallographic studies of antibody–protein complexes have shown that the paratope–epitope interface involves a surface area of about 700-900 Å^2 consisting of about 15-22 amino acid residues each, from both the antigen surface or the paratope [11,139]. In some other reports, however, the epitope was denominated to consist of 8-12 amino acid residues [25]. After applying the epitope mapping methods developed in this thesis to identify the epitope peptide of a previously unknown antigen (rhTNFα), the identified epitope consisted of 8 amino acid residues encompassing a surface area of ~680 Å^2, which is on the low end of the average but consistent with previous results.

Albeit structure-based methods (e.g. X-ray crystallography and NMR) have been successfully used to map epitopes of protein antigens even at atomic resolution; they are not always readily appropriate. For instance, the usually high amount of sample required, proteins which crystallize poorly, and the complex data analysis involved limit their application. The use of phage display peptide libraries have also been employed for mapping antibody epitopes [140-142]. Typically, a phage library containing millions of random

peptides is used and the antibody whose epitope is to be identified is allowed to select and bind to peptides having reasonable affinity for their paratopes. From the consensus motifs observed in the multiple peptide sequences which bind to the antibody, the regions on the antigen containing the identified consensus motifs are matched as the epitope [141]. In most cases of epitope mapping by phage display, a major computational challenge exists as the identified peptides may have no obvious similarity to any linear sequence on the antigen, thereby requesting for huge algorithmic task [143]. Most in-solution epitope mapping procedures such as competition experiments [144], hydrogen/deuterium exchange (HDX) [145], fast photochemical oxidation of proteins (FPOP) [146] which use mass spectrometry as read out are usually met with drawbacks such as time consuming preparations, complex data analysis, high material consumption, just to mention but a few. Using our ITEM methods, one can easily overcome these challenges.

The antigen-binding sites of many IgGs are known to cross-react with a variety of related but different antigenic determinants, making the antibody defense force even more formidable [33]. Whilst antibody cross reactivity appears to be relevant for ensuring that the immune system fights against a myriad of infections, it has also been discussed to initiate autoimmune diseases by molecular mimicry [147]. Moreover, in most biotechnological applications with antibodies, antibody cross reactivity often leads to poor reproducibility of results - a phenomenon known as the antibody reproducibility crisis [148]. Consequently, an important question that remains to be answered is how cross-reactivities observed with antibody recognition can be estimated and whether engineered antibodies' applicabilities can be broadened.

In addition to identifying the epitope peptide by accurately determining the mass of the complex released peptides in ITEM-ONE [137], with ITEM-THREE [136], the experimentalist can obtain in a single experiment, amino acid sequence information of epitope peptide(s) and the originating antigen, thereby allowing possible cross-reactivities to be estimated by performing a BLAST search of the amino acid sequence of the identified epitope(s). Mass spectrometric epitope mapping, molecular modeling and site-directed mutagenesis studies on antibodies and protein antigens have also revealed that within an epitope, there is a subset of residues that contributed most of the free binding energy [106,149,150]. Applying ITEM-THREE we were able to study the effect of single amino acid substitutions in epitope peptides [136].

Whereas certain in-solution handling steps, such as trimming of the epitope by employing different enzymes can be performed equally well in MALDI-based epitope mapping methods as well as ITEM, with ITEM-ONE and ITEM-THREE, no antibody immobilization steps are required and therefore these newly developed methods drastically reduce the in-solution handling. As most currently available MALDI-MS based methods for epitope mapping [63,106,144] require immobilization of the antibody of interest on a protein A or protein G resin or on some kind of a substrate (e.g. beads or columns), there is the likely risk of non-specific adsorption of the antigen / epitope peptide to the surface of the substrate. The non-specific attachment of antigen / peptides onto the substrate may become a likely source of experimental artefacts if washing procedures are not effective enough, and therefore, appropriate control experiments become necessary - a procedure not mandatory in ITEM. The experimentalist thus does not only save time by using our newly developed epitope mapping methods described in this thesis, but also reduces sample consumption.

Another important feature of ITEM-THREE is that, it enables one to check whether an antibody-epitope peptide complex has been formed. This is done by recording mass spectra with higher *m/z* range prior to dissociation of the complex. When using a MALDI MS-based method [144,151,152], the formation of the immune complex is not directly observable as upon addition of the matrix, mostly because of the acidic solution in which

the matrix is typically dissolved in, non-covalent complexes are typically destroyed. This lack of information may become particularly important when one has to distinguish non-specific adsorption from specific paratope-epitope interactions. Whereas in ITEM-THREE only one source of non-specific interactions is present, i.e. peptides non-specifically attached to other sites of the antibody surface, in MALDI based methods, apart from other sites of the antibody being a source of non-specific attachment, the protein G or protein A substrate – or any other surface – could also result in non-specific attachments.

Apart from characterizing antibodies by precisely identifying the epitopes, our studies on determining the gas phase activation energies required for dissociating protein-protein complexes open the field for investigating gas phase stabilities of protein-peptides and other protein complexes in general. As the molecular recognition and functions of proteins can be adversely altered by single amino acid substitutions [116], the method described in this thesis which allows gas phase stabilities of protein-protein complexes to be determined will pave a way for life scientists to elucidate the effect of amino acid exchanges in the binding strengths of protein complexes.

The order of the gas phase dissociation energies for the different protein-protein complexes we studied matched to that from in-solution measurements very well [116]. Conventionally, binding strengths of protein complexes are determined using in-solution methods like calorimetry [153,154], surface plasmon resonance [54,155], surface acoustic wave biosensor [156] etc. Apart from the high sample amounts required for these in-solution methods, they also do not generally provide any information about the stoichiometry and structural details of the interactors. By employing our gas phase procedure for determining the binding energies of protein-protein complexes [116], one is able to simultaneously obtain the stoichiometry of the interaction as well as some structural details of the interactors.

Evidently, understanding the various molecular recognitions of IgG has enormous benefits in drug design. For example, a good understanding of ligatope-efcetope interactions could unveil strategies that will improve treatment of not only autoimmune diseases, but also graft versus host rejections. FcR–IgG-Fc interactions can be manipulated by mutagenesis at either the efcetope or ligatope to enhance the therapeutic efficacy of cytotoxic antibodies in neoplastic diseases [157-159], or to antagonize their ability to trigger effector responses as a means of treating IgG antibody-mediated autoimmune diseases [160,161]. After identifying residues involved in ligatope-efcetope contacts, efcetope peptides can be synthesized and by competition experiments the ability of such peptides to block antibody-receptor interactions can be explored. The success of a synthesized efcetope being able to block antibody Fc binding to an FcR could pave the way for designing new therapeutics to treat antibody-mediated autoinflammatory response in autoimmune diseases such as systemic erythematosus and rheumatoid arthritis [162,163].

To conclude, the mass spectrometric methods which have been developed in this thesis will enhance our understanding of molecular recognition of not only antibodies, but could also be extended for elucidating, in general, the molecular recognitions involved in protein-protein interactions. The methods will essentially provide a means of characterizing antibody recognition by providing precise information about their epitopes, thereby improving our current understanding of how antibody applications can be broadened. Moreover, the method that was developed to study gas phase binding energies of protein-protein interactions can allow one to precisely examine the influences of amino acid substitutions on antibody recognition, therefore providing a means to better understand molecular mechanisms of disease processes as well as give insights about design of novel biotherapeutics.

1.6 References

(1) Jozefowicz, M.; Jozefonvicz, J. *Biomaterials* **1997**, *18*, 1633-1644.
(2) Gellman, S. H. *Chemical reviews* **1997**, *97*, 1231-1232.
(3) Lodish, H.; Berk, A.; Zipursky, S. L.; Matsudaira, P.; Baltimore, D.; Darnell, J. In *Molecular Cell Biology. 4th edition*; WH Freeman, **2000**.
(4) Berg, J.; Tymoczko, J.; Stryer, L. *Biochemistry, 5th ed.; WH Freeman: New York, NY, USA* **2002**.
(5) Cooper, G. M.; Sinauer Associates, **2000**.
(6) Ho, B.; Baryshnikova, A.; Brown, G. W. *Cell systems* **2018**, *6*, 192-205 e193.
(7) Lockett, M. R.; Lange, H.; Breiten, B.; Heroux, A.; Sherman, W.; Rappoport, D.; Yau, P. O.; Snyder, P. W.; Whitesides, G. M. *Angew Chem Int Edit* **2013**, *52*, 7714-7717.
(8) Pavletich, N. P.; Pabo, C. O. *Science* **1991**, *252*, 809-817.
(9) Thiesen, H. J.; Bach, C. *FEBS letters* **1991**, *283*, 23-26.
(10) Dehnen, W. *Mon Not R Astron Soc* **2001**, *324*, 273-291.
(11) Van Regenmortel, M. H. V. *Methods* **1996**, *9*, 465-472.
(12) Tamura, M.; Milenic, D. E.; Iwahashi, M.; Padlan, E.; Schlom, J.; Kashmiri, S. V. *Journal of immunology* **2000**, *164*, 1432-1441.
(13) Solem, S. T.; Brandsdal, B. O.; Smalas, A.; Jorgensen, T. O. *Molecular immunology* **2004**, *40*, 1347-1360.
(14) Chen, G.; Dubrawsky, I.; Mendez, P.; Georgiou, G.; Iverson, B. L. *Protein engineering* **1999**, *12*, 349-356.
(15) Ye, K.; Feenstra, K. A.; Heringa, J.; Ijzerman, A. P.; Marchiori, E. *Bioinformatics* **2008**, *24*, 18-25.
(16) Padlan, E. A.; Abergel, C.; Tipper, J. P. *FASEB journal : official publication of the Federation of American Societies for Experimental Biology* **1995**, *9*, 133-139.
(17) Chagoyen, M.; Garcia-Martin, J. A.; Pazos, F. *Briefings in bioinformatics* **2016**, *17*, 255-261.
(18) Niv, M. Y.; Skrabanek, L.; Roberts, R. J.; Scheraga, H. A.; Weinstein, H. *Proteins* **2008**, *71*, 631-640.
(19) Donald, J. E.; Shakhnovich, E. I. *Nucleic acids research* **2005**, *33*, 4455-4465.
(20) Irwin, M. R. *Biological reviews of the Cambridge Philosophical Society* **1946**, *21*, 93-100.
(21) Ochsenbein, A. F.; Zinkernagel, R. M. *Immunology today* **2000**, *21*, 624-630.
(22) Haji-Ghassemi, O.; Blackler, R. J.; Martin Young, N.; Evans, S. V. *Glycobiology* **2015**, *25*, 920-952.
(23) Haji-Ghassemi, O.; Muller-Loennies, S.; Rodriguez, T.; Brade, L.; Kosma, P.; Brade, H.; Evans, S. V. *The Journal of biological chemistry* **2015**, *290*, 19629-19640.
(24) Watanabe, E.; Kubo, H.; Kanzaki, Y.; Nakazawa, H. *Analytica chimica acta* **2010**, *658*, 56-62.
(25) Opuni, K. F. M.; Al-Majdoub, M.; Yefremova, Y.; El-Kased, R. F.; Koy, C.; Glocker, M. O. *Mass spectrometry reviews* **2018**, *37*, 229-241.
(26) Chait, B. T.; Cadene, M.; Olinares, P. D.; Rout, M. P.; Shi, Y. *Journal of the American Society for Mass Spectrometry* **2016**, *27*, 952-965.
(27) Stickle, D. F.; Presta, L. G.; Dill, K. A.; Rose, G. D. *Journal of molecular biology* **1992**, *226*, 1143-1159.
(28) Baker, E. N.; Hubbard, R. E. *Prog Biophys Mol Bio* **1984**, *44*, 97-179.
(29) Janeway, C. A.; Travers, P.; Walport, M.; Shlomchik, M. *Immunobiology: the immune system in health and disease*; Vol. 7.
(30) Kopp, Z. A.; Jain, U.; Van Limbergen, J.; Stadnyk, A. W. *Frontiers in immunology* **2015**, *6*.
(31) Wootla, B.; Denic, A.; Rodriguez, M. *Methods in molecular biology* **2014**, *1060*, 79-110.

(32) Forthal, D. N. *Microbiology spectrum* **2014**, *2*, 1-17.
(33) Alberts, B.; Johnson, A.; Lewis, J.; Morgan, D.; Raff, M.; Roberts, K.; Walter, P. *Molecular Biology of the Cell, Sixth Edition* **2015**, 1-1342.
(34) Tonegawa, S. *Nature* **1983**, *302*, 575-581.
(35) Tonegawa, S.; Steinberg, C.; Dube, S.; Bernardini, A. *Proceedings of the National Academy of Sciences of the United States of America* **1974**, *71*, 4027-4031.
(36) French, D. L.; Laskov, R.; Scharff, M. D. *Science* **1989**, *244*, 1152-1157.
(37) Gold, M. R. *Trends Pharmacol Sci* **2002**, *23*, 316-324.
(38) Huber, R. *Science* **1986**, *233*, 702-703.
(39) Schroeder, H. W., Jr.; Cavacini, L. *The Journal of allergy and clinical immunology* **2010**, *125*, S41-52.
(40) Irani, V.; Guy, A. J.; Andrew, D.; Beeson, J. G.; Ramsland, P. A.; Richards, J. S. *Molecular immunology* **2015**, *67*, 171-182.
(41) Spiegelberg, H. L. *International archives of allergy and applied immunology* **1989**, *90 Suppl 1*, 22-27.
(42) Jefferis, R. *Expert opinion on biological therapy* **2007**, *7*, 1401-1413.
(43) Ritter, M. A. *Methods in molecular medicine* **2000**, *40*, 23-34.
(44) Lee, A.; Sun, S.; Sandler, A.; Hoang, T. *Current opinion in chemical biology* **2018**, *44*, 56-65.
(45) Bartolome, R. A.; Aizpurua, C.; Jaen, M.; Torres, S.; Calvino, E.; Imbaud, J. I.; Casal, J. I. *Clinical cancer research : an official journal of the American Association for Cancer Research* **2018**, *24*, 433-444.
(46) Chan, A. C.; Carter, P. J. *Nature reviews. Immunology* **2010**, *10*, 301-316.
(47) Birch, J. R.; Racher, A. J. *Advanced drug delivery reviews* **2006**, *58*, 671-685.
(48) Wolter, M.; Rower, C.; Koy, C.; Rath, W.; Pecks, U.; Glocker, M. O. *Journal of proteomics* **2016**, *149*, 44-52.
(49) Heitner, J. C.; Koy, C.; Kreutzer, M.; Gerber, B.; Reimer, T.; Glocker, M. O. *Journal of chromatography. B, Analytical technologies in the biomedical and life sciences* **2006**, *840*, 10-19.
(50) Wolter, M.; Okai, C. A.; Smith, D. S.; Russ, M.; Rath, W.; Pecks, U.; Borchers, C. H.; Glocker, M. O. *Proteomics. Clinical applications* **2018**, *12*, e1800017.
(51) Muller, K. M.; Arndt, K. M.; Bauer, K.; Pluckthun, A. *Analytical biochemistry* **1998**, *259*, 54-61.
(52) Chaga, G.; Bochkariov, D. E.; Jokhadze, G. G.; Hopp, J.; Nelson, P. *Journal of chromatography. A* **1999**, *864*, 247-256.
(53) Kimple, M. E.; Brill, A. L.; Pasker, R. L. *Current protocols in protein science* **2013**, *73*, Unit 9 9.
(54) Li, Y. J.; Bi, L. J.; Zhang, X. E.; Zhou, Y. F.; Zhang, J. B.; Chen, Y. Y.; Li, W.; Zhang, Z. P. *Analytical and bioanalytical chemistry* **2006**, *386*, 1321-1326.
(55) Dorn, I. T.; Neumaier, K. R.; Tampe, R. *Journal of the American Chemical Society* **1998**, *120*, 2753-2763.
(56) Sadoine, M.; Cerminara, M.; Kempf, N.; Gerrits, M.; Fitter, J.; Katranidis, A. *Analytical chemistry* **2017**, *89*, 11278-11285.
(57) Sahu, I. D.; Lorigan, G. A. *BioMed research international* **2018**, *2018*, 3248289.
(58) Forster, K.; Gardiner, E.; Hsieh, S. *Cancer Res* **2017**, *77*.
(59) Dumitru, C. D.; Gardiner, E.; Williams, J.; Zer, C. *Cancer Res* **2016**, *76*.
(60) Gardiner, E.; Forster, K.; Dumitru, C. *J Clin Oncol* **2016**, *34*.
(61) Tang, Z.; Shangguan, D.; Wang, K.; Shi, H.; Sefah, K.; Mallikratchy, P.; Chen, H. W.; Li, Y.; Tan, W. *Analytical chemistry* **2007**, *79*, 4900-4907.
(62) Liu, Z. F.; Wang, F. *Curr Pharm Biotechno* **2010**, *11*, 610-619.
(63) Baschung, Y.; Lupu, L.; Moise, A.; Glocker, M.; Rawer, S.; Lazarev, A.; Przybylski, M. *Journal of the American Society for Mass Spectrometry* **2018**, *29*, 1881-1891.

(64) Mannironi, C.; Scerch, C.; Fruscoloni, P.; Tocchini-Valentini, G. P. *Rna* **2000**, *6*, 520-527.
(65) Tainer, J. A.; Cunningham, R. P. *Current opinion in biotechnology* **1993**, *4*, 474-483.
(66) Belien, T.; Van Campenhout, S.; Vanden Bosch, A.; Bourgois, T. M.; Rombouts, S.; Robben, J.; Courtin, C. M.; Delcour, J. A.; Volckaert, G. *Journal of molecular recognition : JMR* **2007**, *20*, 103-112.
(67) Conroy, P. J.; Hearty, S.; Leonard, P.; O'Kennedy, R. J. *Seminars in cell & developmental biology* **2009**, *20*, 10-26.
(68) Sela-Culang, I.; Kunik, V.; Ofran, Y. *Frontiers in immunology* **2013**, *4*, 302.
(69) Jones, P. T.; Dear, P. H.; Foote, J.; Neuberger, M. S.; Winter, G. *Nature* **1986**, *321*, 522-525.
(70) CRUMPTON, M. J. In *The antigens*; Elsevier, **1974**, pp 1-78.
(71) Shields, R. L.; Namenuk, A. K.; Hong, K.; Meng, Y. G.; Rae, J.; Briggs, J.; Xie, D.; Lai, J.; Stadlen, A.; Li, B.; Fox, J. A.; Presta, L. G. *The Journal of biological chemistry* **2001**, *276*, 6591-6604.
(72) Pincetic, A.; Bournazos, S.; DiLillo, D. J.; Maamary, J.; Wang, T. T.; Dahan, R.; Fiebiger, B. M.; Ravetch, J. V. *Nature immunology* **2014**, *15*, 707-716.
(73) Nimmerjahn, F.; Ravetch, J. V. *Adv Immunol* **2007**, *96*, 179-204.
(74) Fridman, W. H. *Current opinion in immunology* **1993**, *5*, 355-360.
(75) Selvaraj, P.; Fifadara, N.; Nagarajan, S.; Cimino, A.; Wang, G. *Immunologic research* **2004**, *29*, 219-230.
(76) Perussia, B. *Current topics in microbiology and immunology* **1998**, *230*, 63-88.
(77) *Bulletin of the World Health Organization* **1994**, *72*, 809-810.
(78) Kubagawa, H.; Kubagawa, Y.; Jones, D.; Nasti, T. H.; Walter, M. R.; Honjo, K. *Curr Top Microbiol* **2014**, *382*, 3-28.
(79) Sondermann, P.; Huber, R.; Oosthuizen, V.; Jacob, U. *Nature* **2000**, *406*, 267-273.
(80) Radaev, S.; Motyka, S.; Fridman, W. H.; Sautes-Fridman, C.; Sun, P. D. *Journal of Biological Chemistry* **2001**, *276*, 16469-16477.
(81) Solomon, S.; Kassahn, D.; Illges, H. *Arthritis research & therapy* **2005**, *7*, 129-135.
(82) Swanson, J. A.; Hoppe, A. D. *Journal of leukocyte biology* **2004**, *76*, 1093-1103.
(83) Sun, P. D. *Immunologic research* **2003**, *27*, 539-548.
(84) Kiyoshi, M.; Caaveiro, J. M.; Kawai, T.; Tashiro, S.; Ide, T.; Asaoka, Y.; Hatayama, K.; Tsumoto, K. *Nature communications* **2015**, *6*, 6866.
(85) Sakae, Y.; Satoh, T.; Yagi, H.; Yanaka, S.; Yamaguchi, T.; Isoda, Y.; Iida, S.; Okamoto, Y.; Kato, K. *Scientific reports* **2017**, *7*, 13780.
(86) Hanson, Q. M.; Barb, A. W. *Biochemistry* **2015**, *54*, 2931-2942.
(87) Gergely, J.; Sarmay, G. *FASEB journal : official publication of the Federation of American Societies for Experimental Biology* **1990**, *4*, 3275-3283.
(88) Gahoual, R.; Heidenreich, A. K.; Somsen, G. W.; Bulau, P.; Reusch, D.; Wuhrer, M.; Haberger, M. *Analytical chemistry* **2017**, *89*, 5404-5412.
(89) Jensen, P. F.; Larraillet, V.; Schlothauer, T.; Kettenberger, H.; Hilger, M.; Rand, K. D. *Molecular & cellular proteomics : MCP* **2015**, *14*, 148-161.
(90) Yefremova, Y.; Melder, F. T. I.; Danquah, B. D.; Opuni, K. F. M.; Koy, C.; Ehrens, A.; Frommholz, D.; Illges, H.; Koelbel, K.; Sobott, F.; Glocker, M. O. *Anal Bioanal Chem* **2017**.
(91) Dalgleish, A. G.; Kennedy, R. C. *Vaccine* **1988**, *6*, 215-220.
(92) Harding, F. A.; Stickler, M. M.; Razo, J.; DuBridge, R. B. *mAbs* **2010**, *2*, 256-265.
(93) Webster, C. I.; Bryson, C. J.; Cloake, E. A.; Jones, T. D.; Austin, M. J.; Karle, A. C.; Spindeldreher, S.; Lowe, D. C.; Baker, M. P. *mAbs* **2016**, *8*, 253-263.
(94) Sgro, C. *Toxicology* **1995**, *105*, 23-29.
(95) Natvig, J. B.; Kunkel, H. G. *Adv Immunol* **1973**, *16*, 1-59.
(96) Jefferis, R.; Lefranc, M. P. *mAbs* **2009**, *1*, 332-338.
(97) Chersi, A.; Mage, R. *Molecular immunology* **1980**, *17*, 135-138.

(98) Appella, E.; Rejnek, J.; Reisfeld, R. A. *Journal of molecular biology* **1969**, *41*, 473-&.
(99) Capra, J. D.; Kindt, T. J. *Immunogenetics* **1975**, *1*, 417-427.
(100) Johnson, W. E.; Kohn, P. H.; Steinberg, A. G. *Clinical immunology and immunopathology* **1977**, *7*, 97-113.
(101) Sauer-Eriksson, A. E.; Kleywegt, G. J.; Uhlen, M.; Jones, T. A. *Structure* **1995**, *3*, 265-278.
(102) Frick, I. M.; Wikstrom, M.; Forsen, S.; Drakenberg, T.; Gomi, H.; Sjobring, U.; Bjorck, L. *Proceedings of the National Academy of Sciences of the United States of America* **1992**, *89*, 8532-8536.
(103) Warren, K. G.; Catz, I. *Journal of the neurological sciences* **1991**, *103*, 90-96.
(104) Fountoulakis, M.; Mesa, C.; Schmid, G.; Gentz, R.; Manneberg, M.; Zulauf, M.; Dembic, Z.; Garotta, G. *The Journal of biological chemistry* **1995**, *270*, 3958-3964.
(105) Chiu, H. H.; Liao, H. W.; Shao, Y. Y.; Lu, Y. S.; Lin, C. H.; Tsai, I. L.; Kuo, C. H. *Analytica chimica acta* **2018**, *1019*, 93-102.
(106) Al-Majdoub, M.; Opuni, K. F.; Koy, C.; Glocker, M. O. *Analytical chemistry* **2013**, *85*, 10479-10487.
(107) Anderson, G. P.; Jacoby, M. A.; Ligler, F. S.; King, K. D. *Biosensors & bioelectronics* **1997**, *12*, 329-336.
(108) Carter-Franklin, J. N.; Victa, C.; McDonald, P.; Fahrner, R. *Journal of chromatography. A* **2007**, *1163*, 105-111.
(109) Jendeberg, L.; Nilsson, P.; Larsson, A.; Denker, P.; Uhlen, M.; Nilsson, B.; Nygren, P. A. *Journal of immunological methods* **1997**, *201*, 25-34.
(110) Seppala, I.; Sarvas, H.; Peterfy, F.; Makela, O. *Scandinavian journal of immunology* **1981**, *14*, 335-342.
(111) Sheoran, A. S.; Holmes, M. A. *Veterinary immunology and immunopathology* **1996**, *55*, 33-43.
(112) Viera, C.; Yang, H. W.; Etzel, M. R. *Ind Eng Chem Res* **2000**, *39*, 3356-3363.
(113) Choe, W.; Durgannavar, T. A.; Chung, S. J. *Materials* **2016**, *9*.
(114) Mouratou, B.; Behar, G.; Pecorari, F. *Biomolecules* **2015**, *5*, 60-75.
(115) Pabst, T. M.; Palmgren, R.; Forss, A.; Vasic, J.; Fonseca, M.; Thompson, C.; Wang, W. K.; Wang, X.; Hunter, A. K. *Journal of chromatography. A* **2014**, *1362*, 180-185.
(116) Yefremova, Y.; Melder, F. T. I.; Danquah, B. D.; Opuni, K. F. M.; Koy, C.; Ehrens, A.; Frommholz, D.; Illges, H.; Koelbel, K.; Sobott, F.; Glocker, M. O. *Analytical and bioanalytical chemistry* **2017**, *409*, 6549-6558.
(117) Giese, G.; Williams, A.; Rodriguez, M.; Persson, J. *Biotechnology progress* **2018**, *34*, 397-404.
(118) Baker, J. J.; McDaniel, D.; Cain, D.; Lee Tao, P.; Li, C.; Huang, Y.; Liu, H.; Zhu-Shimoni, J.; Ninonuevo, M. *Analytical chemistry* **2019**, *91*, 965-976.
(119) Krishnamurthy, A.; Jimeno, A. *Pharmacology & therapeutics* **2018**, *185*, 122-134.
(120) Trivedi, A.; Stienen, S.; Zhu, M.; Li, H.; Yuraszeck, T.; Gibbs, J.; Heath, T.; Loberg, R.; Kasichayanula, S. *Clinical and translational science* **2017**, *10*, 147-162.
(121) Das, D.; Suresh, M. R. *Methods in molecular medicine* **2005**, *109*, 329-346.
(122) Donaldson, J. M.; Zer, C.; Avery, K. N.; Bzymek, K. P.; Horne, D. A.; Williams, J. C. *Proceedings of the National Academy of Sciences of the United States of America* **2013**, *110*, 17456-17461.
(123) Bzymek, K. P.; Ma, Y.; Avery, K. A.; Horne, D. A.; Williams, J. C. *Acta crystallographica. Section F, Structural biology communications* **2016**, *72*, 434-442.
(124) Matho, M. M.; Gardiner, E. M.; Dumitru, C. D. *Cancer Research* **2015**, *75*.
(125) Kovar, M.; Strohalm, J.; Etrych, T.; Ulbrich, K.; Rihova, B. *Bioconjugate chemistry* **2002**, *13*, 206-215.
(126) Kovtun, Y. V.; Audette, C. A.; Ye, Y.; Xie, H.; Ruberti, M. F.; Phinney, S. J.; Leece, B. A.; Chittenden, T.; Blattler, W. A.; Goldmacher, V. S. *Cancer Res* **2006**, *66*, 3214-3221.

(127) Gromek, S. M.; Balunas, M. J. *Current topics in medicinal chemistry* **2015**, *14*, 2822-2834.
(128) Strop, P.; Liu, S. H.; Dorywalska, M.; Delaria, K.; Dushin, R. G.; Tran, T. T.; Ho, W. H.; Farias, S.; Casas, M. G.; Abdiche, Y.; Zhou, D.; Chandrasekaran, R.; Samain, C.; Loo, C.; Rossi, A.; Rickert, M.; Krimm, S.; Wong, T.; Chin, S. M.; Yu, J.; Dilley, J.; Chaparro-Riggers, J.; Filzen, G. F.; O'Donnell, C. J.; Wang, F.; Myers, J. S.; Pons, J.; Shelton, D. L.; Rajpal, A. *Chemistry & biology* **2013**, *20*, 161-167.
(129) Agarwal, P.; Bertozzi, C. R. *Bioconjugate chemistry* **2015**, *26*, 176-192.
(130) Kline, T.; Steiner, A. R.; Penta, K.; Sato, A. K.; Hallam, T. J.; Yin, G. *Pharmaceutical research* **2015**, *32*, 3480-3493.
(131) Wakankar, A. A.; Feeney, M. B.; Rivera, J.; Chen, Y.; Kim, M.; Sharma, V. K.; Wang, Y. J. *Bioconjugate chemistry* **2010**, *21*, 1588-1595.
(132) Acchione, M.; Kwon, H.; Jochheim, C. M.; Atkins, W. M. *mAbs* **2012**, *4*, 362-372.
(133) Adem, Y. T.; Schwarz, K. A.; Duenas, E.; Patapoff, T. W.; Galush, W. J.; Esue, O. *Bioconjugate chemistry* **2014**, *25*, 656-664.
(134) Bzymek, K. P.; Avery, K. A.; Ma, Y.; Horne, D. A.; Williams, J. C. *Acta crystallographica. Section F, Structural biology communications* **2016**, *72*, 820-830.
(135) Bzymek, K. P.; Ma, Y.; Avery, K. N.; Horne, D. A.; Williams, J. C. *Acta crystallographica. Section F, Structural biology communications* **2017**, *73*, 688-694.
(136) Danquah, B. D.; Rower, C.; Opuni, K. F. M.; ElKased, R.; Frommholz, D.; Illges, H.; Koy, C.; Glocker, M. O. *Molecular & cellular proteomics : MCP* **2019**.
(137) Yefremova, Y.; Opuni, K. F. M.; Danquah, B. D.; Thiesen, H. J.; Glocker, M. O. *Journal of the American Society for Mass Spectrometry* **2017**, *28*, 1612-1622.
(138) El-Kased, R. F.; Koy, C.; Deierling, T.; Lorenz, P.; Qian, Z.; Li, Y.; Thiesen, H. J.; Glocker, M. O. *European journal of mass spectrometry* **2009**, *15*, 747-759.
(139) Davies, D. R.; Padlan, E. A.; Sheriff, S. *Annual review of biochemistry* **1990**, *59*, 439-473.
(140) Dottavio, D. In *Epitope Mapping Protocols*; Springer, 1996, pp 181-193.
(141) Böttger, V.; Böttger, A. In *Epitope Mapping Protocols*; Springer, 2009, pp 181-201.
(142) Moreira, G.; Fuhner, V.; Hust, M. *Methods in molecular biology* **2018**, *1701*, 497-518.
(143) Mayrose, I.; Shlomi, T.; Rubinstein, N. D.; Gershoni, J. M.; Ruppin, E.; Sharan, R.; Pupko, T. *Nucleic acids research* **2007**, *35*, 69-78.
(144) Baerga-Ortiz, A.; Hughes, C. A.; Mandell, J. G.; Komives, E. A. *Protein science : a publication of the Protein Society* **2002**, *11*, 1300-1308.
(145) Wei, H.; Mo, J.; Tao, L.; Russell, R. J.; Tymiak, A. A.; Chen, G.; Iacob, R. E.; Engen, J. R. *Drug discovery today* **2014**, *19*, 95-102.
(146) Jones, L. M.; J, B. S.; J, A. C.; Gross, M. L. *Analytical chemistry* **2011**, *83*, 7657-7661.
(147) Cusick, M. F.; Libbey, J. E.; Fujinami, R. S. *Clin Rev Allerg Immu* **2012**, *42*, 102-111.
(148) Baker, M. *Nature* **2015**, *521*, 274-276.
(149) Li, J.; Wei, H.; Krystek, S. R., Jr.; Bond, D.; Brender, T. M.; Cohen, D.; Feiner, J.; Hamacher, N.; Harshman, J.; Huang, R. Y.; Julien, S. H.; Lin, Z.; Moore, K.; Mueller, L.; Noriega, C.; Sejwal, P.; Sheppard, P.; Stevens, B.; Chen, G.; Tymiak, A. A.; Gross, M. L.; Schneeweis, L. A. *Analytical chemistry* **2017**, *89*, 2250-2258.
(150) Opuni, K.; Solomon, S.; Metzen, F.; Frommholz, D.; Koy, C.; Röwer, C.; Glocker, M.; Illges, H.; Anderson, P. *J Proteomics Bioinform* **2017**, *10*, 60-72.
(151) El-Kased, R.; Koy, C.; Lorenz, P.; Montgomery, H.; Tanaka, K.; Thiesen, H.; Glocker, M. *J Proteomics Bioinform* **2011**, *4*, 001-009.
(152) Al-Majdoub, M.; Opuni, K. F.; Yefremova, Y.; Koy, C.; Lorenz, P.; El-Kased, R. F.; Thiesen, H. J.; Glocker, M. O. *Journal of molecular recognition : JMR* **2014**, *27*, 566-574.
(153) Pierce, M. M.; Raman, C. S.; Nall, B. T. *Methods* **1999**, *19*, 213-221.

(154) Duff, M. R., Jr.; Grubbs, J.; Howell, E. E. *Journal of visualized experiments : JoVE* **2011**.
(155) Tang, Y.; Zeng, X.; Liang, J. *Journal of chemical education* **2010**, *87*, 742-746.
(156) Gronewold, T. M. *Analytica chimica acta* **2007**, *603*, 119-128.
(157) Koch, J.; Tesar, M. *Transfusion medicine and hemotherapy : offizielles Organ der Deutschen Gesellschaft fur Transfusionsmedizin und Immunhamatologie* **2017**, *44*, 337-350.
(158) Redman, J. M.; Hill, E. M.; AlDeghaither, D.; Weiner, L. M. *Molecular immunology* **2015**, *67*, 28-45.
(159) Nimmerjahn, F.; Gordan, S.; Lux, A. *Trends in immunology* **2015**, *36*, 325-336.
(160) Krueger, J. G. *Journal of the American Academy of Dermatology* **2002**, *46*, 1-23; quiz 23-26.
(161) Ludwig, R. J.; Vanhoorelbeke, K.; Leypoldt, F.; Kaya, Z.; Bieber, K.; McLachlan, S. M.; Komorowski, L.; Luo, J.; Cabral-Marques, O.; Hammers, C. M.; Lindstrom, J. M.; Lamprecht, P.; Fischer, A.; Riemekasten, G.; Tersteeg, C.; Sondermann, P.; Rapoport, B.; Wandinger, K. P.; Probst, C.; El Beidaq, A.; Schmidt, E.; Verkman, A.; Manz, R. A.; Nimmerjahn, F. *Frontiers in immunology* **2017**, *8*.
(162) Al-Majdoub, M.; Koy, C.; Lorenz, P.; Thiesen, H. J.; Glocker, M. O. *Journal of mass spectrometry : JMS* **2013**, *48*, 651-659.
(163) El-Kased, R. F.; Koy, C.; Lorenz, P.; Drynda, S.; Guthke, R.; Qian, Z.; Koczan, D.; Li, Y.; Kekow, J.; Thiesen, H. J.; Glocker, M. O. *European journal of mass spectrometry* **2010**, *16*, 443-451.

2 Publication collection

Yelena Yefremova, Kwabena F.M Opuni, **Bright D. Danquah**, Hans.-J Thiesen, and Michael O. Glocker. Intact transition epitope mapping. *J. Am. Soc. Mass Spectrom.* 28, 1612-1622 **(2017)**

Bright D. Danquah, Claudia Röwer, Kwabena F.M. Opuni, Reham El-Kased, David Frommholz, Harald Illges, Cornelia Koy, and Michael O. Glocker. Intact transition epitope mapping- Targeted High-Energy Rupture of Extracted Epitopes (ITEM-THREE). *Mol. Cell. Proteom.* 18, 2-14 **(2019)**

Yelena Yefremova, F. Teresa I. Melder, **Bright D. Danquah**, Kwabena F.M. Opuni, Cornelia Koy, Alexandra Ehrens, David Frommholz, Harald Illges, Knut Koelbel, Frank Sobott, and Michael O. Glocker. Apparent activation energies of protein-protein complex dissociation in the gas phase determined by electrospray mass spectrometry. *Anal. Bioanal Chem*. 409, 6549-6558 **(2017)**

2.1 Intact Transition Epitope Mapping (ITEM)

J. Am. Soc. Mass Spectrom. (2017) 28:1612–1622
DOI: 10.1007/s13361-017-1654-7

RESEARCH ARTICLE

Intact Transition Epitope Mapping (ITEM)

Yelena Yefremova,[1] Kwabena F. M. Opuni,[1] Bright D. Danquah,[1] Hans-Juergen Thiesen,[2] Michael O. Glocker[1]

[1]Proteome Center Rostock, University Medicine Rostock, Schillingallee 69, 18057, Rostock, Germany
[2]Institute of Immunology, University Medicine Rostock, Schillingallee 70, 18057, Rostock, Germany

Abstract. Intact transition epitope mapping (ITEM) enables rapid and accurate determination of protein antigen-derived epitopes by either epitope extraction or epitope excision. Upon formation of the antigen peptide-containing immune complex in solution, the entire mixture is electrosprayed to translate all constituents as protonated ions into the gas phase. There, ions from antibody–peptide complexes are separated from unbound peptide ions according to their masses, charges, and shapes either by ion mobility drift or by quadrupole ion filtering. Subsequently, immune complexes are dissociated by collision induced fragmentation and the ion signals of the "complex-released peptides," which in effect are the epitope peptides, are recorded in the time-of-flight analyzer of the mass spectrometer. Mixing of an antibody solution with a solution in which antigens or antigen-derived peptides are dissolved is, together with antigen proteolysis, the only required in-solution handling step. Simplicity of sample handling and speed of analysis together with very low sample consumption makes ITEM faster and easier to perform than other experimental epitope mapping methods.

Keywords: Native electrospray mass spectrometry, Ion mobility separation, Quadrupole time-of-flight mass spectrometry, Antibody–antigen interactions, Antibody–epitope reactivities

Received: 23 January 2017/Revised: 6 March 2017/Accepted: 7 March 2017/Published Online: 14 June 2017

Introduction

Antibodies are most relevant and indispensable tools for analytical laboratory assays, such as enzyme linked immunosorbent assay (ELISA), Western blot, and immunohistochemistry [1–3], all of which are applied routinely in numerous laboratories around the world. Antibodies contribute a great share to disease diagnostics [4] with huge market values [5]. In addition, antibodies have become of immense clinical importance as diagnostic biomarkers [4], and with "Personalized Medicine" concepts gaining momentum, antibody-based therapeutics constitute the fastest growing class of medication with increased sales volumes of billions of US$ [6–9]. Obviously, reliance on the functionality of an antibody either as a therapeutic agent or as a bioanalytical reagent is huge and the pitfalls that one might step into when an antibody's functionality has not been understood in detail have been extensively discussed in high impact journals [5, 10, 11]. To increase reliability of such precious reagents, there is a tremendous demand for antibody characterization, both structurally and functionally.

Since the most specific property of an antibody is its capability to bind to its antigen in a unique fashion via precise paratope-epitope recognition, experimental determination of epitopes (i.e., partial surfaces on the antigen to which an antibody binds) is of utmost importance for antibody characterization. The two most important strategies for epitope mapping either apply methods for precise structural determinations of antigen partial surfaces (X-ray diffraction, NMR) or make use of functional methods that include competition assays (ELISA, biosensors), antigen modification (H/D exchange, chemical modification of side chains), proteolytic or chemical antigen fragmentation, and synthetic peptides [12, 13]. The bottleneck of all available experimental epitope mapping procedures lies in the rather sophisticated, but up to now unavoidable, multi-step in-solution handling procedures [14], leaving an unmet need for rapid and reliable epitope mapping methods [15, 16]. Facilitating in-solution handling is expected to generate a real breakthrough in routine epitope mapping.

Electronic supplementary material The online version of this article (doi:10.1007/s13361-017-1654-7) contains supplementary material, which is available to authorized users.

Correspondence to: Michael Glocker; *e-mail:* michael.glocker@med.uni–rostock.de

Upon its introduction, ion mobility mass spectrometry [17, 18] enjoys vastly growing interest and finds many new applications in studies on biomolecular structures and dynamics thanks to an additional separation dimension in the gas phase according to the ions' mobilities in a cell filled with a neutral gas [19–22]. Commercial systems have now become available in which such ion mobility drift cells have been flanked by collision cells. The latter enable gas-phase ion reactions and thereby give access to deeper insights into protein structures and into protein–protein complex properties [23–25].

In this paper, we present the development and application of a fast and easy to apply epitope mapping method that identifies the epitope peptide of an antibody of interest in a single experiment. The intact transition epitope mapping (ITEM) procedure makes use of (1) the determining property of an antibody (i.e., its ability to strongly bind to its antigen), (2) the survival of the intact immune-complex when transitioned into the gas phase, (3) ion separation by ion mobility and/or quadrupole filtering, (4) dissociation of the immune complex by collision induced dissociation, and (5) time-of-flight analysis of the complex constituents, all within the mass spectrometer.

Experimental

Preparation of Antibody and Antigen Solutions

Anti-hnRNP-A2/B1 mouse IgG2a (antiRA33; product no. R4653, lot no. 044K4766; Sigma, St. Louis, MO, USA), anti-His-tag mouse IgG1 (product no. MCA1396, batch no. 0309, AbD Serotec, Oxford, UK), and anti-FLAG M2 mouse IgG1 (product no. F3165, lot no. 128H9200; Sigma, St. Louis, MO, USA) monoclonal antibodies and recombinant human TNF protein (rhTNFα) were subjected to buffer exchange using Amicon Ultra centrifugal filters with cutoff 50 K (Millipore Corporation, Ireland). The respective volumes of antibody and antigen stock solutions (as delivered by suppliers) containing 50 µg of antibodies and antigen, were each loaded onto one filter unit. The volumes on the filter units were filled up to 500 µL with 200 mM ammonium acetate buffer (pH 7.1). Then, the units were centrifuged for 10 min at 13,000 rpm. After centrifugation, 430 µL of 200 mM ammonium acetate buffer (pH 7.1) was added on top of the residual volumes above the filters (ca. 70 µL) and centrifugation (10 min at 13,000 rpm) was repeated. Refilling and centrifugation were repeated eight times. After that, filter units were placed upside down into a new vial and the retentates (ca. 50 µL volumes) were collected by centrifugation for 2 min at 4500 rpm. Such re-buffered antibody solutions were directly used for preparation of antigen/peptide-antibody mixtures. Aliquots (ca. 2 µg) were subjected to protein concentration determinations with the fluorescence-based Qubit assay (Invitrogen, Carlsbad, CA, USA). To prepare the Qubit working solution, 1990 µL of Qubit buffer was mixed with 10 µL Qubit reagent. Next, 190 µL of the Qubit working solution was mixed with 10 µL of the three calibration standards (0, 200, and 400 ng/µL). The mixtures were vortexed and incubated for 15 min and after that they were used to calibrate the Qubit 2.0 fluorometer. An antibody solution (ca. 2 µg of antibody) was mixed with the Qubit working solution to reach a final volume of 200 µL, and the mixture was incubated for 15 min. Then, raw fluorescence values were measured and the concentration of the protein in the assay tube was automatically calculated. Antibody solutions were stored at –20 °C for future use.

In-Solution Peptide Mixture Preparation

A peptide mixture (solution 1) was generated by combining 10 µL of each of the following six peptide solutions (peptide concentrations: 0.1 µg/µL, dissolved in 200 mM ammonium acetate, pH 7.1): FLAG peptide, $[M + H]^+$ 1013.39; angiotensin II, $[M + H]^+$ 1046.54; GPI tryptic peptide, $[M + H]^+$ 1142.59; TRIM21 tryptic peptide, $[M + H]^+$ 2098.11 and $[M + 2H]^{2+}$ 1050.5; substance P, $[M + H]^+$ 1347.74; and RA33 tryptic peptide, $[M + H]^+$ 1633.87 and $[M + 2H]^{2+}$ 817.44. To 3 µL of an antiFLAG M2 monoclonal antibody solution with a concentration of 1 µg/µL (6.7 µM) in 200 mM ammonium acetate buffer, pH 7.1 (solution 2), was added 1.2 µL of the peptide mixture (solution 1) to yield a molar ratio of the antiFLAG M2 antibody to the FLAG peptide of 1:1. The antibody-peptide mixture (solution 3) was kept at room temperature and was directly used for nanoESI-MS/MS and nanoESI-IMS-MS/MS analysis, respectively.

Proteolysis of Antigen Proteins

The His-RA33 protein (Euroimmun, Luebeck, Germany; 50 µL, 0.48 µg/µL, dissolved in 8 M urea, 1 M sodium chloride, 50 mM sodium phosphate, pH 7.4), was subjected to in-solution digestion with LysC (Roche Diagnostics GmbH, Mannheim, Germany; reconstituted according to the manufacturer's protocol) using an enzyme to substrate ratio of 1:50 (w/w). Digestion was performed at room temperature overnight and subsequently at 37 °C for 6 h. The proteolytic peptide-containing digestion mixture was desalted with RP-packed tips (ZipTip C18 tips; Millipore, Billerica, MA, USA) loading 5 µL portions onto one tip, which was reconstituted using 50% ACN, and equilibrated using 0.1% TFA solution (pH 1.7). Washing was performed twice using 10 µL of 0.1% TFA solution (pH 1.7) each time and peptides were eluted with 5 µL 80% ACN/0.1% TFA solution (pH 1.7), each. Ten desalted peptide portions (total volume 50 µL) were pooled and 10 µL of 5 M BrCN solution in ACN was added and incubated at 25 °C in the dark for 20 h [26]. Protein G′e (Sigma, St. Louis, MO, USA; 50 µL, 1 µg/µL, dissolved in 100 mM ammonium bicarbonate, pH 8), was subjected to in-solution digestion with trypsin (Promega, Madison, WI, USA, reconstituted according to the manufacturer's protocol) using an enzyme to substrate ratio of 1:20 (w/w). Digestion was performed at 37 °C for 48 h. The proteolytic peptide-containing digestion mixture (5 µL) was loaded onto an RP-packed tip (ZipTip C18 tips, Millipore, Billerica, MA, USA), which was reconstituted using 50% ACN, and equilibrated using 0.1% TFA solution (pH 1.7). Washing was performed twice using 10 µL of 0.1% TFA solution (pH 1.7) each time, and peptides were eluted with 5

μL of 80% ACN/0.1% TFA solution (pH 1.7) [27]. Peptide mixtures were lyophilized using a SpeedVac concentrator (Martin Christ GmbH, Osterode, Germany), re-solubilized in 10 μL of 200 mM ammonium acetate buffer, pH 7.1, and stored at –20 °C for future use.

Preparation of Peptide-Antibody Mixtures for Epitope Extraction

Synthetic RA33 epitope peptide (MAARPHSIDGRVVEP-NH_2; Peptides&Elephants, Potsdam, Germany) and synthetic FLAG peptide (DYKDDDDK; Thermo Fisher Scientific GmbH, Ulm, Germany) were each dissolved in 200 mM ammonium acetate buffer (pH 7.1) to obtain concentrations of 0.01 μg/μL (6.1 μM and 9.8 μM, respectively). AntiRA33 and anti-FLAG M2 monoclonal antibodies with concentrations of 1 μg/μL (6.7 μM each, in 200 mM ammonium acetate buffer, pH 7.1) were mixed with each of the peptide solutions to yield molar ratios of 1:1. To the peptide mixture (10 μL) that derived from LysC/BrCN digestion of His-tag-containing RA33 protein was added 1 μL of synthetic RA33 epitope peptide (0.1 μg/μL) solution. To 1 μL of this peptide mixture were added 3 μL of antiRA33 antibody solution (1 μg/μL). To the peptide solution derived from tryptic digestion of protein G′e (5 μL) were added 5 μL of antiHis-tag antibody solution (1 μg/μL) yielding in a molar ratio of ca. 1:14 between antiHis-tag antibody and His-tag carrying peptide. All antibody-peptide mixtures were prepared at room temperature and directly used for nano-ESI-IMS-MS/MS analysis. Excesses of the prepared mixtures were stored at +4 °C for a maximum 1 wk.

Preparation of Antigen-Antibody Mixtures and Proteolysis of Immune Complexes for Epitope Excision

Five μL of rhTNFα (0. 36 μg/μL; 92 pmol) in 200 mM ammonium acetate buffer (pH 7.1) was mixed with 10 μL of anti-His-tag antibody (0.68 μg/μL; 46 pmol) in 200 mM ammonium acetate buffer (pH 7.1), and the immune complex mixture was incubated overnight at room temperature. Trypsin (Promega, Madison, WI, USA) was first reconstituted in 3 mM HCl with a concentration of 1 μg/μL (stock solution). From this, a working solution with a trypsin concentration of 2 ng/μL was prepared with 200 mM ammonium acetate buffer (pH 7.0). Next, 1 μL of trypsin working solution was added to the immune complex mixture (generating a ratio of 100:1 between rhTNFα and trypsin). After 10 min incubation, this mixture was directly applied for nano-ESI-IMS-MS/MS analysis.

NanoESI-IMS-MS/MS Acquisition Conditions

Nano-ESI capillaries were prepared in-house from borosilicate glass tubes of 1 mm outer diameter and 0.5 mm inner diameters (Sutter Instrument, Novato, CA, USA) using a P-1000 Flaming/Brown Micropipette Puller System (Sutter Instrument). Capillaries were gold-coated using a sputter coater BalTec SCD 004 (Bal-Tech, Balzers, Liechtenstein). For each measurement, 3 μL of antibody-antigen/peptide mixtures was loaded into nano-ESI capillaries using a microloader pipette tip (Eppendorf, Hamburg, Germany). Nano-ESI-IMS-MS/MS measurements were performed on a Synapt G2-S mass spectrometer (Waters MS-Technologies, Manchester, UK) equipped with a traveling-wave ion mobility cell (TW-IMS). Stability of arrival times and gas pressures of the instrument were checked by performing 10 ESI-IMS-MS experiments, five of which were performed on day 1 and 5 others after 2 days' time. We used for the 10 measurements the RA33 peptide (exp. molecular mass: 1632.879 ± 0.021 Da) and the FLAG peptide (exp. molecular mass: 1012.402 ± 0.012 Da). The mean arrival time of the doubly protonated RA33 peptide was 8.202 ± 0.115 ms and that of the singly protonated FLAG peptide was 13.922 ± 0.090 ms. The IMS gas pressures during the measurement series were 3.256 ± 0.006 mbar and 3.254 ± 0.002 mbar, respectively. The instrumental parameters were optimized as follows: source temperature, 50 °C; source offset, 80 V; trap collision energy, 4 V; trap gas flow, 10 mL/min; helium cell gas flow, 180 mL/min; IMS gas flow, 102 mL/min; wave velocity, 650 m/s; wave amplitude, 40 V. Purge gas was set to 600 L/h. EDC delay coefficient of the instrument was 1.41. Capillary and sample cone voltages were optimized for each measurement and were varied between 1.3–2 kV and 60–150 V, respectively. Transfer collision energy (TCE) was raised from 2 to 220 V in a stepwise manner (20–30 V/step). Mass spectra were acquired in positive-ion mode applying a mass window of *m/z* 200–10,000. External mass calibration was performed with 1 mg/mL sodium iodide dissolved in an isopropanol/water solution (50:50, v/v). Data acquisition and processing were performed with the MassLynx software ver. 4.1 (Waters MS-Technologies, Manchester, UK) and the DriftScope software ver. 2.4. CorelDraw X4 was used for data visualization [28].

NanoESI-MS/MS Acquisition Conditions for ITEM with Quadrupole Ion Filtering

The instrumental parameters were optimized as follows: source temperature, 50 °C; source offset, 150 V; capillary voltage, 1.8 V; cone voltage, 150 V; trap collision energy, 4 V; and purge gas, 600 L/h. Transfer collision energy (TCE) was set to either 2 or 220 V for low and high fragmenting conditions, respectively. To record peptide ion signals at low TCE, the quadrupole profile was set to "auto" which corresponds to dwelling at 250 *m/z* for 25% of the scan time, and then using 75% of the scan time to ramp up to 6640 *m/z*. For suppressing the ions in the low *m/z* range the quadrupole profile was manually set to: M_1 = 4000 with dwell time of 25% and ramp time of 25%; M_2 = 5000 with dwell time of 25% and ramp time of 25%; M_3 = 6000. All times are given in % of the mass window scan time. Mass spectra were acquired in positive-ion mode applying a mass window of *m/z* 200–8000. External mass calibration was performed with 1 mg/mL sodium iodide dissolved in an isopropanol/water solution (50:50, v/v). Data acquisition and processing was performed with the MassLynx software ver. 4.1 (Waters MS-Technologies, Manchester, UK). CorelDraw X4 was used for data visualization [28].

Results

Method Development

The ITEM method was developed using synthetic peptides (Table 1) in conjunction with commercially available monoclonal antibodies. In each case, three solutions were prepared and subsequently analyzed. Solution 1 contained just the peptide(s), solution 2 contained the antibody, and solution 3 was a mixture of solutions 1 and 2.

Key operation for determining a peptide as an epitope was to compare the electro-sprayed peptides' and antibodies' ion abundances and their arrival-times from the mixtures (solution 3) after passing the ions through an ion filtering device, such as an ion mobility drift cell or a quadrupole, and upon exposing all those ions that passed the ion filter (i.e., the unbound peptides, the free antibodies, and the immune complexes) to different collision energies in the subsequently aligned collision cell (transfer cell energy; TCE). Two transfer cell energy conditions were chosen for comparisons: low collision induced dissociation (CID) conditions (2 V TCE), and high CID conditions (220 V or 120 V TCE). With ion mobility separation ion signals were recorded and displayed as arrival-time versus mass-over-charge plots (AToMZ plots), i.e., digital images in which the ions' different intensities are represented by grey-scaled pixels. Analysis of peptides (solutions 1) and antibodies (solutions 2) alone is not needed for epitope identification but was performed for comparisons and controls.

In the first experiment, the FLAG peptide was dissolved in 200 mM ammonium acetate buffer (solution 1) from which it was electro-sprayed. The protonated peptide ion was allowed to travel through the ion mobility drift cell, and was exposed to 2 V TCE (i.e., conditions that did not cause excessive fragmentation). The resulting mass spectrum showed a singly charged ion signal of the peptide, referred to as unbound peptide (UBP), at *m/z* 1013.4 and its sodium adduct at *m/z* 1035.4 (Figure 1a). These FLAG peptide ion signals were observed with arrival times of 13.3 ms in the AToMZ plot (solid line circle in Figure 1b). They were accompanied by a few rather low-intensity fragment ions, forming a diagonal trend line in the AToMZ plot on which all singly charged ions were lined up. When the collision energy in the transfer cell of the mass spectrometer was elevated to 220 V TCE, the ion signals of the intact FLAG peptide completely disappeared because under these conditions the peptide was entirely fragmented. As a result of harsh fragmentation conditions, no resolved ion fragments were observed in the AToMZ plot; instead, fragment ion signals were found in a "cloud" with low *m/z* values (at the very left of the *m/z* scale), all with arrival times of their precursors, i.e., ca. 13.3 ms (Figure 1c).

When the mixture consisting of the anti-FLAG M2 antibody and the synthetic FLAG peptide (solution 3) was electro-sprayed and ions passed through the ion mobility drift cell and were subjected to 2 V TCE, the resulting mass spectrum and AToMZ plot (low mass range) resembled the one from solution 1 at low TCE (Figure 1f). By contrast, when solution 3 was exposed to high collision energy (220 V TCE), a singly charged ion signal at *m/z* 1013.4 for the protonated FLAG peptide was observed in the AToMZ plot (dotted circle in Figure 1g). Strikingly, the arrival time of the FLAG peptide ion was now 18.8 ms, which corresponds to the arrival time of the multiply charged antibody or its fragments (Figure 2). Of note, the other singly charged ion in this spectrum at *m/z* 810.40 could not be assigned to any of the ion signals from solution 1 and, therefore, was assumed as being an antibody-derived fragment.

This later arrival time of the FLAG peptide ion is explained by the formation of the noncovalent immune complex in-solution and, upon transition into the gas phase, its migration through the ion mobility cell as "cargo" of the antibody followed by release of the intact FLAG peptide from the antibody, referred to as complex-released peptide (CoRP). Dissociation of the complex is caused by the high collision energy in the transfer cell. For comparison, electro-spraying the antibody solution (solution 2), multiply charged ion signals were recorded with arrival times of 18.6 ms (Supplementary Table S1). From this result, two main features of CoRPs are deduced that allow distinguishing them from UBPs in the peptide-antibody mixture:

1. CoRPs survive the peptide fragmenting conditions in the transfer cell.
2. CoRPs possess arrival times that match the drift times of the antibody ions.

As the ion mobility arrival-time shift of CoRPs in comparison to UBPs is one of the two important features that ITEM takes into account, the epitope peptide ion to be identified by this method must be fast enough to provide an observable arrival-time difference when comparing UBP and CoRP ion

Table 1. Antibody-Binding Peptides

Peptide name	Amino acid sequence [a]	Charge [n]	$[M + nH]^{n+}$ (calcd)	*m/z* (exp.)
FLAG tag	DYKDDDDK	1+	1013.4	1013.4
RA33 epitope	MAARPHSIDGRVVEP	1+	1633.8	1633.8
		2+	817.4	817.4
His-tag (protein G´e and TNFα)	GSSHHHHHHSSGLVPR	1+	1768.8	1768.9
		2+	884.9	884.9
		3+	590.3	590.3
IgG-Fc-binding (protein G´e)	QYANDNGVDGEWTYDDATK	1+	2161.9	2161.9
		2+	1081.5	1081.4
	pQYANDNGVDGEWTYDDATK	1+	2144.9	2144.9

a pQ = pyroglutamic acid

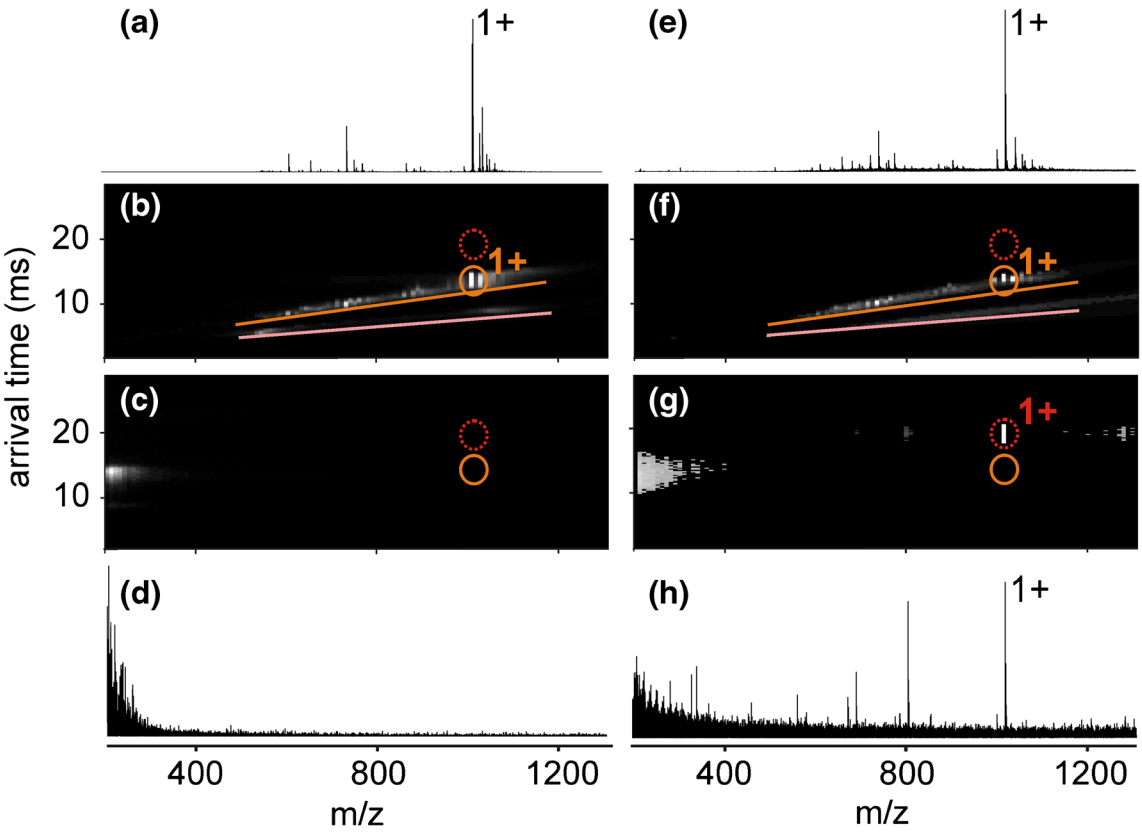

Figure 1. NanoESI mass spectra and AToMZ plots from the FLAG epitope peptide. (**a**), (**b**) Ion signals from solution 1 at low TCE (2 V), and (**c**), (**d**) at high TCE (220 V). (**e**), (**f**) Ion signals from FLAG epitope peptide in the presence of antiFLAG M2 antibody (solution 3) at low TCE (2 V), and (**g**), (**h**) at high TCE (220 V). Solvent: 200 mM ammonium acetate, pH 7.1. UBP positions are marked with orange *solid line circles*; CoRP positions with *red dotted line circles*. Charge states of selected UBPs and CoRPs are given. Trend lines of ions are emphasized by *orange and light red lines*. For *m/z* values of selected ion signals see Table 1

signals in the AToMZ plots. This has been true for the fairly small FLAG peptide (8 amino acid residues in length).

By contrast, the singly charged ion signal of the 15 amino acid residue long RA33 epitope peptide that is recognized by the anti-RA33 antibody [26] migrates with similar arrival times as do the multiply charged ions from the antibody. Yet, the doubly charged peptide ion signal provides the telltale distinctive shift in arrival times in the AToMZ plots. More details on our studies with longer peptides as well as with quadrupole ion filtering or with non-epitope peptide–antibody interactions can be found in sections I–III of the Supplementary Results. In general, in our experiments we observed that the chance that a doubly protonated ion was produced as the most abundant ion by the ESI process – as opposed to the singly protonated ion – increased with the length of the peptide. As only longer peptides with single charges would cause the problem of arival time overlapping with the antibodies' arrival times, the double-charging effect of "longer" peptides automatically resolves the problem of potential ambiguity (see Supplementary Results, section I).

To test whether the experimental settings for ITEM are effective enough to clearly identify epitopes from samples with high complexity, we generated a peptide mixture by proteolytic digestion of full-length proteins. The peptide mixture (solution 1) was obtained by digesting the His-RA33 protein with LysC through which rather long peptides were created. These were further cleaved chemically by BrCN into smaller peptides. Although this procedure produced many peptides with ion signals in the mass range between *m/z* 500 and 1200 (ca. 40 ion signals were recorded with adequate intensities; cf. Supplementary Figure S1a), the "native" epitope peptide was not among them. This observation is consistent with previous findings [26] that place the His-RA33 protein into the group of difficult to digest proteins. Therefore, the synthetic RA33 epitope peptide, resembling the partial amino acid sequence aa78-92 of the His-RA33 protein (underlined partial sequence in Supplementary Figure S1b), was spiked into the mixture (solution 1).

Upon electro-spraying solution 1 and after passing all ions through the ion mobility cell and when 2 V TCE was applied, the RA33 epitope peptide was observed as doubly charged UBP ion with *m/z* 817.4 in the ESI-MS spectrum of the peptide mixture (Figure 3 and Table 1). In the AToMZ plots of solutions 1 and/or 3, the doubly charged UBP ion signal of the RA33 epitope peptide was observed along the drift-time trend line of the doubly charged peptides with an arrival time of 8.2 ms (Figure 3b).

By contrast, when ion mobility-separated ions from solution 3 were exposed to 220 V TCE, the only singly and doubly

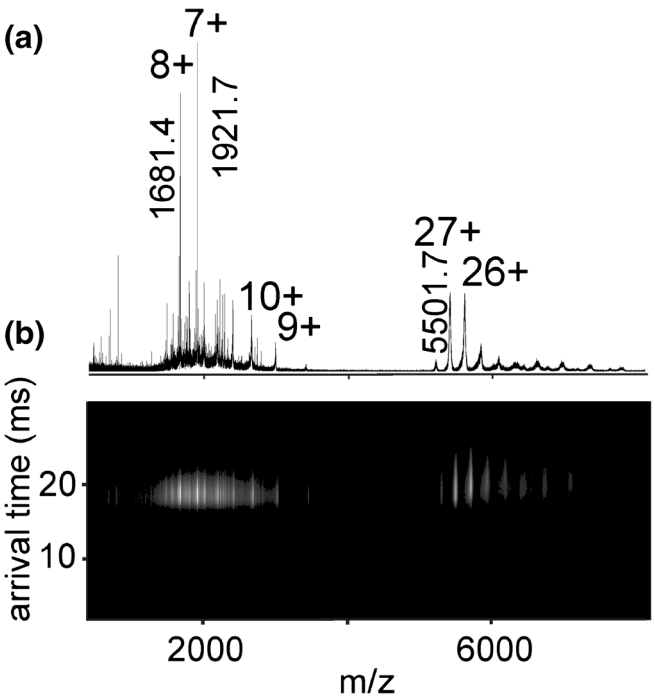

Figure 2. NanoESI mass spectrum and AToMZ plot of antiFLAG antibody. (**a**), (**b**) Ion signals from solution 2 at high TCE (220 V). Solvent: 200 mM ammonium acetate, pH 7.1. Selected multiply charged ion signals from the intact antibody and its fragments and/or contaminants are labeled (cf. Supplementary Table S1)

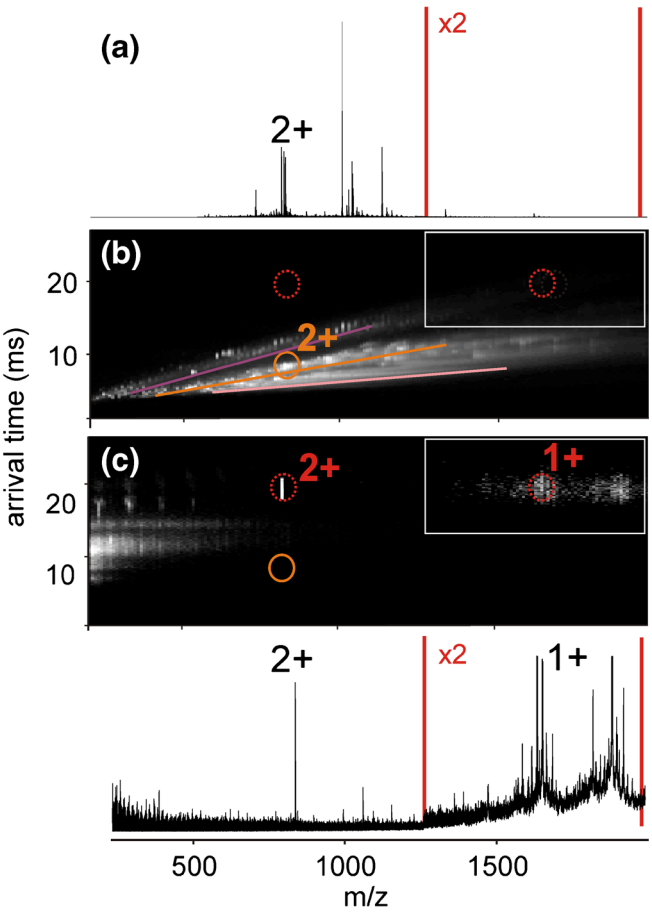

Figure 3. NanoESI mass spectra and AToMZ plots from the His-RA33 peptides from in-solution digestion in the presence of antiRA33 antibody. (**a**), (**b**) Ion signals from solution 3 at low TCE (2 V), and (**c**), (**d**) at high TCE (220 V). Solvent: 200 mM ammonium acetate, pH 7.1. UBP positions are marked with *orange solid line circles*, CoRP positions with *red dotted line circles*. Charge states of selected UBPs and CoRPs are given. Contrast enhanced region is boxed; magnification factor is given. For *m/z* values of selected ion signals see Table 1

charged ion signals in the AToMZ plot were CoRPs from the RA33 epitope peptide (dotted circles in Figure 3c). Consistent with previous observations, the arrival time of the doubly charged RA33 CoRP (i.e., the epitope peptide) was now shifted to 18.7 ms and corresponded with the arrival time of the ions from the antibody (Figure 4).

Of note, the accuracy of determination of the RA33 epitope peptide in this experiment was 18 ppm (the experimentally determined mass of the epitope peptide was 1633.8654, which agrees well with the theoretical mass of 1633.8359). This finding highlights the ITEM feature of determining the epitope peptide mass with isotopic resolution and high mass accuracy because at low *m/z* range monoisotopic masses of CoRPs can be determined very precisely. Conversely, in the high *m/z* range of the mass spectrum of solution 3, three ion series were observed for the antibody and the immune complexes with molecular masses of 150,019.3 ± 72.5 Da, 151,640.3 ± 42.3 Da, and 153,273.1 ± 48.7 Da with average mass differences of 1621.0 Da and 1632.9 Da, respectively (Figure 5).

Hence, when using the experimentally determined masses of the immune complexes to calculate the epitope peptide mass directly from the ESI mass spectra, the accuracy with which the RA33 epitope peptide (Mr 1633.8359) was determined was 7871 ppm and 573 ppm, respectively. Obviously, subtracting experimentally determined masses of the antibody from the masses of the immune complexes leads to rather imprecise determination of the epitope peptide mass, independent of the mass spectrometer performance. The primary reason for the poor resolution of around 160 (FWHM) at this mass range is due to the mean peak widths of the antibody/immune complex ion signals, which were between 25 and 30 Th, caused mostly by antibody heterogeneity.

The observations on AToMZ plot resolutions and inspections of *m/z* traces prompted us to investigate alternative quadrupole ion filtering as an approach within the ITEM method (see Supplementary Results, section II). In contrast to quadrupole ion filtering, which functions like an off-switch with respect to transmission of low *m/z* ions from the ESI source, ion mobility filtering spreads out the ions that are produced in the ESI source on a traveling time scale and allows adding an extra dimension to the mass spectrum. This feature enables to display the data as two-dimensional plots, termed AToMZ plots, and affords instant identification of an ion signal as deriving from a UBP or a CoRP without ambiguity.

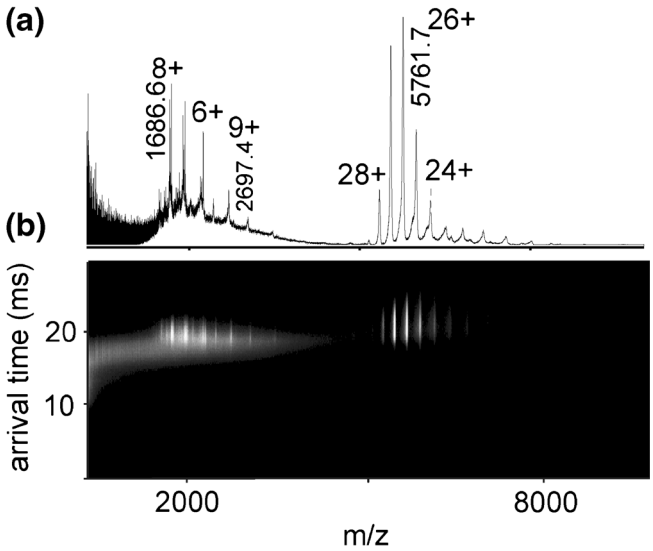

Figure 4. NanoESI mass spectrum and AToMZ plot of antiRA33 antibody. (**a**), (**b**) Ion signals from solution 2 at high TCE (220 V). Solvent: 200 mM ammonium acetate, pH 7.1. Selected multiply charged ion signals from the intact antibody and its fragments and/or contaminants are labeled (cf. Supplementary Table S1)

Application Examples

Epitope extraction We first applied the ITEM method to identify the His-tag epitope from recombinant protein G´e by epitope extraction. Protein G´e is a commercial protein [27] from which 25 assignable peptide ion signals with adequate intensities were produced by tryptic digestion (cf. Supplementary Figure S2a), yielding 100% sequence coverage. The complex peptide mixture containing the His-tag carrying peptide served as solution 1. Solution 3 consisted of solution 1 to which an antiHis-tag antibody (solution 2) was added. When solution 3 was electrosprayed and ions were ion mobility separated and exposed to 2 V TCE, the His-tag peptide was recorded in the AToMZ plot as doubly and triply charged ion signals at *m/z* 884.9 and *m/z* 590.3 with arrival times of 8.2 ms and 5.8 ms, respectively (solid line circles in Figure 6; Table 1).

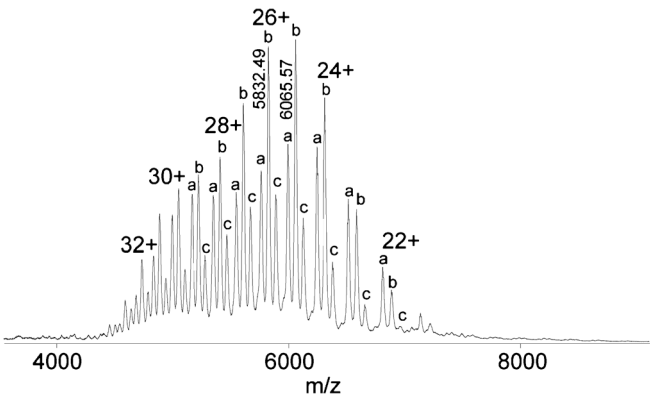

Figure 5. NanoESI mass spectrum of the mixture of antiRA33 antibody and RA33 epitope peptide at 2 V TCE. Solvent: 200 mM ammonium acetate, pH 7.1. The 1:2 (antibody:epitope) mixture shows ion signals belonging to the antibody (series "a") and to the immune complexes in which one epitope peptide (series "b") and two epitope peptides (series "c") were bound, respectively. Selected charge states and *m/z* values are indicated

Electrospraying solution 3, separating all ions in the ion mobility cell, and exposing the ions to 120 V TCE afforded in the AToMZ plot singly charged ion signals for the His-tag peptide at *m/z* 1768.9 (Table 1) but now with 21.5 ms arrival time (dashed line circle in Figure 6c), which matched the arrival time of the antibody ions and their respective fragment ions (Supplementary Figure S3). This characteristic change in position in the AToMZ plots qualified the His-tag peptide ions as CoRPs, i.e., identified the peptide as epitope (underlined partial sequence in Supplementary Figure S2b).

Interestingly, another peptide ion signal that survived fragmentation when 120 V TCE was applied was found at m/z 1535.6. It was assigned to the partial sequence aa17-31 from protein G´e (cf. Supplementary Figure S2). However, the position of this ion signal in the AToMZ plots did not match the arrival time of the antibody, indicating that it was not a CoRP but survived fragmentation, at least partially, because of its stability. Of note, in all spectra from the antiHis-tag antibody (solution 2), rather strong ion signals within the mass range of *m/z* 2000 and 4000 at arrival times above 12 ms were observed from which molecular masses of ca. 38 kDa were calculated (Supplementary Table S1). As these ion signals were present in the AToMZ plots at both low TCE (data not shown) and high TCE (Supplementary Figure S3), they were assigned as unknown contaminants. Owing to their multiple charge states, they did not interfere with assignment of epitope peptide ions as the latter typically were doubly or singly protonated.

Even more intriguing was that in addition to the His-tag carrying epitope peptide, two more closely spaced, singly charged peptide ion signals with *m/z* 2144.9 and 2161.9 and with arrival times of 24.2 ms each, were recorded in the AToMZ plots when solution 3 was investigated with high CID conditions (120 V TCE). As the arrival times of these two ions matched those of the antibody (dashed squares in Figure 6c), their positions in the AToMZ plots marked them as CoRPs as well. The ion signal at *m/z* 2161.9 was assigned to the identical partial amino acid sequences aa77-95 and/or aa147-165 of protein G´e (dashed lines in Supplementary Figure S2b), and the ion signal at *m/z* 2144.9 was regarded as a deamination product therefrom (Table 1). The latter was most likely produced by CID from the N-terminal Q residue [29] of this peptide. Reexamination of the AToMZ plot from solution 3 with 2 V TCE revealed the presence of the respective doubly charged peptide ion at *m/z* 1081.4 with 9.8 ms arrival time (solid line rectangle in Figure 6b; the ion signal is marked with "#" in Supplementary Figure S2a). From X-ray crystallography data it is known that protein G´e binds strongly to Fc parts of antibodies [30] and the region of protein G´e that makes contact with the antibodies encompasses the partial amino acid sequences aa77-95 and/or aa147-165 [31]. Hence, our ITEM result stands in full agreement with crystal structure analyses.

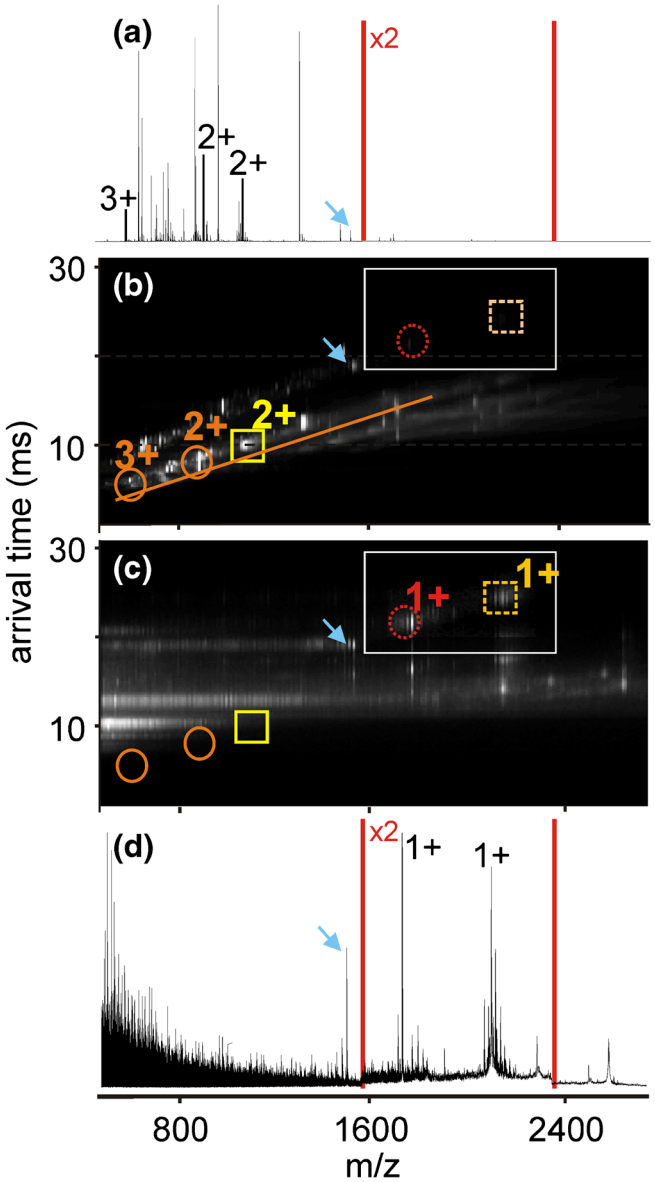

Figure 6. NanoESI mass spectra and AToMZ plots from the protein G´e peptides derived from in-solution digestion. (**a**), (**b**) Ion signals from digest peptide mixture in the presence of antiHis-tag antibody (solution 3) at low TCE (2 V), and (**c**), (**d**) at high TCE (120 V). Solvent: 200 mM ammonium acetate, pH 7.1. UBP positions are marked with *orange solid line circles* and *yellow squares*; CoRP positions with *red dotted line circles* and *dark yellow dotted squares*. The *blue arrow* points to a non-fragmenting peptide. Charge states of selected UBPs and CoRPs are given. Trend lines of ions are emphasized by orange and light red lines. Contrast-enhanced region is boxed; magnification factor is given. For *m/z* values of selected ion signals see Table 1

More specific investigations on antibody-protein G binding can be found in the Supplementary Results (section III).

Epitope Excision For epitope excision, we first prepared solution 3 by mixing rhTNFα (as a full-length antigen) with the antiHis-tag antibody and subjected this immune complex-containing mixture to enzymatic digestion with trypsin. All solvent mixing was done using 200 mM ammonium acetate buffer (pH 7). Then, following the standard ITEM procedure, we electrosprayed the resulting peptide and protein mixture as a whole and exposed the ion mobility-separated ions first to low (2 V TCE) and second to high (200 V TCE) fragmentation conditions. When solution 3 was subjected to 2 V TCE (Figure 7b, c, and Supplementary Figure S4), a few peptide ion signals, which were formed upon digestion of the antigen with trypsin, were observed in the low *m/z* range of the mass spectrum, all with less than 15 ms arrival times. The His-tag-carrying peptide was found as a doubly charged ion signal at *m/z* 884.89 with an arrival time of 7.95 ms. The presence of the

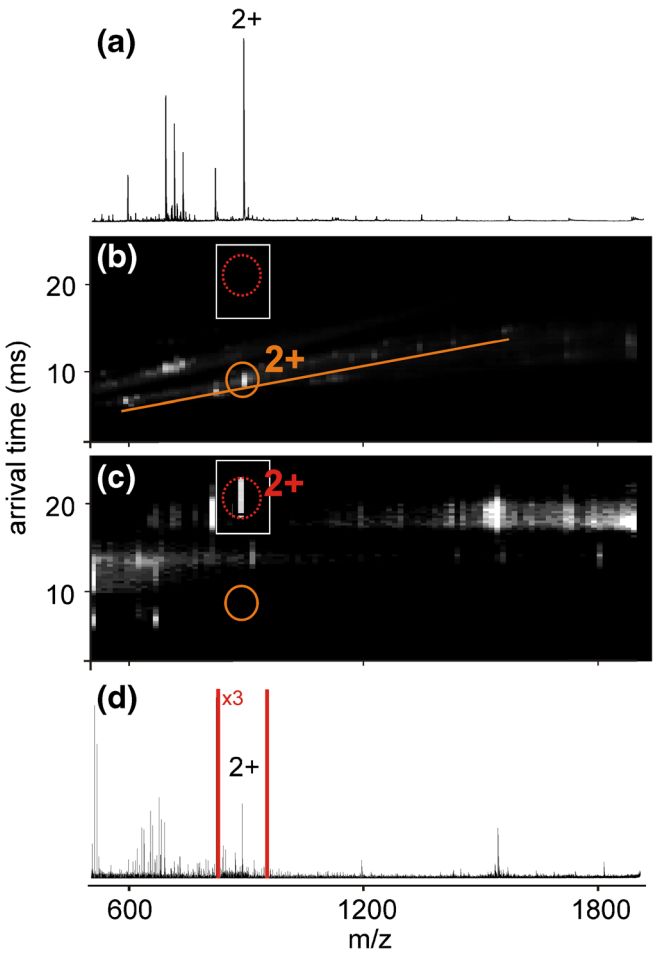

Figure 7. NanoESI mass spectra and AToMZ plots from the rhTNFα peptides derived from epitope excision. (**a**), (**b**) Ion signals from digest peptide mixture in the presence of the antiHis-tag antibody (solution 3) at low TCE (2 V), and (**c**), (**d**) at high TCE (120 V). Solvent: 200 mM ammonium acetate, pH 7.1. UBP positions are marked with *orange solid line circles*; CoRP positions with *red dotted line circles*. Charge states of selected UBPs and CoRPs are given. Trend line of ions is emphasized by an *orange line*. Contrast enhanced region is boxed; magnification factor is given. For *m/z* values of selected ion signals see Table 1

unbound His-tag peptide in this mixture can be explained by the fact that rhTNFα is a trimer, potentially leaving some of the His-tag peptides inaccessible to the antibody.

When the ion mobility-separated ions from solution 3 were exposed to high TCE voltage, unbound peptides were fragmented and the only nonfragmented ion signal that could be attributed to the antigen was that of the doubly charged His-tag-carrying peptide at *m/z* 884.88. But now its arrival time of 21.4 ms matched that of the antibody (Figure 7c). Again, the antiHis-Tag antibody was prone to degradation when exposed to high TCE voltage, producing many multiply charged and some singly charged fragment ions (cf. Supplementary Table S1). The fact that the peptide with *m/z* 884.88 survived high TCE conditions and possessed an arrival time like that of the anti-His-tag antibody proves that this peptide is a CoRP and, consequently, the epitope peptide.

Discussion

We have developed the ITEM method to provide a facile and routinely applicable procedure to rapidly determine antigen-derived epitopes of an antibody of interest using both epitope extraction and epitope excision. These two epitope mapping methods have proven to be well applicable to identify assembled (conformational, discontinuous) as well as sequential (linear, continuous) epitopes [14, 32] by mass spectrometry, and typically afford peptide masses as read-outs by which the epitopes are defined. It has been proven that higher-order structured peptides are able to bind to antibodies. Peptides of a certain length (ca. 6–10 amino acids and more) are known to be able to adopt higher order structures such as alpha-helices in solution [19, 33, 34], and peptides are known to be able to bind to antibodies (or other binding partners) via a mechanism that is called "induced fit" [35]. For instance, with Western blotting as well as with so-called peptide chips, one is able to identify epitopes [26, 36] independent of the fact that by applying these methods the structures that are bound by the antibodies are taken out of the context of their highly structured "natively folded" antigen proteins. Despite not knowing the precise structure of the bound amino acids in an immune complex, the experimentally determined epitope is sufficiently encoded by the peptide that contains the partial structure which is recognized by the antibody. Hence, the identified CoRPs reflect the epitope peptides with high accuracy.

Our ITEM approach, in fact, follows the same step-wise experimental sequence as was developed for in-solution epitope mapping methods, yet without immobilization of the antibody and/or the immune complex. Instead, after in-solution formation of the specific antibody–peptide complex, a transition of this complex into the gas phase is induced together with all other constituents in that mixture. Sample preparation for ITEM has, thus, been minimized to the generation of antigen/peptide-antibody mixtures using volatile buffers. The demand on purity for both the antigen/peptide solution (solution 1) and the antibody solution (solution 2) is rather moderate. With nanospray capillaries, the consumed volume in one experiment is ca. 3–5 μL and the amount of required peptide and antibody is in the low pmol range for each. In our hands, as long as a suitable electrospray was obtained from the mixture (solution 3) the epitope mapping experiment was successful.

Already during the desolvation step, electrospray conditions can be selected such that weakly bound molecules and nonspecifically bound "stickier" peptides are efficiently removed from the specific immune complex while antibody–epitope interactions are not broken; they are typically very strong with K_D values of around 10 nM [32]. Therefore, the traditional "washing step" that is implemented to remove nonspecific or unbound mixture components occurs predominantly in the transition step from solution to the gas phase in the source and to a lesser extent within the ion mobility drift cell. "Elution" of the epitope peptide from the immune complex is achieved by efficient collision induced dissociation in the transfer cell (or the collision cell). Simultaneously, peptides that are not bound to the antibody (UBPs) but that passed the ion filter are efficiently fragmented under the applied CID conditions. After these simultaneous gas-phase processes, which are equivalent to "washing" and "elution", only a few peptides survived, resulting in just a few ion signals (i.e., spots in an AToMZ plot) which, therefore, are easy to interpret.

It turned out that the harshness of both the electrospray and the gas-phase dissociation conditions were to be fine-tuned to match the individual stabilities of all constituents of the sprayed mixture, including those of the antibodies [37], the peptides, and the contaminants in order to obtain good signal intensities (signal to noise values) and to simultaneously avoid generation of too many Ab-derived fragment ion signals. In cases when milder collision energy regimens in the transfer cell were selected for successful ITEM analysis (e.g., 120 V as opposed to 220 V), some fairly stable UBPs may survive unfragmented. However, they can be easily identified by comparing their arrival times with the arrival times of the antibody ion signals (from solution 3) and by the absence of arrival time shifts.

Of note, since CoRP ions are not produced by the ESI process in the source region of the mass spectrometer, they receive/retain their protons (charges) from the antibody–epitope complexes during CID in the transfer cell. Thus, in principle it may be possible that neutral CoRPs are obtained by CID, which would not be detectable in the mass spectrometer and, therefore, ITEM might be limited. Yet a number of studies have shown that via CID an asymmetric distribution of charges on the dissociated components occurs [38] in which the smaller of the two complex partners takes the relatively larger numbers of protons upon dissociation. This stands in agreement with our observations that showed that the CoRPs were either singly or doubly protonated upon dissociation of the immune complex. Also, the fact that ionization of CoRPs is not taking place in the ESI source makes them free from so-called "matrix effects" where peptides from a more or less complex mixture are competing for the available protons under the respective

solution ionization conditions. Therefore, ion yields which are observed for peptides that are ionized from complex peptide mixtures are not decisive for the abundance by which the epitope peptide ion signals will be observed by the ITEM method. For comparison, high resolution structure analysis techniques, such as X-ray diffraction [39, 40] or NMR [41] of immune complexes, also suffer from limitations like high material demands, time-consuming preparations, and molecular size restrictions [42].

In addition to alternative ion filtering methods like ion mobility and quadrupole separation that can be applied with ITEM, there are several mass spectrometric methods that have found application for gas-phase fragmentation of protein–protein complexes. Black-body infrared dissociation (BIRD) seems one potential alternative for fragmentation of noncovalent peptide–protein bonds. Yet BIRD is so far not routinely available with commercial mass spectrometers [43, 44]. The closest alternative to CID breakage of noncovalent bonds in the gas phase seems to be surface induced dissociation (SID) [45, 46]. However, it was reported that in SID experiments, charge distribution is more symmetric and charges are distributed proportionally to the masses of dissociated constituents [47].

In summary, ITEM is very powerful and allows the direct identification of an epitope as in-solution handling is reduced to mixing of antigen/epitope peptide and antibody solutions. Since suitable mass spectrometry equipment has become available, our ITEM method seems to be easily adaptable by mass spectrometry laboratories around the world.

Acknowledgements

The authors express their thanks to Dr. Stephan Mikkat for providing his expertise on mass spectrometry and to Dr. Cornelia Koy and Dr. Peter Lorenz for critically reading the manuscript. The authors also thank Dr. Harald Illges for providing rhTNFα and Dr. Marcus Frank for providing access to the capillary sputter. We acknowledge the German Academic Exchange Service (DAAD) for providing scholarships for Y.Y., B.D., and K.O. The WATERS Synapt G2S mass spectrometer has been bought through a EU grant (EFRE-UHROM 9) made available to M.O.G.

References

1. Bjorling, E., Uhlen, M.: Antibodypedia, a portal for sharing antibody and antigen validation data. Mol. Cell. Proteom. **7**, 2028–2037 (2008)
2. Dubel, S., Stoevesandt, O., Taussig, M.J., Hust, M.: Generating recombinant antibodies to the complete human proteome. Trends Biotechnol. **28**, 333–339 (2010)
3. Uhlen, M., Ponten, F.: Antibody-based proteomics for human tissue profiling. Mol. Cell. Proteom. **4**, 384–393 (2005)
4. Andresen, H., Grotzinger, C.: Deciphering the antibodyome-peptide arrays for serum antibody biomarker diagnostics. Curr. Proteom. **6**, 1–12 (2009)
5. Baker, M.: Reproducibility crisis: blame it on the antibodies. Nature **521**, 274–276 (2015)
6. Aggarwal, S.R.: A survey of breakthrough therapy designations. Nat. Biotechnol. **32**, 323–330 (2014)
7. Ecker, D.M., Jones, S.D., Levine, H.L.: The therapeutic monoclonal antibody market. MAbs **7**, 9–14 (2015)
8. Fekete, S., Guillarme, D., Sandra, P., Sandra, K.: Chromatographic, electrophoretic, and mass spectrometric methods for the analytical characterization of protein biopharmaceuticals. Anal. Chem. **88**, 480–507 (2016)
9. Walsh, G.: Biopharmaceutical benchmarks 2014. Nat. Biotechnol. **32**, 992–1000 (2014)
10. Egelhofer, T.A., Minoda, A., Klugman, S., Lee, K., Kolasinska-Zwierz, P., Alekseyenko, A.A., Cheung, M.S., Day, D.S., Gadel, S., Gorchakov, A.A., Gu, T., Kharchenko, P.V., Kuan, S., Latorre, I., Linder-Basso, D., Luu, Y., Ngo, Q., Perry, M., Rechtsteiner, A., Riddle, N.C., Schwartz, Y.B., Shanower, G.A., Vielle, A., Ahringer, J., Elgin, S.C., Kuroda, M.I., Pirrotta, V., Ren, B., Strome, S., Park, P.J., Karpen, G.H., Hawkins, R.D., Lieb, J.D.: An assessment of histone-modification antibody quality. Nat. Struct. Mol. Biol. **18**, 91–93 (2011)
11. Michel, M.C., Wieland, T., Tsujimoto, G.: How reliable are G-protein-coupled receptor antibodies? [Naunyn Schmiedebergs Arch. Pharmacol.] **379**, 385–388 (2009)
12. Abbott, W.M., Damschroder, M.M., Lowe, D.C.: Current approaches to fine mapping of antigen-antibody interactions. Immunology **142**, 526–535 (2014)
13. Morris, G.E.: Epitope mapping: identification of antibody-binding sites on protein antigens. In: Walker, J.M., Rapley, R. (eds.) Molecular biomethods handbook. Humana Press, Totowa (2008)
14. Opuni, K.F., Al-Majdoub, M., Yefremova, Y., El-Kased, R.F., Koy, C., Glocker, M.O.: Mass spectrometric epitope mapping. Mass Spectrom. Rev. (2016)
15. Buus, S., Rockberg, J., Forsstrom, B., Nilsson, P., Uhlen, M., Schafer-Nielsen, C.: High-resolution mapping of linear antibody epitopes using ultrahigh-density peptide microarrays. Mol. Cell. Proteom. **11**, 1790–1800 (2012)
16. Sharon, J., Rynkiewicz, M.J., Lu, Z., Yang, C.Y.: Discovery of protective B-cell epitopes for development of antimicrobial vaccines and antibody therapeutics. Immunology **142**, 1–23 (2014)
17. Clemmer, D.E., Jarrold, M.F.: Ion mobility measurements and their applications to clusters and biomolecules. J. Mass Spectrom. **32**, 577–592 (1997)
18. Hoaglund, C.S., Valentine, S.J., Sporleder, C.R., Reilly, J.P., Clemmer, D.E.: Three-dimensional ion mobility/TOFMS analysis of electrosprayed biomolecules. Anal. Chem. **70**, 2236–2242 (1998)
19. Al-Majdoub, M., Opuni, K.F., Koy, C., Glocker, M.O.: Facile fabrication and instant application of miniaturized antibody-decorated affinity columns for higher-order structure and functional characterization of TRIM21 epitope peptides. Anal. Chem. **85**, 10479–10487 (2013)
20. Uetrecht, C., Rose, R.J., van Duijn, E., Lorenzen, K., Heck, A.J.R.: Ion mobility mass spectrometry of proteins and protein assemblies. Chem. Soc. Rev. **39**, 1633–1655 (2010)
21. Valentine, S.J., Liu, X.Y., Plasencia, M.D., Hilderbrand, A.E., Kurulugama, R.T., Koeniger, S.L., Clemmer, D.E.: Developing liquid chromatography ion mobility mass spectometry techniques. Expert Rev. Proteom. **2**, 553–565 (2005)
22. Wyttenbach, T., Pierson, N.A., Clemmer, D.E., Bowers, M.T.: Ion mobility analysis of molecular dynamics. Annu. Rev. Phys. Chem. **65**, 175–196 (2014)
23. Erba, E.B., Ruotolo, B.T., Barsky, D., Robinson, C.V.: Ion mobility-mass spectrometry reveals the influence of subunit packing and charge on the dissociation of multiprotein complexes. Anal. Chem. **82**, 9702–9710 (2010)
24. Jones, L.M., Zhang, H., Cui, W.D., Kumar, S., Sperry, J.B., Carroll, J.A., Gross, M.L.: Complementary MS methods assist conformational characterization of antibodies with altered S–S Bonding Networks. J. Am. Soc. Mass Spectrom. **24**, 835–845 (2013)
25. Ruotolo, B.T., Benesch, J.L.P., Sandercock, A.M., Hyung, S.J., Robinson, C.V.: Ion mobility-mass spectrometry analysis of large protein complexes. Nat. Protoc. **3**, 1139–1152 (2008)
26. El-Kased, R.F., Koy, C., Deierling, T., Lorenz, P., Qian, Z., Li, Y., Thiesen, H.J., Glocker, M.O.: Mass spectrometric and peptide chip epitope mapping of rheumatoid arthritis autoantigen RA33. Eur. J. Mass Spectrom. **15**, 747–759 (2009)
27. Yefremova, Y., Al-Majdoub, M., Opuni, K.F.M., Koy, C., Cui, W.D., Yan, Y.T., Gross, M.L., Glocker, M.O.: "De-novo" amino acid sequence

elucidation of protein G'e by combined "Top-Down" and "Bottom-Up" mass spectrometry. J. Am. Soc. Mass Spectrom. **26**, 482–492 (2015)
28. Yefremova, Y., Al-Majdoub, M., Opuni, K.F., Koy, C., Yan, Y., Gross, M.L., Glocker, M.O.: A dynamic model of pH-induced protein G'e higher order structure changes derived from mass spectrometric analyses. Anal. Chem. **88**, 890–897 (2016)
29. Neta, P., Pu, Q.L., Kilpatrick, L., Yang, X.Y., Stein, S.E.: Dehydration versus deamination of N-terminal glutamine in collision-induced dissociation of protonated peptides. J. Am. Soc. Mass Spectrom. **18**, 27–36 (2007)
30. Akerstrom, B., Bjorck, L.: A physicochemical study of protein-G, a molecule with unique immunoglobulin-G-binding properties. J. Biol. Chem. **261**, 240–247 (1986)
31. Sauererikssson, A.E., Kleywegt, G.J., Uhl, M., Jones, T.A.: Crystal-structure of the C2 fragment of streptococcal protein-G in complex with the Fc domain of human-IGG. Structure **3**, 265–278 (1995)
32. Hager-Braun, C., Tomer, K.B.: Determination of protein-derived epitopes by mass spectrometry. Expert Rev. Proteom. **2**, 745–756 (2005)
33. Al-Majdoub, M., Koy, C., Lorenz, P., Thiesen, H.J., Glocker, M.O.: Mass spectrometric and peptide chip characterization of an assembled epitope: analysis of a polyclonal antibody model serum directed against the Sjogren/systemic lupus erythematosus autoantigen TRIM21. J. Mass Spectrom. **48**, 651–659 (2013)
34. Al-Majdoub, M., Opuni, K.F.M., Yefremova, Y., Koy, C., Lorenz, P., El-Kased, R.F., Thiesen, H.J., Glocker, M.O.: A novel strategy for the rapid preparation and isolation of intact immune complexes from peptide mixtures. J. Mol. Recognit. **27**, 566–574 (2014)
35. Weikl, T.R., von Deuster, C.: Selected-fit versus induced-fit protein binding: kinetic differences and mutational analysis. Proteins **75**, 104–110 (2009)
36. Lustrek, M., Lorenz, P., Kreutzer, M., Qian, Z.L., Steinbeck, F., Wu, D., Born, N., Ziems, B., Hecker, M., Blank, M., Shoenfeld, Y., Cao, Z.W., Glocker, M.O., Li, Y.X., Fuellen, G., Thiesen, H.J.: Epitope predictions indicate the presence of two distinct types of epitope-antibody-reactivities determined by epitope profiling of intravenous immunoglobulins. Plos One **8**(11), e78605 (2013)
37. Ugwu, S.O., Apte, S.P.: The effect of buffers on protein conformational stability. Pharm. Technol. **28**, 86 (2004)
38. Benesch, J.L.P., Aquilina, J.A., Ruotolo, B.T., Sobott, F., Robinson, C.V.: Tandem mass spectrometry reveals the quaternary organization of macromolecular assemblies. Chem. Biol. **13**, 597–605 (2006)
39. Chen, Y., Wiesmann, C., Fuh, G., Li, B., Christinger, H.W., McKay, P., de Vos, A.M., Lowman, H.B.: Selection and analysis of an optimized anti-VEGF antibody: crystal structure of an affinity-matured Fab in complex with antigen. J. Mol. Biol. **293**, 865–881 (1999)
40. Ultsch, M., Bevers, J., Nakamura, G., Vandlen, R., Kelley, R.F., Wu, L.C., Eigenbrot, C.: Structural basis of signaling blockade by anti-IL-13 antibody lebrikizumab. J. Mol. Biol. **425**, 1330–1339 (2013)
41. Zilber, B., Scherf, T., Levitt, M., Anglister, J.: NMR-derived model for a peptide-antibody complex. Biochemistry **29**, 10032–10041 (1990)
42. Gershoni, J.M., Roitburd-Berman, A., Siman-Tov, D.D., Freund, N.T., Weiss, Y.: Epitope mapping—the first step in developing epitope-based vaccines. Biodrugs **21**, 145–156 (2007)
43. Dunbar, R.C.: BIRD (blackbody infrared radiative dissociation): evolution, principles, and applications. Mass Spectrom. Rev. **23**, 127–158 (2004)
44. Wang, W., Kitova, E.N., Sun, J., Klassen, J.S.: Blackbody infrared radiative dissociation of nonspecific protein–carbohydrate complexes produced by nanoelectrospray ionization: the nature of the noncovalent interactions. J. Am. Soc. Mass Spectrom. **16**, 1583–1594 (2005)
45. Harvey, S.R., Yan, J., Brown, J.M., Hoyes, E., Wysocki, V.H.: Extended gas-phase trapping followed by surface-induced dissociation of noncovalent protein complexes. Anal. Chem. **88**, 1218–1221 (2016)
46. Quintyn, R.S., Zhou, M.W., Yan, J., Wysocki, V.H.: Surface-induced dissociation mass spectra as a tool for distinguishing different structural forms of gas-phase multimeric protein complexes. Anal. Chem. **87**, 11879–11886 (2015)
47. Zhou, M., Dagan, S., Wysocki, V.H.: Protein subunits released by surface collisions of noncovalent complexes: native-like compact structures revealed by ion mobility mass spectrometry. Angew. Chem. Int. Ed. Engl. **51**, 4336–4339 (2012)

Supplemental data

Intact Transition Epitope Mapping (ITEM)

SUPPLEMENTARY RESULTS

Yelena Yefremova[a)], Kwabena F.M. Opuni[a)], Bright D. Danquah [a)],

Hans-Juergen Thiesen[b)], and Michael O. Glocker[a)]

1) Proteome Center Rostock, University Medicine Rostock, Schillingallee 69, 18057 Rostock, Germany
2) Institute of Immunology, University Medicine Rostock, Schillingallee 70, 18057 Rostock, Germany

Section I (larger peptides)

To test whether larger peptides with more than ten amino acids in length, i.e. with arrival times longer than 20 ms of the singly protonated ions, could be subjected to ITEM, again three solutions were prepared. Solution 1 consisted of the RA33 epitope peptide and solution 3 was a mix of the RA33 epitope peptide with the antiRA33 antibody (solution 2). Using solution 1 for electro-spraying, singly and doubly charged ion signals of the RA33 epitope peptide with m/z 817.4 and m/z 1,633.8 (Table 1), and arrival times of 8.8 ms and 20.4 ms, respectively, were observed in the AToMZ plot as the major ion signals (solid line circles in Figure S5b) when 2 V TCE was applied. These ion signals were accompanied by low intensity fragment ion signals. As expected, the doubly charged ion signal was dominant. The mass spectrum of solution 2 at high TCE showed the multiply charged ions of the antibody as well as some multiply charged fragment ions (Figure 4; Table S1). When solution 3, consisting of a mixture of the RA33 epitope peptide (solution 1) and the anti-hnRNP-A2/B1 antibody (solution 2), was electro-sprayed and the ions passed through the ion mobility drift cell and were exposed to 220 V TCE, the corresponding AToMZ plot exhibited ion signals of the singly and doubly protonated RA33 epitope peptide. Yet, in contrast to the results from solution 1, both ion signals were observed with arrival times of 19.5 ms (Figure S5c), matching with the arrival times of the ion signals of the antibody and its fragments. The overlaying antibody fragment ions did not interfere with epitope peptide assignment because multiply charged ions can easily be distinguished from singly charged ions.

(Figure S5a-d)

Although at the moment the graphical means for visualization of AToMZ plots are somewhat low in resolution on the m/z scale, the assignment of an ion signal as UBP and/or CoRP was in all investigated cases unambiguous. The shift of arrival time of the epitope peptide could be tracked instantly by comparing AToMZ plots of solutions 3. Yet, if higher resolution on the m/z scale was needed, one can independently consult the m/z trace of the underlying data. Similarly, in case higher resolution on the arrival time scale was needed, one can plot the arrival time trace of an ion of interest and determine its intensity maximum using standard peak analysis software. But even without arrival time differences of longer epitope peptides, as in the case of the intact RA33 epitope peptide, the appearance of the singly charged ion signal under the selected high TCE conditions is indicative for the peptide to be derived from the immune-complex, i.e. being a CoRP, since the respective UBP would be completely fragmented under those conditions.

Section II (quadrupole filtering)

Quadrupole filtering was performed using a mixture of six synthetic peptides (solution 1), one of which was the Flag epitope peptide. Solution 3 was obtained by adding the antiFLAG M2 antibody (solution 2) and was subjected to mass spectrometric analysis (Figure S6). TCE was kept at 2 V and the quadrupole filter was set to full transmission, i.e. all ions traversed the quadrupole, for recording all the ions from the peptide mixture (Figure S6a). Five ion signals were observed with different intensities. Then, the quadrupole was tuned to suppress all peptide ions in the low m/z range between m/z 500 and m/z 3000 (Figure S6b). Under these conditions only the ions of the antibody and of the immune complexes, respectively, were observed in the high m/z range between m/z 3000 and 8000, showing broad multiply charged ion signals.

(Figure S6a-c)

When TCE voltage was set to 200 V ion signals appeared again in the low m/z range. Since ion transmission from the ESI source was completely blocked, these low m/z ions must originate from the dissociated immune complex. We observed a singly charged ion signal of the epitope peptide at m/z 1013.40 together with fragment ion signals from the antibody, most of which were multiply charged (Figure S6c). The 7+ to 10+ ions signals indicated the presence of the light chain of the antibody with a molecular mass of 24215.84 ± 1.23 Da. Another fragment with a molecular mass of 13444.73 ± 0.89 Da was represented by 9+ and 6+ charged ion signals (Table S1). Of note, the other singly charged ion in this spectrum at m/z 810.40 could not be assigned to any of the peptides from solution 1 and, therefore, was assumed as being an antibody-derived fragment as well.

The matching ion mobility filtering experiment with the exact same peptide mixture (solution 1) showed upon electro-spraying solution 3 and after passing all ions through the ion mobility cell and when 2 V TCE was applied, the FLAG epitope peptide as singly charged UBP ion with m/z 1013.4 and an arrival time of 13.3 ms in the AToMZ plot; located along the arrival time trend line of the singly charged peptides (Figure S7b).

(Figure S7a-d)

By contrast, when ion mobility separated ions from solution 3 were exposed to 220 V TCE the only singly charged ion signal in the AToMZ plot was a CoRP from the FLAG epitope peptide (dotted circle in Figure S7c). Consistent with previous observations, the arrival time of the singly charged FLAG CoRP, i.e. the epitope peptide, was now shifted to 18.8 ms and corresponded with the arrival time of the ions from the antibody (cf. Figure 2).

Section III (non-epitope peptide – antibody interactions)

More specific investigations on antibody – protein G binding have been conducted to prove that the appearance of the peptides of solution 3 with ion signals at *m/z* 2,161.9 and *m/z* 2,144.9, both at 24.2 ms arrival time, was in fact reflecting a specific non-covalent in-solution bonding of this peptide to the Fc part of IgG. We performed an additional ITEM experiment using the antiFLAG M2 antibody (solution 2). As solution 1 we again applied the peptide mixture that was derived from tryptic digestion of protein G´e. As expected, the AToMZ plot from solution 3, i.e. the mixture of solutions 1 and 2, showed at 2 V TCE (Figure S8b) the presence of the Fc binding peptide of protein G´e that is indicated by the doubly charged ion at *m/z* 1,081.4 and 9.8 ms arrival time (solid line rectangle in Figure 8b).

(Figure 8a-d)

When examining solution 3 at high TCE, the only singly charged CoRP ion signal was recorded in the AToMZ plot at *m/z* at 2,144.9 and 24.0 ms arrival time (Figure 8c), proving that the peptides with partial sequences aa77-95 and/or aa147-165 from protein G´e had been bound to the Fc part of the antiFLAG M2 antibody in-solution. Again, the explanation is that the in-solution complex between the protein G´e-derived peptide and the antiFLAG M2 antibody had been transitioned into the gas phase, had been separated from the UBPs of the protein G´e digest by ion mobility, and had been dissociated in the transfer cell under high fragmenting conditions. This finding, in fact, expands the applicability of our ITEM method for probing antigen-antibody, i.e. epitope-paratope interactions, to also other specific and stable in-solution protein-peptide interactions. The fact that the antiHis-tag antibody recognized the His-tag peptide from the protein G´e-derived peptide mixture as its epitope whereas the antiFlag M2 antibody, which can be considered a “dummy”, i.e. a nonbinding antibody, did not, enhances the confidence in our ITEM method.

Intact Transition Epitope Mapping (ITEM)

Yelena Yefremova[a)], Kwabena F.M. Opuni[a)], Bright D. Danquah[a)],

Hans-Juergen Thiesen[b)], and Michael O. Glocker[a)]

SUPPLEMENTARY TABLES and FIGURES

1) Proteome Center Rostock, University Medicine Rostock, Schillingallee 69, 18057 Rostock, Germany
2) Institute of Immunology, University Medicine Rostock, Schillingallee 70, 18057 Rostock, Germany

SUPPLEMENTARY TABLES

Table S1: Antibody and fragment ions in nanoESI-MS/MS spectra and AToMZ plots of solutions 2 at high TCE.

antibody	charge states of ion series	arrival times [ms]	exp. masses [Da]
antiHis-tag [a)]	27+ – 23+	21.5	148,889.97 ± 19.25
	14+ – 11+	>12	37,833.15 ± 240.86
antiRA33 [b)]	28+ – 24+	18.7	149,723.07 ± 54.94
	8+ – 10+	18.7	24,279.42 ± 11.07
	9+ – 6+	18.7	13,207.11 ± 1.16
antiFLAG M2 [b)]	28+ – 24+	18.6	148,430.43 ± 76.68
	7+ – 10+	18.6	24,215.84 ± 1.23
	9+ – 6+	18.6	13,444.73 ± 0.89

a) 120 V TCE
b) 200 V TCE

SUPPLEMENTARY FIGURES

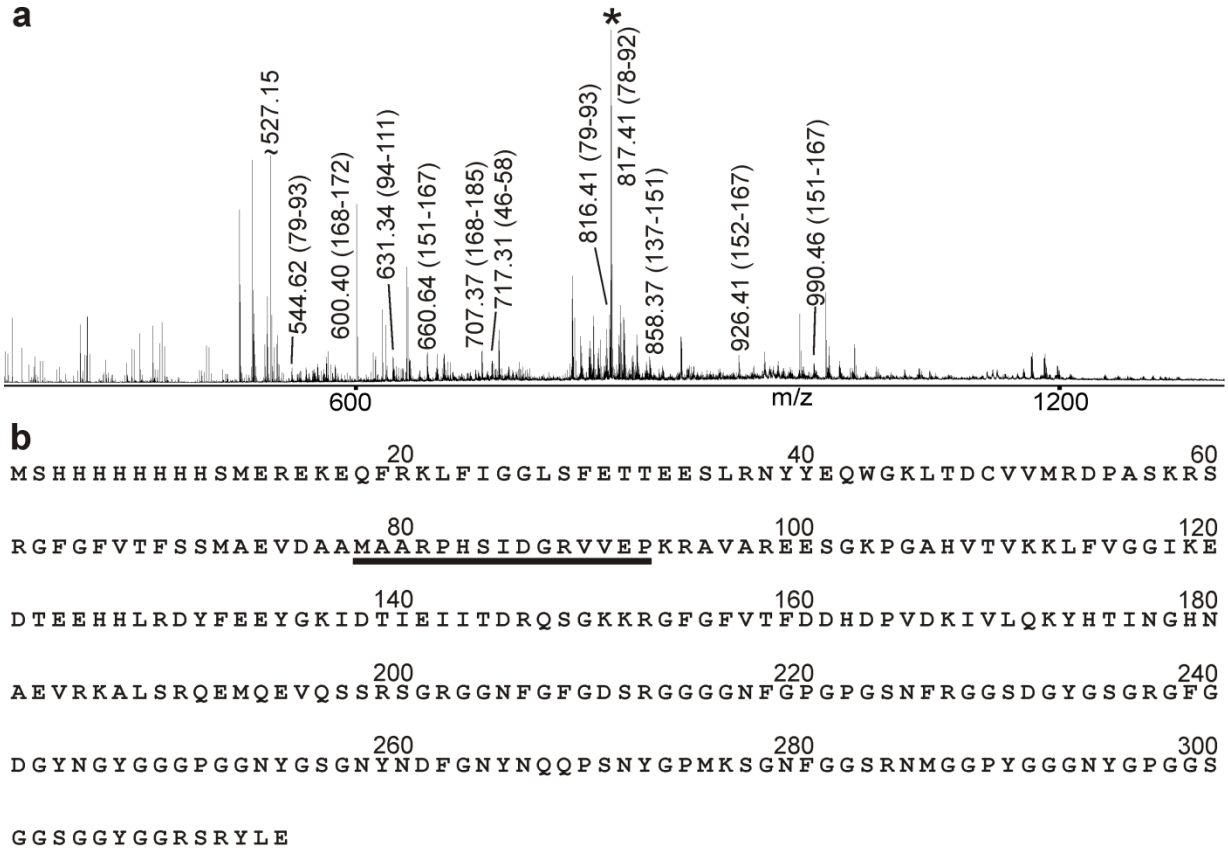

Figure S1: NanoESI mass spectrum of peptide mixture after in-solution digestion of His-RA33 antigen and amino acid sequence. **(a)** Ion signals from solution 1 at low TCE (2 V). Solvent: 200 mM ammonium acetate, pH 7.1. Selected ion signals are labeled with m/z values. Amino acid sequence ranges are indicated in parentheses. ✸: RA33 epitope peptide. Sequence coverage: 35 %. **(b)** Amino acid sequence of His-RA33 in single letter code. The epitope sequence for the antiRA33 antibody is underlined.

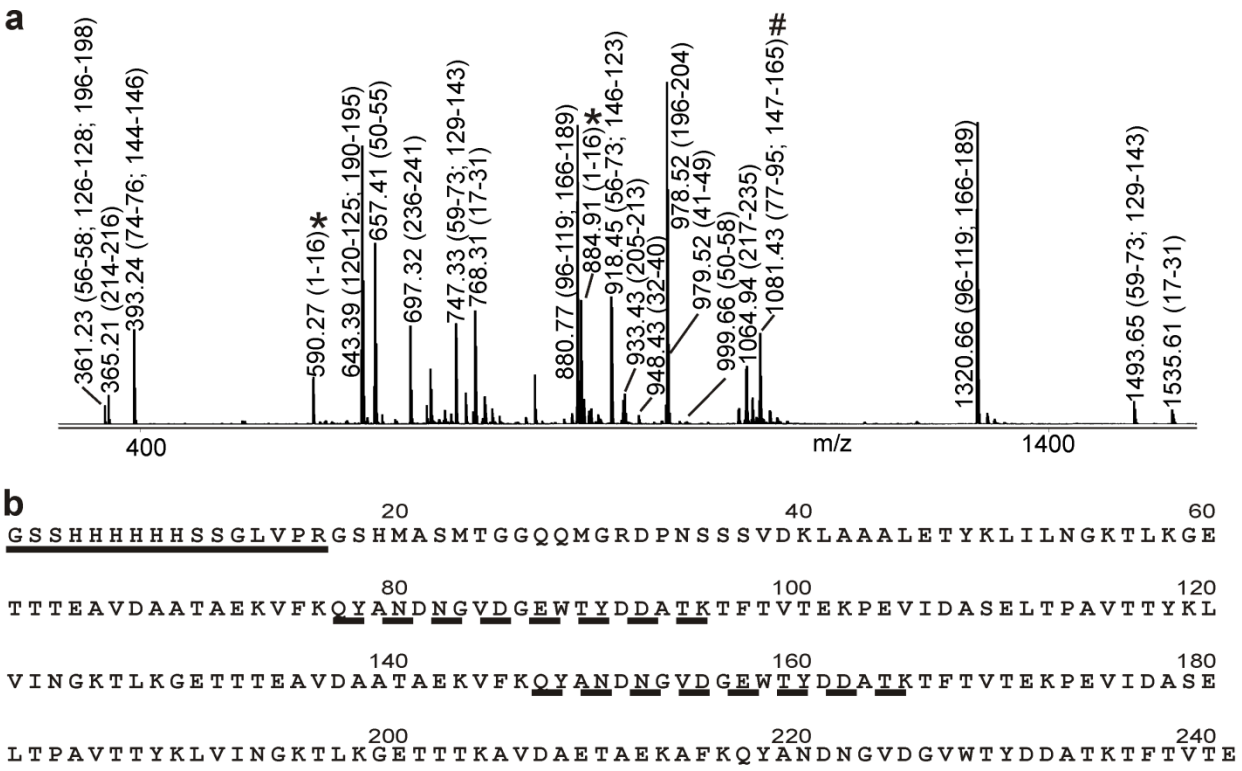

Figure S2: NanoESI mass spectrum of peptide mixture after in-solution digestion of protein G´e antigen and amino acid sequence. **(a)** Ion signals from solution 1 at low TCE (2 V). Solvent: 200 mM ammonium acetate, pH 7.1. Selected ion signals are labeled with m/z values. Amino acid sequence ranges are indicated in parentheses. ✱: His-tag epitope peptide. #: peptides that bind to the Fc part of an IgG1 antibody. Sequence coverage: 100 %. **(b)** Amino acid sequence of protein G´e in single letter code. The epitope sequence for the antiHis-tag antibody (solid line) and the sequences that bind to the Fc part of an IgG1 antibody (dashed lines) are underlined.

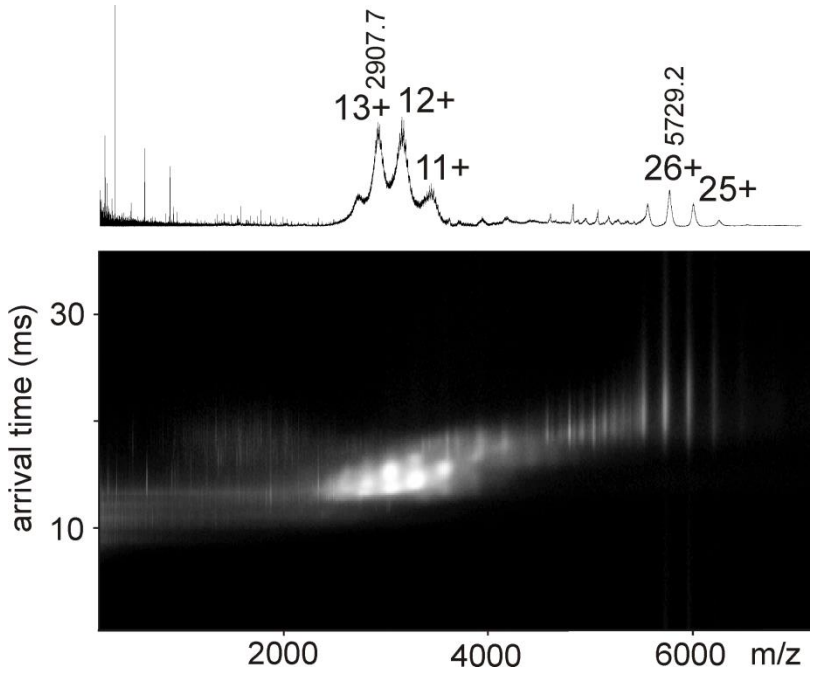

Figure S3: NanoESI mass spectrum and AToMZ plot of antiHis-tag antibody. **(a,b)** Ion signals from solution 2 at high TCE (120 V). Solvent: 200 mM ammonium acetate, pH 7.1.Selected multiply charged ion signals from the intact antibody and its fragments and/or contaminants are labeled (cf. Table S1).

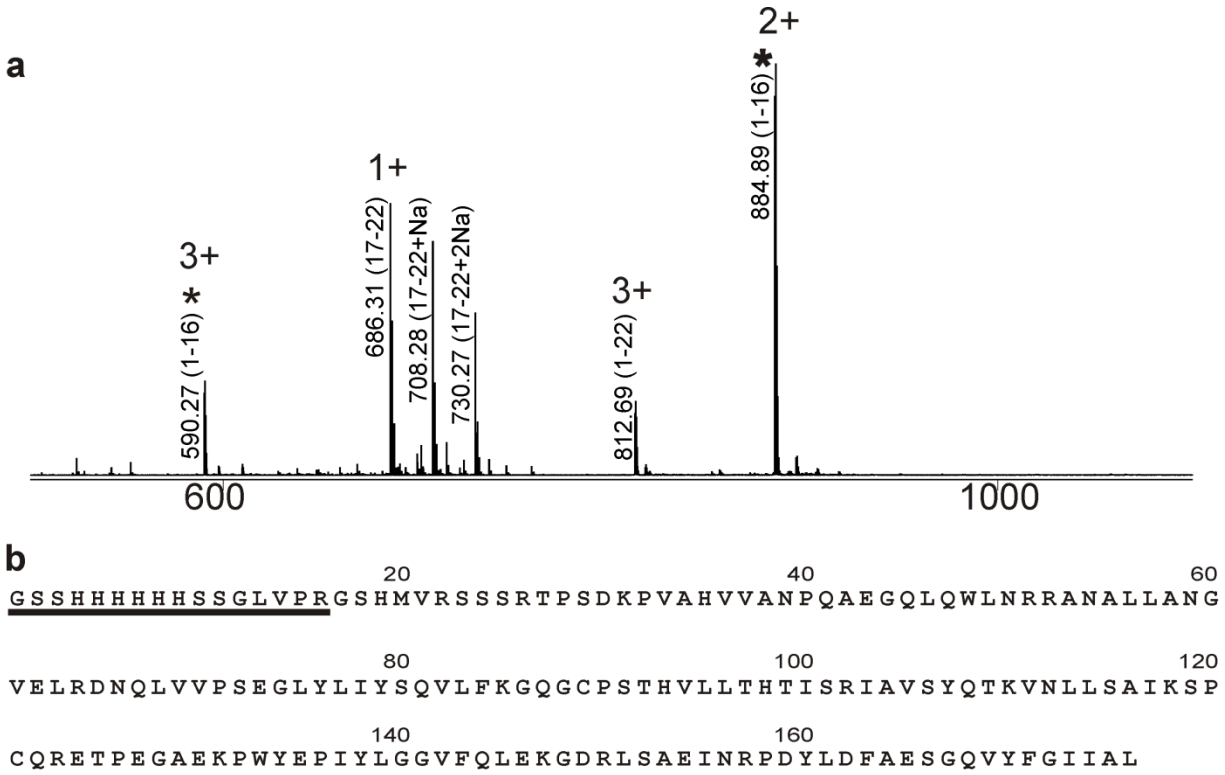

Figure S4: NanoESI mass spectrum of peptide mixture after in-solution digestion (epitope excision) of the immune complex consisting of the rhTNFα antigen and the anti-His-tag antibody. **(a)** Ion signals from solution 3 at low TCE (2 V). Solvent: 200 mM ammonium acetate, pH 7.1. Ion signals are labeled with m/z values. Amino acid sequence ranges are indicated in parentheses. ✱: His-tag epitope peptide. **(b)** Amino acid sequence of rhTNFα in single letter code. The epitope sequence for the antiHis-tag antibody is underlined.

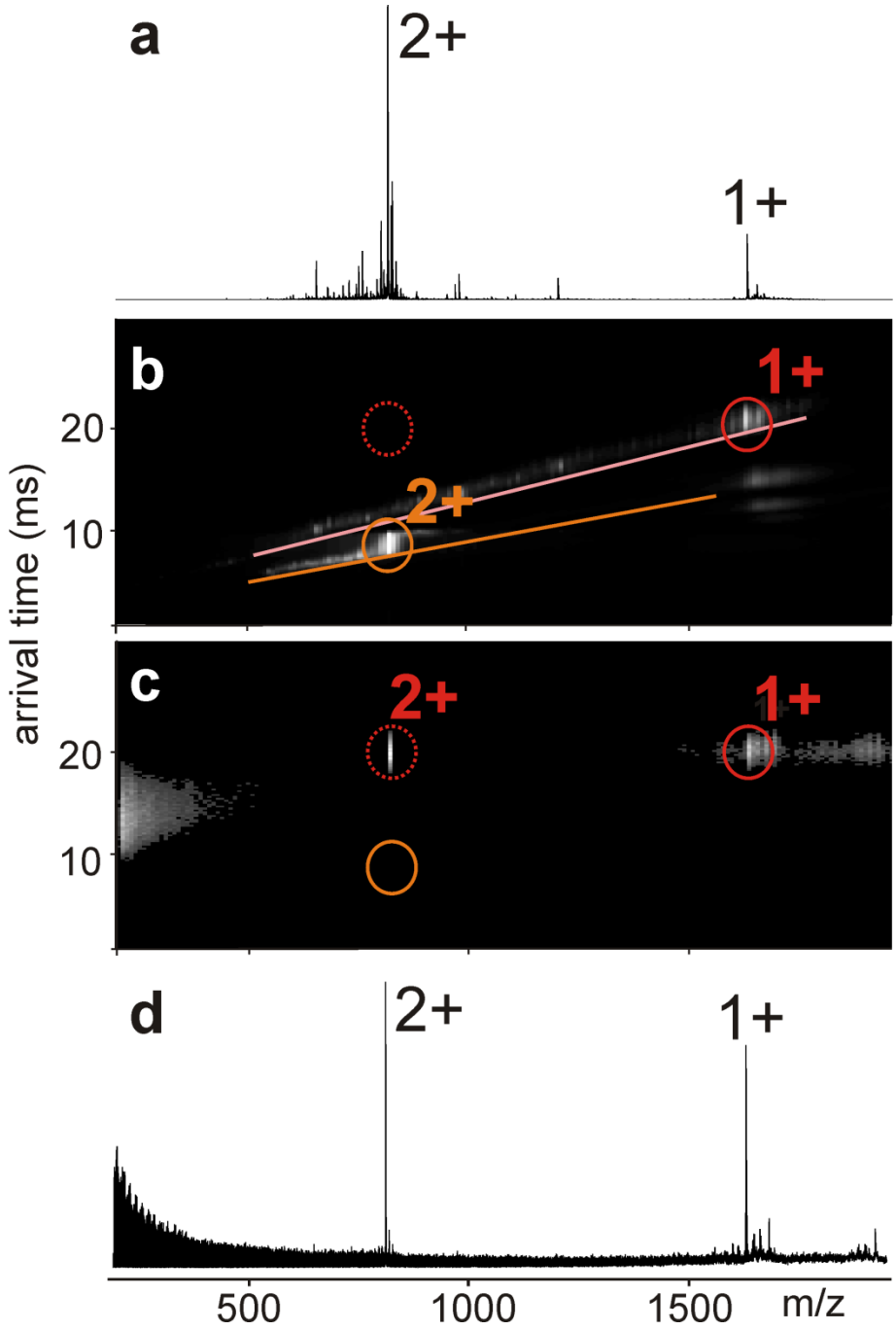

Figure S5: NanoESI mass spectra and AToMZ plots from the RA33 epitope peptide. **(a,b)** Ion signals from solution 3 at low TCE (2 V) and **(c,d)** at high TCE (220 V). Solvent: 200 mM ammonium acetate, pH 7.1. UBP positions are marked with orange solid line circles, CoRP positions with red dotted line circles. Charge states of selected UBPs and CoRPs are given. Trend lines of ions are emphasized by orange and light red lines. For m/z values of selected ion signals see Table 1.

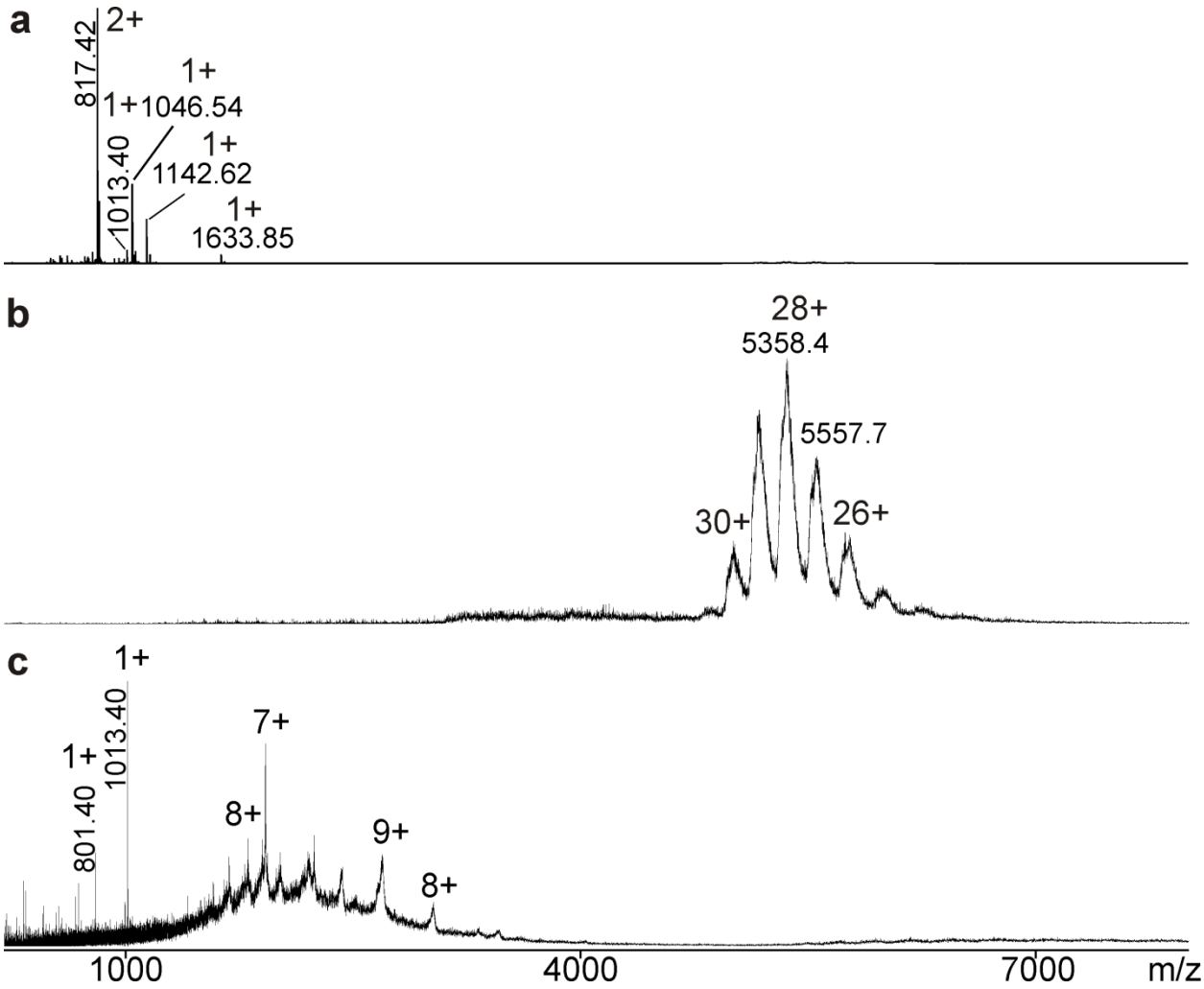

Figure S6: NanoESI mass spectra of a synthetic peptide mixture and the anti-FLAG M2 antibody. Ion signals from solution 1 **(a)** at low TCE (2 V). Ion signals from solution 3 **(b)** at low TCE (2 V) and **(c)** at high TCE (220 V). Solvent: 200 mM ammonium acetate, pH 7.1. The quadrupole profile in (a) was set to fully transmit all ions, in (b) and (c) it was set to block transmission of ions below m/z 3000. Selected ion signals are labeled with m/z values and charge states are given (cf. Table S1).

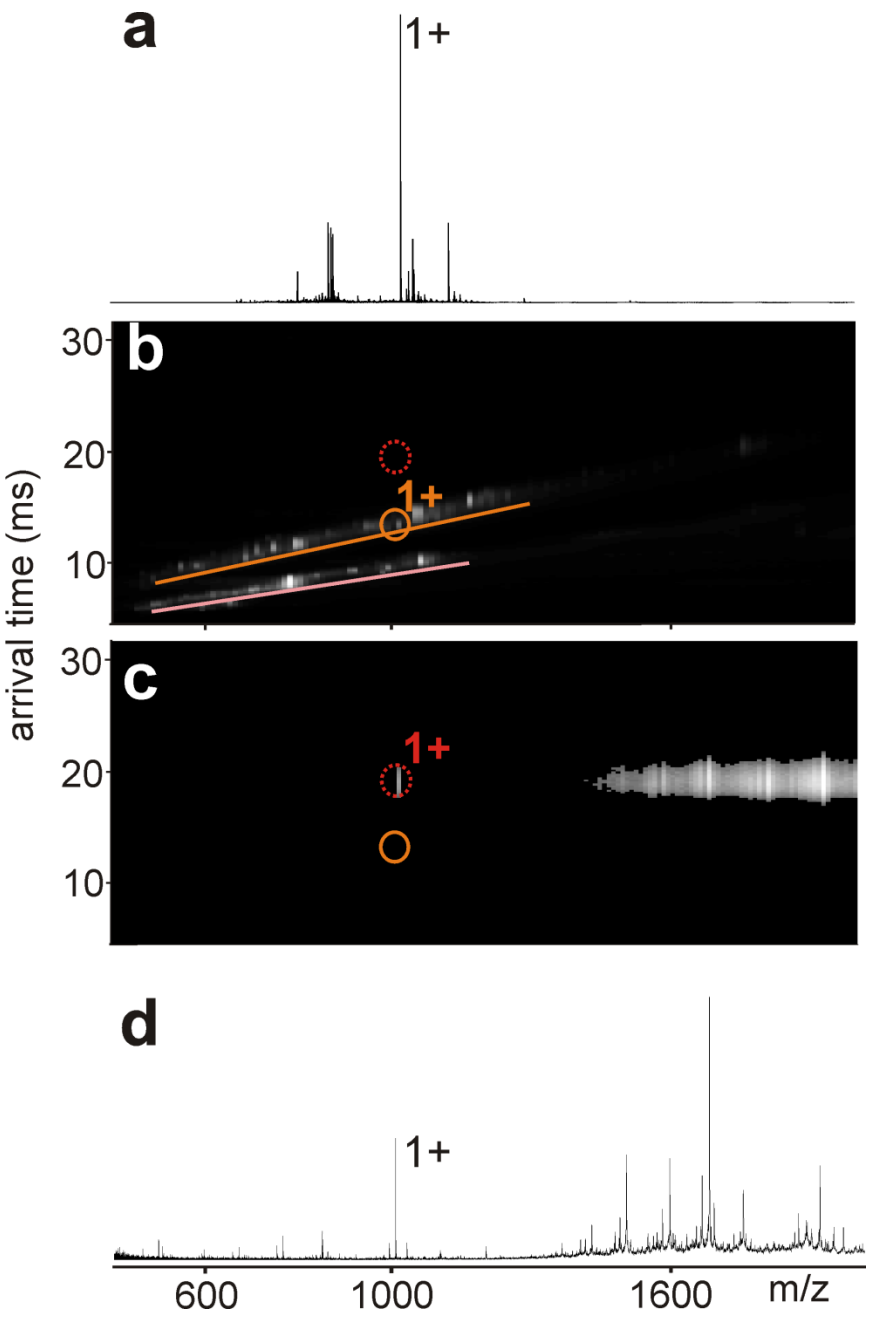

Figure S7: NanoESI mass spectra and AToMZ plots from the synthetic peptide mixture that includes the FLAG epitope peptide. **(a,b)** Ion signals from solution 3, i.e. in the presence of the antiFLAG antibody, at low TCE (2 V) and **(c,d)** at high TCE (220 V). Solvent: 200 mM ammonium acetate, pH 7.1. UBP positions are marked with orange solid line circles; CoRP positions with red dotted line circles. Charge states of selected UBPs and CoRPs are given. Trend lines of ions are emphasized by orange and light red lines. For m/z values of selected ion signals see Table 1.

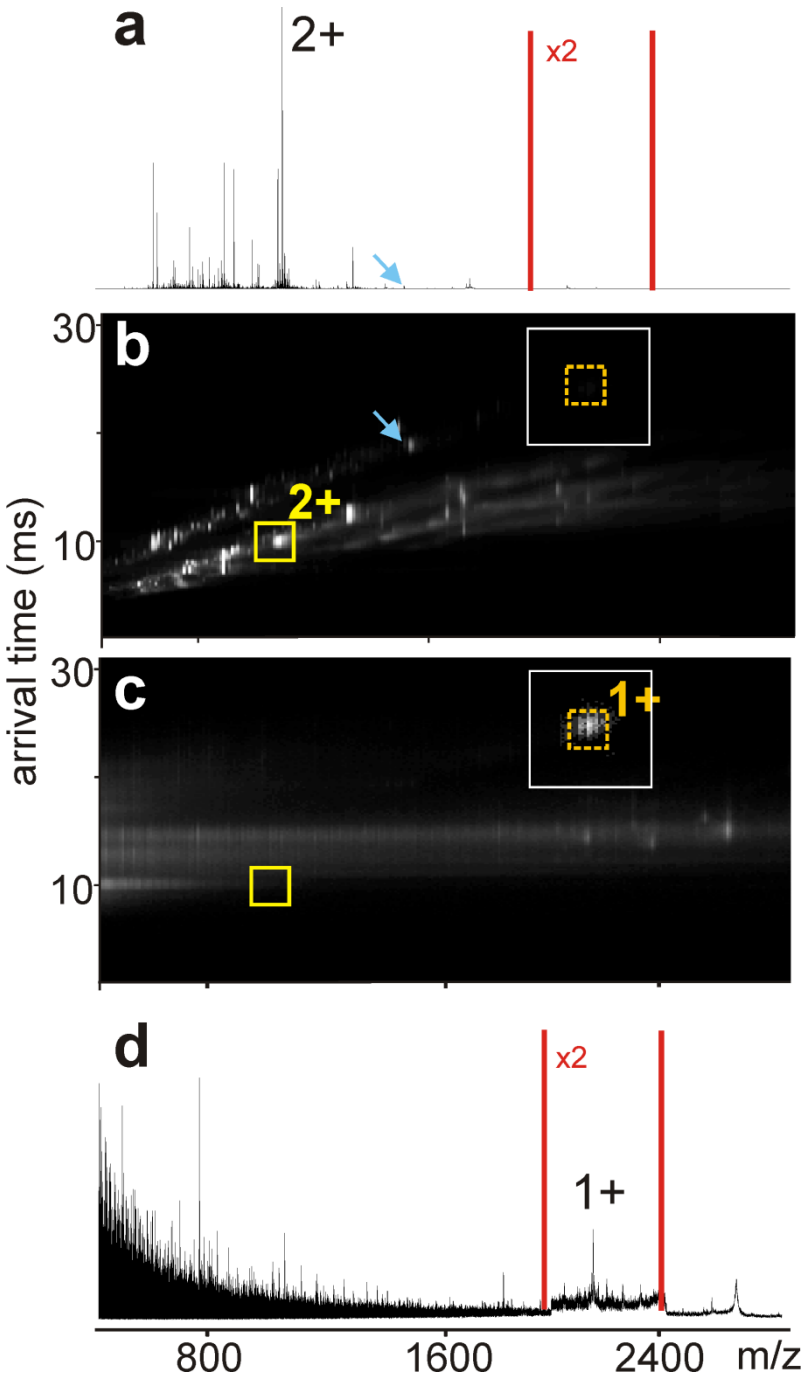

Figure S8: NanoESI mass spectra and AToMZ plots from the protein G´e peptides from in-solution digestion in the presence of antiFLAG-M2 antibody. **(a,b)** Ion signals from solution 3 at low TCE (2 V) and **(c,d)** at high TCE (220 V). Solvent: 200 mM ammonium acetate, pH 7.1. UBP positions are marked with orange solid line circles, CoRP positions with red dotted line circles. Charge states of selected UBPs and CoRPs are given. Contrast enhanced region is boxed; magnification factor is given. For m/z values of selected ion signals see Table 1.

2.2 Intact Transition Epitope Mapping - Targeted High-Energy Rupture of Extracted Epitopes (ITEM-THREE)

Intact Transition Epitope Mapping – Targeted High-Energy Rupture of Extracted Epitopes (ITEM-THREE)

Authors

Bright D. Danquah, Claudia Röwer, Kwabena F. M. Opuni, Reham El-Kased, David Frommholz, Harald Illges, Cornelia Koy, and Michael O. Glocker

Correspondence

michael.glocker@med.uni-rostock.de

Graphical Abstract

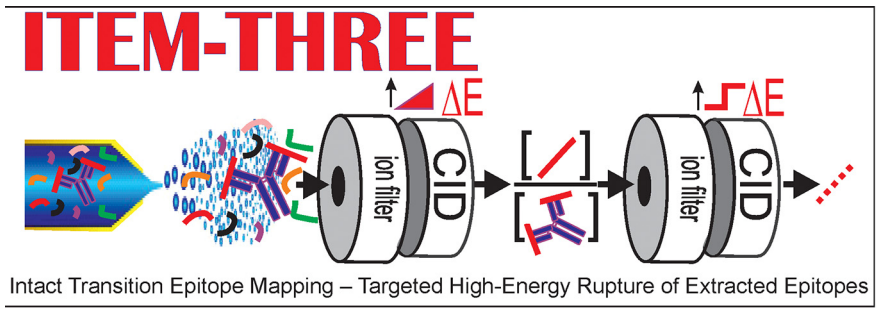

Intact Transition Epitope Mapping – Targeted High-Energy Rupture of Extracted Epitopes

In Brief

ITEM-THREE enables rapid epitope mapping. Sample consumption is minimized and in-solution handling reduced to mixing of antibody and antigen peptide solutions. After immune complex formation in solution, epitope mapping is performed in the gas phase using the mass spectrometer for sophisticated ion manipulation and filtering. Because amino acid sequence information is obtained from the epitope peptide, unknown antigens can be identified. Knowing the epitope broadens the application of antibodies to unspecified target proteins from any organism.

Highlights

- Multiplex epitope mapping/antigenic determinant identification in the gas phase.
- Intact transition and controlled dissociation of immune complexes by MS.
- Simultaneous identification and amino acid sequence determination of epitopes.
- Simplified in-solution sample handling because of ion manipulation and filtering by MS.

Danquah et al., 2019, Molecular & Cellular Proteomics *18*, 2–14

https://doi.org/10.1074/mcp.RA119.001429

Intact Transition Epitope Mapping – Targeted High-Energy Rupture of Extracted Epitopes (ITEM-THREE)*[S]

Bright D. Danquah‡, Claudia Röwer‡, Kwabena F. M. Opuni§, Reham El-Kased¶, David Frommholz‖, Harald Illges‖**, Cornelia Koy‡, and Michael O. Glocker‡‡

Epitope mapping, which is the identification of antigenic determinants, is essential for the design of novel antibody-based therapeutics and diagnostic tools. ITEM-THREE is a mass spectrometry-based epitope mapping method that can identify epitopes on antigens upon generating an immune complex in electrospray-compatible solutions by adding an antibody of interest to a mixture of peptides from which at least one holds the antibody's epitope. This mixture is nano-electrosprayed without purification. Identification of the epitope peptide is performed within a mass spectrometer that provides an ion mobility cell sandwiched in-between two collision cells and where this ion manipulation setup is flanked by a quadrupole mass analyzer on one side and a time-of-flight mass analyzer on the other side. In a stepwise fashion, immune-complex ions are separated from unbound peptide ions and dissociated to release epitope peptide ions. Immune complex-released peptide ions are separated from antibody ions and fragmented by collision induced dissociation. Epitope-containing peptide fragment ions are recorded, and mass lists are submitted to unsupervised data base search thereby retrieving both, the amino acid sequence of the epitope peptide and the originating antigen. ITEM-THREE was developed with antiTRIM21 and antiRA33 antibodies for which the epitopes were known, subjecting them to mixtures of synthetic peptides of which one contained the respective epitope. ITEM-THREE was then successfully tested with an enzymatic digest of His-tagged recombinant human β-actin and an antiHis-tag antibody, as well as with an enzymatic digest of recombinant human TNFα and an antiTNFα antibody whose epitope was previously unknown. ***Molecular & Cellular Proteomics 18: 2–14, 2019. DOI: 10.1074/mcp.RA119.001429.***

The identification of epitopes or antigenic determinants is essential for the design of novel antibody-based therapeutics and vaccines (1–4). With current personalized medicine concepts (4, 5), epitope mapping, *i.e.* accurate identification of antigenic determinants (epitopes) of protein antigens (6–8), is very useful in the design of novel antibody-based diagnostic tools, particularly for companion diagnostics (9, 10). Although structure-based methods, such as X-ray crystallography (11, 12) and NMR (13, 14) have been regarded as "gold standard" to map epitopes because they achieve atomic resolution, they are not always readily applicable because a given antigen-antibody pair may lie beyond the scope of either or both of these methods, *e.g.* when the immune complex is not crystallizable or is too large for NMR (15, 16). One great disadvantage of X-ray crystallography and NMR is that both require rather large sample amounts (17, 18).

By contrast, the relatively low amounts of samples required (19) and the rapidity (6) by which mass spectrometric epitope mapping is executed is of great advantage in this respect (20). Chemical cross-linking mass spectrometry (21, 22), hydrogen/deuterium exchange (HDX)[1] mass spectrometry (23) and mass spectrometric methods that employ chemical modification on proteins, such as Fast Photochemical Oxidation of Proteins (FPOP) (24, 25) or chemical modification of surface exposed residues (26, 27) have been applied in epitope mapping experiments (28) and in determinations of protein - protein interaction sites in general (29), but their application may be limited when rather demanding chemistries are involved, or when performing such experiments becomes laborious, and/or requires sophisticated laboratory equipment (20, 30). Significant advances in epitope mapping protocols/methods have been reached with the two most commonly used mass spectrometric methods: epitope extraction and epitope excision (20, 31, 32). These techniques have matured either through automation of solution handling procedures (33) or by minimizing in-solution handling, *i.e.* avoiding immobilization procedures and other chemical reactions (6, 34).

From the ‡Proteome Center Rostock, University Medicine Rostock, Rostock, Germany; §School of Pharmacy, University of Ghana, Legon, Ghana; ¶Microbiology and Immunology Faculty of Pharmacy, The British University in Egypt, Cairo, Egypt; ‖University of Applied Sciences Bonn-Rhein-Sieg, Immunology and Cell Biology, Rheinbach, Germany; **University of Applied Sciences Bonn-Rhein-Sieg, Institute for Functional Gene Analytics, Rheinbach, Germany

Received March 4, 2019, and in revised form, May 14, 2019
Published, MCP Papers in Press, May 30, 2019, DOI 10.1074/mcp.RA119.001429

Advanced mass spectrometer designs have led to increased flexibility by coupling various ion filtering devices with different mass analyzers, and have opened new opportunities for performing ion reactions, such as CID and SID (19, 35–39) in the gas phase and/or laser irradiation and UV irradiation of ions, respectively (36, 40, 41). The availability of mass spectrometers equipped with ion-mobility separation chambers provide an additional dimension for the separation of ions based on not only their *m/z* values but also on their shapes and sizes (42–44). This new generation of mass spectrometers led to the development of fast and easy to apply epitope mapping methods by which epitope peptides of an antibody of interest can be identified in a relatively simple and robust fashion (6, 20). Based on our gas phase epitope mapping strategy, termed ITEM-ONE (6), where epitopes of known antigens have been identified by precisely determining the mass of the extracted epitope peptide, we have now advanced to ITEM-THREE, where mass spectrometric amino acid sequencing of unknown epitope peptides is performed to identify an antigenic determinant on an antigen surface.

MATERIALS AND METHODS

Proteins and Peptides—Mouse antiRA33 antibody (monoclonal anti-hnRNP-A2/B1; clone DP3B3 lot: 044K4766) was obtained from Sigma-Aldrich (Steinheim, Germany). Rabbit antiTRIM21 antibody (polyclonal anti-52kDa Ro/SSA antibody; sc-20960 lot: F0503) raised against amino acids 141–280 of TRIM21 (52kDa Ro/SSA) of human origin was obtained from Santa Cruz Biotechnology, Inc. (Heidelberg, Germany). Mouse antiHis-tag antibody (monoclonal antibody MCA 1396; Batch no. 0309) was supplied by Bio-Rad, (Munich, Germany) and mouse antiTNFα antibody (monoclonal antibody; catalogue no. MA5-23720) was produced by ThermoFisher Scientific GmbH (Ulm, Germany). Recombinant human TNF alpha (rhTNFα) was a gift from Prof. Harald Illges, Hochschule Bonn-Rhein-Sieg University of Applied Sciences, Germany. Actin, cytoplasmic 1 recombinant protein was purchased from GenWay Biotech (Catalogue no. 10-288-23014F, San Diego, CA). RA33 peptide (MAARPHSIDGRVVEP-NH_2), GPI peptide (ALKPYSPGGPR), Angiotensin II (DRVYIHPF), TRIM21A peptide (LQELEKDEREQLRILGE), TRIM21B peptide (LQPLEKDEREQLRILGE) and TRIM21C peptide (LQELEKDEPEQLRILGE) were synthesized by Peptides and Elephants GmbH (Potsdam, Germany). The synthetic FLAG peptide (DYKDDDDK; article no. 020015) was obtained from ThermoFisher Scientific GmbH and sequencing grade, modified trypsin was obtained from Promega Corporation (Madison, WI).

Preparation of the Synthetic Peptide Mixture Solution (Solution 1)—A mixture of equimolar concentrations of seven synthetic peptides (10 μM each; GPI peptide, FLAG peptide, Angiotensin II, TRIM21A peptide, TRIM21B peptide, TRIM21C peptide, and RA33 peptide) was prepared by dissolving the appropriate amounts of the individual lyophilized peptide powders in freshly prepared 200 mM ammonium acetate, pH 7.1 and mixing the appropriate volumes. The peptide mixture-containing solution was shock-frozen and kept at −20 °C until either mass spectrometric analysis or immune complex formation were performed.

Tryptic Digestion of Recombinant Human Beta Actin (Solution 1)—Recombinant human beta actin (rhβactin) was digested with trypsin (26, 34, 45) using a modified Filter Aided Sample Preparation (FASP) protocol. To 10 μl of 200 mM DTT, dissolved in 0.1 M Tris/HCl containing 8 M urea was added 20 μl of rhβactin solution (protein concentration 1 μg/μl). This mixture was incubated at 37 °C for 30 min. Then, this solution was transferred into an equilibrated 30K Amicon centrifugal filter (equilibration with 1% formic acid according to protocol (46)) and 170 μl of 8 M urea in 0.1 M Tris/HCl, pH 8.5, were added and centrifuged at 13,000 rpm for 15 min. After discarding the filtrate, 150 μl of 8 M urea in 0.1 M Tris/HCl, pH 8.5, were added to the retentate in the filter unit and centrifuged again at 13,000 rpm for 15 min. A further wash of the retentate was done by adding 100 μl of 8 M urea in 0.1 M Tris/HCl, pH 8.5, to the filter unit and centrifuging at 13,000 rpm for 12 min. The filtrates were discarded and the retentate was further washed for three times, first by adding 100 μl, then 75 μl, and lastly 50 μl of 50 mM ammonium bicarbonate solution, pH 8.6, and each time centrifugation was performed at 13,000 rpm for 10 min, 12,000 rpm for 8 min, and 12,000 rpm for 6 min, respectively. After the three washings, the filter unit containing the retentate (ca. 5 μl) was transferred into a new collection tube. A volume of 35 μl of 11.42 ng/μl of trypsin in 50 mM ammonium bicarbonate, pH 8.6, was added to the protein that was dissolved in the solution on the filter unit to obtain an enzyme/substrate ratio of 1:50 (w/w). The mixture was incubated at room temperature in a wet chamber for 16 h and then centrifuged at 8000 rpm for 5 min and at 12,000 rpm for 3 min. Next, a volume of 40 μl of 10 mM ammonium bicarbonate, pH 8.6, and a further amount of 4 μl of 0.1 μg/μl trypsin solution (composition see above) was added and incubated at 37 °C for 2 h. Finally, the mixture was centrifuged at 12,000 rpm for 8 min and the filtrate (ca. 80 μl), which contained the tryptic peptides, was collected for further analysis. The peptide concentration of the solution was determined using the Qubit® 2.0 Fluorometer (Carlsbad, CA), following described procedures (6, 47). Aliquots (10 μl, each), were shock-frozen and kept at −20 °C until either mass spectrometric analysis or immune complex formation were performed.

Tryptic Digestion of Recombinant Human TNF Alpha (Solution 1)—Tryptic digestion of recombinant human TNF alpha (26, 34, 45) (rhTNFα, 1 μg/μl) was performed by adding 15 μl of the rhTNFα dissolved in 200 mM ammonium acetate, pH 7.1, to 32 μl of trypsin solution (9.4 ng/μl in 4.8 mM Tris/HCl with 5 mM DTT) to yield an enzyme/substrate ratio of 1:50 (w/w). This mixture was incubated at 37 °C for 20 h. The resulting tryptic peptide solution was divided into nine aliquots, each of which contained a volume of 5 μl. Each aliquot was desalted by loading the entire 5 μl volume onto one C18 ZipTip Pipette Tip (Merck Millipore Ltd, Tullagreen, Carrigtwohill, Co. Cork, Ireland) that had been wetted with a mixture of deionized H_2O/ACN (50:50, v/v). Equilibration and washing solutions consisted of 1% HCOOH in deionized H_2O; two times 10 μl were used for each step. The affinity-bound peptides were eluted into 5 μl of 1% HCOOH in H_2O : 1% HCOOH in ACN (50:50, v/v) (46, 48). Next, all nine desalted portions of the tryptic peptide-containing solutions were pooled to obtain a total volume of 45 μl. This solution was aliquoted into 10 μl volumes, shock-frozen and kept at −20 °C until either mass spectrometric analysis or immune complex formation were performed.

Preparation of Antibody Solutions (Solution 2)—As described previously (6), a volume of 30 μl of 0.8 μg/μl of antiRA33 antibody solution was loaded onto a 50K Amicon centrifugal filter (Merck Millipore Ltd, Tullagreen, Carrigtwohill, Co. Cork, Ireland) and 470 μl of 200 mM ammonium acetate, pH 7.1, was added. The resulting

[1] The abbreviations used are: HDX, hydrogen deuterium exchange; Nano-ESI, nano-electrospray ionization; IMS, ion mobility separation; ToF, time of flight; CID, collision induced dissociation; ΔCV, collision cell voltage difference; UBPs, unbound peptide ions; CoRPs, complex-released peptide ions; BLAST, basic local alignment search tool.

solution was centrifuged at 13,000 rpm for 10 min for eight times. Each time the filtrates were discarded and 470 μl of 200 mM ammonium acetate, pH 7.1, were added to the retentates. After the last centrifugation the filter units were inverted and placed into new tubes and centrifuged at 4500 rpm for 5 min to collect the retentates of ca. 20 μl antibody solution in each case. Protein concentrations were determined using the Qubit® 2.0 Fluorometer following described procedures (6). Similarly, 100 μl of 0.2 μg/μl of antiTRIM21 antibody solution, 20 μl of 1.0 μg/μl antiHis-tag antibody solution, and 40 μl of 0.5 μg/μl of antiTNFα antibody solution, which were all obtained from suppliers in PBS buffer, were buffer exchanged into 200 mM ammonium acetate buffer, pH 7.1.

Preparation of Immune Complex-containing Solutions (Solution 3)—For immune complex formation, a final concentration of ca. 0.2 μg/μl of each antibody-containing solution (solution 2) was prepared by diluting the solutions obtained from the buffer exchange with 200 mM ammonium acetate, pH 7.1. Solutions 3 were binary mixtures of one Solution 1 with one Solution 2 to obtain the molar ratios of ~2.2:1 (epitope peptide/antibody) in each of Solutions 3. Immune complex-containing mixtures (Solutions 3) were incubated at room temperature for at least 1 h.

NanoESI-IMS-MS/MS Instrument Settings and Spray Needle Preparation—NanoESI-IMS-MS/MS measurements were carried out in positive ion mode on a quadrupole ion-mobility separation time-of-flight mass spectrometer (Synapt G2-S, Waters MS-Technologies, Manchester, United Kingdom) as described (6). The *m/z* range 200–8000 of the time-of-flight analyzer was calibrated externally using a 1 mg/ml sodium iodide solution dissolved in an isopropanol/water mixture (50:50, v/v). Measurements were performed with the following instrumental settings; source temperature, 50 °C; capillary voltage, 1.60–1.90 kV; source offset, 80–100 V; sample cone voltage, 90–120 V; TRAP cell gas flow, 6.0 ml/min; cone gas flow, 100 liters/h. Gas controls were set to automatic as follows: TRAP cell gas flow, 2.0 ml/min; helium cell gas flow, 180 ml/min; IMS cell gas flow, 90 ml/min. IMS wave velocity and wave height were manually set to 650 m/s and 40 V, respectively. Start wave height and end wave height were also optimized with 30–35 V and 20–25 V, respectively, for each experiment to obtain adequate ion mobility separation. Pusher width and pusher cycle times were both set to automatic. Scan duration of 1.0 s and inter scan delay of 0.015 s were set for both IMS and MS measurements. Reflectron grid, flight tube and reflectron voltages were 1.46 kV, 10.00 kV and 3.78 kV, respectively, and detector sensitivity was set to normal. Pressure settings within the various parts of the mass spectrometer were as follows: TRAP cell, $\sim 2.2 \times 10^{-2}$ mbar; Helium cell, $\sim 1.35 \times 10^{3}$ mbar; IMS cell, $\sim 3.5 \times 10^{0}$ mbar; TRANSFER cell, $\sim 2.6 \times 10^{-2}$ mbar; ToF analyzer, $\sim 8.0 \times 10^{-7}$ mbar. Spray needles were prepared in-house from borosilicate glass tubes of 1 mm outer and 0.5 mm inner diameters with a P-1000 Flaming/Brown™ Micropipette Puller System (Sutter Instruments, Novato, CA, USA) followed by gold coating, applying the Sputter Coater SCD 005 (BAL-TEC Inc., Balzers, Liechtenstein) (6, 47).

NanoESI-IMS-MS/MS Measurements for Epitope Mapping—To perform ITEM-THREE experiments, solutions 3 (ca. 3 μl, each) were loaded into spray needles with the aid of 20 μl microloader pipette tips (Eppendorf AG, Hamburg, Germany) and were electrosprayed without any purification. In the mass spectrometer, the quadrupole analyzer was first used to block transmission of lower molecular weight ions (filter off ions below *m/z* 5000) by manually setting the quadrupole appropriately (6). The epitope peptide-antibody complexes were able to transit the quadrupole intact. Next, dissociation of the epitope peptide-antibody complexes in the TRAP cell (first collision cell) was achieved by increasing the collision cell voltage difference (ΔCV) to between 50 and 80 V. The collision voltage differences in the TRAP cell were raised in a stepwise manner (5–20 V/step) and were so optimized for each experiment to ensure adequate dissociation of the antibody - peptide complex with minimal antibody fragmentation. The dissociated complex constituents then entered the ion mobility chamber where they were separated according to their *m/z* values, sizes and shapes. Finally, the collision cell voltage differences (ΔCV) in the TRANSFER cell (second collision cell) were also increased to 40–70 V to cause enough fragmentation of the complex released peptides (CoRPs). Again, the collision voltage differences in the TRANSFER cell were raised in a stepwise manner (5–20 V/step) to adjust optimized peptide ion fragmentation conditions for each experiment. Both ion mobility raw data (arrival time of ions) and mass spectral raw data were collected and stored using MassLynx software 4.1 (Waters MS-Technologies). The mass spectrometry data have been deposited in the PRIDE database (49).

Mascot Database Search with MS/MS Fragment Ions—After selecting the arrival time of the released epitope peptide ion, raw data from an MS/MS spectrum were de-convoluted and de-isotoped and then converted into peak lists using the MaxEnt3 algorithm on the MassLynx version 4.1 software. The peak list was then saved as a SEQUEST file (*.DTA) that was then uploaded onto the Mascot (Matrix Science Ltd., London, UK) search engine (50, 51), using the UniProt database (release 2018_06) that contained 557,713 sequences and an "amended UniProt" database that was generated to contain the amino acid sequences of the recombinant antigens in addition to all the amino acid sequence entries of the UniProt database (release 2018_06). The search parameters were set as follows: taxonomy, all entries; enzyme, none or trypsin (where tryptic digests were used), and up to 1 missed cleavage was allowed. Fixed modifications, carbamidomethylation of cysteine, and variable modifications, dicarbamidomethylation of lysine, were selected where necessary. Peptide mass tolerance and MS/MS ion mass tolerance were both set to 0.3 Da. Threshold ion scores were used in accepting the individual spectra. The ion scores above these thresholds indicated amino acid sequence with significant homology to the sequence entries from the data base.

NCBI BLAST of Identified Epitope Peptides—The amino acid sequence of the first hit from the Mascot search (epitope peptide) was submitted to an NCBI BLAST search using the following parameters: database, Uniprot (release 2018_06); organisms, all; max target sequence, 250; expect threshold, 2000; matrix PAM50 (52).

RESULTS

Method Development—

Immune Complex Formation and Epitope Identification for the antiRA33 Antibody—On electrospraying a peptide mixture that consists of seven synthetic peptides dissolved in aqueous ammonium acetate (solution 1) and operating the mass spectrometer in positive ion and ion mobility separation modes, the arrival times of the peptide ions at the end of the ion mobility separation chamber were recorded between 4 ms and 14 ms, respectively. The mass spectrum showed all ion signals from this arrival time regime as mainly singly and doubly charged ion signals within the mass range between *m/z* 300 and *m/z* 1600 (Fig. 1*A*–1*B*). In addition, fragment ions from the FLAG peptide and the GPI peptide were recorded as well (supplemental Table S1), despite low voltage differences (ca. 2 V to 4 V) in both, the TRAP cell that is the first collision cell located behind the quadrupole but in front of the ion mobility separation chamber, and the TRANSFER cell, which is the second collision cell, located behind the ion mobility

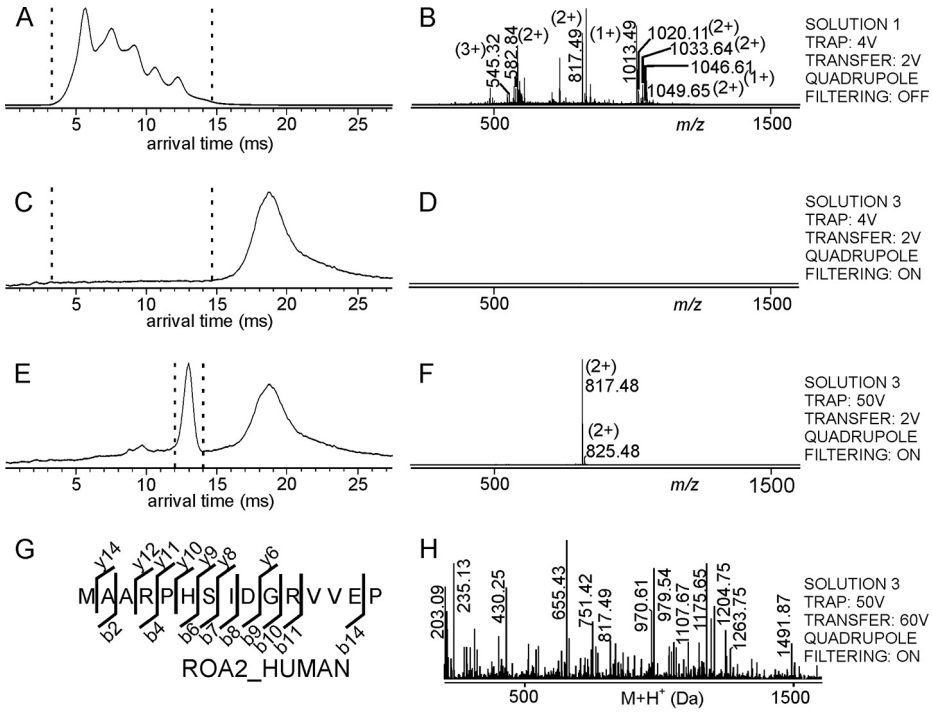

FIG. 1. **Mass spectrometric dissociation of the RA33 epitope peptide – antiRA33 antibody complex and amino acid sequence determination of the complex-released peptide by mass spectrometric fragmentation.** Ion mobility arrival time plots of *A*, Solution 1, *C*, and *E*, Solution 3. Dashed lines mark the regions for mass spectra selections. Settings of the TRAP cell, the TRANSFER cell, and the quadrupole are indicated at the right. *B*, *D*, and *F*, nanoESI mass spectra (low *m/z* range) of ions from selected arrival time ranges. Selected *m/z* values are given and charge states are indicated in parentheses. For ion signal assignments see supplemental Table S1. *G*, Amino acid sequence of the complex-released peptide (single letter code) as determined by the matched mass spectrometric fragment ions (fragment ion types and numbers are indicated). The Uniprot protein ID of the peptide source protein (first hit) is shown. *H*, Pseudo mass spectrum (after charge deconvolution and de-isotoping) of fragment ions derived by selecting arrival time of the complex-released peptide with *m/z* 817.48. For ion signal assignments see supplemental Table S2.

separation chamber but in front of the ToF analyzer. As expected, in later arrival time regimes, *i.e.* above 16 ms, the mass spectrum of this peptide mixture did not show any ion signals (supplemental Fig. S1*A*–S1*B*).

Adding the antiRA33 antibody (solution 2) to the synthetic peptide mixture (solution 1) produced solution 3 in which formation of the immune complex occurred, consisting of RA33 epitope peptide and antiRA33 antibody. Electrospraying solution 3 and setting the quadrupole to block transmission of ions with *m/z* values below *m/z* 5000, only the intact immune complex ions as well as free antibody ions were able to traverse the quadrupole ion filter. The high molecular weight components of solution 3 produced multiply charged ions, ranging from 24+ to 30+ charge states, which all appeared above *m/z* 5000 (supplemental Fig. S1*C*–S1*D*, cf. supplemental Table S3). All these multiply charged ion signals were recorded with arrival times between 16 ms and 22 ms at the end of the ion mobility separation chamber (Fig. 1*C*). On looking at the arrival time regime where the unbound peptide ions (UBPs) were expected to reach the end of the ion mobility separation chamber (4 ms to 14 ms), there appeared no peptide ion signals within the mass range of *m/z* 300 to *m/z* 1600 (Fig. 1*D*).

However, when higher collision cell voltage differences (50 V) were applied in the TRAP cell, collision of the immune complex ions with argon gas atoms caused dissociation of singly and/or doubly charged peptide ions from the multiply charged immune complex ions. The complex-released peptide ions (CoRPs) were detected with arrival times of around 13 ms and the corresponding arrival time-matched mass spectrum showed doubly charged ions at *m/z* 817.48 and at *m/z* 825.48 for the RA33 epitope peptide and its oxygenated product, both with mass accuracies of 61 ppm (Fig. 1*E*–1*F*). Obviously, after intact transition into the gas phase, the respective multiply charged immune complex ions traversed the quadrupole mass filter while the quadrupole effectively blocked transmission of all UBPs (Fig. 1*C*–1*D*).

Next, the collision cell voltage difference in the TRANSFER cell was increased to 60 V to fragment (rupture) the CoRPs, which had been generated in the TRAP cell. Thus, at high collision cell voltage differences in both the TRAP cell (50 V) and the TRANSFER cell (60 V) fragment ions of the RA33 epitope peptide were recorded with the same arrival times (ca. 13 ms) as the precursor CoRP ions (Fig. 1*H*). Additionally, when high collision cell voltage differences in both collision cells are applied, multiply charged antibody fragment ions

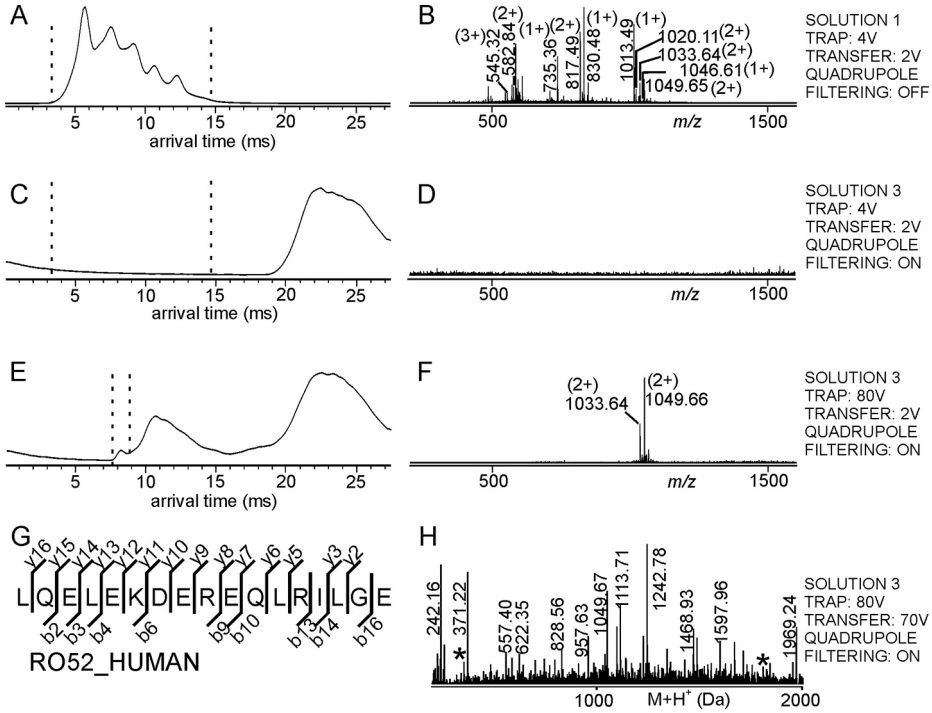

FIG. 2. **Mass spectrometric dissociation of the TRIM21 epitope peptide – antiTRIM21 antibody complex and amino acid sequence determination of the complex-released peptides by mass spectrometric fragmentation.** Ion mobility arrival time plots of *A*, Solution 1, *C*, and *E*, Solution 3. Dashed lines mark the regions for mass spectra selections. Settings of the TRAP cell, the TRANSFER cell, and the quadrupole are indicated at the right. *B*, *D*, and *F*, nanoESI mass spectra (low *m/z* range) of ions from selected arrival time ranges. Selected *m/z* values are given, and charge states are indicated in parentheses. For ion signal assignments see supplemental Table S1. *G*, Amino acid sequence of the complex-released peptide (single letter code) as determined by the matched mass spectrometric fragment ions (fragment ion types and numbers are indicated). The Uniprot protein ID of the peptide source protein (first hit) is shown. *H*, Pseudo mass spectrum (after charge deconvolution and de-isotoping) of fragment ions derived by selecting arrival time of the complex-released peptide with *m/z* 1049.66. The " " marks ions that belong to the peptide with ion signal at *m/z* 1033.64. For ion signal assignments see supplemental Tables S4 and S5.

appeared at around *m/z* 2000 with arrival times similar to those of the intact immune complex ions and/or the ions of the free antibody (supplemental Fig. S1*E*–S1*F*).

After processing the raw data from the CoRP fragment ion mass spectra by de-isotoping and deconvolution of charge states, and after submitting the list of fragment ions to data base search using the Mascot search engine, the best hit from the search result reported the amino acid sequence of the RA33 peptide (Fig. 1*G*). In addition to *b*-type and *y*-type ions, some *b*-type and *y*-type ions that had lost ammonia were identified as well (supplemental Table S2). The best hit reported a score of 43 (threshold 34), indicating that the determined amino acid sequence had a significant homology to the sequence entry from the data base. In addition to the amino acid sequence the data base entry revealed the name of the originating protein, hence the antigen.

Although the CoRPs, *i.e.* epitope peptides, which had been generated in the TRAP cell could be identified with high mass accuracies by comparing their monoisotopic masses to the known masses of all the peptides in the peptide mixture (solution 1), fragmenting the CoRP ions by increasing the collision cell voltage difference in the TRANSFER cell enabled experimental determination of the respective partial amino acid sequence on data base search, thereby substantiating epitope identification.

Immune Complex Formation and Epitope Identification for the antiTRIM21 Antibody—To further test our ITEM-THREE workflow an antiTRIM21 antibody (solution 2) was added to the mixture of synthetic peptides (solution 1), thereby obtaining TRIM21 epitope peptide - antiTRIM21 antibody complexes in solution 3. As before, the arrival times of the peptide ions at the end of the ion mobility separation chamber were recorded between 4 ms and 14 ms, respectively. The mass spectrum showed all ion signals from this arrival time regime as mainly singly and doubly charged ion signals within the mass range between *m/z* 300 and *m/z* 1600 (Fig. 2*A*–2*B*). Again, and as expected, the mass spectrum of this peptide mixture did not show any ion signals in later arrival time regimes, *i.e.* above 16 ms (supplemental Fig. S2*A*–S2*B*).

Electrospraying solution 3 and setting the quadrupole to block transmission of ions below *m/z* 5000, only the multiply charged ions of the intact immune complex and of the free antibody traversed the quadrupole and the ion mobility separation chamber with arrival times of between 19 ms and 28 ms (Fig. 2*C*). Like before, within the time regime at which the peptides' arrivals at the end of the ion mobility separation

chamber were expected (4 ms to 14 ms), no peptide ion signals were seen in the mass range below *m/z* 1600 (Fig. 2*D*).

However, contrary to the case of antiRA33 antibody-RA33 epitope peptide complex, the mass spectrum that covered the arrival time range of 19 ms to 28 ms of the TRIM21 epitope peptide - antiTRIM21 antibody complex showed the presence of unresolved antiTRIM21 antibody together with TRIM21 epitope peptide-antiTRIM21 antibody complex ion signals at above *m/z* 5000. Their charge states ranged from 23+ to 28+ (supplemental Fig. S2*C*–S2*D*, cf. supplemental Table S6). Despite the unresolved multiply charged ion signals, this result repeatedly showed that the quadrupole was effectively filtering off UBPs.

On raising the TRAP cell voltage difference to 80 V and looking at the mass spectra that matched to the arrival times of CoRPs, in this case approx. 8 ms (Fig. 2*E*–2*F*), there appeared two doubly charged peptides, one at *m/z* 1049.66 and one at *m/z* 1033.64. By comparing the monoisotopic masses of these ions to the masses of the peptide ions that were contained in the peptide mixture (solution 1), the ion signal at *m/z* 1049.66 was assigned to the TRIM21A peptide with a mass accuracy of 85 ppm. Likewise, the ion signal at *m/z* 1033.64 was assigned to the TRIM21B peptide with a mass accuracy of 68 ppm (cf. supplemental Table S1). It is worth noting that the TRIM21C peptide, which was a constituent of the peptide mixture (solution 1) had not bound to the antiTRIM21 antibody and, hence, did not show up as a CoRP but remained a UBP.

When the TRANSFER cell voltage difference was increased to 70 V, both doubly charged precursor CoRP ions were simultaneously fragmented. The respective fragment ion spectrum that corresponded to the arrival time of the doubly charged precursor ions (ca. 8 ms) showed a mixture of the fragment ions. On performing data base search with the deconvoluted and de-isotoped fragment mass list, only the TRIM21A peptide sequence was reported as best hit with a score of 46 (threshold 37; Fig. 2*G*–2*H*, cf. supplemental Table S4), because only the wild type epitope peptide sequence was included in the Uniprot database. The TRIM21B peptide was identified (score 27; threshold 35) when repeating the data base search and applying the amended Uniprot database that contained the manually added amino acid sequence with the respective amino acid exchange (Fig. 2*H*, cf. supplemental Table S5). For the TRIM21A peptide both, *b*-type and *y*-type ions were assigned. Additionally, ion signals were observed for *b*-type and *y*-type fragment ions that had lost ammonia or water (supplemental Table S4). For the TRIM21B peptide barely *b*-type ions with loss of ammonia or water were seen (supplemental Table S5).

The mass spectra that were recorded at high collision cell energies in both, the TRAP cell and the TRANSFER cell, and selection of arrival times from 19 ms to 28 ms, where the multiply charged ion signals of unresolved TRIM21 epitope peptide - antiTRIM21 antibody immune complexes and free antibody had appeared, showed in addition to these ion signals the presence of multiply charged antibody fragment ions (supplemental Fig. S2*E*–S2*F*, cf. supplemental Table S6). To unequivocally assign antibody fragment ion signals we performed control experiments by individually electrospraying the antibody solutions (solutions 2), one after the other, under the same fragmentation conditions for comparisons (data not shown).

Application Examples—

*Immune Complex Formation and Epitope Identification for the antiHis-tag Antibody—*As a first application example, we performed our ITEM-THREE method to identify a His-tag epitope peptide from the 6-times histidine tagged recombinant human beta actin (rhβactin) using an antiHis-tag antibody. To generate solution 1 an in-solution tryptic digestion of the His-tagged rhβactin was performed. The arrival times of the tryptic peptide ions from solution 1, after traversing the quadrupole and the ion mobility separation chamber, ranged from 4 ms to 14 ms when measured at low collision cell voltage differences in both, the TRAP cell (4V) and the TRANSFER cell (2V). The corresponding mass spectrum showed ion signals below *m/z* 1600, which covered 55% of the amino acid sequence of the full length rhβactin (Fig. 3*A*–3*B*, cf. supplemental Fig. S5, supplemental Table S7). However, none of the peptide masses from the mass spectrum could be assigned to the C-terminal tryptic peptide, which contained the His-tag. In the mass range above *m/z* 5000, there were no ion signals present (supplemental Fig. S4*A*–S4*B*).

The antiHis-tag antibody (solution 2) was added to solution 1 and the mixture (solution 3) was electrosprayed without any further purification after an incubation period of 1 h at room temperature. When analyzing solution 3 at low collision cell voltage differences in both the TRAP cell and the TRANSFER cell and with setting the quadrupole to block transmission of UBPs, no ion signals appeared in the mass spectrum below *m/z* 1600 (Fig. 3*C*–3*D*). In the mass range above *m/z* 5000 multiply charged ion signals of unresolved antiHis-tag antibody and His-tag peptide-anti-Histag antiHis-tag antibody complex were recorded with charge states ranging from 22+ to 27+ (supplemental Fig. S4*C*–S4*D*, cf. supplemental Table S10).

After raising the collision cell voltage difference to 50 V in the TRAP cell, there appeared a doubly charged CoRP ion signal at *m/z* 695.82 with an arrival time of around 11 ms (Fig. 3*E*–3*F*). Surprisingly, the mass of this ion signal did not match to any of the predicted tryptic peptide masses from rhβactin. With an additional high collision cell voltage difference (40 V) in the TRANSFER cell, we were able to obtain the fragment ions of the corresponding CoRP, *i.e.* the peptide that was pulled out by the antiHis-tag antibody, hence the epitope containing peptide. After processing the ion signals from the

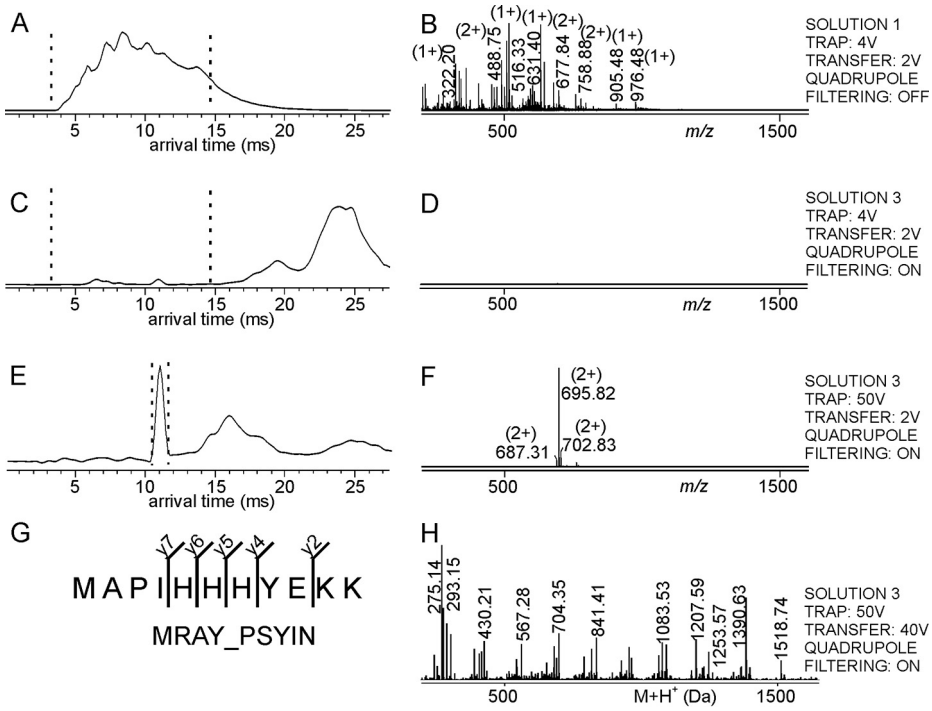

FIG. 3. **Mass spectrometric dissociation of the His-tag epitope peptide – antiHis-tag antibody complex and amino acid sequence determination of the complex-released peptide by mass spectrometric fragmentation.** Ion mobility arrival time plots of *A*, Solution 1, *C*, and *E*, Solution 3. Dashed lines mark the regions for mass spectra selections. Settings of the TRAP cell, the TRANSFER cell, and the quadrupole are indicated at the right. *B*, *D*, and *F*, nanoESI mass spectra (low *m/z* range) of ions from selected arrival time ranges. Selected *m/z* values are given and charge states are indicated in parentheses. For ion signal assignments see supplemental Table S7. *G*, Amino acid sequence of the complex-released peptide (single letter code) as determined by the matched mass spectrometric fragment ions (fragment ion types and numbers are indicated). The Uniprot protein id of the peptide source protein (first hit) is shown. *H*, Pseudo mass spectrum (after charge deconvolution and de-isotoping) of fragment ions derived by selecting arrival time of the complex-released peptide with *m/z* 695.82. For ion signal assignments see supplemental Table S8.

fragment ion spectrum of the low *m/z* range and submitting the mass list to Uniprot data base search using the Mascot search engine, an assignment of the doubly charged CoRP was obtained for a peptide with three histidine residues in a row (Fig. 3*G*–3*H*), originating from Phospho-N-acetylmuramoyl-pentapeptide-transferase (MRAY_PSYIN) from *Psychromonas ingrahamii (strain 37*). The reported peptide sequence only provided 33% homology to the His-tag peptide from rhβactin that was used in the experiment. Although the search engine reported a false positive hit (score 18), the thereby suggested amino acid sequence indicated that the epitope peptide indeed contained a set of consecutively arranged histidine residues. After including the amino acid sequence of the His-tagged rhβactin into the amended Uniprot database, we obtained the C-terminal peptide from rhβactin as chemically modified six histidine residue encompassing peptide as best hit (score 22; threshold 23) for the fragmented epitope peptide, *i.e.* the precursor ion at *m/z* 695.82. Of note, the mass difference of 114.04 Da between the measured and the theoretical masses of the tryptic His-tag peptide KC(carb)FHHHHHH was assumed to be because of di-carbamidomethylation on the lysine K373 residue (supplemental Fig. S3, cf. supplemental Table S9) in addition to carbamidomethylation of the cysteine C374 residue. Chemical modification on the K373 residue stands in agreement with shielding this lysine residue from enzymatic cleavage; explaining the "missed cleavage" at this amino acid residue (cf. supplemental Table S7).

At high collision cell energies in both the TRAP cell and the TRANSFER cell, the mass spectrum of high *m/z* range (above *m/z* 5000) with arrival times between 15 ms and 23 ms showed multiply charged ion signals of intact antibody unresolved from immune complex ions together with antibody fragments ions (supplemental Fig. S4*E*–S4*F*).

Immune Complex Formation and Epitope Identification for the antiTNFα Antibody—Because the ITEM-THREE method successfully identified epitope peptides from either synthetic peptide mixtures or from peptide mixtures originating from digested antigen proteins when exposed to the respective antibody, we applied our procedure to the identification of the unknown epitope of an antiTNFα antibody. Like before, solution 1 was generated by tryptic digestion of the protein, in this case the trimeric recombinant human TNFα (rhTNFα). The rhTNFα tryptic peptides' arrival times ranged from 4 ms to 12 ms and produced ion signals below *m/z* 1600 that covered 100% of the entire amino acid sequence of the full length

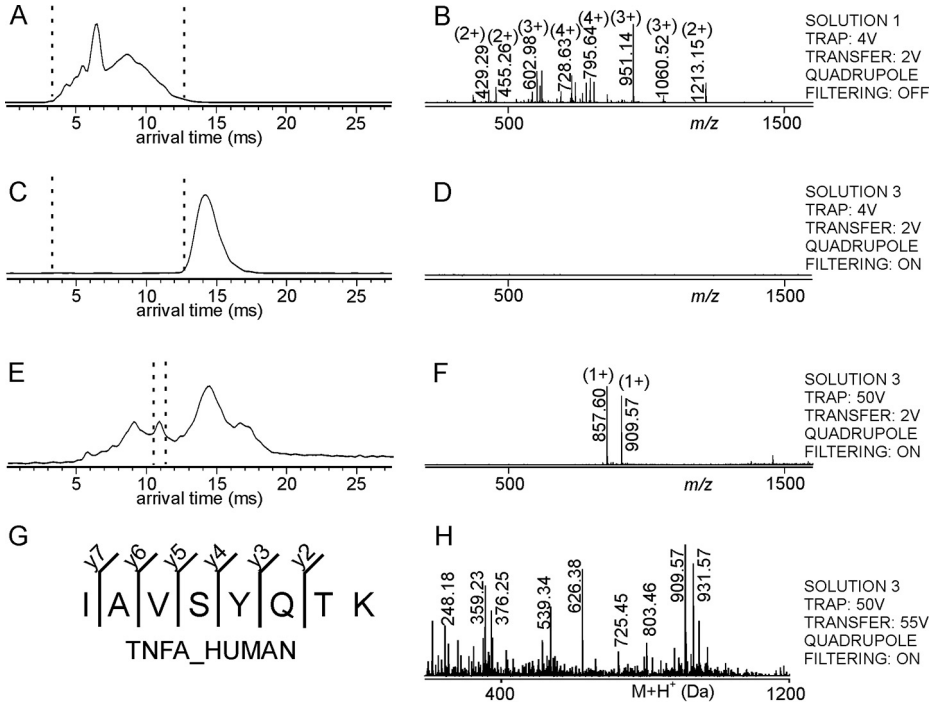

FIG. 4. **Mass spectrometric dissociation of the TNFα epitope peptide – anti TNFα antibody complex and amino acid sequence determination of the complex-released peptide by mass spectrometric fragmentation.** Ion mobility arrival time plots of *A*, Solution 1, *C*, and *E*, Solution 3. Dashed lines mark the regions for mass spectra selections. Settings of the TRAP cell, the TRANSFER cell, and the quadrupole are indicated at the right. *B*, *D*, and *F*, nanoESI mass spectra (low *m/z* range) of ions from selected arrival time ranges. Selected *m/z* values are given, and charge states are indicated in parentheses. For ion signal assignments see supplemental Table S11. *G*, Amino acid sequence of the complex-released peptide (single letter code) as determined by the matched mass spectrometric fragment ions (fragment ion types and numbers are indicated). The Uniprot protein id of the peptide source protein (first hit) is shown. *H*, Pseudo mass spectrum (after charge deconvolution and de-isotoping) of fragment ions derived by selecting arrival time of the complex-released peptide with *m/z* 909.57. For ion signal assignments see supplemental Table S12.

protein monomer (Fig. 4*A*–4*B*). After addition of the antiTNFα antibody (solution 2) and incubation for 1 h at room temperature, solution 3 was electrosprayed. Setting the quadrupole analyzer to block transmission of unbound peptide ions from solution 3, there appeared no peptide ions in the lower mass range (*m/z* below 1600) but in the higher mass range (*m/z* above 5000) there appeared unresolved ion signals of antiTNFα antibody and rhTNFα epitope peptide-antiTNFα antibody immune complexes with charge states ranging from 22+ to 27+ (Fig. 4*C*–4*D* and supplemental Fig. S7). Then, on raising the TRAP cell voltage difference to 50 V, two singly charged ion signals, one at *m/z* 857.60 and one at *m/z* 909.57 showed up with significant intensities in the corresponding mass spectrum (Fig. 4*E*–4*F*). Albeit these two CoRPs overlapped with respect to their arrival times of approx. 11 ms, they could be separately fragmented by applying different TRANSFER cell voltage differences. A TRANSFER cell voltage difference of 50 V was required to efficiently fragment the precursor CoRP ion at *m/z* 857.60 whereas a TRANSFER cell voltage difference of 55 V was needed to obtain high enough yields of fragment ions of the precursor CoRP ion at *m/z* 909.57. Subsequent submission of the two different mass lists from the processed fragment ion mass spectra to Uniprot data base search revealed two amino acid sequences, VNLLSAIK for the CoRP with *m/z* 857.60 (score 14; threshold 26, aa79–86) and IAVSYQTK for the CoRP with *m/z* 909.57 (score 35; threshold 26, aa87–94), respectively (Fig. 4*G*–4*H* and supplemental Fig. S6, cf.supplemental Tables S12–S13). The lower score for VNLLSAIK can be explained by the fact that at the TRANSFER cell collision voltage of 50 V that was applied to sufficiently fragment the precursor ion at *m/z* 857.60 some rather high intensity fragments of the IAVSYQTK precursor peptide were seen as well, now characterized as noise. Because unmatched ion signals generate a penalty in the Mascot algorithm, the ion score for the amino acid sequence of the target peptide is low. Interestingly, the two peptides are located adjacent to each other in the amino acid sequence of the rhTNFα (supplemental Fig. S8).

To examine whether both peptides together form the antiTNFα antibody epitope or, alternatively, to decide which of the two peptide contained the specific epitope, we compared their hydrophobicity values and solvent accessible surface areas (asa) using X-ray crystallographic data (1tnf.pdb). Our computational investigations revealed that the amino acid residues of the VNLLSAIK peptide (aa79–86) were highly hydrophobic and only surface accessible when assuming the

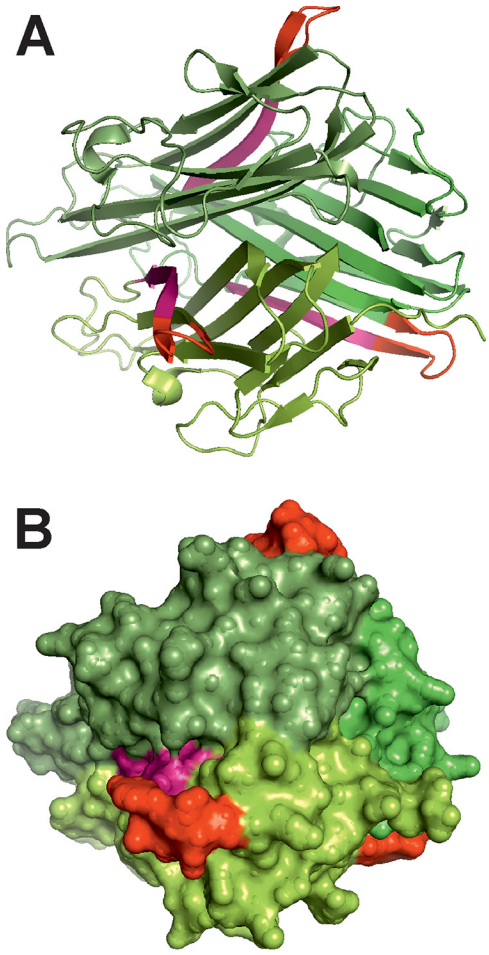

FIG. 5. **3D structure images of the human TNFα protein trimer.** *A*, The cartoon display shows ribbons with backbone atom coordinates. *B*, Display of vanderWaals surfaces. Monomer surfaces are shown in different green shades. The epitope peptides′ surfaces on each monomer (aa79 – aa86: IAVSYGTK) are displayed in red, the adjacent peptides′ surfaces (aa87 – aa94: VNNLSAIK) in purple (cf. supplemental Fig. S9).

presence of monomeric rhTNFα. By contrast, the residues of the IAVSYQTK peptide were highly surface accessible in both, trimeric and monomeric rhTNFα. The IAVSYQTK peptide (aa87–94) is rather hydrophilic as compared with the VNLLSAIK peptide (supplemental Fig. S9).

From this comparison it can be concluded that on the trimeric rhTNFα the IAVSYQTK peptide is highly surface exposed and, hence, is better accessible for antibody (paratope) recognition than the VNLLSAIK peptide. On the other hand it can be argued that the residues of VNLLSAIK are involved in the trimerization interface of TNFα and, consistent with the three dimensional structure of TNFα, only become surface exposed on destroying the rhTNFα trimer (Fig. 5). Thus, the appearance of the VNLLSAIK peptide in the ITEM-THREE experiment may be a result of nonspecific interaction of this peptide to the antibody that could be attributed to its "stickiness" because of its many hydrophobic residues.

However, when in control experiments either rituximab or a mouse monoclonal anti-actin antibody (solutions 2) was added to the rhTNFα tryptic peptide mixtures (solution 1) not a single peptide was fished out by either of the two negative control antibodies in ITEM-THREE (data not shown). Hence, we are tempted to speculate that the antiTNFα antibody may not be monoclonal. If we were to assume that the commercially available antiTNFα antibody was in fact containing two antibody clones, then, one might bind to the surface accessible peptide (IAVSYQTK) as the "expected" epitope and the other could bind to the "sticky" peptide (VNLLSAIK). In this case both peptides fully satisfied the properties of epitope peptides.

DISCUSSION

ITEM-THREE differs from MALDI MS-based epitope mapping methods (20, 53–55) in several aspects. Most currently available MALDI-MS approaches for epitope mapping require immobilization of the capturing antibody on a protein A (or protein G) substrate or on some other sort of a substrate (beads or columns) when chemically immobilized. Using a substrate is usually associated with the risk of nonspecific adsorption of the antigen/epitope peptide to its surface. Respective control experiments that test for nonspecific adsorption of antigens and/or epitope peptides onto the substrate material become mandatory, thereby doubling or tripling the amount of antigen/epitope peptides to be consumed. In ITEM-THREE one does not need to fix the capturing antibody on any substrate and therefore a respective negative control experiment with only substrate (bead or column surfaces, protein A or protein G, etc.) is obsolete. Hence, with ITEM-THREE sample consumption is reduced and the experimenter′s time is saved as well. Perhaps more importantly, ITEM-THREE allows one to check whether an antibody-epitope peptide complex has been formed in the first place. This is done by recording mass spectra with higher *m/z* range before dissociation of the complex. Using a MALDI MS-based method, the formation of the immune complex is not directly observable as on addition of the matrix (mostly because of the acidic solution in which the matrix is typically dissolved in), immune complexes are destroyed.

Of note, in MALDI-MS-based methods, mass spectrometry is applied "only" as a readout for the *in-solution* enzymatic/chemical processing steps, whereas in ITEM-THREE the mass spectrometer′s capabilities of ion manipulation and sorting become part of the experimental process. For one, we have observed that loosely (nonspecifically) attached peptides can be "shaken off" from the antibody surface during transition between the condensed and the gas phase by adjusting desorption/ionization conditions. Stronger bound epitope-containing peptides mostly survive this "cleansing" step and are dissociated later by applying CID conditions in a collision cell within the mass spectrometer. A comparable "clean-up" effect within the ionization regime may be difficult

to achieve by applying a MALDI-based method, as dissociation of peptides is not controlled but forced by denaturation of the antibody/immune complex under acidic matrix preparation conditions.

Also worth mentioning is the fact that dissociation of the epitope-containing peptide from the antibody by CID generates the charged epitope peptide ions in an ionization process that is completely different than that in an ionization source of a mass spectrometer. In the ion source all analytes compete for obtaining charge carriers (protons in positive ion mode) and there is a selection taking place by which in general more basic peptides become better ionized than less basic peptides. In MALDI-MS ionization the "lucky survivor concept" has found acceptance (56, 57). This in the end may have an impact in the detection sensitivity because there is the risk that some peptides simply may not ionize well and, hence their ion signals are weak and, depending on the noise, may be overlooked. By contrast, as has been amply described (6, 47, 58, 59) CID results in an asymmetric charge distribution and the epitope-containing peptide, being the smaller partner of the to be dissociated complex, receives at least one proton. At least in our hands, ionization yields were not limiting detection of the epitope peptides.

Further, additional in-solution handling steps, such as trimming of the epitope by applying different enzymes (60) can be done equally well in both of the two methods, MALDI-based and ITEM-THREE, at least as long as the proteases that in ITEM-THREE are to be added to one and the same sample without purification are stable enough and not digest each other faster than the time needed for trimming of the epitope peptide. Another prerequisite for ITEM-THREE is that the applied proteases should work in ammonium acetate buffer at pH 7. Yet, also in MALDI-based epitope mapping methods, during "trimming" the experimental conditions have to be kept such that the immune complex is not destroyed, *i.e.* a pH value of about neutral.

The fact that ITEM-THREE reveals partial amino acid sequences of epitope peptides as well as the respective protein name of the antigen in one experiment, principally allows one to identify unknown antigens of an antibody of interest in a given protein extract. An example for the identification of an unknown epitope amino acid sequence is presented by the chemically modified His-tag containing C-terminal epitope peptide, KCFHHHHHH, of rhβactin that was found to be triply carbamidomethylated. Both, the epitope peptide amino acid sequence and the location of the modifications were clearly identified by mass spectrometric fragmentation, thereby proving the versatility of ITEM-THREE. The observed double-carbamidomethylation at the lysine residue of the epitope peptide is consistent with reports that have shown that lysine residues might be modified by iodoacetamide, depending on the lysine residues' microenvironment (61, 62). In addition to the highly abundant $[M+2H]^{2+}$ ion at *m/z* 695.82 that was released from the immune complex, we also observed ion signals of two low-abundance doubly charged ion signals (*m/z* 687.31 and 702.83) with mass differences of −17.04 Da and +14.02 Da with respect to the epitope peptide's mass (Fig. 3*F*). The −17.04 Da likely was because of a loss of ammonia (63), whereas +14.02 Da can be explained by methylation of the K373 residue (64). Although loss of ammonia is produced from the peptide at elevated collision energies, methylation of the peptide was observed already in the peptide mixture of the tryptic digest of rhβactin (supplemental Table S7). Obviously, epitope peptides that contain modified residues because of post-translational modifications or as a result of chemical conversions during sample preparation are still identified by ITEM-THREE, provided that the modification not affects recognition of the epitope by the antibody's paratope. This stands in agreement with findings of methionine oxidized His-tag containing peptides, where oxidation did not prevent recognition of the epitope by the antibody under investigation or with partially carbamylated epitope peptides, where the chemical modification of a lysine residue was tolerated by the antibody as well (34). Such results illustrate the importance of ITEM-THREE as a method that can study amino acid modification-related effects on antigen-antibody binding.

Once an epitope peptide's sequence has been determined, one becomes able to search for amino acid sequence similarities on other proteins, thereby allowing to estimate cross-reactivities of the investigated antibody, or even to predict which unrelated proteins might bind to an antibody of interest in addition to its specific antigen. Such information becomes particularly relevant when one aims at using antibodies to identify proteins in species for which an antibody has not been produced or specified. When the amino acid sequence of the protein of interest is known, one can predict whether a given antibody might be a good binder, *i.e.* suitable for immune assays within a research project of a different species. Based on epitope peptide sequence similarities, the applicability of a precious antibody was securely broadened (8, 65). Practicality of this approach is illustrated by NCBI BLAST searches using the here identified epitope peptide sequences without taxonomy restrictions. The obtained lists of proteins that shared amino acid sequences that were like the query sequences from the identified epitope peptides, for instance, provided lists with more than 250 entries, each. Within the top 50 listed proteins in the report from the BLAST search applying the RA33 epitope peptide, only the top 6 proteins contained amino acid sequence stretches that were 100% identical to the query sequence. The next 16 proteins in the list had 100% identity to shorter query sequence stretches (Table I). The following amino acid sequences in the list were from unrelated proteins that possessed partial amino acid sequences with still high homologies to the original epitope peptide sequence.

The same type of results, which match with reports from cross-reactivity-studies with diagnostic heart muscle troponin

TABLE I
BLAST search results with identified epitope peptide amino acid sequences

Epitope peptide sequence (query)[a,b]	Protein IDs of 1st hit list entry[a,c]	No. of peptides identical[d]/similar[e] to query	Query/urp hit length[f]	1st urp's epitope-related amin o acid sequence[g]	Protein IDs of 1st urp[g]	List pos. of 1st urp[g]
M**AARPH**SI**DGR**VVEP	ROA2_HUMAN	6/16	15/15	L**ASRPH**TL**DGR**NIDP	DAZP1_XENLA	24
LQE**LEK**D**EREQLRIL**GE	RO52_HUMAN	1/26	17/17	TF**LEK**T**ER**L**EQLRIL**EN	KDSB_RICTY	3
KC**FHHHHHH**[h]	rhβ-actin_HUMAN	1/0	9/22	QHHHQHH**FHHHHHH**H HHHHNHG	SUV42_DROME	2
I**AVSYQTK**	TNFA_HUMAN	15/17	8/8	G**AV**N**YQTK**	HPUB_NEIMC	20

[a]Uniprot database was searched.
[b]Sequence parts which are identical to the query sequence are printed in bold.
[c]Number of subjects (entries in hit list) was limited to 250.
[d]Number of subjects (entries in hit list) identified with 100% sequence coverage and 100% sequence identity to query.
[e]Number of subjects (entries in hit list) identified with 100% sequence coverage and less than 100% sequence identity to query.
[f]rp: unrelated protein.
[g]First subject (entry in hit list) which belongs to an unrelated protein.
[h]Amended Uniprot database was searched.

T antibodies (65), can be obtained with any epitope peptide amino acid sequence (Table I). Because of amino acid sequence similarities it is likely that the antibody of interest was able to recognize binding motifs on unrelated proteins, as long as the targeted amino acid sequence was surface exposed and the partial peptide assumed a somewhat similar three dimensional structure compared with that of the original epitope peptide, even when the respective antibody was not raised against the unrelated protein.

ITEM-THREE is an electrospray mass spectrometry-based method that determines an utmost important antibody feature, its molecular recognition code. Except for mixing the antibody of interest with a peptide mixture that contains the epitope peptide, all experimental steps, such as epitope extraction and epitope peptide sequencing are performed in a single mass spectrometry experiment. Followed by an in-silico search, which starts with subjecting the experimentally determined mass lists to unsupervised data base search, the epitopes' peptide amino acid sequences are defined, and the originating antigens thereby unequivocally determined while homologues are retrievable and cross-reactivities estimated using BLAST search tools.

Acknowledgment—We thank Mr. Michael Kreutzer for providing his expertise on bioinformatics.

DATA AVAILABILITY

The mass spectrometry data have been deposited to the ProteomeXchange Consortium via the PRIDE partner repository with the dataset identifier PXD013823 (http://www.ebi.ac.uk/pride/archive/projects/PXD013823).

* We acknowledge the German Academic Exchange Service (DAAD) for providing scholarships for BD (No. 91566064). The WATERS Synapt G2S mass spectrometer has been bought through an EU grant [EFRE-UHROM 9] made available to MOG.

S This article contains supplemental material.

‡‡ To whom correspondence should be addressed: Proteome Center Rostock, University Rostock Medical Center and Natural Science Faculty, University of Rostock, Schillingallee 69, 18057 Rostock, Germany. Tel.: +49 - 381 - 494 4930; Fax: +49 - 381 - 494 4932; E-mail: michael.glocker@med.uni-rostock.de.

Author contributions: B.D.D. and C.R. performed research; B.D.D., C.R., K.F.M.O., R.E.-K., C.K., and M.O.G. analyzed data; B.D.D., C.R., K.F.M.O., R.E.-K., H.I., C.K., and M.O.G. wrote the paper; D.F. and H.I. contributed new reagents/analytic tools; C.K. and M.O.G. designed research.

REFERENCES

1. Baraniak, I., Kropff, B., McLean, G. R., Pichon, S., Piras-Douce, F., Milne, R. S. B., Smith, C., Mach, M., Griffiths, P. D., and Reeves, M. B. (2018) Epitope-specific humoral responses to human cytomegalovirus glycoprotein-B vaccine with MF59: anti-AD2 levels correlate with protection from viremia. *J. Infect. Dis.* **217,** 1907–1917
2. Xu, K., Acharya, P., Kong, R., Cheng, C., Chuang, G. Y., Liu, K., Louder, M. K., O'Dell, S., Rawi, R., Sastry, M., Shen, C. H., Zhang, B., Zhou, T., Asokan, M., Bailer, R. T., Chambers, M., Chen, X., Choi, C. W., Dandey, V. P., Doria-Rose, N. A., Druz, A., Eng, E. T., Farney, S. K., Foulds, K. E., Geng, H., Georgiev, I. S., Gorman, J., Hill, K. R., Jafari, A. J., Kwon, Y. D., Lai, Y. T., Lemmin, T., McKee, K., Ohr, T. Y., Ou, L., Peng, D., Rowshan, A. P., Sheng, Z., Todd, J. P., Tsybovsky, Y., Viox, E. G., Wang, Y., Wei, H., Yang, Y., Zhou, A. F., Chen, R., Yang, L., Scorpio, D. G., McDermott, A. B., Shapiro, L., Carragher, B., Potter, C. S., Mascola, J. R., and Kwong, P. D. (2018) Epitope-based vaccine design yields fusion peptide-directed antibodies that neutralize diverse strains of HIV-1. *Nat. Med.* **24,** 857–867
3. Volk, A. L., Hu, F. J., Berglund, M. M., Nordling, E., Stromberg, P., Uhlen, M., and Rockberg, J. (2016) Stratification of responders towards eculizumab using a structural epitope mapping strategy. *Sci. Rep.* **6,** 31365
4. Pritchard, A. L. (2018) Targeting neoantigens for personalised immunotherapy. *BioDrugs* **32,** 99–109
5. Linnebacher, M., Lorenz, P., Koy, C., Jahnke, A., Born, N., Steinbeck, F., Wollbold, J., Latzkow, T., Thiesen, H. J., and Glocker, M. O. (2012) Clonality characterization of natural epitope-specific antibodies against the tumor-related antigen topoisomerase IIa by peptide chip and proteome analysis: a pilot study with colorectal carcinoma patient samples. *Anal. Bioanal. Chem.* **403,** 227–238
6. Yefremova, Y., Opuni, K. F. M., Danquah, B. D., Thiesen, H. J., and Glocker, M. O. (2017) Intact transition epitope mapping (ITEM). *J. Am. Soc. Mass. Spectrom.* **28,** 1612–1622
7. Al-Majdoub, M., Koy, C., Lorenz, P., Thiesen, H. J., and Glocker, M. O. (2013) Mass spectrometric and peptide chip characterization of an assembled epitope: analysis of a polyclonal antibody model serum directed against the SjOgren/systemic lupus erythematosus autoantigen TRIM21. *J. Mass Spectrom.* **48,** 651–659
8. El-Kased, R. F., Koy, C., Deierling, T., Lorenz, P., Qian, Z., Li, Y., Thiesen, H. J., and Glocker, M. O. (2009) Mass spectrometric and peptide chip

epitope mapping of rheumatoid arthritis autoantigen RA33. *Eur. J. Mass Spectrom.* **15,** 747–759
9. Weidele, K., Stojanovic, N., Feliciello, G., Markiewicz, A., Scheitler, S., Alberter, B., Renner, P., Haferkamp, S., Klein, C. A., and Polzer, B. (2018) Microfluidic enrichment, isolation and characterization of disseminated melanoma cells from lymph node samples. *Int. J. Cancer* **145,** 232–241
10. Mankoff, D. A., Edmonds, C. E., Farwell, M. D., and Pryma, D. A. (2016) Development of companion diagnostics. *Semin. Nucl. Med.* **46,** 47–56
11. Davies, D. R., Padlan, E. A., and Sheriff, S. (1990) Antibody-antigen complexes. *Annu. Rev. Biochem.* **59,** 439–473
12. Toride King, M., and Brooks, C. L. (2018) Epitope mapping of antibody-antigen interactions with X-ray crystallography. *Methods Mol. Biol.* **1785,** 13–27
13. Bardelli, M., Livoti, E., Simonelli, L., Pedotti, M., Moraes, A., Valente, A. P., and Varani, L. (2015) Epitope mapping by solution NMR spectroscopy. *J. Mol. Recognit.* **28,** 393–400
14. Simonelli, L., Pedotti, M., Bardelli, M., Jurt, S., Zerbe, O., and Varani, L. (2018) Mapping antibody epitopes by solution NMR spectroscopy: practical considerations. *Methods Mol. Biol.* **1785,** 29–51
15. Chiliveri, S. C., and Deshmukh, M. V. (2016) Recent excitements in protein NMR: Large proteins and biologically relevant dynamics. *J. Biosci.* **41,** 787–803
16. Pan, J. X., Zhang, S. P., Chou, A., and Borchers, C. H. (2016) Higher-order structural interrogation of antibodies using middle-down hydrogen/deuterium exchange mass spectrometry. *Chem. Sci.* **7,** 1480–1486
17. Gershoni, J. M., Roitburd-Berman, A., Siman-Tov, D. D., Tarnovitski Freund, N., and Weiss, Y. (2007) Epitope mapping: the first step in developing epitope-based vaccines. *BioDrugs* **21,** 145–156
18. Mackay, J. P., Landsberg, M. J., Whitten, A. E., and Bond, C. S. (2017) Whaddaya know: a guide to uncertainty and subjectivity in structural biology. *Trends Biochem. Sci.* **42,** 155–167
19. Al-Majdoub, M., Opuni, K. F., Koy, C., and Glocker, M. O. (2013) Facile fabrication and instant application of miniaturized antibody-decorated affinity columns for higher-order structure and functional characterization of TRIM21 epitope peptides. *Anal. Chem.* **85,** 10479–10487
20. Opuni, K. F. M., Al-Majdoub, M., Yefremova, Y., El-Kased, R. F., Koy, C., and Glocker, M. O. (2018) Mass spectrometric epitope mapping. *Mass Spectrom. Rev.* **37,** 229–241
21. Pimenova, T., Nazabal, A., Roschitzki, B., Seebacher, J., Rinner, O., and Zenobi, R. (2008) Epitope mapping on bovine prion protein using chemical cross-linking and mass spectrometry. *J. Mass Spectrom*. **43,** 185–195
22. Horne, J. E., Walko, M., Calabrese, A. N., Levenstein, M. A., Brockwell, D. J., Kapur, N., Wilson, A. J., and Radford, S. E. (2018) Rapid mapping of protein interactions using tag-transfer photocrosslinkers. *Angewandte Chemie-International Edition* **57,** 16688–16692
23. Artigues, A., Nadeau, O. W., Rimmer, M. A., Villar, M. T., Du, X., Fenton, A. W., and Carlson, G. M. (2016) Protein structural analysis via mass spectrometry-based proteomics. *Adv. Exp. Med. Biol.* **919,** 397–431
24. Jones, L. M., Sperry, J. B., Carroll, J. A., and Gross, M. L. (2011) Fast photochemical oxidation of proteins for epitope mapping. *Anal. Chem.* **83,** 7657–7661
25. Li, J., Wei, H., Krystek, S. R., Jr, Bond, D., Brender, T. M., Cohen, D., Feiner, J., Hamacher, N., Harshman, J., Huang, R. Y., Julien, S. H., Lin, Z., Moore, K., Mueller, L., Noriega, C., Sejwal, P., Sheppard, P., Stevens, B., Chen, G., Tymiak, A. A., Gross, M. L., and Schneeweis, L. A. (2017) Mapping the energetic epitope of an antibody/interleukin-23 interaction with hydrogen/deuterium exchange, fast photochemical oxidation of proteins mass spectrometry, and alanine shave mutagenesis. *Anal. Chem.* **89,** 2250–2258
26. Glocker, M. O., Nock, S., Sprinzl, M., and Przybylski, M. (1998) Characterization of surface topology and binding area in complexes of the elongation factor proteins EF-Ts and EF-Tu center dot GDP from Thermus thermophilus: A study by protein chemical modification and mass spectrometry. *Chemistry* **4,** 707–715
27. Suckau, D., Mak, M., and Przybylski, M. (1992) Protein surface topology-probing by selective chemical modification and mass spectrometric peptide mapping. *Proc. Natl. Acad. Sci. U.S.A.* **89,** 5630–5634
28. Dhungana, S., Fessler, M. B., and Tomer, K. B. (2009) Epitope mapping by differential chemical modification of antigens. *Methods Mol. Biol.* **524,** 119–134
29. Glocker, M. O., Borchers, C., Fiedler, W., Suckau, D., and Przybylski, M. (1994) Molecular characterization of surface topology in protein tertiary structures by amino-acylation and mass spectrometric peptide mapping. *Bioconjug. Chem.* **5,** 583–590
30. Yefremova, Y., Danquah, B. D., Opuni, K. F., El-Kased, R., Koy, C., and Glocker, M. O. (2017) Mass spectrometric characterization of protein structures and protein complexes in condensed and gas phase. *Eur. J. Mass Spectrom.* **23,** 445–459
31. Suckau, D., Kohl, J., Karwath, G., Schneider, K., Casaretto, M., Bitter-Suermann, D., and Przybylski, M. (1990) Molecular epitope identification by limited proteolysis of an immobilized antigen-antibody complex and mass spectrometric peptide mapping. *Proc. Natl. Acad. Sci. U.S.A.* **87,** 9848–9852
32. Macht, M., Fiedler, W., Kurzinger, K., and Przybylski, M. (1996) Mass spectrometric mapping of protein epitope structures of myocardial infarct markers myoglobin and troponin T. *Biochemistry* **35,** 15633–15639
33. Baschung, Y., Lupu, L., Moise, A., Glocker, M., Rawer, S., Lazarev, A., and Przybylski, M. (2018) Epitope ligand binding sites of blood group oligosaccharides in lectins revealed by pressure-assisted proteolytic excision affinity mass spectrometry. *J. Am. Soc. Mass Spectrom.* **29,** 1881–1891
34. El-Kased, R., Koy, C., Lorenz, P., Montgomery, H., Tanaka, K., Thiesen, H., and Glocker, M. (2011) A novel Mass spectrometric epitope mapping approach without immobilization of the antibody. *J. Proteomics Bioinform.* **4,** 001–009
35. Uetrecht, C., Rose, R. J., van Duijn, E., Lorenzen, K., and Heck, A. J. (2010) Ion mobility mass spectrometry of proteins and protein assemblies. *Chem. Soc. Rev.* **39,** 1633–1655
36. Valentine, S. J., Liu, X., Plasencia, M. D., Hilderbrand, A. E., Kurulugama, R. T., Koeniger, S. L., and Clemmer, D. E. (2005) Developing liquid chromatography ion mobility mass spectometry techniques. *Expert Rev. Proteomics* **2,** 553–565
37. Wyttenbach, T., Pierson, N. A., Clemmer, D. E., and Bowers, M. T. (2014) Ion mobility analysis of molecular dynamics. *Annu. Rev. Phys. Chem.* **65,** 175–196
38. VanAernum, Z. L., Gilbert, J. D., Belov, M. E., Makarov, A. A., Horning, S. R., and Wysocki, V. H. (2019) Surface-induced dissociation of noncovalent protein complexes in an extended mass range orbitrap mass spectrometer. *Anal. Chem.* **91,** 3611–3618
39. Busch, F., VanAernum, Z. L., Ju, Y., Yan, J., Gilbert, J. D., Quintyn, R. S., Bern, M., and Wysocki, V. H. (2018) Localization of protein complex bound ligands by surface-induced dissociation high-resolution mass spectrometry. *Anal. Chem.* **90,** 12796–12801
40. Zhang, X., Li, H., Moore, B., Wongkongkathep, P., Ogorzalek Loo, R. R., Loo, J. A., and Julian, R. R. (2014) Radical-directed dissociation of peptides and proteins by infrared multiphoton dissociation and sustained off-resonance irradiation collision-induced dissociation with Fourier transform ion cyclotron resonance mass spectrometry. *Rapid Commun. Mass Spectrom.* **28,** 2729–2734
41. Halim, M. A., Girod, M., MacAleese, L., Lemoine, J., Antoine, R., and Dugourd, P. (2016) Combined infrared multiphoton dissociation with ultraviolet photodissociation for ubiquitin characterization. *J. Am. Soc. Mass Spectrom.* **27,** 1435–1442
42. Ben-Nissan, G., and Sharon, M. (2018) The application of ion-mobility mass spectrometry for structure/function investigation of protein complexes. *Curr. Opin. Chem. Biol.* **42,** 25–33
43. Clemmer, D. E., and Jarrold, M. F. (1997) Ion mobility measurements and their applications to clusters and biomolecules. *J. Mass Spectrom.* **32,** 577–592
44. Hoaglund, C. S., Valentine, S. J., Sporleder, C. R., Reilly, J. P., and Clemmer, D. E. (1998) Three-dimensional ion mobility/TOFMS analysis of electrosprayed biomolecules. *Anal. Chem.* **70,** 2236–2242
45. Glocker, M. O., Arbogast, B., and Deinzer, M. L. (1995) Characterization of disulfide linkages and disulfide bond scrambling in recombinant human macrophage colony stimulating factor by fast-atom bombardment mass spectrometry of enzymatic digests. *J. Am. Soc. Mass Spectrom.* **6,** 638–643
46. Yang, J., Rower, C., Koy, C., Russ, M., Ruger, C. P., Zimmermann, R., von Fritschen, U., Bredell, M., Finke, J. C., and Glocker, M. O. (2015) Mass spectrometric characterization of limited proteolysis activity in human plasma samples under mild acidic conditions. *Methods* **89,** 30–37

47. Yefremova, Y., Melder, F. T. I., Danquah, B. D., Opuni, K. F. M., Koy, C., Ehrens, A., Frommholz, D., Illges, H., Koelbel, K., Sobott, F., and Glocker, M. O. (2017) Apparent activation energies of protein-protein complex dissociation in the gas-phase determined by electrospray mass spectrometry. *Anal. Bioanal. Chem.* **409,** 6549–6558
48. Wolter, M., Okai, C. A., Smith, D. S., Russ, M., Rath, W., Pecks, U., Borchers, C. H., and Glocker, M. O. (2018) Maternal apolipoprotein B100 serum levels are diminished in pregnancies with intrauterine growth restriction and differentiate from controls. *Proteomics Clin. Appl.* **12,** e1800017
49. Perez-Riverol, Y., Csordas, A., Bai, J., Bernal-Llinares, M., Hewapathirana, S., Kundu, D. J., Inuganti, A., Griss, J., Mayer, G., Eisenacher, M., Perez, E., Uszkoreit, J., Pfeuffer, J., Sachsenberg, T., Yilmaz, S., Tiwary, S., Cox, J., Audain, E., Walzer, M., Jarnuczak, A. F., Ternent, T., Brazma, A., and Vizcaino, J. A. (2019) The PRIDE database and related tools and resources in 2019: improving support for quantification data. *Nucleic Acids Res.* **47,** D442–D450
50. Pecks, U., Seidenspinner, F., Rower, C., Reimer, T., Rath, W., and Glocker, M. O. (2010) Multifactorial analysis of affinity-mass spectrometry data from serum protein samples: a strategy to distinguish patients with preeclampsia from matching control individuals. *J. Am. Soc. Mass Spectrom.* **21,** 1699–1711
51. Kienbaum, M., Koy, C., Montgomery, H. V., Drynda, S., Lorenz, P., Illges, H., Tanaka, K., Kekow, J., Guthke, R., Thiesen, H. J., and Glocker, M. O. (2009) MS characterization of apheresis samples from rheumatoid arthritis patients for the improvement of immunoadsorption therapy - a pilot study. *Proteomics Clin. Appl.* **3,** 797–809
52. Madi, A., Mikkat, S., Ringel, B., Ulbrich, M., Thiesen, H. J., and Glocker, M. O. (2003) Mass spectrometric proteome analysis for profiling temperature-dependent changes of protein expression in wild-type Caenorhabditis elegans. *Proteomics* **3,** 1526–1534
53. Al-Majdoub, M., Opuni, K. F., Yefremova, Y., Koy, C., Lorenz, P., El-Kased, R. F., Thiesen, H. J., and Glocker, M. O. (2014) A novel strategy for the rapid preparation and isolation of intact immune complexes from peptide mixtures. *J. Mol. Recognit.* **27,** 566–574
54. Rinaldi, F., Lupu, L., Rusche, H., Kukacka, Z., Tengattini, S., Bernardini, R., Piubelli, L., Bavaro, T., Maeser, S., Pollegioni, L., Calleri, E., Przybylski, M., and Temporini, C. (2019) Epitope and affinity determination of recombinant Mycobacterium tuberculosis Ag85B antigen towards anti-Ag85 antibodies using proteolytic affinity-mass spectrometry and biosensor analysis. *Anal. Bioanal. Chem.* **411,** 439–448
55. Raska, C. S., Parker, C. E., Sunnarborg, S. W., Pope, R. M., Lee, D. C., Glish, G. L., and Borchers, C. H. (2003) Rapid and sensitive identification of epitope-containing peptides by direct matrix-assisted laser desorption/ionization tandem mass spectrometry of peptides affinity-bound to antibody beads. *J. Am. Soc. Mass Spectrom.* **14,** 1076–1085
56. Jaskolla, T. W., and Karas, M. (2011) Compelling evidence for Lucky Survivor and gas phase protonation: the unified MALDI analyte protonation mechanism. *J. Am. Soc. Mass Spectrom.* **22,** 976–988
57. Karas, M., Gluckmann, M., and Schafer, J. (2000) Ionization in matrix-assisted laser desorption/ionization: singly charged molecular ions are the lucky survivors. *J. Mass Spectrom.* **35,** 1–12
58. Sciuto, S. V., Liu, J., and Konermann, L. (2011) An electrostatic charge partitioning model for the dissociation of protein complexes in the gas phase. *J. Am. Soc. Mass Spectrom.* **22,** 1679–1689
59. Zhou, M., Dagan, S., and Wysocki, V. H. (2012) Protein subunits released by surface collisions of noncovalent complexes: nativelike compact structures revealed by ion mobility mass spectrometry. *Angew Chem. Int. Ed. Engl.* **51,** 4336–4339
60. Parker, C. E., Papac, D. I., Trojak, S. K., and Tomer, K. B. (1996) Epitope mapping by mass spectrometry: determination of an epitope on HIV-1 IIIB p26 recognized by a monoclonal antibody. *J. Immunol.* **157,** 198–206
61. Svozil, J., and Baerenfaller, K. (2017) A cautionary tale on the inclusion of variable posttranslational modifications in database-dependent searches of mass spectrometry data. *Proteomics Biol.* **586,** 433–452
62. Mukouyama, E. B., Oguchi, M., Kodera, Y., Maeda, T., and Suzuki, H. (2004) Low pKa lysine residues at the active site of sarcosine oxidase from Corynebacterium sp. U-96. *Biochem. Biophys. Res. Commun.* **320,** 846–851
63. Sun, S., Yu, C., Qiao, Y., Lin, Y., Dong, G., Liu, C., Zhang, J., Zhang, Z., Cai, J., Zhang, H., and Bu, D. (2008) Deriving the probabilities of water loss and ammonia loss for amino acids from tandem mass spectra. *J. Proteome Res.* **7,** 202–208
64. Lanouette, S., Mongeon, V., Figeys, D., and Couture, J. F. (2014) The functional diversity of protein lysine methylation. *Mol. Syst. Biol.* **10,** 724
65. Macht, M., Marquardt, A., Deininger, S. O., Damoc, E., Kohlmann, M., and Przybylski, M. (2004) 'Affinity-proteomics': direct protein identification from biological material using mass spectrometric epitope mapping. *Anal. Bioanal. Chem.* **378,** 1102–1111

Supplemental data

Intact Transition Epitope Mapping –

Targeted High-Energy Rupture of Extracted Epitopes

(ITEM - THREE)

Bright D. Danquah[1)], Claudia Röwer[1)], Kwabena F.M. Opuni[2)], Reham El-Kased[3)], David Frommholz[4)], Harald Illges[4,5)], Cornelia Koy[1)], and Michael O. Glocker[1)]

1) Proteome Center Rostock, University Medicine Rostock, Rostock, Germany

2) School of Pharmacy, University of Ghana, Legon, Ghana

3) Microbiology and Immunology Faculty of Pharmacy, The British University in Egypt, Cairo, Egypt

4) University of Applied Sciences Bonn-Rhein-Sieg, Immunology and Cell Biology, Rheinbach, Germany

5) University of Applied Sciences Bonn-Rhein-Sieg, Institute for Functional Gene Analytics, Rheinbach, Germany

Supplemental Tables

Supplemental Figures

Table S1: Amino acid sequences and molecular masses of synthetic peptides [a].

peptide name	amino acid sequence	[p] [c]	$[M+pH]^{p+}$ (calcd)	*m/z* (exp)
RA33	MAARPHSIDGRVVEP-NH_2	2 3	817.43 545.29	817.49 545.32
TRIM21 A	LQELEKDEREQLRILGE	2 3	1049.56 700.04	1049.64 700.09
TRIM21 B	LQ<u>P</u>LEKDEREQLRILGE	2	1033.57	1033.64
TRIM21 C	LQELEKDE<u>P</u>EQLRILGE	2	1020.04	1020.11
FLAG	DYKDDDDK	1	1013.41	1013.49
FLAG (3-8) [b]	KDDDDK	1	735.32	735.36
FLAG (4-8) [b]	DDDDK	1	607.22	607.26
FLAG (5-8) [b]	DDDK	1	492.19	492.22
angiotensin II	DRVYIHPF	1	1046.54	1046.61
GPI	ALKPYSPGGPR	1 2	1142.63 571.82	1142.72 571.85
GPI (4-11) [b]	PYSPGGPR	1	830.42	830.48
GPI (6-11) [b]	SPGGPR	1	570.30	570.34
GPI (7-11) [b]	PGGPR	1	483.27	483.30

a) solution 1 (cf. Figures 1 and 2)
b) sequence range of fragments observed at higher collision energies
c) positively charged ions

Table S2: MS/MS fragmentation of MAARPHSIDGRVVEP showing matches used for scoring [a,b)]

no.	b	b^{++}	b*	b^{*++}	b^{0}	b^{0++}	seq [c,d,e)].	y	y^{++}	y*	y^{*++}	y^{0}	y^{0++}	no.
1	132.0478	66.5275					M							15
2	***203.0849***	102.0461					A	***1502.8186***	751.9130	1485.7921	743.3997	1484.8081	742.9077	14
3	274.1220	137.5646					A	1431.7815	716.3944	1414.7550	707.8811	1413.7710	707.3891	13
4	***430.2231***	215.6152	413.1966	207.1019			R	1360.7444	680.8758	1343.7179	672.3626	1342.7338	671.8706	12
5	527.2759	264.1416	510.2493	255.6283			P	***1204.6433***	602.8253	1187.6167	594.3120	1186.6327	593.8200	11
6	***664.3348***	332.6710	647.3082	324.1578			H	***1107.5905***	554.2989	1090.5640	545.7856	1089.5800	545.2936	10
7	***751.3668***	376.1870	734.3403	367.6738	733.3562	367.1818	S	***970.5316***	485.7694	953.5051	477.2562	952.5211	476.7642	9
8	***864.4509***	432.7291	847.4243	424.2158	846.4403	423.7238	I	***883.4996***	442.2534	866.4730	433.7402	865.4890	433.2482	8
9	***979.4778***	490.2425	962.4513	481.7293	961.4672	481.2373	D	770.4155	385.7114	753.3890	377.1981	752.4050	376.7061	7
10	***1036.4993***	518.7533	1019.4727	510.2400	1018.4887	509.7480	G	***655.3886***	328.1979	638.3620	319.6847	637.3780	319.1926	6
11	***1192.6004***	596.8038	1175.5738	588.2906	1174.5898	587.7985	R	598.3671	299.6872	581.3406	291.1739	580.3566	290.6819	5
12	1291.6688	646.3380	1274.6423	637.8248	1273.6582	637.3328	V	442.2660	221.6366			424.2554	212.6314	4
13	1390.7372	695.8722	1373.7107	687.3590	1372.7266	686.8670	V	343.1976	172.1024			325.1870	163.0972	3
14	***1519.7798***	760.3935	1502.7533	751.8803	1501.7692	751.3883	E	244.1292	122.5682			226.1186	113.5629	2
15							P	115.0866	58.0469					1

[a)] 21 of 140 fragment ion masses were assigned using 43 most intense peaks from the spectrum (c.f. Figure 1): bold italic print means the series contributed to the score; bold print means that the number of matches in the ion series is greater than would be expected by chance, indicating that the ion series is present; non-bold underlined print means that the number of matches in the ion series is no greater than would be expected by chance, so that the matches themselves may be by chance; non-bold non-underlined print means that this mass was not represented by an ion signal in the mass spectrum.

[b)] ions score: 43; random score (expectation value): 4.7

[c)] monoisotopic mass of neutral peptide M_r: 1632.8518

[d)] fixed modification: amidated C-terminus

[e)] **$^{++}$:** doubly charged fragment ion, * : fragment ion with loss of ammonia, ^{0} :fragment ion with loss of water

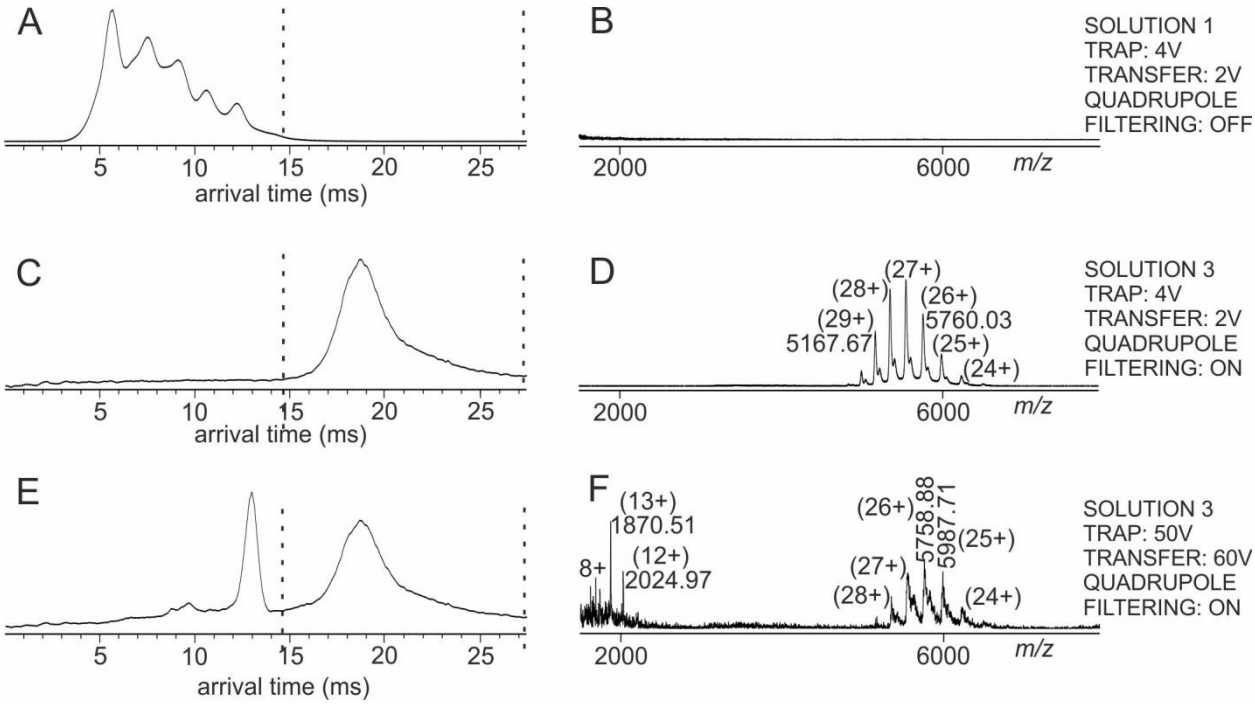

Figure S1: Mass spectrometric dissociation of the RA33 epitope peptide – antiRA33 antibody complex. Ion mobility arrival time plots of **A:** Solution 1, **C:** and **E:** Solution 3. Dashed lines mark the regions for mass spectra selections. Settings of the TRAP cell, the TRANSFER cell, and the quadrupole are indicated at the right. **B**, **D**, and **F**: nanoESI mass spectra (high *m/z* range) of ions from selected arrival time ranges. Selected *m/z* values are given and charge states are indicated in parentheses. For ion signal assignments see Table S3.

Table S3: List of protein ion signals from antiRA33 antibody [a].

molecular species	charge state [d]	exp. *m/z*	exp. mass
antibody	24	6235.51	149628.24
	25	5988.58	149689.50
	26	5760.03	149734.78
	27	5548.13	149772.51
	28	5351.02	149800.56
	29	5167.67	149833.43
	30	4997.90	149907.00
antibody-peptide complex [b]	25	6052.22	151280.50
	26	5820.40	151304.40
	27	5604.22	151286.94
	28	5411.10	151482.80
	29	5222.54	151424.66
	30	5052.56	151546.80
antibody fragments [c]	12	2024.97	24287.64
	13	1870.51	24303.63
	14	1736.53	24297.42
	7	1887.64	13206.48
	8	1651.83	13206.64
	9	1468.43	13206.87

a) solutions 2 and 3; (cf. Figure S1)
b) antibody bound to one peptide
c) observed at high collision voltages
d) positively charged ions

Table S4: MS/MS fragmentation of LQELEKDEREQLRILGE showing matches used for scoring [a,b)]

no.	b	b^{++}	b*	b^{*++}	b^{0}	b^{0++}	seq [c,d)].	y	y^{++}	y*	y^{*++}	y^{0}	y^{0++}	no.
1	114.0913	57.5493					L							17
2	**242.1499**	121.5786	225.1234	113.0653			Q	***1985.0298***	993.0185	1968.0033	984.5053	1967.0192	984.0133	16
3	**371.1925**	186.0999	354.1660	177.5866	353.1819	177.0946	E	***1856.9712***	928.9893	1839.9447	920.4760	1838.9607	919.9840	15
4	**484.2766**	242.6419	467.2500	234.1287	466.2660	233.6366	L	***1727.9286***	**864.4680**	1710.9021	855.9547	1709.9181	855.4627	14
5	**613.3192**	307.1632	596.2926	298.6499	595.3086	298.1579	E	***1614.8446***	807.9259	1597.8180	799.4127	1596.8340	798.9206	13
6	741.4141	371.2107	724.3876	362.6974	723.4036	362.2054	K	***1485.8020***	**743.4046**	1468.7754	734.8914	1467.7914	734.3993	12
7	856.4411	428.7242	839.4145	420.2109	838.4305	419.7189	D	***1357.7070***	**679.3571**	1340.6805	670.8439	1339.6965	670.3519	11
8	985.4837	493.2455	968.4571	484.7322	967.4731	484.2402	E	***1242.6801***	621.8437	1225.6535	613.3304	1224.6695	612.8384	10
9	**1141.5848**	571.2960	1124.5582	562.7828	1123.5742	562.2907	R	***1113.6375***	**557.3224**	1096.6109	548.8091	1095.6269	548.3171	9
10	1270.6274	635.8173	1253.6008	627.3040	1252.6168	626.8120	E	***957.5364***	**479.2718**	940.5098	470.7585	939.5258	470.2665	8
11	1398.6859	699.8466	1381.6594	691.3333	1380.6754	690.8413	Q	***828.4938***	414.7505	811.4672	406.2373	810.4832	405.7452	7
12	1511.7700	756.3886	1494.7435	747.8754	1493.7594	747.3834	L	***700.4352***	350.7212	683.4087	342.2080	682.4246	341.7160	6
13	**1667.8711**	834.4392	1650.8446	825.9259	1649.8606	825.4339	R	***587.3511***	294.1792	570.3246	285.6659	569.3406	285.1739	5
14	1780.9552	890.9812	1763.9286	882.4680	1762.9446	881.9759	I	431.2500	216.1287			413.2395	207.1234	4
15	1894.0393	947.5233	1877.0127	939.0100	1876.0287	938.5180	L	***318.1660***	159.5866			300.1554	150.5813	3
16	**1951.0607**	976.0340	1934.0342	967.5207	1933.0502	967.0287	G	205.0819	103.0446			187.0713	94.0393	2
17							E	148.0604	74.5339			130.0499	65.5286	1

[a)] 53 of 178 fragment ion masses were assigned using 140 most intense peaks from the spectrum (c.f. Figure 2): bold italic print means the series contributed to the score; bold print means that the number of matches in the ion series is greater than would be expected by chance, indicating that the ion series is present; non-bold underlined print means that the number of matches in the ion series is no greater than would be expected by chance, so that the matches themselves may be by chance; non-bold non-underlined print means that this mass was not represented by an ion signal in the mass spectrum.

[b)] ions score: 46; random score (expectation value): 1.6

[c)] monoisotopic mass of neutral peptide M_r: 2098.1065

[d)] **$^{++}$:** doubly charged fragment ion, * : fragment ion with loss of ammonia, ^{0} :fragment ion with loss of water

Table S5: MS/MS fragmentation of LQ*P*LEKDEREQLRILGE showing matches used for scoring [a,b)]

no.	b	b^{++}	b*	b^{*++}	b^{0}	b^{0++}	seq [c,d)]	y	y^{++}	y*	y^{*++}	y^{0}	y^{0++}	no.
1	114.0913	57.5493					L							17
2	242.1499	121.5786	225.1234	113.0653			Q	1953.0400	977.0236	1936.0134	968.5104	1935.0294	968.0183	16
3	339.2027	170.1050	322.1761	161.5917			P	***1824.9814***	912.9943	1807.9549	904.4811	1806.9708	903.9891	15
4	452.2867	226.6470	435.2602	218.1337			L	***1727.9286***	**864.4680**	1710.9021	855.9547	1709.9181	855.4627	14
5	581.3293	291.1683	564.3028	282.6550	563.3188	282.1630	E	***1614.8446***	807.9259	1597.8180	799.4127	1596.8340	798.9206	13
6	709.4243	355.2158	692.3978	346.7025	691.4137	346.2105	K	***1485.8020***	**743.4046**	1468.7754	734.8914	1467.7914	734.3993	12
7	824.4512	412.7293	807.4247	404.2160	806.4407	403.7240	D	***1357.7070***	**679.3571**	1340.6805	670.8439	1339.6965	670.3519	11
8	953.4938	477.2506	936.4673	468.7373	935.4833	468.2453	E	***1242.6801***	621.8437	1225.6535	613.3304	1224.6695	612.8384	10
9	1109.5949	555.3011	1092.5684	546.7878	1091.5844	546.2958	R	***1113.6375***	**557.3224**	1096.6109	548.8091	1095.6269	548.3171	9
10	1238.6375	619.8224	1221.6110	611.3091	1220.6270	610.8171	E	***957.5364***	**479.2718**	940.5098	470.7585	939.5258	470.2665	8
11	1366.6961	683.8517	1349.6696	675.3384	1348.6856	674.8464	Q	***828.4938***	414.7505	811.4672	406.2373	810.4832	405.7452	7
12	1479.7802	740.3937	1462.7536	731.8805	1461.7696	731.3884	L	***700.4352***	350.7212	683.4087	342.2080	682.4246	341.7160	6
13	1635.8813	818.4443	1618.8547	809.9310	1617.8707	809.4390	R	***587.3511***	294.1792	570.3246	285.6659	569.3406	285.1739	5
14	1748.9654	874.9863	1731.9388	866.4730	1730.9548	865.9810	I	431.2500	216.1287			413.2395	207.1234	4
15	1862.0494	931.5283	1845.0229	923.0151	1844.0389	922.5231	L	***318.1660***	159.5866			300.1554	150.5813	3
16	1919.0709	960.0391	1902.0443	951.5258	1901.0603	951.0338	G	205.0819	103.0446			187.0713	94.0393	2
17							E	148.0604	74.5339			130.0499	65.5286	1

[a)] 34 of 174 fragment ion masses were assigned using 127 most intense peaks from the spectrum (c.f. Figure 2): bold italic print means the series contributed to the score; bold print means that the number of matches in the ion series is greater than would be expected by chance, indicating that the ion series is present; non-bold underlined print means that the number of matches in the ion series is no greater than would be expected by chance, so that the matches themselves may be by chance; non-bold non-underlined print means that this mass was not represented by an ion signal in the mass spectrum.

[b)] ions score: 27; random score (expectation value): 96)

[c)] monoisotopic mass of neutral peptide M_r: 2065.1167

[d)] **$^{++}$:** doubly charged fragment ion, * : fragment ion with loss of ammonia, ^{0} :fragment ion with loss of water

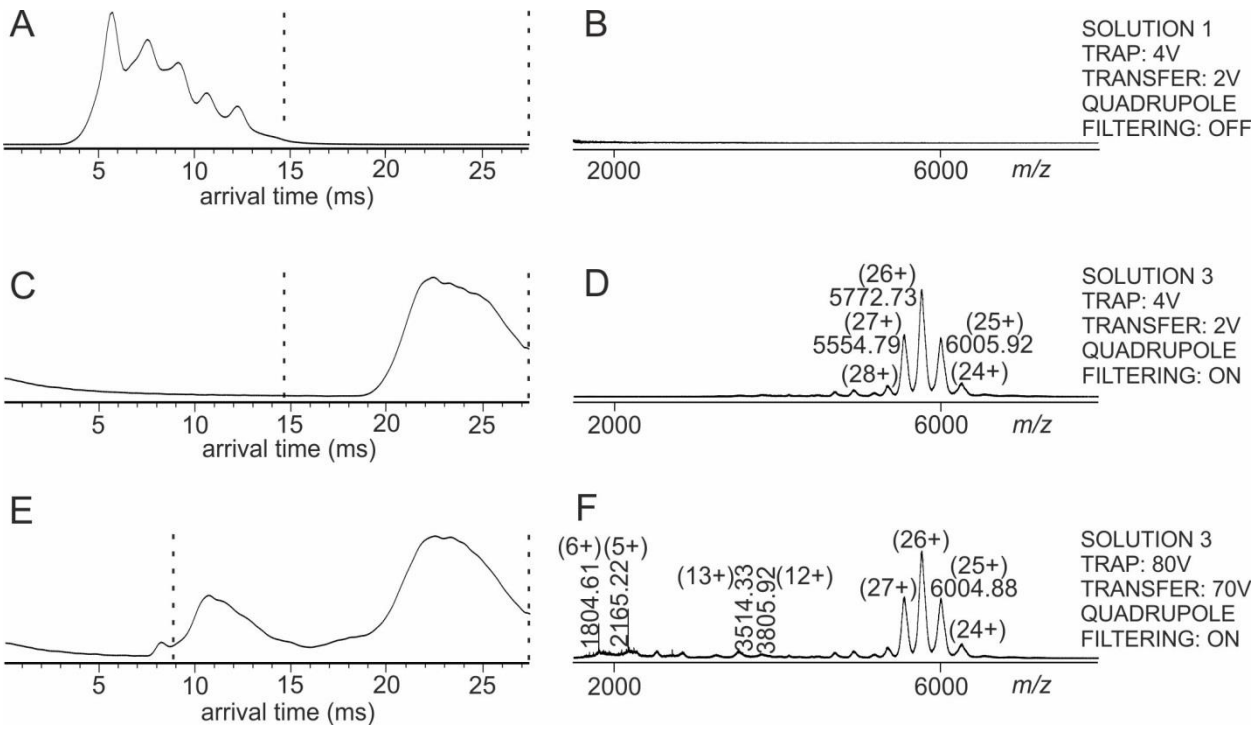

Figure S2: Mass spectrometric dissociation of the TRIM21 epitope peptide – TRIM21 antibody complex. Ion mobility arrival time plots of **A:** Solution 1, **C:** and **E:** Solution 3. Dashed lines mark the regions for mass spectra selections. Settings of the TRAP cell, the TRANSFER cell, and the quadrupole are indicated at the right. **B**, **D**, and **F**: nanoESI mass spectra (high *m/z* range) of ions from selected arrival time ranges. Selected *m/z* values are given and charge states are indicated in parentheses. For ion signal assignments see Table S6.

Table S6: List of protein ion signals from antiTRIM21 antibody [a].

molecular species	charge state [d]	exp. *m/z*	exp. mass
antibody-peptide complex [b]	23	6544.84	150508.32
	24	6266.54	150372.96
	25	6005.92	150123.00
	26	5772.73	150064.98
	27	5554.79	149952.33
	28	5351.85	149823.80
antibody fragments[c]	12	3805.92	45659.04
	13	3514.33	45673.29
	14	3248.82	45469.48
	8	2834.63	22669.04
	9	2512.70	22605.30
	4	2706.05	10820.20
	5	2165.23	10821.15
	6	1804.61	10821.66

a) solutions 2 and 3 (cf. Figure S2)
b) antibody bound to peptide not resolved from antibody ion signals
c) observed at high collision voltages
d) positively charged ions

Table S7: List of peptide ion signals upon tryptic digestion of rhβactin [a].

sequence range	charge state [b]	*m/z* (exp)	peptide mass (Mr)
19-28	2	488.75	975.44
19-28	1	976.48	975.44
29-39	2	599.82	1197.70
40-50	2	586.31	1170.56
51-61	2	599.82	1197.51
51-61	1	1198.56	1197.70
51-62	2	677.84	1353.62
51-62	1	1354.67	1353.62
63-68	1	644.43	643.43
69-84	2	973.99	1945.89
85-95	1	1515.75	1514.74
96-113	3	652.05	1953.06
96-113	2	977.57	1953.06
114-116	1	360.21	359.19
117-118	1	276.17	275.15
178-183	1	644.40	643.37
184-191	2	499.73	997.48
184-191	1	998.52	997.48
192-196	1	631.40	630.37
197-206	2	566.79	1131.52
197-206	1	1132.56	1131.52
207-210	1	516.33	515.31
207-213	2	436.78	871.51
207-215	2	565.35	1128.65
211-213	1	375.24	374.22
211-215	2	316.69	631.35
239-254	2	895.98	1789.88
255-256	1	322.20	321.18
285-291	2	453.24	904.44
285-291	1	905.48	904.44
313-315	1	406.22	405.20
316-326	2	581.34	1160.61
316-326	1	1161.65	1160.61
327-328	1	260.21	259.19
327-335	2	518.73	1035.64
327-335	1	1036.46	1035.64
329-335	1	795.50	794.50
329-336	2	462.30	922.56
360-372	2	758.88	1515.70
360-372	1	1516.72	1515.70
360-373	2	822.93	1643.79
360-373 [c]	2	829.93	1657.81
373-381 [d]	3	464.23	1389.60
373-381 [e]	3	468.89	1403.62
373-381 [d]	2	695.82	1389.60
373-381 [e]	2	702.83	1403.62

a) solution 1 (cf. Figure 3 and Figure S5)
b) positively charged ions
c) singly methylated peptide
d) triply carbamidomethylated peptide containing the epitope
e) singly methylated and triply carbamidomethylated peptide containing the epitope

Table S8: MS/MS fragmentation of MAPIHHHYEKK showing matches used for scoring [a,b)]

no.	b	b^{++}	b*	b^{*++}	b^{0}	b^{0++}	seq [c,d,e)]	y	y^{++}	y*	y^{*++}	y^{0}	y^{0++}	no.
1	132.0478	66.5275					M							11
2	203.0849	102.0461					A	1259.6644	630.3358	1242.6378	621.8225	1241.6538	621.3305	10
3	300.1376	150.5725					P	1188.6273	594.8173	1171.6007	586.3040	1170.6167	585.8120	9
4	413.2217	207.1145					I	1091.5745	546.2909	1074.5479	537.7776	1073.5639	537.2856	8
5	550.2806	275.6439					H	978.4904	489.7489	961.4639	481.2356	960.4799	480.7436	7
6	687.3395	344.1734					H	***841.4315***	421.2194	824.4050	412.7061	823.4209	412.2141	6
7	824.3984	412.7029					H	***704.3726***	352.6899	687.3461	344.1767	686.3620	343.6847	5
8	987.4618	494.2345					Y	***567.3137***	284.1605	550.2871	275.6472	549.3031	275.1552	4
9	1116.5044	558.7558			1098.4938	549.7505	E	404.2504	202.6288	387.2238	194.1155	386.2398	193.6235	3
10	1244.5993	622.8033	1227.5728	614.2900	1226.5888	613.7980	K	***275.2078***	138.1075	258.1812	129.5942			2
11							K	147.1128	74.0600	130.0863	65.5468			1

[a)] 8 of 80 fragment ion masses were assigned using 12 most intense peaks from the spectrum (c.f. Figure 3): bold italic print means the series contributed to the score; bold print means that the number of matches in the ion series is greater than would be expected by chance, indicating that the ion series is present; non-bold underlined print means that the number of matches in the ion series is no greater than would be expected by chance, so that the matches themselves may be by chance; non-bold non-underlined print means that this mass was not represented by an ion signal in the mass spectrum.

[b)] ions score: 18; random score (expectation value): 11

[c)] monoisotopic mass of neutral peptide M_r: 1389.6975

[d)] fixed modification: carbamidomethyl

[e)] **$^{++}$:** doubly charged fragment ion, * : fragment ion with loss of ammonia, ^{0} :fragment ion with loss of water

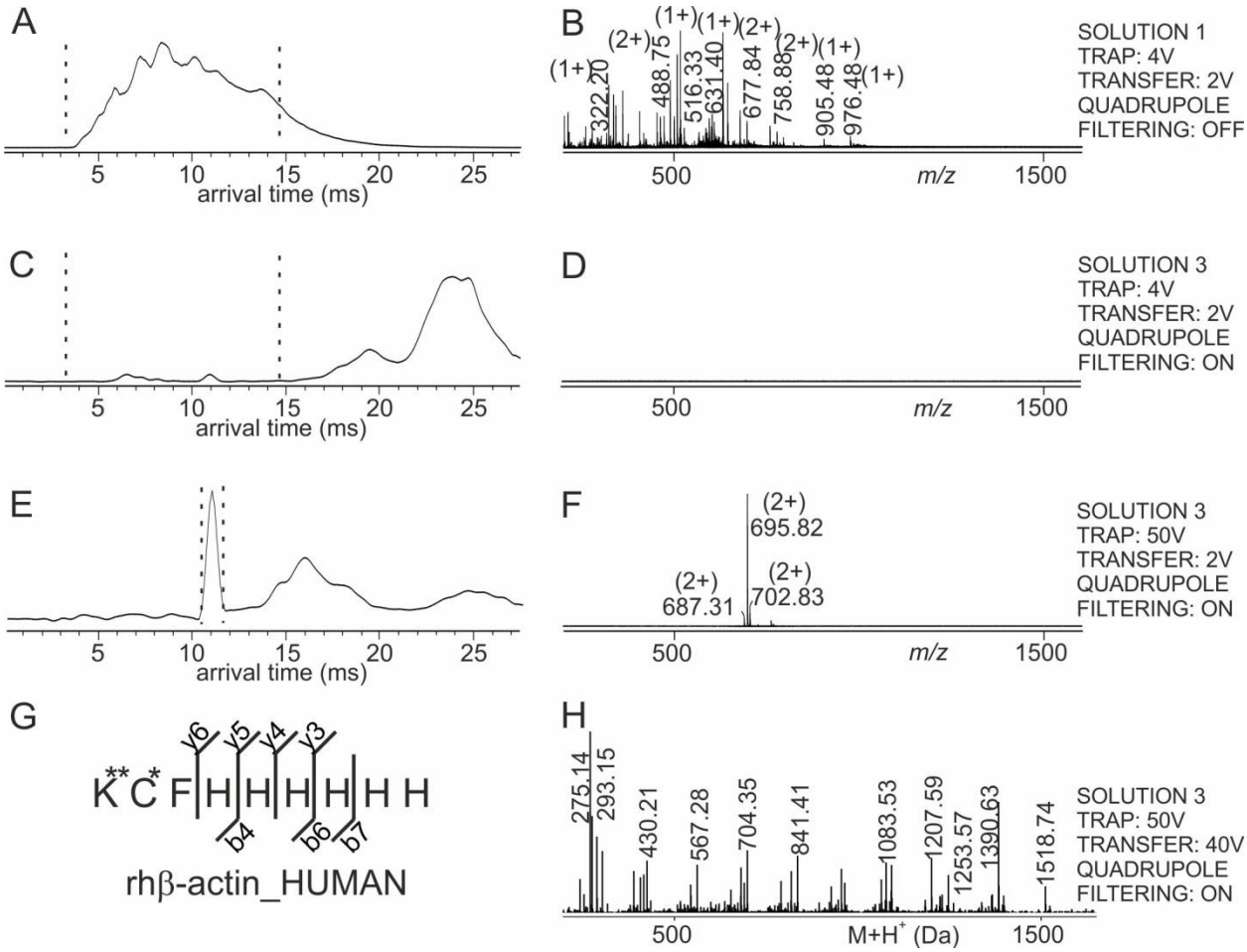

Figure S3: Mass spectrometric dissociation of the His-tag epitope peptide – antiHis-tag antibody complex and amino acid sequence determination of the complex-released peptide by mass spectrometric fragmentation. Ion mobility arrival time plots of **A:** Solution 1, **C:** and **E:** Solution 3. Dashed lines mark the regions for mass spectra selections. Settings of the TRAP cell, the TRANSFER cell, and the quadrupole are indicated at the right. **B**, **D**, and **F**: nanoESI mass spectra (low *m/z* range) of ions from selected arrival time ranges. Selected *m/z* values are given and charge states are indicated in parentheses. For ion signal assignments see Table S7. **G**: Amino acid sequence of the complex-released peptide (single letter code) as determined by the matched mass spectrometric fragment ions (fragment ion types and numbers are indicated). Carbamidomethylation is indicated by *. The amended Uniprot protein id of the peptide source protein (first hit) is shown. **H**: Pseudo mass spectrum (after charge deconvolution and de-isotoping) of fragment ions derived by selecting arrival time of the complex-released peptide with *m/z* 695.82. For ion signal assignments see Table S9.

Table S9: MS/MS fragmentation of KCFHHHHHH showing matches used for scoring [a,b)]

no.	b	b^{++}	b*	b^{*++}	seq [c,d,e)]	y	y^{++}	y^{*++}	no.
1	243.1452	122.0762	226.1186	113.5629	K				9
2	403.1758	202.0915	386.1493	193.5783	C	1148.4704	574.7388		8
3	550.2442	275.6258	533.2177	267.1125	F	988.4397	494.7235		7
4	***687.3031***	344.1552	670.2766	335.6419	H	***841.3713***	421.1893		6
5	824.3621	412.6847	807.3355	404.1714	H	***704.3124***	352.6598		5
6	***961.4210***	481.2141	944.3944	472.7008	H	***567.2535***	284.1304		4
7	***1098.4799***	549.7436	1081.4533	541.2303	H	***430.1946***	215.6009		3
8	1235.5388	618.2730	1218.5122	609.7598	H	293.1357	147.0715		2
9					H	156.0768	78.5420		1

[a)] 7 of 48 fragment ion masses were assigned using 12 most intense peaks from the spectrum (c.f. Figure S3): bold italic print means the series contributed to the score; bold print means that the number of matches in the ion series is greater than would be expected by chance, indicating that the ion series is present; non-bold underlined print means that the number of matches in the ion series is no greater than would be expected by chance, so that the matches themselves may be by chance; non-bold non-underlined print means that this mass was not represented by an ion signal in the mass spectrum.

[b)] ions score: 22; random score (expectation value): 7.8

[c)] monoisotopic mass of neutral peptide M_r: 1389.6010

[d)] fixed modification: carbamidomethyl; variable modification: dicarbamidomethyl

[e)] **$^{++}$:** doubly charged fragment ion, * : fragment ion with loss of ammonia

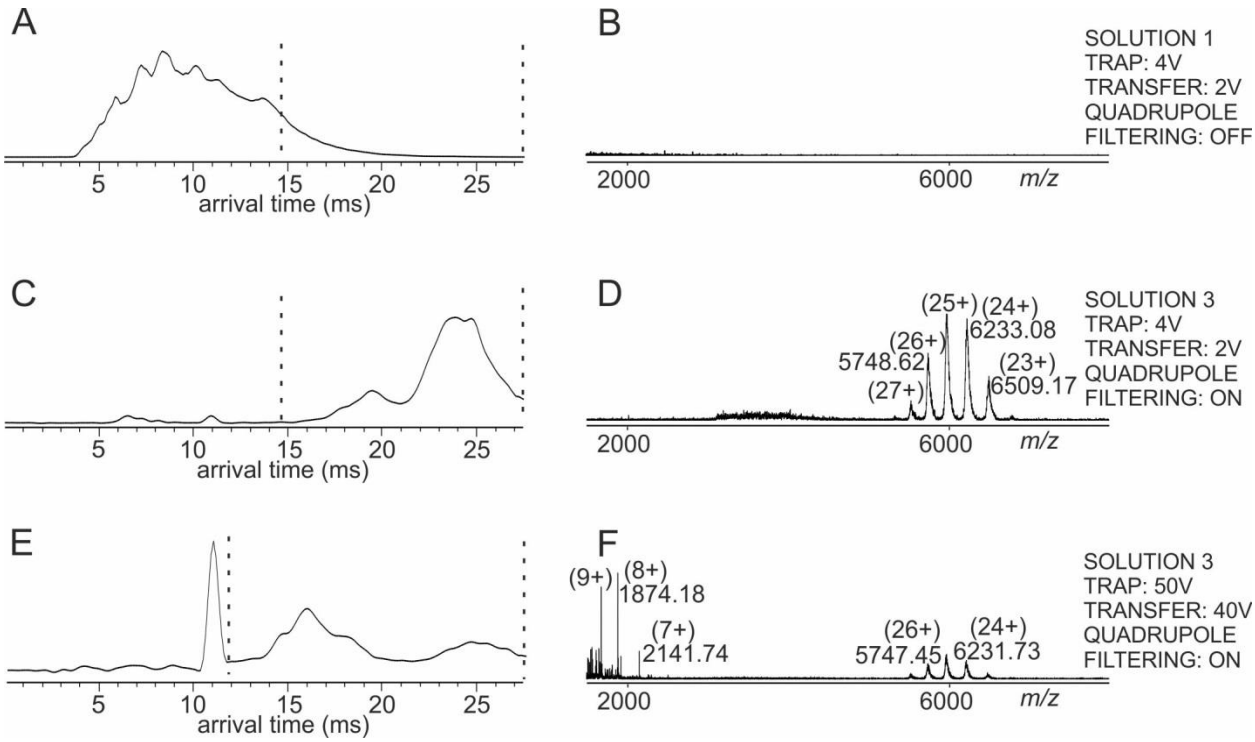

Figure S4: Mass spectrometric dissociation of the His-tag epitope peptide – antiHis-tag antibody complex. Ion mobility arrival time plots of **A:** Solution 1, **C:** and **E:** Solution 3. Dashed lines mark the regions for mass spectra selections. Settings of the TRAP cell, the TRANSFER cell, and the quadrupole are indicated at the right. **B**, **D**, and **F**: nanoESI mass spectra (high *m/z* range) of ions from selected arrival time ranges. Selected *m/z* values are given and charge states are indicated in parentheses. For ion signal assignments see Table S10.

Table S10: List of protein ion signals from antiHis-tag antibody [a].

molecular species	charge state [d]	exp. *m/z*	exp. mass
antibody-peptide complex [b]	22	6803.40	149652.80
	23	6509.17	149687.91
	24	6233.08	149569.92
	25	5978.56	149439.00
	26	5748.62	149438.12
	27	5534.18	149395.86
antibody fragments [c]	11	3472.98	38191.78
	12	3176.01	38100.12
	7	2141.62	14984.34
	8	1874.07	14984.56
	9	1665.97	14984.73

a) solutions 2 and 3 (cf. Figure S4)
b) antibody bound to peptide not resolved from antibody ion signals
c) observed at high collision voltages
d) positively charged ions

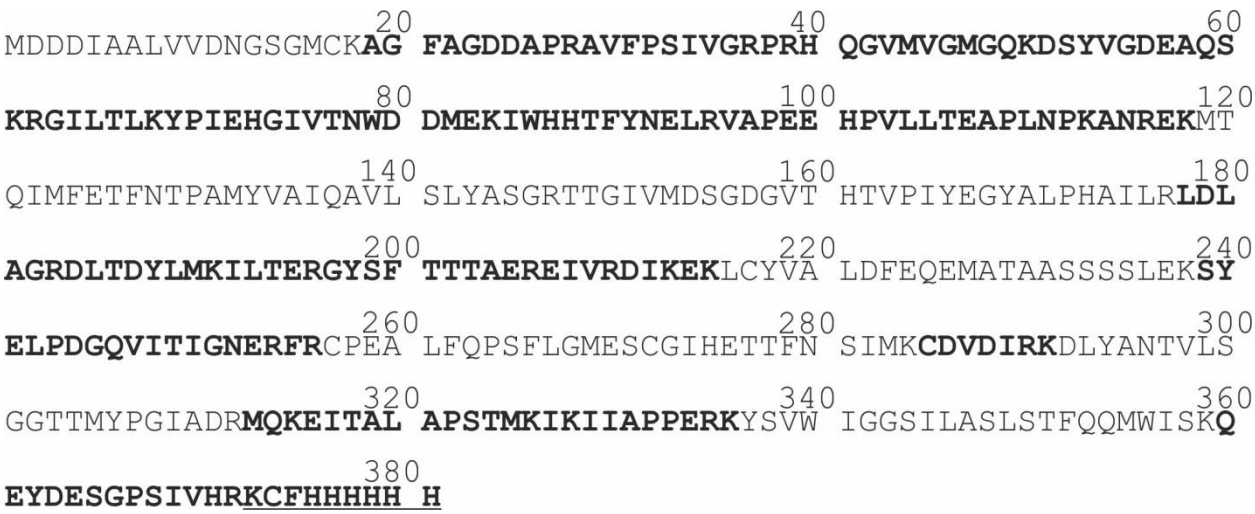

Figure S5: Amino acid sequence of recombinant human β-actin protein with C-terminal His-tag in single letter code. Partial amino acid sequences that were matched to ion signals from the nanoESI mass spectra (cf. Figure 3) are printed in bold. The amino acid sequence of the epitope peptide (aa373 – aa381) is underlined. For peptide assignments see Table S7.

Table S11: List of peptide ion signals upon tryptic digestion of rhTNFα [a].

sequence range	charge state [b]	*m/z* (exp)	peptide mass (Mr)
1-28	5	631.73	3153.65
2-27	5	583.14	2910.52
2-27	4	728.63	2910.52
2-28	6	512.11	3066.62
2-28	5	614.33	3066.62
2-28	4	767.66	3066.62
3-27	4	689.61	2754.42
3-27	3	919.15	2754.42
3-28	5	583.14	2910.52
3-28	4	728.63	2910.52
28-40	3	466.28	1395.79
29-40	2	620.86	1239.69
29-61	3	1216.32	3645.98
31-40	2	528.31	1054,61
31-61	3	1154.63	3460.90
33-40	1	871.48	870.49
34-40	2	379.72	757.41
34-40	1	758.45	757.41
34-61	3	1055.57	3163.69
41-61	3	809.10	2424.29
41-61	2	1213.15	2424.29
62-78	4	452.49	1805.92
62-78	3	602.98	1805.92
79-86 c)	2	455.26	908.50
79-86 c)	1	909.54	908.50
87-94 d)	2	429.29	856.54
87-94 d)	1	857.56	856.54
87-99	3	476.94	1427.79
100-124	3	951.14	2850.41
100-124	2	1426.19	2850.41
100-127	4	795.64	3178.56
100-127	3	1060.52	3178.56
125-153	3	1077.2	3228.61
128-153	3	967.82	2900.46
128-153	2	1451.22	2900.46

a) solution 1 (cf. Figure 4 and Figure S8)
b) positively charged ions
c) peptide containing the epitope
d) peptide adjacent to the epitope

Table S12: MS/MS fragmentation of IAVSYQTK showing matches used for scoring [a,b)]

no.	a	a*	b	b*	seq [c,d)]	y	y*	no.
1	86.0964		114.0913		I			8
2	157.1335		185.1285		A	***796.4199***	779.3934	7
3	256.2020		284.1969		V	***725.3828***	708.3563	6
4	343.2340		371.2289		S	***626.3144***	609.2879	5
5	506.2973		534.2922		Y	***539.2824***	522.2558	4
6	634.3559	617.3293	662.3508	645.3243	Q	***376.2191***	359.1925	3
7	735.4036	718.3770	763.3985	746.3719	T	***248.1605***	231.1339	2
8					K	147.1128	130.0863	1

[a)] 7 of 32 fragment ion masses using 16 most intense peaks from the spectrum (c.f. Figure 4): bold italic print means the series contributed to the score; bold print means that the number of matches in the ion series is greater than would be expected by chance, indicating that the ion series is present; non-bold underlined print means that the number of matches in the ion series is no greater than would be expected by chance, so that the matches themselves may be by chance; non-bold non-underlined print means that this mass was not represented by an ion signal in the mass spectrum.
[b)] ions score: 35; random score (expectation value): 0.25
[c)] monoisotopic mass of neutral peptide M_r: 909.4967
[d)] * : fragment ion with loss of ammonia

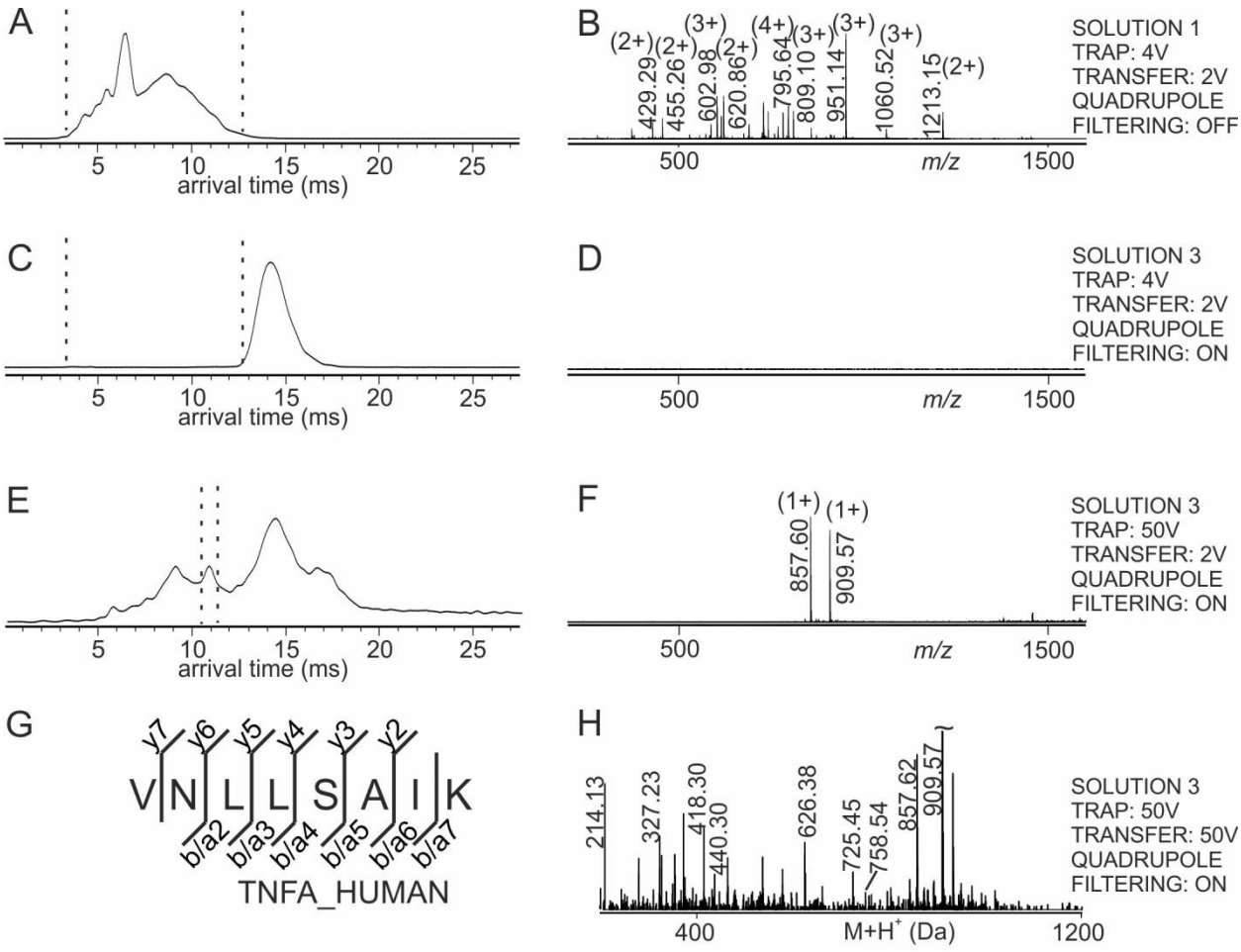

Figure S6: Mass spectrometric dissociation of the TNFα epitope peptide – anti TNFα antibody complex and amino acid sequence determination of the complex-released peptide by mass spectrometric fragmentation. Ion mobility arrival time plots of **A:** Solution 1, **C:** and **E:** Solution 3. Dashed lines mark the regions for mass spectra selections. Settings of the TRAP cell, the TRANSFER cell, and the quadrupole are indicated at the right. **B**, **D**, and **F**: nanoESI mass spectra (low *m/z* range) of ions from selected arrival time ranges. Selected *m/z* values are given and charge states are indicated in parentheses. For ion signal assignments see Table S11. **G**: Amino acid sequence of the complex-released peptide (single letter code) as determined by the matched mass spectrometric fragment ions (fragment ion types and numbers are indicated). The Uniprot protein id of the peptide source protein (first hit) is shown. **H**: Pseudo mass spectrum (after charge deconvolution and de-isotoping) of fragment ions derived by selecting arrival time of the complex-released peptide with *m/z* 857.60. For ion signal assignments see Table S13.

Table S13: MS/MS fragmentation of VNLLSAIK showing matches used for scoring [a,b)]

no.	a	a*	b	b*	seq. [c,d)]	y	y*	no.
1	72.0808		100.0757		V			8
2	186.1237	169.0972	**214.1186**	197.0921	N	***758.4771***	741.4505	7
3	299.2078	282.1812	**327.2027**	310.1761	L	***644.4341***	627.4076	6
4	412.2918	395.2653	**440.2867**	423.2602	L	***531.3501***	514.3235	5
5	499.3239	482.2973	527.3188	510.2922	S	***418.2660***	401.2395	4
6	570.3610	553.3344	**598.3559**	581.3293	A	***331.2340***	314.2074	3
7	683.4450	666.4185	711.4400	694.4134	I	***260.1969***	243.1703	2
8					K	147.1128	130.0863	1

[a)] 15 of 40 fragment ion masses were assigned using 63 most intense peaks from the spectrum (c.f. Figure S6): bold italic print means the series contributed to the score; bold print means that the number of matches in the ion series is greater than would be expected by chance, indicating that the ion series is present; non-bold underlined print means that the number of matches in the ion series is no greater than would be expected by chance, so that the matches themselves may be by chance; non-bold non-underlined print means that this mass was not represented by an ion signal in the mass spectrum.
[b)] ions score: 14; random score (expectation value): 41
[c)] monoisotopic mass of neutral peptide M_r: 856.5382
[d)] * : fragment ion with loss of ammonia

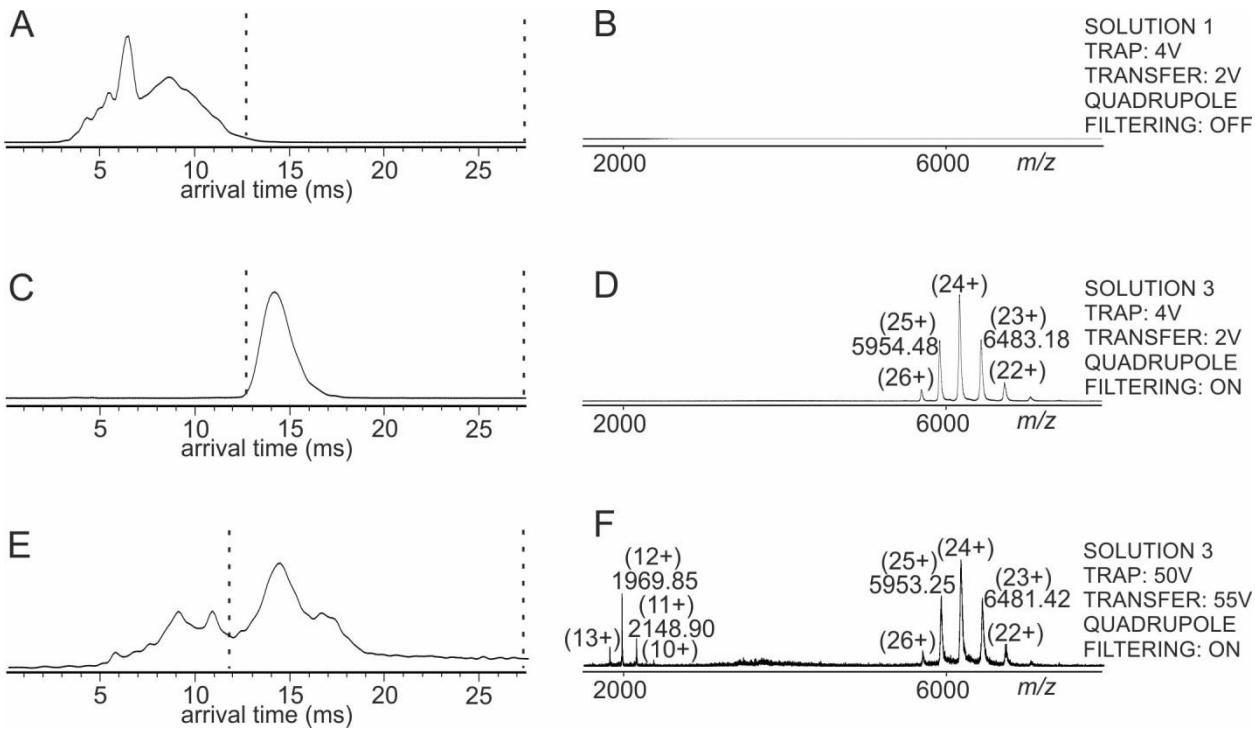

Figure S7: Mass spectrometric dissociation of the TNFα epitope peptide – anti TNFα antibody complex. Ion mobility arrival time plots of **A:** Solution 1, **C:** and **E:** Solution 3. Dashed lines mark the regions for mass spectra selections. Settings of the TRAP cell, the TRANSFER cell, and the quadrupole are indicated at the right. **B**, **D**, and **F**: nanoESI mass spectra (high *m/z* range) of ions from selected arrival time ranges. Selected *m/z* values are given and charge states are indicated in parentheses. For ion signal assignments see Table S14.

Table S14: List of protein ion signals from antiTNFα antibody [a].

molecular species	charge state [d]	exp. *m/z*	exp. mass
antibody-peptide complex [b]	22	6779.89	149135.58
	23	6483.18	149090.14
	24	6203.56	148861.44
	25	5954.48	148837.00
	26	5720.10	148696.60
	27	5506.67	148653.09
antibody fragments [c]	10	2363.79	23627.90
	11	2148.90	23626.90
	12	1969.85	23626.20
	13	1818.49	23627.37
	7	2059.88	14412.16
	8	1802.59	14412.72
	9	1603.87	14425.83

a) solutions 2 and 3 (cf. Figure S7)
b) antibody bound to peptide not resolved from antibody ion signals
c) observed at high collision voltages
d) positively charged ions

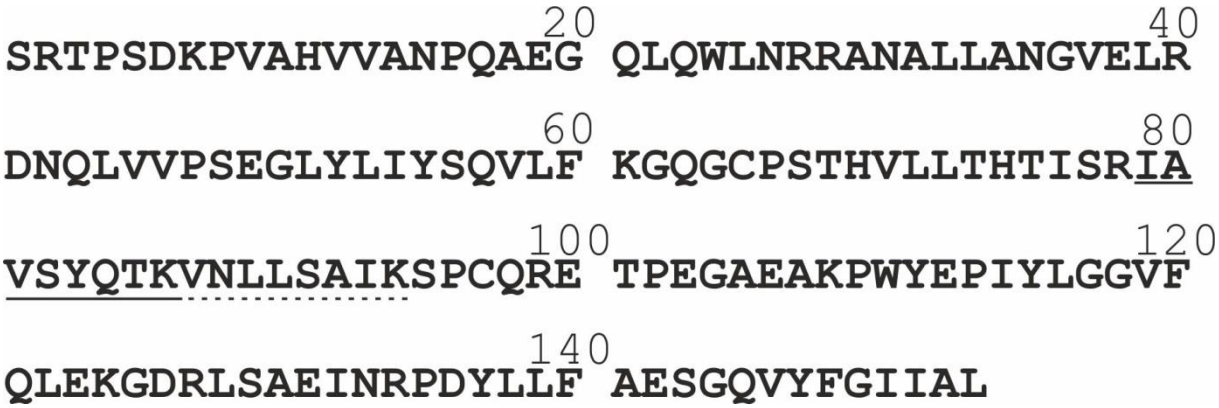

Figure S8: Amino acid sequence of recombinant human TNFα protein monomer with N-terminal His-tag in single letter code. Partial amino acid sequences that were matched to ion signals from the nanoESI mass spectra (cf. Figure 4) are printed in bold. The amino acid sequence of the epitope peptide (aa79 – aa86) is underlined. The adjacent peptide (aa87 – aa94) is dotted underlined. For peptide assignments see Table S11.

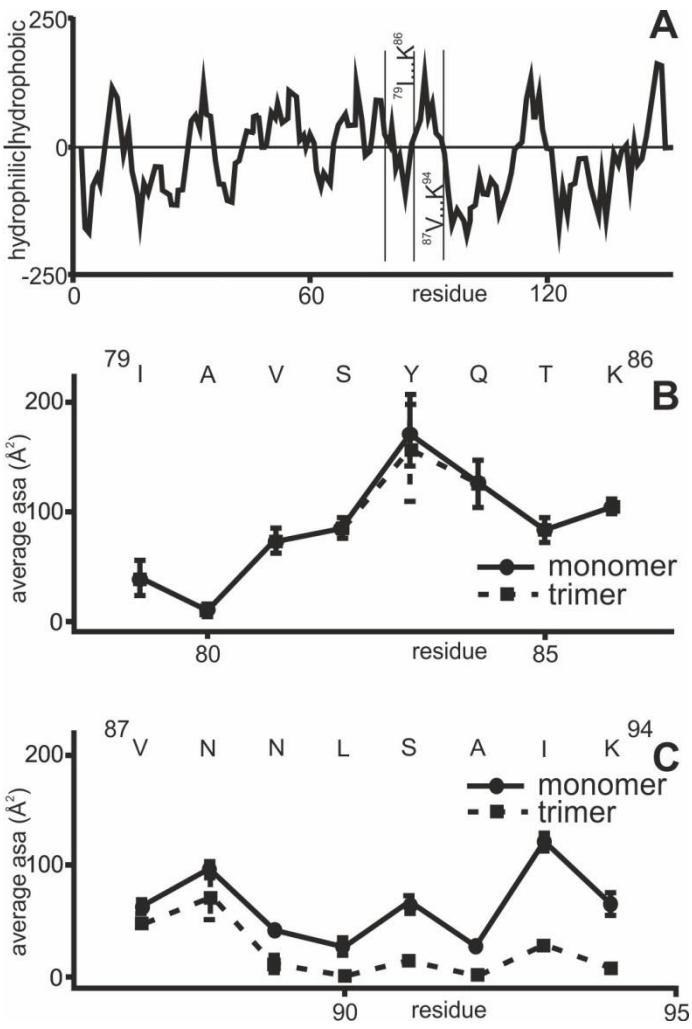

Figure S9: Physico-chemical properties of recombinant human TNFα protein. **A**: Hydrophobicity plot. The epitope peptide (aa79 – aa86) is hydrophilic. The adjacent peptide (aa87 – aa94) is hydrophobic. **B**: Partial amino acid surface areas of the amino acids of the epitope peptide (aa79 – aa86). **C**: Partial amino acid surface areas of the amino acids of the adjacent peptide (aa87 – aa94). Values for monomers (filled dots and solid line) and of the trimer (filled squares and dotted line) represent means and standard deviations are shown. Amino acid residues are displayed in single letter code (cf. Figure S8).

2.3 Apparent activation energies of protein-protein complex dissociation in the gas phase determined by electrospray mass spectrometry

Anal Bioanal Chem (2017) 409:6549–6558
DOI 10.1007/s00216-017-0603-4

RESEARCH PAPER

Apparent activation energies of protein–protein complex dissociation in the gas–phase determined by electrospray mass spectrometry

Yelena Yefremova[1] · F. Teresa I. Melder[1] · Bright D. Danquah[1] · Kwabena F.M. Opuni[1,2] · Cornelia Koy[1] · Alexandra Ehrens[3,4] · David Frommholz[3] · Harald Illges[3] · Knut Koelbel[5] · Frank Sobott[5,6,7] · Michael O. Glocker[1]

Received: 22 June 2017 / Revised: 9 August 2017 / Accepted: 23 August 2017 / Published online: 12 September 2017

Abstract We have developed a method to determine apparent activation energies of dissociation for ionized protein–protein complexes in the gas phase using electrospray ionization mass spectrometry following the Rice-Ramsperger-Kassel-Marcus quasi-equilibrium theory. Protein–protein complexes were formed in solution, transferred into the gas phase, and separated from excess free protein by ion mobility filtering. Afterwards, complex disassembly was initiated by collision-induced dissociation with step-wise increasing energies. Relative intensities of ion signals were used to calculate apparent activation energies of dissociation in the gas phase by applying linear free energy relations. The method was developed using streptavidin tetramers. Experimentally determined apparent gas-phase activation energies for dissociation ($E^{\#}_{A\ m0g}$) of complexes consisting of Fc parts from immunoglobulins (IgG-Fc) and three closely related protein G' variants (IgG-Fc•protein G'e, IgG-Fc•protein G'f, and IgG-Fc•protein G'g) show the same order of stabilities as can be inferred from their in-solution binding constants. Differences in stabilities between the protein–protein complexes correspond to single amino acid residue exchanges in the IgG-binding regions of the protein G' variants.

Keywords Protein–protein interaction · Native mass spectrometry · Ion mobility · Collision induced dissociation · Quasi equilibrium conditions

Yelena Yefremova and F. Teresa I. Melder contributed equally to this work.

Electronic supplementary material The online version of this article (https://doi.org/10.1007/s00216-017-0603-4) contains supplementary material, which is available to authorized users.

✉ Michael O. Glocker
michael.glocker@med.uni-rostock.de

[1] Proteome Center Rostock, University Rostock Medical Center, Schillingallee 69, 18059 Rostock, Germany

[2] Present address: School of Pharmacy, University of Ghana, P.O. Box LG43, Legon Accra, Ghana

[3] University of Applied Sciences Bonn-Rhein-Sieg, von-Liebig-Str. 20, 53359 Rheinbach, Germany

[4] Present address: University Hospital of Bonn, Sigmung-Freud-Str. 25, 53105 Bonn, Germany

[5] Department of Chemistry, University of Antwerp, Groenenborgerlaan 171, 2020 Antwerp, Belgium

[6] Astbury Centre for Structural Molecular Biology, University of Leeds, Leeds LS2 9JT, UK

[7] School of Molecular and Cellular Biology, University of Leeds, Leeds LS2 9JT, UK

Abbreviations

ESI	electrospray ionization
$E^{\#}_{A\ m0g}$	E_A: energy of activation, #: apparent (with merged temperature term), m: mean of charge states, 0: at E_{com} = 0 eV, g: gas phase
Fc part	fragment crystallizable part
IgG	immunoglobulin G
IVIG	intravenous immunoglobulin
$K_{D\ s}$	dissociation constant in solution
$K^{\#}_{D\ m0g}$	K_D: dissociation constant, #: apparent (with merged temperature term), m: mean of charge states, 0: at E_{com} = 0 eV, g: gas phase
LFE	linear free energy
Protein G′	protein G prime
Protein G′e	protein G prime e (extended)

Protein G′f	protein G prime f
Protein G′g	protein G prime g
ToF	time of flight
ΔG_s	Gibbs free energy difference in solution

Introduction

Already in the mid-90s of the last century, the possibility to characterize non-covalent bio-macromolecular complexes using electrospray mass spectrometry became evident [1, 2]. More recent studies provided strong indications that upon transfer into the gas-phase proteins retained compact conformations [3] that could be investigated by so-called "native ESI-MS" and ion mobility MS (IM-MS) [4–6]. These methods are now widely applied for determining qualitative properties of protein complexes, such as topology, size, subunit organization, and stoichiometry [7–9].

In solution, protein–protein interactions are characterized quantitatively by dissociation constants ($K_{D\ s}$) and Gibbs free binding energies (ΔG_s^0) at equilibrium [10], which are typically determined using calorimetric or spectroscopic methods [11]. In some cases, mass spectrometry-based methods have been applied as readouts for determining in-solution K_D values of protein–protein complexes by comparing ion signal intensities of free and complexed proteins at different solution concentrations of the complex components [12–15]. Introducing correction factors for differences of surface activities of analytes in the droplet as well as for additional gas-phase ion suppression effects [16] yielded satisfactory correlation with results from conventional methods.

There are, however, currently no universally accepted gas-phase equivalents to typical thermodynamic and/or kinetic methods for evaluating protein–protein complex properties. In one case, activation energies of thermal protein–protein complex dissociation in the gas phase were deduced by observing complex dissociation kinetics upon blackbody infrared radiation using Fourier-transform ion cyclotron resonance mass spectrometry [17]. In another study, factors that affected gas-phase stabilities of non-covalent protein–peptide complexes were interrogated but without determining strengths of interactions [18].

Here, we describe a method to estimate apparent activation energies of dissociation of charged protein–protein complexes in the gas phase ($E_{A\ m0g}^{\#}$) directly under quasi-equilibrium conditions. After protein–protein complexes have been formed in solution, electrospray mass spectrometry is used to ionize and transfer them into the gas phase intact. Upon ion mobility separation of the ionized intact complexes from excess non-complexed constituents, dissociation of the complexes is initiated. Relative intensities of ion signals were used to calculate apparent activation energies of dissociation in the gas phase according to the Rice-Ramsperger-Kassel-Marcus quasi-equilibrium theory (RRKM–QET), which assumes that dissociation of molecular complexes in the gas phase is unidirectional and irreversible, i.e., not reaching equilibrium conditions. The energy that is applied to dissociate a protein–protein complex in the mass spectrometer is, thus, in correlation with its activation energy [19–21].

To develop our method, we investigated dissociation of the streptavidin tetramer and applied the procedure to three closely related protein–protein complexes consisting of Fc parts of immunoglobulins (IgG) and protein G' isoforms (IgG-Fc•protein G'e, IgG-Fc•protein G'f, and IgG-Fc•protein G'g). Apparent activation energies of dissociation in the gas phase were compared with thermodynamic data from in-solution measurements.

Materials and methods

Materials

Protein G'e was obtained from Sigma-Aldrich, Steinheim, Germany (catalog no. P4689-5MG; lot no.SLBB8536V). Protein G'f was produced by the University of Applied Sciences Bonn-Rhein-Sieg (Bonn, Germany). Protein G'g was a gift from Rainin Corp. (Oakland, CA, USA). Active human IgG-Fc fragment was from Abcam, Cambridge, UK (product no. ab90285, lot no. GR149467–12). All stock solutions contained 50 μg of protein. Polyclonal intravenous immunoglobulins (IVIG) were obtained from Omrix Biopharmaceuticals (Nes-Ziona, Israel). 16-Mercaptohexadecanoic acid, phosphate buffered saline powder, ethanolamine, *N*-hydroxysuccinimide, 2-[*N*-morpholino] ethanesulfonic acid, 1-ethyl-3-[3-dimethylaminopropyl] carbodiimide were from Sigma-Aldrich. Details on streptavidin can be found in the Electronic Supplementary Material (ESM).

IgG-Fc and protein G'-containing solutions

Solutions of active human IgG-Fc and protein G' isoforms (protein G'e, protein G'f, and protein G'g) were buffer-exchanged using Amicon ultra centrifugal filters with 10 K cutoff (Millipore Corporation, Ireland) according to the manufacturer's protocol. Protein concentrations (aliquots of ca. 2 μg in 5 μl, each) were determined with the fluorescence-based Qubit™ assay (Invitrogen, Carlsbad, USA). For calibration, Qubit™ working solution (Qubit™ reagent diluted 1/100 in Qubit™ buffer) and three calibration standards (0, 200, and 400 ng/μl) were mixed (190 and 10 μl, respectively), incubated for 15 min, and measured in the Qubit® 2.0 Fluorimeter. Raw fluorescence values were used to calculate the concentrations of the similarly treated proteins in the assay tubes and in the original stocks. Typical protein concentrations were between 0.2 and 0.6 μg/μl. Sample

solutions were either directly used for preparation of complexes consisting of protein G' isoforms and IgG-Fc or stored at −20 °C.

Protein G'–IgG-Fc complex preparations

IgG-Fc (3.6 μM; ca. 20–35 μl) in 200 mM ammonium acetate buffer, pH 7.1, was mixed with one of the buffer-exchanged protein G' isoforms at a time (ca. 6.5–13 μl) to yield a molar ratio of 1:1.3 (protein G' isoform: IgG-Fc). Small excess of protein G' was found to be optimal for both, generating an in-solution complex with 1:1 stoichiometry and avoiding precipitation. All protein G' isoform–IgG-Fc complexes were prepared in this manner at room temperature. Solutions with protein–protein complexes were either directly used for nano-ESI-IMS-MS/MS analysis or kept at +4 °C for maximally 1 week.

Nano-ESI-IMS-MS/MS acquisition conditions

Capillaries for nano-ESI-IMS-MS/MS measurements were prepared in-house [22] from borosilicate glass tubes of 1 mm outer and 0.5 mm inner diameters using a P-1000 Flaming / Brown™ Micropipette Puller System (all Sutter Instrument, Novato, CA, USA) and gold-coated using a BalTec SCD 004 sputter coater (Bal-Tech, Balzers, Liechtenstein). For each measurement, 3 μl of sample was loaded using a micro-loader pipette tip (Eppendorf, Hamburg, Germany). Measurements were performed on a Synapt G2-S mass spectrometer (Waters MS-Technologies, Manchester, UK) equipped with a traveling-wave ion mobility cell (TW-IMS). The instrumental parameters were optimized as follows: source temperature, 50 °C; sample cone, 150 V; source offset, 150 V; trap collision energy, 4 V; trap DC bias, 45 V; trap gas flow, 10 ml/min; helium cell gas flow, 180 ml/min; IMS gas flow, 80 ml/min; wave velocity, 700 m/s; wave amplitude, 35 V. The capillary voltage was adjusted individually for each measurement (1.3–2 kV). The transfer collision energy (TCE) was raised from 2 to 220 V in a stepwise manner (20–30 V steps) to induce protein–protein complex dissociation. Mass spectra were acquired in positive-ion mode applying a mass window of m/z 200–10,000. External mass calibration was performed with 1 mg/ml sodium iodide dissolved in an isopropanol/water solution (50:50, *v*/*v*). Data acquisition and processing were performed with the MassLynx software version 4.1 (Waters MS-Technologies, Manchester, UK) [22]. Data analysis and calculation of gas-phase activation energy are outlined in the ESM.

In-solution K_D value determinations

Real time bio-affinity analyses were performed with the K5S-Sens® SAW biosensor (SAW Instruments, Bonn, Germany). The chip surface was cleaned by a 45-min sonication in 20-ml piranha solution (30% H_2O_2/H_2SO_4 1:1) and subsequent 15 min washing steps with ca. 20 ml deionized water and with ca. 20 ml ethanol, respectively. When dried, the plain gold surface of the chip was functionalized by incubating the chip in 30 ml 10 μM 16-mercaptohexadecanoic acid in $CHCl_3$ at 25 °C for 12–16 h to generate the self-assembled monolayer (SAM). Afterwards, the SAM was washed with ca. 5-ml ethanol and the chip was allowed to dry. The functionalized chip was inserted into the sensor unit of the instrument, and immobilization of the antibody (ligand) was performed online in the microfluidic cell of the biosensor as follows. After washing with immobilization buffer (10 mM acetate buffer, pH 5) for 30 min, 250 μl of 30 mg/ml EDC (dissolved in a mixture of 100 mM NHS: 50 mM MES, pH 6.3) was injected to activate the free carboxyl groups on the SAM. Ligand molecules were immobilized by injecting 250 μl of IVIG (2.5 μg/μl in 10 mM acetate buffer, pH 5). The remaining active sites were quenched by injecting 250 μl of aqueous 1 M ethanolamine (pH 8.5). A flow rate of 20 μl/min was maintained throughout the immobilization procedure. Binding experiments were performed at 22 °C using 10 mM PBS (pH 7.4) running buffer in a two frequency mode (optimum frequency 150.8 MHz). Serial dilutions of analytes were prepared after determining stock solution concentrations (1200 nM, each) using the Qubit® 2.0 Fluorometer (Invitrogen, Carlsbad, USA) as described above. Sample concentrations of 25, 50, 100, 400, and 500 nM (protein G'e); 50, 200, 300, 400, and 500 nM (protein G'f); and 100, 300, 400, 600, and 800 nM (protein G'g) all in 10 mM PBS (pH 7.4) were used. The measurements (binding curves) were recorded as changes in the phases of the acoustic waves (in degree) due to binding as functions of time (in seconds). Data analysis procedures are described in the ESM.

Results

Method development

To develop a mass spectrometry-based method by which apparent dissociation energies of ionized protein–protein complexes could be investigated in the gas phase, we analyzed the dissociation behavior of streptavidin tetramer complexes. Both theoretical considerations as well as details of our development-oriented investigations are provided in the ESM (Figs. S1 to S6). The main findings of our studies with streptavidin are that the RRKM–QE theory can be applied to describe the dissociation behavior of protein–protein complexes in the gas phase semi-quantitatively and that there is no need to investigate the dissociation behavior of each individual charge state of the protein–protein complex ions separately in order to deduce the apparent activation energy of complex dissociation. Instead, it is easier to perform and well suitable for calculating dissociation energies when all multiply

charged ions of a protein–protein complex are simultaneously submitted to dissociation. The abundance-weighted mean of charge states of a protein–protein complex (i) can easily be determined as the maximum position of its precursor ion peak ensemble and (ii) is subsequently applied for all thermodynamic calculations.

Analysis of individual proteins and formation of protein G' complexes with IgG-Fc in-solution

Having established the procedure, we focused on the analysis of gas-phase dissociation of protein–protein complexes consisting of the Fc parts of immunoglobulins (IgG-Fc) and one of three closely related protein G' variants (proteins G'e, G'f, and G'g). Each protein G' molecule contains three independent IgG-binding domains, which according to X-ray crystallography data [23] form part of the binding interface. Amino acid sequence alignment of the three protein G' variants (ESM Fig. S7) shows that protein G'e and protein G'g have identical sequences of the so-called IgG-binding domains I, II, and III as well as of the in-between spacer sequences. They differ only in their flanking sequences that are located on either the N-terminus (protein G'e; FSN) or on the C-terminus (protein G'g; FSC). By contrast, proteins G'f and G'e possess similar N-terminal flanking sequences (FSN), but differ markedly by single amino acid exchanges in the IgG-binding domains (four of them in the relevant region). The introduced single amino acid exchanges of protein G'f have been suggested to increase the overall stability of protein G'f under basic conditions as compared to that of protein G'e [24]. All in all, the parts of proteins G'e and G'g relevant for IgG-binding are identical as opposed to protein G'f. Comparable IgG binding properties are therefore expected for proteins G'e and G'g, but a different one for protein G'f.

When the free proteins G' were sprayed from neutral solutions, multiply charged ion series of high intensities with the highest signals at +10 (G'e) and +9 (G'f and G'g) were observed. Occasionally highly charged, i.e., unfolded proteins were detected as well with, however, only low signal intensities (ESM Fig. S8A-C). Protein G'e and protein G'f are known to be partially gluconoylated [25], yielding satellite ion signals of these protein species which are not always well resolved when sprayed under native ESI conditions (ESM Fig. S8A-B). For the non-gluconoylated proteins, we determined molecular masses, which closely agree with the calculated average masses of these proteins that were obtained from their amino acid sequences (Table 1).

When IgG-Fc was analyzed by nano-ESI-MS under neutral pH conditions, only a few rather broad protein ion signals were observed in the higher *m/z* range corresponding to charge states between 12+ and 15+ with a maximum intensity between the 13+ and the 14+ signal (ESM Fig. S8D). From these ions, the average molecular mass of ca. 53.4 kDa was experimentally determined. We had used IgG-Fc from a pool of polyclonal human IgGs, so several IgG-Fc species were present with amino acid sequence differences and heterogeneous glycosylation, explaining the broad ion signals in the ESI-MS spectra.

Protein G' isoforms were mixed with IgG-Fc at neutral pH (7.1), and the resulting protein–protein complexes were analyzed by nano-ESI-MS (Table 1). All three IgG-Fc•Protein G' complexes adopted a 1:1 stoichiometry, and their charge state distributions followed the same trends as did the free protein G' variants (Fig. 1). Because of slight excess of protein G' in the mixtures, multiply charged ion signals of free protein G' variants were seen in the mass spectra as well.

Dissociation of protein G'–IgG-Fc complexes in the gas phase

The presence of potentially interfering free protein G' ion signals led us to introduce a filtering step prior to inducing dissociation of the IgG-Fc•protein G' complexes. We filtered out ion signals of the unbound protein G' isoforms by ion mobility separation. The specific arrival time windows in which the IgG-Fc•protein G' complex ion signals were found exclusively were determined when collision energy in the transfer cell was turned off. For dissociation analyses without interference of either ion signals of unbound protein G' or of free IgG-Fc, the respective arrival time windows were kept constant and acceleration voltage in the transfer cell (V_{acc}) was raised stepwise from 50 to 220 V. For the IgG-Fc•protein G'e complex, exclusively ion signals of the complex with charge states from 16+ to 19+ were found until a transfer cell energy voltage (V_{acc}) of 70 V (Fig. 2a). The abundance-weighted mean charge state (m) of this complex was 17.40+ (Table 1).

Upon further increase of V_{acc}, the signal intensities of the complex ions decreased, while those of dissociated constituents appeared and increased (Fig. 2b–d). Protein G'e, which is the complex constituent with lower molecular mass, retained relatively more charges than the larger IgG-Fc. Released protein G'e carried 13+ to 11+ charges, whereas IgG-Fc retained 6+ or 7+ charges with low intensities. It should be mentioned that at very high transfer cell energies (V_{acc} 220 V; cf. Fig. 2e) substantial peptide backbone cleavage occurred, producing poorly resolved fragment ions. All gas-phase dissociation experiments were performed in triplicate for each of the three complexes. Abundance-weighted mean charge states (m) of 17.71+ and 16.33+ were calculated from the charge-state distributions of IgG-Fc•protein G'f and IgG-Fc•protein G'g complexes, respectively (Table 1).

Using the series of mass spectra that were recorded with different transfer cell energies, i.e., different center-of-mass energies of the protein–protein complexes, we next determined all areas under the ion signals in a given spectrum that

Table 1 Average molecular masses of starting materials and protein–protein complexes

	Protein			IgG-Fc•proteinG' complex	
	No. of aa	M_r	Exp. mass ± stdv., Da	Exp. mass ± stdv., Da	m
G'e	241	25,999.55	25,999.60 ± 0.09	79,380.20 ± 53.94	17.40
G'f	228	24,415.92	24,415.05 ± 0.16	77,818.48 ± 55.52	17.71
G'g	209	22,809.09	22,809.43 ± 0.10	76,016.77 ± 20.73	16.33
IgG-Fc	n.d.	n.d.	53,392.70 ± 0.83	n.a.	n.d.

aa amino acid residues, *m* abundance-weighted mean charge state, *n.d.* not determined, *n.a.* not applicable

were present with decent intensities. After summing up all these areas under the ion signals, e.g., of protein G'e, the IgG-Fc•protein G'e complex, and their fragments, the ion signal intensities were normalized to the sum of all peak areas. The same procedure was applied with the IgG-Fc•protein G'f and IgG-Fc•protein G'g complex dissociation analyses (ESM Figs. S9 and S10). Normalized and averaged areas under the signals (norm. AUS) corresponding to the IgG-Fc•protein G'e complex and its dissociation products were plotted against center-of-mass collision energy values (E_{com}) (Fig. 3). The data points were fitted to a sigmoidal curve and showed the disappearance of the IgG-Fc•protein G'e complex with increasing energy, while the intensities of the ion signals for the dissociated protein G'e went up to reach a maximum at around E_{com} = 1.5 eV. At higher E_{com}, the ion signal intensities of the backbone fragments increased at the expense of the intact proteins. Dissociation analysis was performed for IgG-Fc•protein G'g and IgG-Fc•protein G'f complexes following the same procedure as described above.

The overlaid normalized AUS curves of all three IgG-Fc•protein G' complexes (Figure 4a) showed similar sigmoidal characteristics of complex disappearance with increasing E_{com} values. The center-of-mass energy at which 50% of the IgG-Fc•protein G'e and IgG-Fc•protein G'g complexes were dissociated was 1.3 eV. However, in case of the IgG-Fc•protein G'f complex, 50% dissociation was achieved already at 1.2 eV (Table 2).

Using the normalized AUS values, we calculated the apparent Gibbs free energy, $\Delta G_g^{\#}$, in the gas phase for individual complex dissociation events and plotted them vs. E_{com} (Fig. 4b). Interestingly, the slopes ("*n* values") of all three fitted lines were very similar. A linear free energy (LFE) evaluation, i.e., linear extrapolation of the lines from the $\Delta G_g^{\#}$ values provided the apparent activation energy ($E_{A\ m0g}^{\#}$) of protein–protein complex dissociation at the intercepts with the y-axis (E_{com} = 0 eV), at which the external energy component is negligible.

It is apparent that the IgG-Fc•protein G'f complex requires less activation energy for dissociation than the IgG-Fc•protein G'e and IgG-Fc•protein G'g complexes, respectively. They both dissociate at comparable activation energies (Table 2).

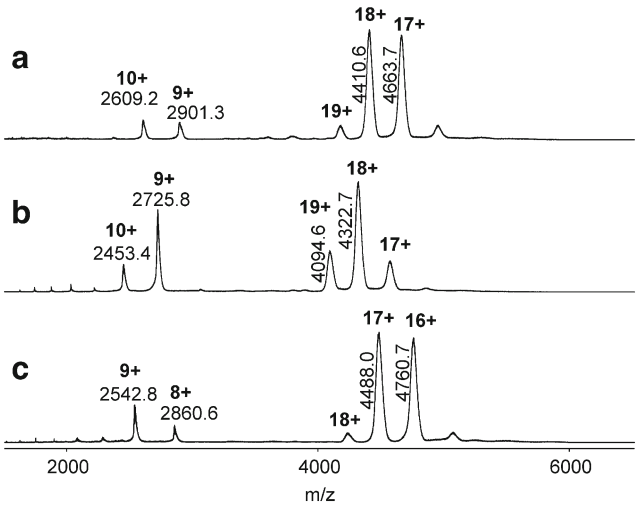

Fig. 1 NanoESI mass spectra of protein complexes derived from protein G' isoforms and IgG-Fc. **A** IgG-Fc•proteinG'e. **B** IgG-Fc•proteinG'f. **C** IgG-Fc•proteinG'g. Charge states and *m/z* values for selected ion signals are given for the complexes (right ion series) and for the respective uncomplexed protein G' isoforms (left ion series). Solvent: 200 mM NH_4OAc

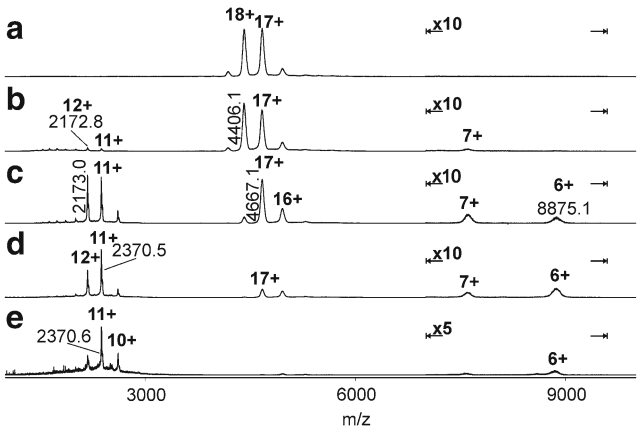

Fig. 2 Nano-ESI mass spectra of IgG-Fc•proteinG'e after ion mobility separation and exposure to different transfer cell energies (TCE; given as acceleration voltages V_{acc}). **A**: 70 V. **B**: 120 V. **C**: 150 V. **D**: 170 V. **E**: 200 V. Charge states and *m/z* values for selected ion signals are given for the complexes (center ion series) and for the respective released protein G'e (left ion series) and IgG-Fc (right ion series). Solvent: 200 mM NH_4OAc. Ranges with 10-fold or 5-fold magnification are marked; *m/z* values of ion signal apexes are labeled. At 200 V, TCE protein ion signals are superimposed by ion signals from fragments

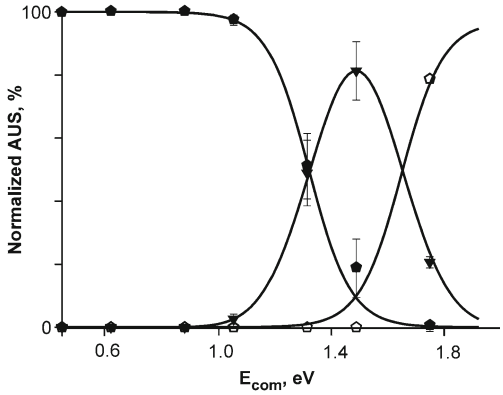

Fig. 3 Normalized areas under signals (AUS) plotted as a function of center-of-mass energy. AUS of IgG-Fc•proteinG'e (*filled pentagons*), intact protein G'e (*filled triangles*), and fragments (*open pentagons*) are shown. Each data point is the mean of three independent measurements, and standard deviations are shown by vertical bars. A Boltzmann function was used to fit the curve for the IgG-Fc•proteinG'e complex, a Gaussian function was used to fit the curve for intact protein G'e, and a logistic function was used to fit the curve for the protein fragment abundances

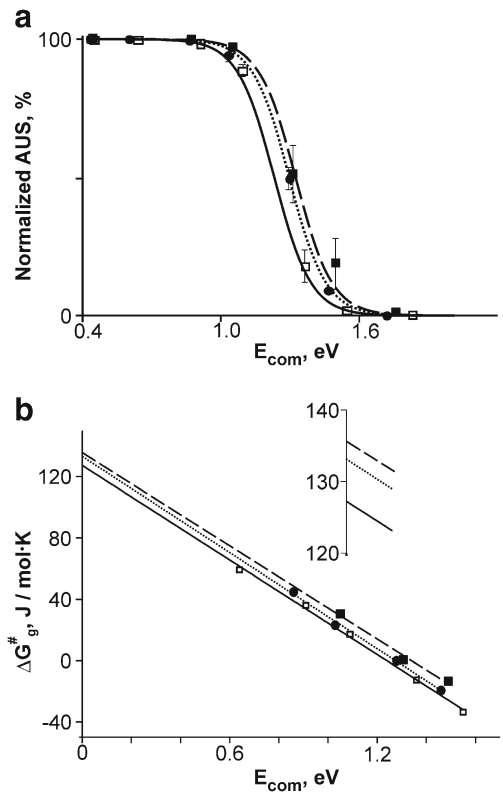

Fig. 4 **A** Normalized areas under signals (AUS) plotted as functions of center-of-mass collision energy for IgG-Fc•proteinG'e (*dashed line*; *filled squares*), IgG-Fc•proteinG'g (*dotted line*; *filled circles*), and IgG-Fc•proteinG'f (*solid line*; *empty squares*). Curves are fitted using Boltzmann functions. **B** Differences of apparent Gibbs free energies in the gas phase ($\Delta G_g^{\#}$) plotted as functions of center-of-mass collision energy for IgG-Fc•proteinG'e (*dashed line*; *filled squares*), IgG-Fc•proteinG'g (*dotted line*; *filled circles*), and IgG-Fc•proteinG'f (*solid line*; *empty squares*). The intercepts with the y-axis (zoomed insert) give $E_{A\ m0g}^{\#}$ values

Table 2 Comparison of gas phase and in-solution parameters of protein G' isoforms complexed with IgG(Fc)

Protein	Solution	Gas phase		
	$K_{D\ s} \pm stdv.$ [nM]	E_{com50} [eV]	$E_{A\ m0g}^{\#}$ $\left[\frac{J}{mol \cdot K}\right]$	$K_{D\ m0g}^{\#}$ [nM]
G'e	54.8 ± 8.3	1.3	135.7	81.6
G'f	133.0 ± 17.5	1.2	127.2	226.7
G'g	56.0 ± 2.8	1.3	133.1	111.5

[a] Center-of-mass energies at which 50% of the IgG-Fc•protein G' complexes were dissociated

Since the IgG-Fc•protein G'f complex was found to be less stable in the gas phase than the complexes with the two other protein G' isoforms, we conclude that amino acid sequence differences in the IgG-binding domains played more dominant roles for complex stability as opposed to the flanking sequences which seemed to be of lesser importance.

Structural analysis of IgG-Fc complex formation by protein G'

From X-ray data of protein G', it is known that IgG-binding domain III is involved in binding to IgG-Fc to a larger degree than the other two domains. Since mixing of protein G' and IgG-Fc in solution resulted in a 1:1 stoichiometry, we conclude that the 3rd domain of protein G' variants made the most important contacts to IgG-Fc. Consequently, the differences in amino acid sequences of the 3rd domains (Fig. 5) between protein G'e or protein G'g and protein G'f were mostly to be made responsible for the observed protein–protein complex stability differences.

As outlined above, the amino acid sequences of the IgG-binding relevant regions of protein G'e and protein G'g are identical (Fig. 5, the two upper and lowermost lines, respectively). Significant deviations within the actually binding-relevant regions only occur in the third

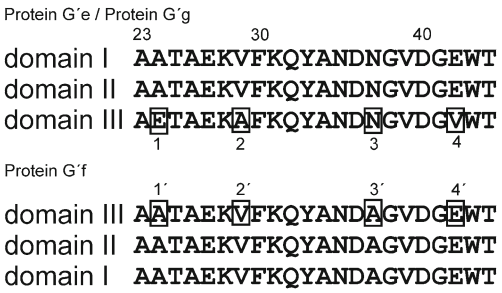

Fig. 5 Partial amino acid sequences of protein G'e, protein G'g, and protein G'f regions that are involved in contacts with IgG-Fc. Amino acid exchanges in the 3rd domains are boxed and numbered

IgG-binding domain of protein G'f as compared to the other two protein G'variants (Fig. 5, the two innermost lines). Out of the four amino acid residues which differ in the IgG-binding regions of protein G'e or protein G'g as compared to protein G'f, residue E24 (boxes marked 1 and 1′ in Fig. 5) has been suggested to cause the largest difference. E24 is involved in hydrogen bonds with residues R255 and/or K248 of IgG-Fc. Disrupting these hydrogen bonds, the E24A exchange results in decreased binding strength of protein G'f to IgG-Fc. By contrast, amino acid exchanges A29V and N37A (boxes marked 2 and 2′ as well as 3 and 3′ in Fig. 5) do not affect binding because the concerned amino acid residues are too remote from the interface region between the two proteins. Finally, the carboxyl group of E42 (boxes marked 4 and 4′ in Fig. 5) is involved in hydrogen bonding with the side chain of Q311 on the Fc part. However, it was reasoned that the E42V exchange neither favored nor disfavored binding, as upon this exchange remote conformational changes occurred and led to new hydrophobic interactions between protein G' and IgG-Fc [23].

In-solution dissociation constants of protein G'–IgG complexes and comparison to gas phase activation energies

To test whether the differences in gas phase binding between protein G' isoforms and IgG-Fc are mirroring in-solution behavior, we determined the dissociation constants ($K_{D\ s}$) of the interactions between polyclonal intravenous immunoglobulins (IVIG) and the three protein G' isoforms using a Surface Acoustic Wave Biosensor assay. The average $K_{D\ s}$ for IgG–protein G'e binding obtained from four independent measurements in two measurement series was 54.8 ± 8.3 nM. For IgG interaction of protein G'f, an average $K_{D\ s}$ value of 133.0 ± 17.5 nM and for protein G'g an average $K_{D\ s}$ value of 56.0 ± 2.8 nM were obtained from two independent measurements, each (Table 2). While the $K_{D\ s}$ values for protein G'e and protein G'g were identical within experimental error, that of protein G'f was roughly twice as high.

The experimentally determined apparent gas-phase activation energy values ($E^{\#}_{A\ m0g}$) were mathematically transformed into apparent gas-phase dissociation constants ($K^{\#}_{D\ m0g}$). Interestingly, the trends of the gas-phase values pretty much resembled those from the in-solution analyses. The $K^{\#}_{D\ m0g}$ values of IgG-Fc•protein G'e and IgG-Fc•G'g were more or less equal and half of that of IgG-Fc•protein G'f (Table 2), again indicating the differences in the binding strengths of the IgG-Fc•protein G'f complex as compared to the other two complexes.

Discussion

The current study opens the field for rapidly and reliably investigating protein–protein complex stabilities in the gas phase using mass spectrometry. Non-covalent complex dissociation under CID conditions requires an energy input above a critical threshold and proceeds irreversibly, but (comparatively) slowly. This concerns the fraction of particles, which, according to the energy-dependent Boltzmann distribution, contain sufficient energy for crossing the dissociation energy barrier. Hence, within this "transition energy region" dissociated complex constituent ions (products) and protein–protein complex ions (educts) are detectable simultaneously with their respective relative abundances. Hence, despite the de facto irreversible character of the dissociation reaction, an apparent equilibrium exists (RRKM-QET).

Of note, E_{com50} values do not represent pure internal energies of protein–protein complexes, as they still contain the ions' kinetic energy and charge-related energy increments. This may explain why in previous reports [26, 27] experimentally determined gas-phase binding strengths did not match with in-solution binding forces. Hence, for semi-quantitative evaluation of gas-phase protein–protein complex dissociation, we emphasize to subtract the ions' charge-related and kinetic energy contributions to the dissociation reaction, i.e., correct for "external" energy increments, by extrapolation to $E_{com} = 0$. The linear fit errors by which the intercepts with the y-axis are determined are within the 10% accuracy of the extrapolation procedure [28, 29]. Increasing the number of repetitions renders the method more robust. To limit the inherent effort, abundance-weighted mean charge states (m) were successfully applied instead of individual charge-state analyses.

As shown here, dissociation energies of protein–protein complexes in the gas phase that have been corrected for "external energy" contributions seem to represent in-solution properties of protein–protein complexes well. As was pointed out in a recent review [30], surface-induced dissociation (SID) seems to be an alternative to CID breakage of non-covalent bonds in the gas phase [31, 32]. However, in SID experiments, charges are distributed proportionally to the masses of dissociated constituents [33]. Dissociation reactions of any kind traverse at least one transition state with its associated energy barrier. This principle applies to both solution [28, 34, 35] and gas-phase reactions [36, 37], thus providing a common thermodynamic background. In solution, the backward reaction ensures that under equilibrium the system is limited by the Gibb's free energy, i.e., the internal energy difference between product and educt. However, in the gas phase, since there is no backward reaction, this role is fulfilled by the Gibb's free activation energy (here $E^{\#}_{A\ m0g}$), representing the energy barrier between ground state and transition state. Both gas phase and in-solution reactions assume, with first approximation, linear responses of product

formation with changing complex energies; thus, nominal stability values can be obtained by linear extrapolation [38, 39]. This model assumes that dissociation is mostly enthalpy driven and not requiring substantial entropy energy terms (hard spheres model), and that transition states are comparable, if not independent, of the ions' charge states. However, applying well-established in-solution equilibrium description (i.e., LFE; see ESM) to inherently irreversible gas-phase dissociation processes needs to take into account typical gas phase reaction features, such as asymmetric charge partitioning [40–43] and simultaneous (partial) unfolding of the dissociated complex components [26, 44].

Applying the LFE concept to describe gas-phase dissociation of protein–protein complexes, i.e., nominal complex stability values ($E^{\#}_{A\ m0g}$), we were able to add experimental evidence to the assumption that particular amino acid residues of the IgG-binding domains of protein G' variants play decisive roles in high affinity binding to IgG-Fc. Our gas-phase results not only confirmed what was expected from previous knowledge but also matched the results from in-solution measurements. Only, since desolvation occurs in the source of the mass spectrometer, hydrophobic interactions that contribute significantly to non-covalent binding in the liquid phase are (partially) lost in the gas phase. The (partial) loss of these hydrophobic forces could be the reason for lower binding constants observed in the gas phase ($K^{\#}_{D\ m0g}$) as opposed to the $K_{D\ s}$ values (cf. Table 2). However, since this is the first report on the issue, we do not exclude exceptions to the observations that have come out from our experiments. With respect to in-solution data, one should keep in mind that available software programs typically assume a 1:1 binding stoichiometry [45, 46]. By contrast, our analyses of protein complexes by mass spectrometry provide definite protein–protein complex stoichiometries.

The method for experimental determination of gas-phase stabilities of protein–protein complexes, as presented here, could, e.g., be used for checking whether or not non-synonymous coding single nucleotide polymorphisms (nsSNPs) affect protein–protein interactions by comparing $E^{\#}_{A\ m0g}$ values of wild-type and mutated proteins. Altering protein function, particularly protein–protein interaction properties, ultimately may lead to disease [47, 48]. The effects of nsSNPs, i.e., genomic mutations that cause specific amino acid substitutions [49], on binding strengths between two proteins can now be analyzed by ESI-MS in detail. To emphasize the importance, it has been found that a nsSNP variant of integrin β-2 (CD18) caused a P178L exchange which affects binding to integrin α-X (CD11) [50]. Patients who carry this mutation in their genomes suffer from leukocyte adherence deficiency (LAD) [51, 52]. LAD is clinically characterized by chronic neutrophilia, impaired wound healing, and severe life-threatening infections [53]. The huge amount of up to 200,000 nsSNPs in the human population shows the dimension of the task that awaits to be tackled, and therefore, any method that helps to characterize stabilities of protein–protein interactions that is less time-consuming and less expensive as conventional methodology clearly is of importance to characterize these effects on protein functions [14].

In sum, determination of gas phase stabilities, i.e., apparent activation energies of dissociation ($E^{\#}_{A\ m0g}$) of protein–protein complexes in the gas phase is a rapid method to obtain useful information for characterizing protein–protein, protein–metabolite, protein–drug, or protein–nucleic acid interactions with only little sample consumption.

Acknowledgements We express our thanks to Dr. Stephan Mikkat for providing expertise on mass spectrometry and to Ms Ursula Glocker for preliminary technical assistance. We also thank Dr. Marcus Frank for providing access to the capillary sputter. We acknowledge the German Academic Exchange Service (DAAD) for providing scholarships for YY (no. 91523785), BD (no. 91566064), and KO (no. 91548123). The WATERS Synapt G2S mass spectrometer has been bought through an EU grant (EFRE-UHROM 9) made available to MOG.

Compliance with ethical standards

Conflict of interest The authors have no conflict of interest to declare.

References

1. Przybylski M, Glocker MO. Electrospray mass spectrometry of biomacromolecular complexes with noncovalent interactions—new analytical perspectives for supramolecular chemistry and molecular recognition processes. Angew Chem Int Ed. 1996;35(8):807–26. https://doi.org/10.1002/anie.199608061.
2. Loo JA. Studying noncovalent protein complexes by electrospray ionization mass spectrometry. Mass Spectrom Rev. 1997;16(1):1–23. https://doi.org/10.1002/(SICI)1098-2787(1997)16.
3. Pagel K, Natan E, Hall Z, Fersht AR, Robinson CV. Intrinsically disordered p53 and its complexes populate compact conformations in the gas phase. Angew Chem Int Ed. 2013;52(1):361–5. https://doi.org/10.1002/anie.201203047.
4. Bornschein RE, Ruotolo BT. Ion mobility-mass spectrometry of charge-reduced protein complexes reveals general trends in the collisional ejection of compact subunits. Analyst. 2015;14(20):7020–9. https://doi.org/10.1039/c5an01242b.
5. Chen F, Gulbakan B, Weidmann S, Fagerer SR, Ibanez AJ, Zenobi R. Applying mass spectrometry to study non-covalent biomolecule complexes. Mass Spectrom Rev. 2016;35(1):48–70. https://doi.org/10.1002/mas.21462.
6. Hoaglund CS, Valentine SJ, Sporleder CR, Reilly JP, Clemmer DE. Three-dimensional ion mobility/TOFMS analysis of electrosprayed biomolecules. Anal Chem. 1998;70(11):2236–42. https://doi.org/10.1021/ac980059c.
7. Konijnenberg A, Butterer A, Sobott F. Native ion mobility-mass spectrometry and related methods in structural biology. Biochim Biophys Acta. 2013;1834(6):1239–56. https://doi.org/10.1016/j.bbapap.2012.11.013.
8. Sobott F, Benesch JL, Vierling E, Robinson CV. Subunit exchange of multimeric protein complexes. Real-time monitoring of subunit exchange between small heat shock proteins by using electrospray

mass spectrometry. J Biol Chem. 2002;277(41):38921–9. https://doi.org/10.1074/jbc.M206060200.
9. Zhong YY, Hyung SJ, Ruotolo BT. Ion mobility-mass spectrometry for structural proteomics. Expert Rev Proteomics. 2012;9(1):47–58. https://doi.org/10.1586/Epr.11.75.
10. Cooper A (1999) Thermodynamic analysis of biomolecular interactions. Curr Opin Chem biol 3 (5):557-563. https://doi.org/10.1016/S1367-5931(99)00008-3.
11. Robertson AD, Murphy KP. Protein structure and the energetics of protein stability. Chem Rev. 1997;97(5):1251–67. https://doi.org/10.1021/Cr960383c.
12. Erba EB, Barylyuk K, Yang Y, Zenobi R. Quantifying protein-protein interactions within noncovalent complexes using electrospray ionization mass spectrometry. Anal Chem. 2011;83(24):9251–9. https://doi.org/10.1021/ac201576e.
13. Jorgensen TJD, Roepstorff P, Heck AJR. Direct determination of solution binding constants for noncovalent complexes between bacterial cell wall peptide analogues and vancomycin group antibiotics by electrospray ionization mass spectrometry. Anal Chem. 1998;70(20):4427–32. https://doi.org/10.1021/Ac980563h.
14. Krishnaswamy SR, Williams ER, Kirsch JF. Free energies of protein-protein association determined by electrospray ionization mass spectrometry correlate accurately with values obtained by solution methods. Prot Sci. 2006;15(6):1465–75. https://doi.org/10.1110/ps.062083406.
15. West GM, Tang L, Fitzgerald MC. Thermodynamic analysis of protein stability and ligand binding using a chemical modification- and mass-spectrometry based strategy. Anal Chem. 2008;80(11):4175–85. https://doi.org/10.1021/ac702610a.
16. Cech NB, Enke CG. Practical implications of some recent studies in electrospray ionization fundamentals. Mass Spectrom Rev. 2001;20(6):362–87. https://doi.org/10.1002/mas.10008.
17. Sinelnikov I, Kitova EN, Klassen JS. Influence of Coulombic repulsion on the dissociation pathways and energetics of multiprotein complexes in the gas phase. J Am Soc Mass Spectrom. 2007;18(4):617–31. https://doi.org/10.1016/j.jasms.2006.11.006.
18. Catalina MI, de Mol NJ, Fischer MJE, Heck AJR. Probing factors affecting the gas phase stabilities of noncovalent complexes formed by peptides bound to the Grb2 SH2 domain protein. Phys Chem Chem Phys. 2004;6(10):2572–9. https://doi.org/10.1039/b315435a.
19. Baer T, Mayer PM. Statistical Rice-Ramsperger-Kassel-Marcus quasiequilibrium theory calculations in mass spectrometry. J Am Soc Mass Spectrom. 1997;8(2):103–15. https://doi.org/10.1016/S1044-0305(96)00212-7.
20. Rosenstock HM, Wallenstein MB, Wahrhaftig AL, Eyring H. Absolute rate theory for isolated systems and the mass spectra of polyatomic molecules. Proc Natl Acad Sci U S A. 1952;38(8):667–78. https://doi.org/10.1073/pnas.38.8.667.
21. Vekey K. Internal energy effects in mass spectrometry. J Mass Spectrom. 1996;31(5):445–63. https://doi.org/10.1002/(Sici)1096-9888(199605)31:5<445::Aid-Jms354>3.0.Co;2-G.
22. Yefremova Y, Al-Majdoub M, Opuni KFM, Koy C, Yan Y, Gross ML, et al. A dynamic model of pH-induced protein G' e higher order structure changes derived from mass spectrometric analyses. Anal Chem. 2016;88(1):890–7. https://doi.org/10.1021/acs.analchem.5b03536.
23. Sauer-Eriksson AE, Kleywegt GJ, Uhlen M, Jones TA. Crystal structure of the C2 fragment of streptococcal protein G in complex with the Fc domain of human IgG. Structure. 1995;3(3):265–78. https://doi.org/10.1016/S0969-2126(01)00157-5.
24. Gulich S, Linhult M, Stahl S, Hober S. Engineering streptococcal protein G for increased alkaline stability. Protein Eng. 2002;15(10):835–42. https://doi.org/10.1093/protein/15.10.835.
25. Yefremova Y, Al-Majdoub M, Opuni KFM, Koy C, Cui WD, Yan YT, et al. "De-novo" amino acid sequence elucidation of protein G'e by combined "top-down" and "bottom-up" mass spectrometry. J Am Soc Mass Spectrom. 2015;26(3):482–92. https://doi.org/10.1007/s13361-014-1053-2.
26. Nesatyy VJ. Gas-phase binding of non-covalent protein complexes between bovine pancreatic trypsin inhibitor and its target enzymes studied by electrospray ionization tandem mass spectrometry. J Mass Spectrom. 2001;36:950–9. https://doi.org/10.1002/jms.199.
27. Nesatyy VJ. Mass spectrometry evaluation of the solution and gas-phase binding properties of noncovalent protein complexes. Int J Mass Spectrom. 2002;221:147–61. https://doi.org/10.1016/S1387-3806(02)00956-9.
28. Pace CN, Shaw KL. Linear extrapolation method of analyzing solvent denaturation curves. Proteins Suppl. 2000;4:1–7. https://doi.org/10.1002/1097-0134(2000)41:4+3.3.
29. Bolen DW, Santoro MM. Unfolding free energy changes determined by the linear extrapolation method. 2. Incorporation of delta G degrees N-U values in a thermodynamic cycle. Biochemistry. 1988;27(21):8069–74. https://doi.org/10.1021/bi00421a014.
30. Yefremova Y, Danquah BD, Opuni KFM, El-Kased RF, Koy C, Glocker MO (2017) Mass spectrometric characterization of protein structures and protein complexes in condensed and gas phase. Eur J Mass Spectrom 23. https://doi.org/10.1177/1469066717722256.
31. Harvey SR, Yan J, Brown JM, Hoyes E, Wysocki VH. Extended gas-phase trapping followed by surface-induced dissociation of noncovalent protein complexes. Anal Chem. 2016;88:1218–21. https://doi.org/10.1021/acs.analchem.5b03479.
32. Quintyn RS, Zhou MW, Yan J, Wysocki VH. Surface-induced dissociation mass spectra as a tool for distinguishing different structural forms of gas-phase multimeric protein complexes. Anal Chem. 2015;87:11879–86. https://doi.org/10.1021/ar400223t.
33. Zhou M, Dagan S, Wysocki VH. Protein subunits released by surface collisions of noncovalent complexes: native-like compact structures revealed by ion mobility mass spectrometry. Angew Chem Int Ed Engl. 2012;51:4336–9. https://doi.org/10.1002/anie.201108700.
34. Myers JK, Pace CN, Scholtz JM. Denaturant m values and heat capacity changes: relation to changes in accessible surface areas of protein unfolding. Protein Sci. 1995;4(10):2138–48. https://doi.org/10.1002/pro.5560041020.
35. Pace CN. Determination and analysis of urea and guanidine hydrochloride denaturation curves. Methods Enzymol. 1986;131:266–80. https://doi.org/10.1016/0076-6879(86)31045-0.
36. Drahos L, Vekey K. Entropy evaluation using the kinetic method: is it feasible? J Mass Spectrom. 2003;38(10):1025–42. https://doi.org/10.1002/jms.538.
37. Wu L, Lemr K, Aggerholm T, Cooks RG. Recognition and quantification of binary and ternary mixtures of isomeric peptides by the kinetic method: metal ion and ligand effects on the dissociation of metal-bound complexes. J Am Soc Mass Spectrom. 2003;14(2):152–60. https://doi.org/10.1016/S1044-0305(02)00868-1.
38. Parker MJ, Spencer J, Clarke AR. An integrated kinetic analysis of intermediates and transition states in protein folding reactions. J Mol Biol. 1995;253(5):771–86. https://doi.org/10.1006/jmbi.1995.0590.
39. Staniforth RA, Burston SG, Smith CJ, Jackson GS, Badcoe IG, Atkinson T, et al. The energetics and cooperativity of protein folding: a simple experimental analysis based upon the solvation of internal residues. Biochemistry. 1993;32(15):3842–51. https://doi.org/10.1021/bi00066a003.
40. Benesch JL, Ruotolo BT, Simmons DA, Robinson CV. Protein complexes in the gas phase: technology for structural genomics and proteomics. Chem Rev. 2007;107(8):3544–67. https://doi.org/10.1021/cr068289b.
41. Jurchen JC, Williams ER. Origin of asymmetric charge partitioning in the dissociation of gas-phase protein homodimers. J Am Chem Soc. 2003;125(9):2817–26. https://doi.org/10.1021/ja0211508.

42. Sciuto SV, Liu JJ, Konermann L. An electrostatic charge partitioning model for the dissociation of protein complexes in the gas phase. J Am Soc Mass Spectrom. 2011;22(10):1679–89. https://doi.org/10.1007/s13361-011-0205-x.
43. Sobott F, Robinson CV. Characterising electrosprayed biomolecules using tandem-MS—the noncovalent GroEL chaperonin assembly. Int J Mass Spectrom. 2004;236(1–3):25–32. https://doi.org/10.1016/j.ijms.2004.05.010.
44. Benesch JL. Collisional activation of protein complexes: picking up the pieces. J Am Soc Mass Spectrom. 2009;20(3):341–8. https://doi.org/10.1016/j.jasms.2008.11.014.
45. Dragusanu M, Petre BA, Slamnoiu S, Vlad C, Tu TT, Przybylski M. On-line bioaffinity-electrospray mass spectrometry for simultaneous detection, identification, and quantification of protein-ligand interactions. J Am Soc Mass Spectrom. 2010;21(10):1643–8. https://doi.org/10.1016/j.jasms.2010.06.011.
46. Gronewold TMA. Surface acoustic wave sensors in the bioanalytical field: recent trends and challenges. Anal Chim Acta. 2007;603(2):119–28. https://doi.org/10.1016/j.aca.2007.09.056.
47. Thomas PD, Kejariwal A. Coding single-nucleotide polymorphisms associated with complex vs. Mendelian disease: evolutionary evidence for differences in molecular effects. Proc Natl Acad Sci U S A. 2004;101(43):15398–403. https://doi.org/10.1073/pnas.0404380101.
48. Zhao N, Han JG, Shyu CR, Korkin D. Determining effects of non-synonymous SNPs on protein-protein interactions using supervised and semi-supervised learning. PLoS Comput Biol. 2014;10(5). ARTN):e1003592. https://doi.org/10.1371/journal.pcbi.1003592.
49. Stunnenberg HG, Hubner NC. Genomics meets proteomics: identifying the culprits in disease. Hum Genet. 2014;133(6):689–700. https://doi.org/10.1007/s00439-013-1376-2.
50. David A, Razali R, Wass MN, Sternberg MJ. Protein-protein interaction sites are hot spots for disease-associated nonsynonymous SNPs. Hum Mutat. 2012;33(2):359–63. https://doi.org/10.1002/humu.21656.
51. Back AL, Kwok WW, Hickstein DD. Identification of two molecular defects in a child with leukocyte adherence deficiency. J Biol Chem. 1992;267(8):5482–7.
52. Ohashi Y, Yambe T, Tsuchiya S, Kikuchi H, Konno T. Familial genetic-defect in a case of leukocyte adhesion deficiency. Hum Mutat. 1993;2(6):458–67. https://doi.org/10.1002/humu.1380020606.
53. Etzioni A. Adhesion molecules—their role in health and disease. Pediatr Res. 1996;39(2):191–8. https://doi.org/10.1203/00006450-199602000-00001.

Supplemental data

Analytical and Bioanalytical Chemistry

Electronic Supplementary Material

Apparent activation energies of protein-protein complex dissociation in the gas-phase determined by electrospray mass spectrometry

Yelena Yefremova, F. Teresa I. Melder, Bright D. Danquah, Kwabena F.M. Opuni, Cornelia Koy, Alexandra Ehrens, David Frommholz, Harald Illges, Knut Koelbel, Frank Sobott, Michael O. Glocker

I) Theoretical background and method development

II) Protein G´ • IgG-Fc

I) Theoretical background and method development

Basic considerations

Thermodynamic evaluation of gas-phase dissociation reactions of protein-protein complexes along well established laws for in-solution reactions, such as linear free energy relationships, is derived from considering the following facts and simplifications [17-21, 26, 27, 29, 30]:

1. Both, the protein-protein complex dissociation reaction itself (because of entropy gain of the products) and concomitant complex constituent unfolding reactions (due to lack of the hydrophobic effect which could drive refolding) are irreversible.
2. Within the energy "transition region" of the protein-protein complex dissociation reaction, the time required for recording single spectra is shorter than that which was needed for reaching complete unfolding/dissociation of protein-protein complexes.
3. Consequently, educt (protein-protein complex) and product (complex constituent) ion signals are simultaneously recorded in the corresponding mass spectra with elevated collision energies as opposed to the exclusive presence of educt ions in the "baseline region" as well as of only product ions in the maximum energy regime (disregarding potential fragmentation).

These considerations permit application of "Linear Free Energy relations" (LFE).

In-solution thermodynamic methods [10-16] were adapted to gas-phase experiments using the following conventions and definitions:

(1) $$\text{Normalized area under signal (norm. AUS)} = \left(f\frac{educts}{\Sigma ed+prod}\right) * [\%]\ (educts) \quad (1)$$

(2) The charge contribution to the kinetic energy was accounted for by converting acceleration voltage (V_{acc}) into center of mass (E_{com}) energy:

$$E_{lab\ frame} = V_{acc} * z \quad (2)$$

$$E_{com} = \left(\frac{N}{m_p+N}\right) * E_{lab\ frame} \quad (3)$$

(N = mass of the neutral collision gas (here Ar, M_r = 39.95); m_p = mass of the protein-protein complex ion; z = charge)

(3) An "in-solution-like" LFE was applied to the "apparent equilibrium":

$$\Delta G_g^{\#} = -R * ln\left(\frac{100\%-norm.AUS}{norm.AUS}\right) = \Delta G_{m0g}^{\#} - \mathrm{n} * [E_{com}] \quad (4)$$

R = gas constant, n = slope, m = mean of charge state, 0 = at E_{com}=0, g = gas phase. Principally, the absolute temperature, T, should be a factor in this equation, too, but since it cannot be determined with certainty, it was merged with the free enthalpy term. $\Delta G_{m0g}^{\#}$ must, therefore, be regarded as apparent.

(4) Extrapolation towards "zero activation", at E_{com}=0, yields the nominal stability (as opposed to observed parameters as threshold values) of complexes. However, because of the de facto irreversibility of the dissociation reaction (see above considerations), this value describes not a

thermodynamic (equilibrium) stability, but has to be regarded as being proportional to the activation energy ($E_{A\,m0g}^{\#}$): $\Delta G_{m0g}^{\#\,0} = E_{A\,m0g}^{\#}$ (5)

Plotting normalized AUS curves as functions of the respective lab frame or center-of-mass energies in order to obtain valid threshold energies has been accepted standard. But, Coulomb repulsion affects the unfolding and dissociation processes ("interface separation") of protein-protein complex ions in the gas phase. This dissociation process comprises two different aspects which need to be considered separately.

1) the charge impact on kinetic energy itself is conveniently corrected for by plotting the peak areas of complex ions and constituent ions, respectively, vs. lab frame or, as in our case, center-of-mass energies (E_{com}).
2) charge repulsion - as driving force for separation - is covered by our analysis by extrapolation towards $E_{com} = 0$.

Further correction is not necessary, since we used the respective educt and product abundances (in the transition region) at energies that limit formation of charge repulsed products. Principally, this simplification is correct as long as the procedure is applied to each charge state separately. Of note, our experiments with streptavidin have shown that extrapolation lines from the different charge states are well represented by the line that is obtained by the data from the mean of the charge states.

Therefore, we determined the activation energy ($E_{A\,m0g}^{\#}$) at E_{com}=0 eV of protein-protein complexes by applying "Linear Free Energy relations" (LFE; cf. Figure S6B).

Ion mobility separation of protein complex ions

Our method was tested by dissociating the streptavidin tetramer (S4) with and without ion mobility selection of individual charge states using a Synapt mass spectrometer as described in the Materials and Methods section. A streptavidin tetramer (S4) stock solution was prepared by dissolving the commercial product (Carl-Roth, Karlsruhe, Germany, article no. 6073, lot no. 025218507; Mr (avg.): 56,116) in 50 mM NH_4OAc, pH 6.9 (final streptavidin (S4) concentration 1 mg/ml). Buffer exchange, using 50 mM NH_4OAc, pH 6.9 for all steps, protein concentration determination, and spectrum acquisition are described in the materials and methods section for IgG-Fc and protein G´-containing solutions.

Despite the fact that the 16+ streptavidin tetramer ion signal is located at the same m/z position as the 4+ streptavidin monomer ion signal, there is no risk of ambiguity in the assignment, since the latter appears at clearly different TCE / E_{com} values as opposed to that of the first one. When dissociating the individual charge states 15+ and 14+ of the tetramer complex there is no overlap of tetramer with monomer ions.

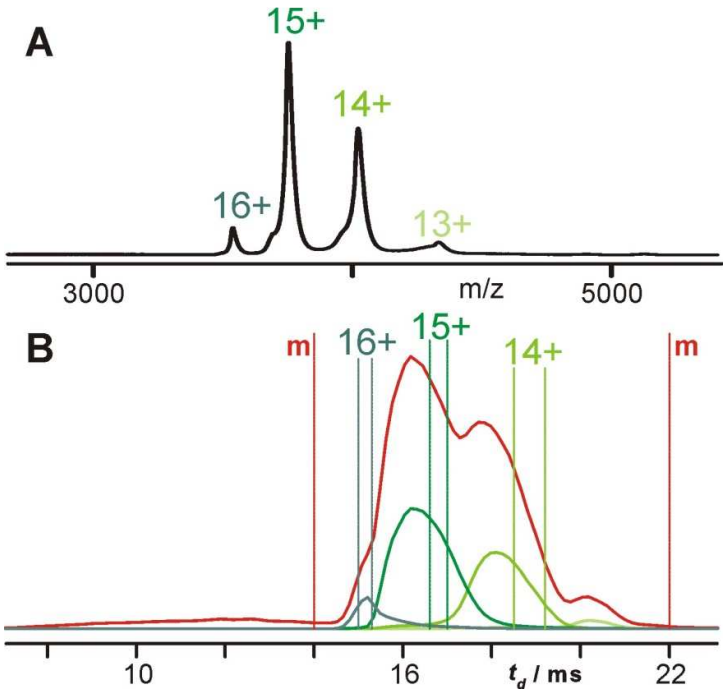

Fig. S1 Ion mobility selection of tetrameric streptavidin ions. A: Precursor ion mass spectrum of the intact streptavidin tetramer recorded with 30 V acceleration voltage (TCE). Individual charge states are indicated above the respective peaks. B: Arrival time distributions corresponding to the complete spectrum (red) or to the individual charge states (same color code as in A). Drift time windows as used for abundance-weighted mean of charge states (m) and charge state-specific ion mobility selections (see Fig. S2-S5) are indicated by vertical ticked lines

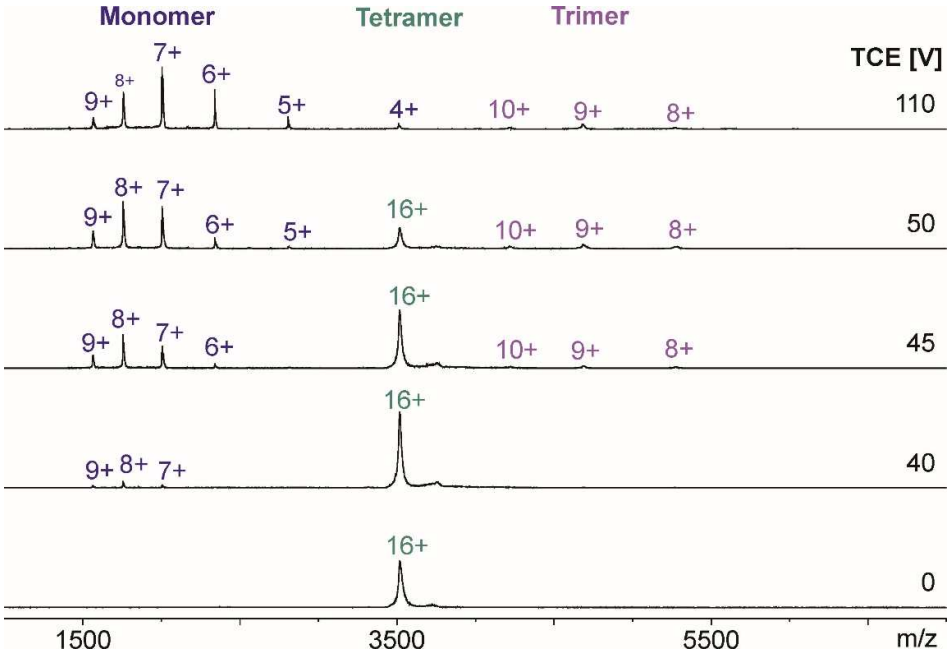

Fig. S2 Collision induced dissociation of 16+ tetrameric streptavidin ion. NanoESI mass spectra of intact and dissociated streptavidin tetramers after ion mobility selection of the 16+ charge state and its subsequent collision induced dissociation by stepwise increasing transfer cell collision energies (TCE, from bottom to top)

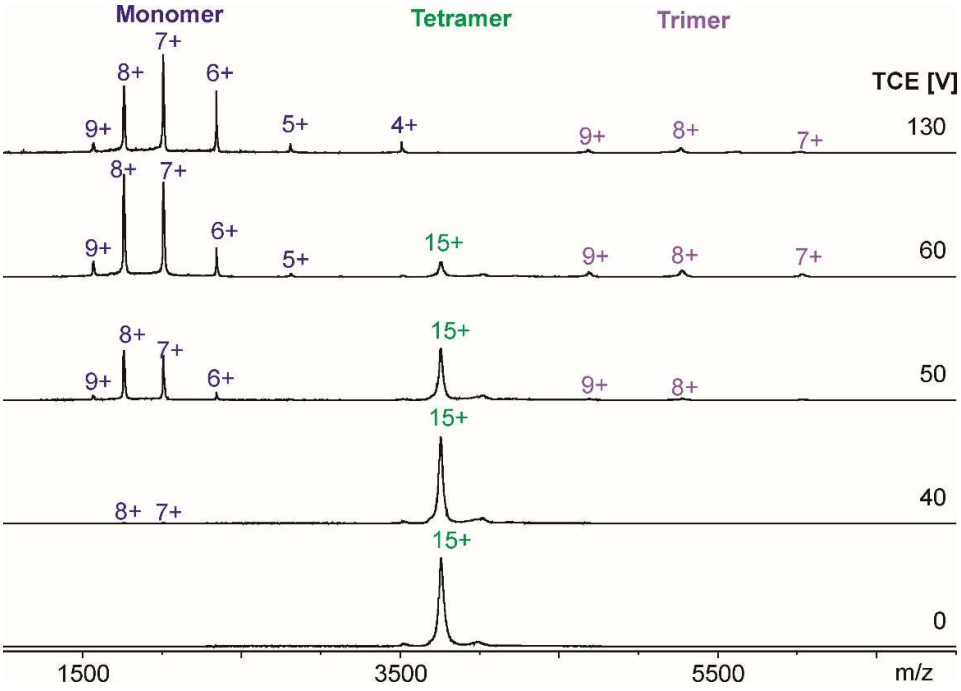

Fig. S3 Collision induced dissociation of 15+ tetrameric streptavidin ion. NanoESI mass spectra of intact and dissociated streptavidin tetramers after ion mobility selection of the 15+ charge state and its subsequent collision induced dissociation by stepwise increasing transfer cell collision energies (TCE, from bottom to top)

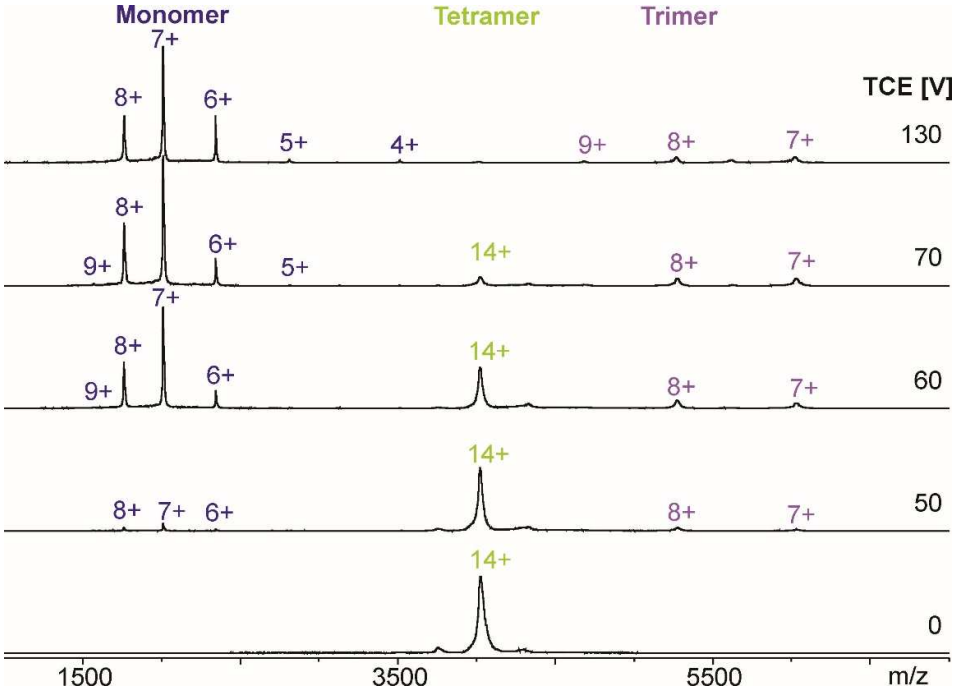

Fig. S4 Collision induced dissociation of 14+ tetrameric streptavidin ion. NanoESI mass spectra of intact and dissociated streptavidin tetramers after ion mobility selection of the 14+ charge state and its subsequent collision induced dissociation by stepwise increasing transfer cell collision energies (TCE, from bottom to top)

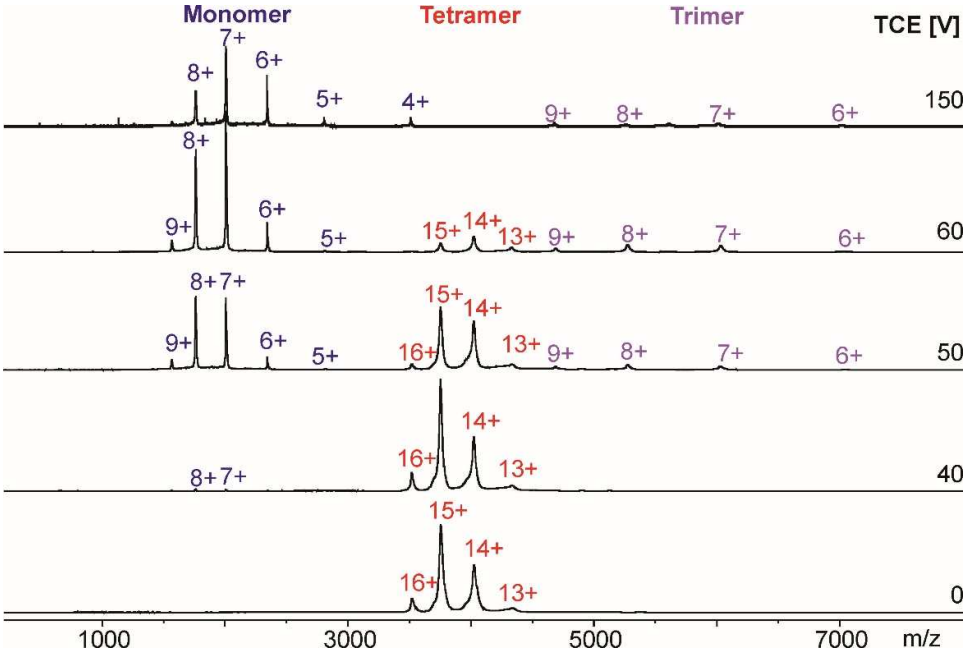

Fig. S5 Collision induced dissociation of n+ tetrameric streptavidin ions. NanoESI mass spectra of intact and dissociated streptavidin tetramers after ion mobility selection of the abundance-weighted mean of charge states (m) and their subsequent collision induced dissociation by stepwise increasing transfer cell collision energies (TCE, from bottom to top)

Evaluation of CID data of ion mobility-selected streptavidin complexes

From Fig. S2-S5 the unaltered pattern of the highly charged monomeric product ions is apparent – regardless of precursor ion charge. Contrarily, the charge states of the respective precursor and dominant trimeric product ions correlate strictly. Since the classical asymmetric charge distribution pattern is adhered to, ion mobility selection can be conveniently used as surrogate of conventional MS/MS.

The unfolding/dissociation transitions of tetrameric streptavidin are steep (Fig. S6A), leaving only four to five data points for LFE evaluation. The potential error margin depends from either keeping or dropping the extreme points from analysis (Fig. S6B). Sufficient numbers of repetitions are therefore required. These, in turn, are more conveniently achieved for the complete sets of precursor ion peaks (m) than for each individual charge state. So, we widened the drift time window to encompass the complete tetrameric ensemble (+16 to +13, m; see Fig. S1) and measured dissociation of tetrameric streptavidin (S4) in triplicate (Fig. S5). An abundance-weighted mean of charge state (m) of 14.6+ was calculated using equation 6:

$$m = \sum z_n * \left(\frac{I_{z_n}}{\sum I}\right) \quad (6)$$

m = abundance weighted mean of charge state of the tetramer ion series
Zn = individual charge states of the tetramer ion series
IZn = individual ion intensities of the tetramer ion series
∑I = sum of the intensities of the tetramer ion series

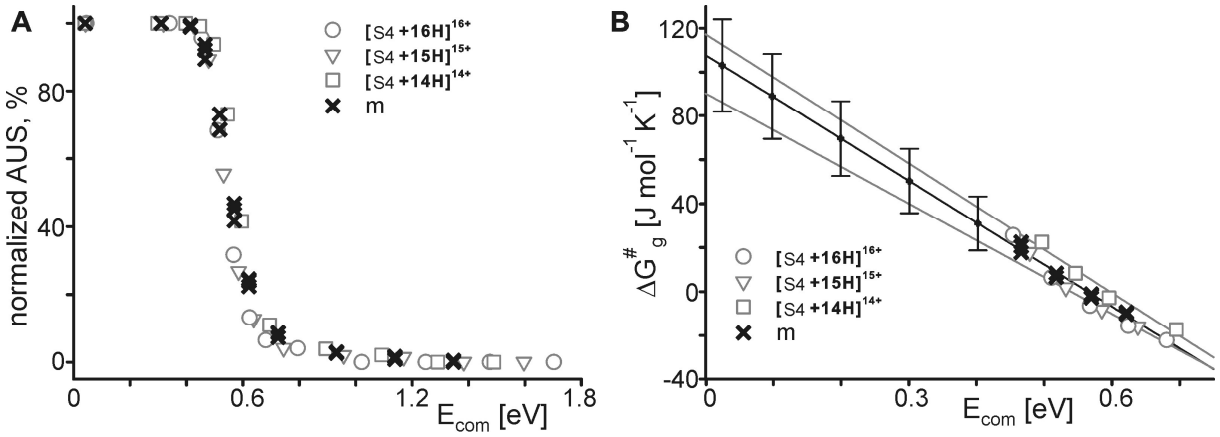

Fig. S6 Evaluation of streptavidin complex gas-phase stabilities by LFE. A: Series of CID measurements using ion mobility-selected (see Fig. **S**1 for the respective drift time windows) tetrameric streptavidin (S4) were conducted and normalized areas under ion signals (normalized AUS) were determined as described. B: LFE evaluation was applied to the normalized AUS data. Selected data points were deliberately dropped from analysis to test for their effects on resulting deviations (maximum effects are within error bars).

Quite reasonably – as the mean of charge states inherently represents the most intense signal within the considered ensemble (+14 and +15 for S4) – LFE evaluation of these data closely resembles the corresponding results of the individual charge state-specific measurements. And, since the most intense native-MS peaks of a given protein are usually adjacent to each other, LFE evaluation of abundance-weighted mean of charge states will yield fairly representative $E_{A\,m0g}^{\#}$ values for the complete charge state ensemble of a given protein-protein complex.

II) Protein G´ • IgG-Fc

Amino acid sequences of protein G´ variants

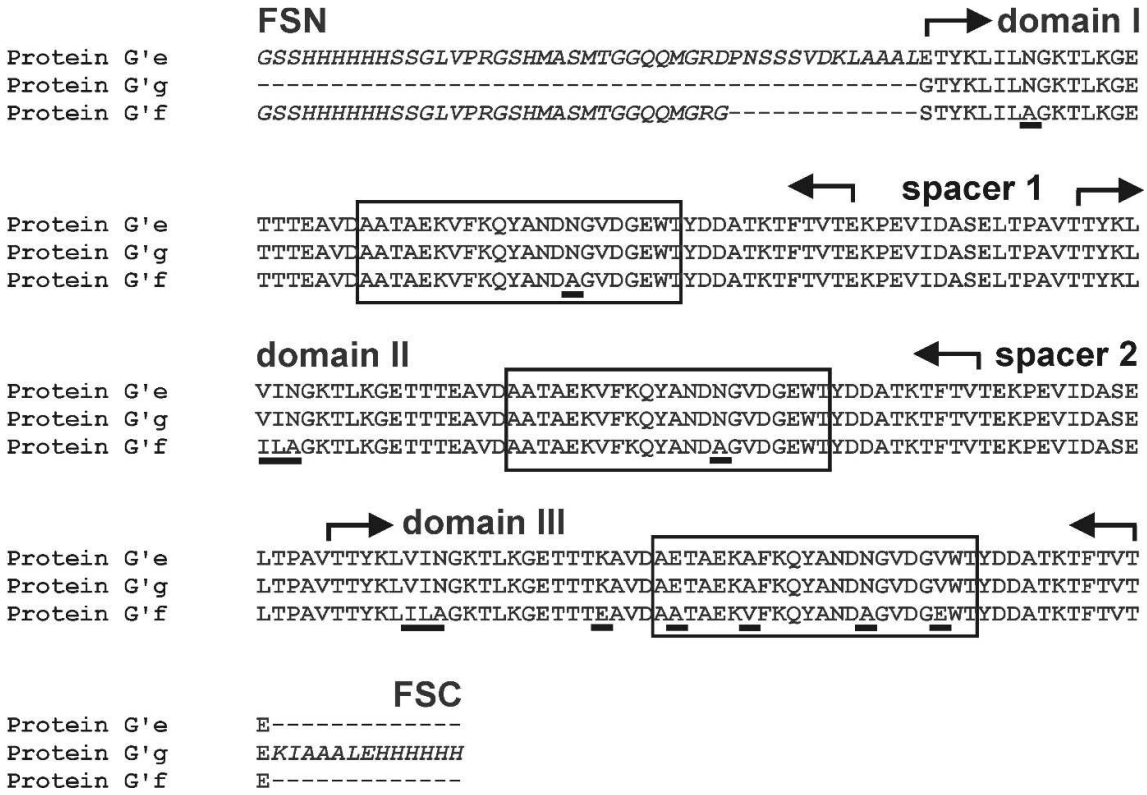

Fig. S7 Amino acid alignment of the three protein G' variants. The amino acid sequences of proteins G'e, G'g and G'f (from top to bottom in each single panel) are aligned with the N- and C-termini shown in italics. Kinked arrows encompass the complete IgG binding domains, whereas boxes indicate regions known to be actually involved in IgG binding. Distinct domains and linkers of the proteins are labeled individually above the sequences: the N- and C-terminal flanking sequences (FSN and FSC, respectively), the three IgG binding domains (I-III) and the spacer regions in between. Residues, the exchanges of which distinguish protein G'f from the other two, are underlined

Data on individual complex constituents

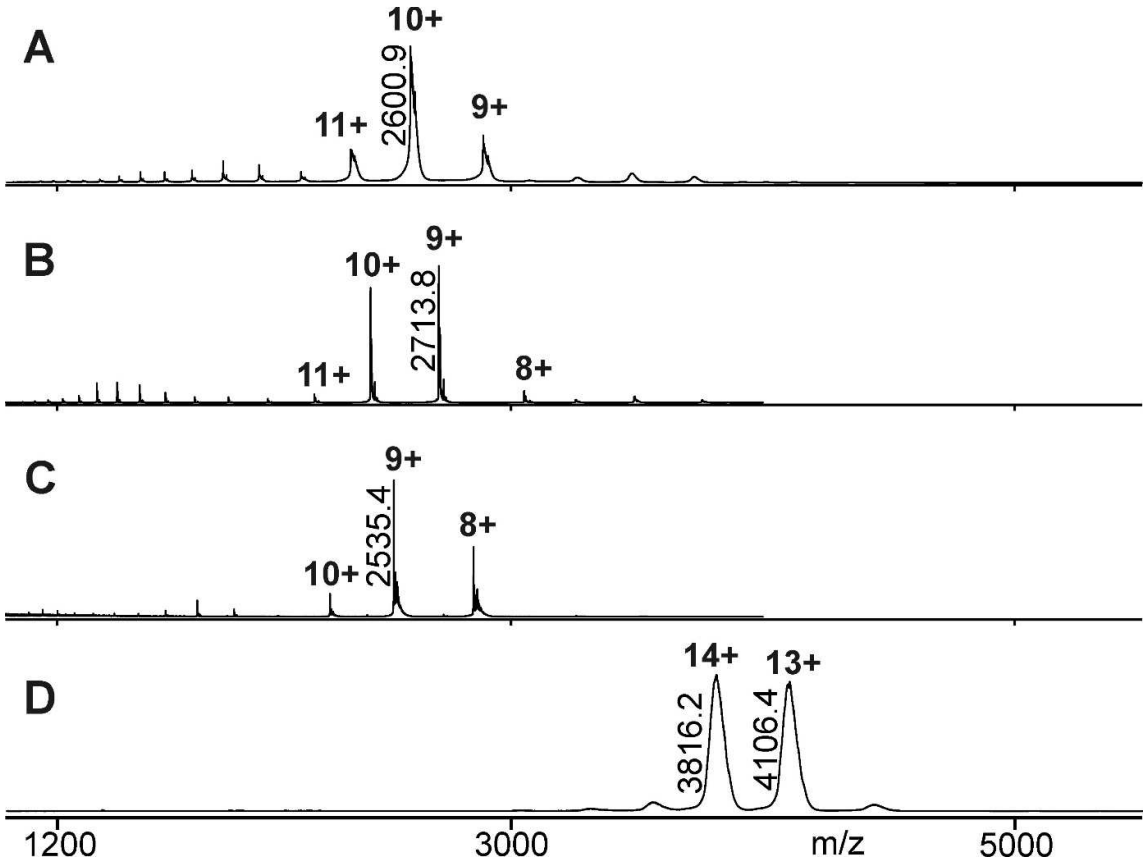

Fig. S8 NanoESI mass spectra of protein G´ isoforms and IgG-Fc. A: protein G´e. B: protein G´f. **C:** protein G´g. **D:** IgG-Fc. Charge states and m/z values for selected ion signals of a respective ion series are given. Solvents: 200 mM NH_4OAc

Collision induced protein-protein complex dissociation

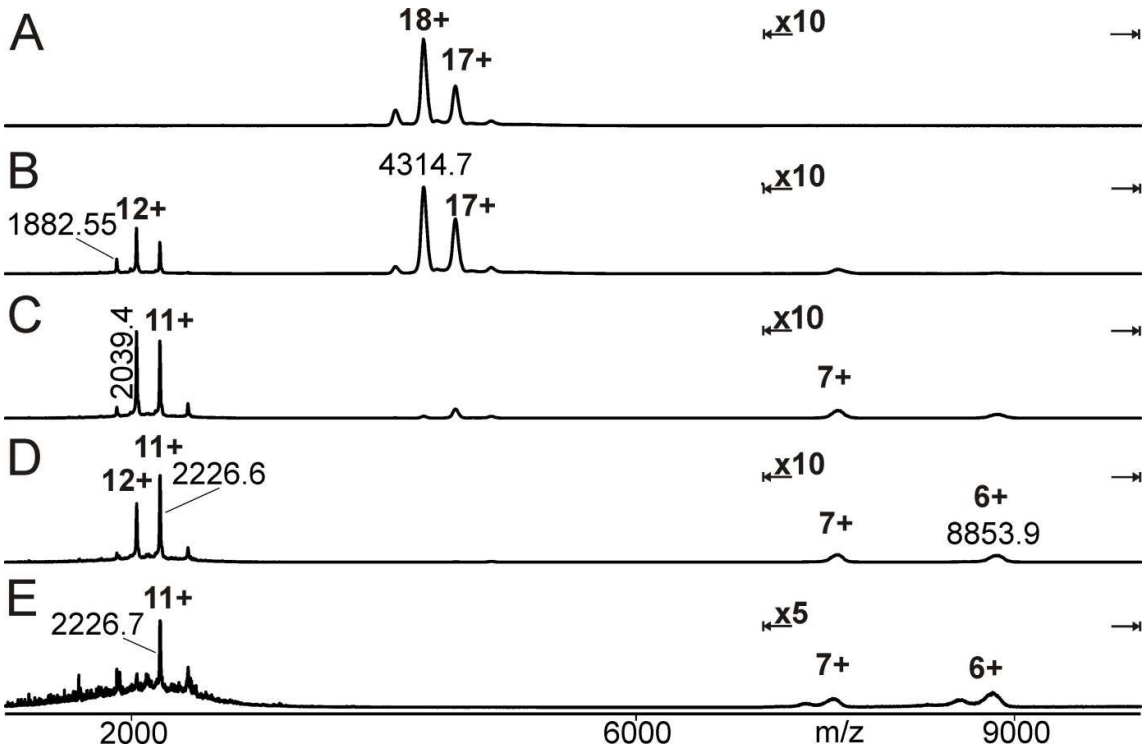

Fig. S9 Collision induced dissociation of the ion mobility-separated IgG-Fc protein G'f complex. The complex was prepared and sprayed from 200 mM NH_4OAc and measurement series with increasing transfer cell collision energies (TCE) were acquired as described. Example spectra recorded at (A) 70 V, (B) 120 V, (C) 150 V, (D) 170 V, and (E) 200 V are presented. Charge states and m/z values (from the apex of each peak in question) of released protein G'f product ions, IgG-Fc G'f precursor ions as, well as of retained IgG-Fc product ions are labeled. *Note*: At 200 V TCE signals of intact protein G'f are superimposed by backbone fragment ion signals

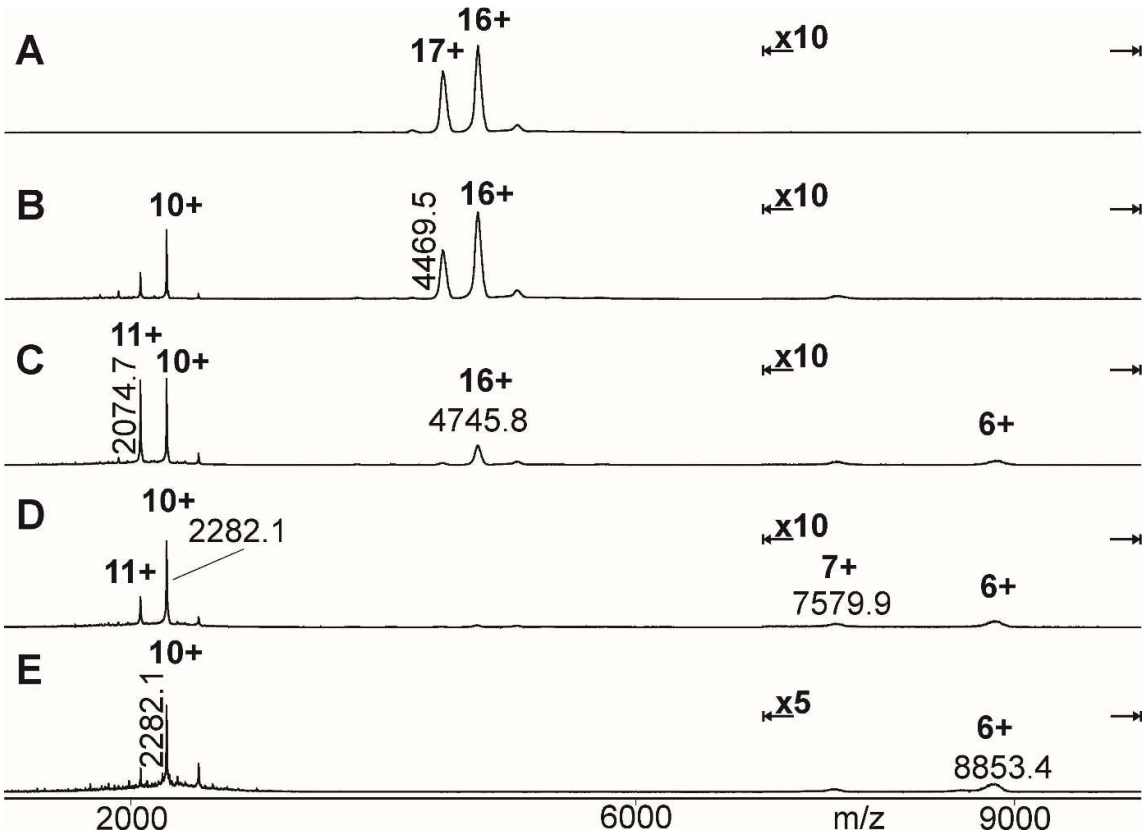

Fig. S10 Collision induced dissociation of the ion mobility-separated IgG-Fc protein G'g complex. The complex was prepared and sprayed from 200 mM NH_4OAc and measurement series with increasing transfer cell collision energies (TCE) were acquired as described. Example spectra recorded at (A) 70 V, (B) 120 V, (C) 150 V, (D) 170 V, and (E) 200 V are presented. Charge states and m/z values (from the apex of each peak in question) of released protein G'g product ions, IgG-Fc G'g precursor ions, as well as of retained IgG-Fc product ions are labeled. *Note*: At 200 V TCE signals of intact protein G'g are superimposed by backbone fragment ion signals

In-solution K_D value determinations

The obtained in-solution data (see Materials and Methods) were stored in the SensMaster software. For evaluation of the sensograms the software FitMaster (Rev. 2.0; SAW Instruments, Bonn, Germany) coupled with Origin 8.1G (OriginLab corporation, Massachusetts, USA) was used. Fitting of the binding curves was done by applying the "1:1 Binding + Residue model" which assumes a permanently bound residue [45, 46]. Since the concentration of immobilised antibodies (IVIG) is in excess and remains almost unchanged during the interactions, the time course of phase changes that occurred during binding was fitted to a pseudo first order kinetics. The pseudo first order kinetic constant (k_{obs}) was determined for the different concentrations of analytes using equation (7), where *A* is the number of bound sites at any given time point (*t*) and A_{eq} is the number of bound sites at equilibrium between absorption and desorption.

$$A(t) = A_{eq} * [1 - \exp\{-k_{obs} * t\}] \quad (7)$$

Next, $k_{obs(n)}$ values determined for different concentrations (c_1, c_2, … c_n) were subjected to linear regression described by equation (8).

$$k_{obs(n)} = k_{on} * c_n + k_{off} \quad (8)$$

A linear regression of concentration of analyte vs $k_{obs(n)}$ was subsequently used to obtain k_{on} and k_{off} values, where k_{on} is the slope of the graph, k_{off} is the intercept on the $k_{obs(n)}$ axis, and c_n is the concentration of analytes. From these, $K_{D\,s}$ values were calculated according to equation (9).

$$K_{D\,s} = \frac{k_{off}}{k_{on}} \quad (9)$$

3 Curriculum vitae

Personal Data

Name	Bright Djan Danquah
Nationality	Ghanaian
Gender	Male
Date of Birth	4th May 1987.
Religion	Christian
Marital status	Married, 1 child
E-mail address	bright.danquah@uni-rostock.de or danquahbright@yahoo.com

Education/ Professional Qualifications

Proteome Center Rostock, Institute of Immunology, Unversity of Rostock. Germany
PhD candidate. October 2015- Date

Kwame Nkrumah University of Science and Technology, Kumasi, Ghana
MPhil Pharmaceutical Chemistry. 2011- 2013. (Degree awarded in June 2014)

Ghana Pharmacy Professional Qualifying Examination (GPPQE), Accra, Ghana
Pharmacy Licensure. 2011

Kwame Nkrumah University of Science and Technology, Kumasi, Ghana
Bachelor of Pharmacy. 2006-2010

St. Peter's Senior Secondary School, Nkwatia- Kwahu, Ghana
Senior Secondary School Certificate (SSCE). 2002-2005

Santa Maria School Complex, Accra, Ghana
Basic Education Certificate Examination (BECE). 2000-2002

Awards

German Academic Exchange Service (DAAD) stipend for doctoral studies, Proteome Center Rostock, University of Rostock, Germany. October 2015 to June 2019

European Cooperation in Science and Technology (COST) travel grant for training school on chemical crosslinking, 7th Symposium on Structural Proteomics, 23-25th October 2017, Vienna, Austria

German Society for Mass Spectrometry (DGMS) travel stipend for European Mass Spectrometry Conference, 11th-15th March, 2018, Saarbruecken, Germany

German Academic Exchange Service (DAAD) Stipend for German language, Carls Duisberg language school, Berlin, June to September 2014

Academic Positions

Part time Lecturer, Department of Pharmaceutical Sciences, Kumasi Technical University. September 2014- April 2015

Graduate Assistant, Department of Pharmaceutical Chemistry, Kwame Nkrumah University of Science and Technology (KNUST). August 2012- July 2013

Postgraduate Researcher, Department of Pharmaceutical Chemistry, Kwame Nkrumah University of Science and Technology (KNUST). August 2011- July 2013

Research Assistant, Department of Pharmaceutical Chemistry, Kwame Nkrumah University of Science and Technology (KNUST). August 2010- July 2011

Academic and Professional Affiliation

Member, Graduate Academy, University of Rostock; Germany
Member, Structured curriculum for MD/PhD students, University Medicine Rostock, University of Rostock, Germany
Member, German Society for Mass Spectrometry (DGMS)
Member, American Society for Mass Spectrometry (ASMS)
Member, Pharmaceutical Society of Ghana (MPSGh)

Leadership Experience

Executive member, 2014-2015. Ashanti regional branch of Pharmaceutical Society of Ghana

President, 2009-2010. Ghana Pharmaceutical Students' Association (GPSA)

Local Representative, National Union of Ghana Students, **2008-2009**
Faculty of Pharmacy and Pharmaceutical Sciences, KNUST- Kumasi. Ghana

Teacher and Staff Secretary, 2005- 2006. Gina International School, Madina, Accra. Ghana

Senior House Prefect, 2004-2005. Kizito House, St. Peter's Secondary School, Nkwatia- Kwahu. Ghana

---

4 List of publications and presentations

Publications

Yelena Yefremova., Kwabena F.M.Opuni, **Bright D. Danquah,** Hans.-J. Thiesen, and Michael O. Glocker. Intact transition epitope mapping. *J. Am. Soc. Mass Spectrom*. 28, 1612–1622 **(2017)**

Yelena Yefremova, **Bright D. Danquah**, Kwabena F.M. Opuni, Reham El-Kased, Cornelia Koy, and Michael O. Glocker. Mass spectrometric characterization of proteins structures and protein complexes in condensed and gas phase. *Eur. J. Mass Spectrom*. 23, 445-459 **(2017)**

Yelena Yefremova, F. Teresa I. Melder, **Bright D. Danquah**, Kwabena F.M. Opuni, Cornelia Koy, Alexandra Ehrens, David Frommholz, Harald Illges, Knut Koelbel, Frank Sobott, and Michael O. Glocker. Apparent activation energies of protein-protein complex dissociation in the gas phase determined by electrospray mass spectrometry. *Anal. Bioanal Chem*. 409, 6549-6558 **(2017)**

Bright D. Danquah, Claudia Röwer, Kwabena F.M. Opuni, Reham El-Kased, David Frommholz, Harald Illges, Cornelia Koy, and Michael O. Glocker. Intact Transition Epitope Mapping- Targeted High-energy Rupture of Extracted Epitopes (ITEM-THREE). *Mol. Cell. Proteom.* 18, 2-14 **(2019)**

Oral presentations

B. D. Danquah, C. Röwer, K.F.M. Opuni, R. El-Kased, D. Frommholz, H. Illges, C. Koy, and M. O. Glocker. Intact Transition Epitope Mapping- Targeted High-energy Rupture of Extracted Epitopes (ITEM-THREE). Proteome Center Rostock/Institute of Immunology Group meeting, 28th May, **2019**, Rostock, Germany

B. D. Danquah, C. Röwer, K.F.M. Opuni, R. El-Kased, D. Frommholz, H. Illges, C. Koy, and M. O. Glocker. Intact Transition Epitope Mapping- Targeted High-energy Rupture of Extracted Epitopes (ITEM-THREE). 52nd Annual German Society for Mass Spectrometry (DGMS) Conference, 10th-13th March, **2019**. Rostock, Germany

B. D. Danquah. Development of novel mass spectrometric methods for antibody characterization and stratification of patients for treatment. Faculty of Pharmacy and Pharmaceutical Sciences Seminar, Kwame Nkrumah University of Science and Technology (KNUST), 30th January, **2019**. Kumasi, Ghana

B. D. Danquah and M. O. Glocker. ITEM-TWO: Nanoelectrospray ionization mass spectrometry enables simultaneous characterization of specificities and affinities of epitope-antibody complexes in the gas phase. International Symposium and Summer School “Mass Spectrometry in Medical Technology and Biotechnology”, 19th-24th August, **2018**, Hochschule RheinMain, Rüsselsheim am Main, Germany

B. D. Danquah and M. O. Glocker. Determination of apparent gas phase dissociation energies of antiHis tag antibody-His tag peptide complex by electrospray ionization mass spectrometry (ITEM-TWO). Participants' Camp Summer Semester 2018, 5th July, **2018**, University Medicine Rostock, Rostock, Germany

B. D. Danquah, Y. Yefremova, K.F.M. Opuni, F. T. I. Melder, C. Koy, and M. O. Glocker. Intact transition epitope mapping- thermodynamic weak-force observation (ITEM-TWO). International Workshop "Affinity- Mass Spectrometry-Clinical Methods Development and Application", 2nd-3rd November, **2017**, Hochschule RheinMain, Rüsselsheim am Main, Germany

B. D. Danquah, H.-J. Thiesen, M. O. Glocker. Epitope-antibody reactivities determuined by electrospray mass spectrometry. Summer Semester 2017 Participants' Camp, 28th-29th June, **2017**, University Medicine Rostock, Rostock, Germany

B. D. Danquah, and M. O. Glocker. Epitope-antigen reactivities probed by biosensor analysis and mass spectrometry. Participants´ Camp Winter Semester 2016/2017, 14–15th December, **2016**, University Medicine Rostock, Rostock, Germany

B. D. Danquah, and M. O. Glocker. Epitope or Meditope? That is the question. Proteome Center Rostock/Institute of Immunology Group meeting, 21st November, **2016**, Rostock, Germany

B. D. Danquah, Determination of affinity constant for the interaction of antiRA33 antibody with its epitope peptide using a love wave biosensor. Participants' Camp Summer Semester, 29th-30th June, **2016**, University Medicine Rostock, Rostock, Germany

B. D. Danquah, and M. O. Glocker. Kinetic and thermodynamic studies of interactions between protein G' isoforms and IVIG. Proteome Center Rostock/Institute of Immunology Group meeting, 8th January, **2016**, Rostock, Germany

B. D. Danquah. Kinetic and thermodynamic studies of antibody-antigen interactions. Participants' camp and 10th Proteome Forum, 2nd-3rd December, **2015**, Rostock, Germany

Poster presentations

Bright D. Danquah, Claudia Röwer, Kwabena F.M. Opuni, Reham El-Kased, David Frommholz, Harald Illges, Cornelia Koy, and Michael O. Glocker. Intact Transition Epitope Mapping- Targeted High-energy Rupture of Extracted Epitopes (ITEM-THREE). 67th American Society for Mass Spectrometry (ASMS) Conference on Mass Spectrometry and Allied Topics, 2nd-6th June, **2019**. Atlanta, USA

Bright D. Danquah, Yelena Yefremova, Kwabena F.M. Opuni, F. Teresa I. Melder, Cornelia Koy, and Michael O. Glocker. ITEM-TWO: Nanoelectrspray ionization mass spectrometry enables simultaneous characterization of specificities and affinities of epitope-antibody complexes in the gas phase. 66th

American Society for Mass Spectrometry (ASMS) conference, 3rd-7th June, **2018**, San Diego CA, USA

Bright D. Danquah, Yelena Yefremova, Kwabena F.M. Opuni, F. Teresa I. Melder, Cornelia Koy, and Michael O. Glocker. Determination of apparent gas phase activation energies and dissociation constants of epitope peptide – antibody complexes by electrospray-mass spectrometry – ITEM TWO. European Mass Spectrometry Conference, 11th -15th March, **2018**, Saarbrücken, Germany

Bright D. Danquah, Yelena Yefremova, Kwabena F.M. Opuni, F. Teresa I. Melder Cornelia Koy, and Michael O. Glocker. Intact transition epitope mapping-thermodynamic weak-force observation (ITEM-TWO). 7th Symposium on Structural Proteomics, 23rd-25th October, **2017**, Vienna, Austria

Yelena Yefremova, F. Teresa I. Melder, **Bright D. Danquah**, Kwabena F.M. Opuni, Cornelia Koy, Knut Koelbel, Frank Sobott, Harald Illges, and Michael O. Glocker. Gas phase activation energies of protein-protein interactions determined by electrospray mass spectrometry. 65th American Society for Mass Spectrometry (ASMS) conference, 4th-8th June, **2017**, Indianapolis IN, USA